Universidade do Minho
Escola de Engenharia

Luís Carlos Martins da Silva

Dynamic analysis of out-of-plane loaded masonry walls using homogenization

abril de 2019

Dynamic analysis of out-of-plane loaded masonry walls using homogenization
Luís Carlos Martins da Silva
UMinho | 2019

FCT Fundação para a Ciência e a Tecnologia
MINISTÉRIO DA CIÊNCIA, TECNOLOGIA E ENSINO SUPERIOR
POPH QUALIFICAR E CRESCER
QREN QUADRO DE REFERÊNCIA ESTRATÉGICO NACIONAL
GOVERNO DA REPÚBLICA PORTUGUESA
UNIÃO EUROPEIA
Fundo Social Europeu

Universidade do Minho
Escola de Engenharia

Luís Carlos Martins da Silva

Dynamic analysis of out-of-plane loaded masonry walls using homogenization

Tese de Doutoramento
Engenharia Civil

Trabalho efetuado sob a orientação do
Professor Doutor Paulo B. Lourenço
Professor Doutor Gabriele Milani

abril de 2019

DIREITOS DE AUTOR E CONDIÇÕES DE UTILIZAÇÃO DO TRABALHO POR TERCEIROS

Acknowledgments

I want to express my sincere gratitude to my thesis supervisor, Professor Paulo Lourenço. Thank you for believing in me, for your support, availability, guidance, scientific advices and for your careful reading of the thesis. You are truly a role model. I want to express, as well, my deepest gratitude to my thesis co-supervisor, Professor Gabriele Milani. I am very grateful for having the opportunity to work by your side. Your guidance throughout this dissertation period was decisive and made me grow as a researcher. Thanks for the knowledge shared, for your inspiring geniality, for the advices and motivation, for the full availability and for the great hospitality during my stay in Milan.

A special thanks to Professor Nuno Dourado for his interest and help provided during an early stage of this work. I also want to express my gratitude to Professor Bahman, Doctor Nuno Mendes, Doctor Rui Silva, and Doctor João Pereira for their interest and support during these years.

Thanks, indeed, to my closest friends for their care and motivation. Thank you Luís M., Bruno, Julien, André, João, Diogo, Hugo, Natália, Rita, Patrícia, Andreia, Tiago, Beatriz, Nuno, Hilário, Rui, and Ricardo. I will be always grateful for your friendship.

I also want to thank my fellow friends from the ISISE research group in UMinho. We shared a lot of good moments together, laughs, talks, discussions and football matches. Thank you Chandan, João A., Joana, Leonardo, Susana, Alberto, Javier, Angelo, Maria Pia, Giorgos, Carlos, Chrysl, Federica, Filipe, Simone, Marilú, and João. Since this work was partially developed at the Technical University of Milan (Italy), I had also the opportunity to make good friends from the ABC department. A special word goes to Nicola, Simone T., Ana, Rafael and Gabriele for all the moments we shared, the *apperitivvi*, and the fruitful discussions.

I would like to dedicate this thesis to my family. It is hard to describe how grateful I am for having you in my life. Your continuous love, friendship and support give me the daily joy and strength I need. In particular, to my beloved parents: João Silva & Ana Luísa; to my beloved half: my twin sister, Ana; to my dear grandmother, Palmira; to the memory of my grandfather who will be always in my heart: João António; to Ricardo and to the newborn João and his contagious happy smile.

Lastly, I would like to acknowledge the financial support provided by the Portuguese Foundation for Science and Technology (FCT) through the individual Ph.D. scholarship SFRH/BD/95086/2013.

STATEMENT OF INTEGRITY

I hereby declare having conducted this academic work with integrity. I confirm that I have not used plagiarism or any form of undue use of information or falsification of results along the process leading to its elaboration.

I further declare that I have fully acknowledged the Code of Ethical Conduct of the University of Minho.

Universidade do Minho,

Signature:

Resumo

Uma estratégia multi-escala baseada em homogeneização computacional é apresentada para a análise não linear material de estruturas de alvenaria simples para os regimes estático e dinâmico de ações. Duas escalas, meso e macro, são consideradas na análise. O modelo tem a capacidade de incorporar potenciais incertezas do sistema estrutural, recorrendo ao método de amostragem por hipercubo latino, com o objetivo de desenvolver análises de fragilidade sísmica.

À mesoescala (nível dos componentes), dois modelos computacionais simples e eficazes de homogeneização são apresentados para realizar a caracterização do comportamento de um elemento representativo de volume (RVE) da alvenaria. Os meso-modelos utilizam elementos finitos (EFs) contínuos de placa e casca (teorias de Kirchhoff-Love e Mindlin-Reissner). Uma técnica de homogeneização periódica de primeira ordem com recurso a tensões de Cauchy é assumida. As unidades de alvenaria são modeladas com EFs quadriláteros lineares com um comportamento elástico. As juntas de argamassa são modeladas com EFs de interface de espessura nula com um comportamento inelástico. O domínio plástico das juntas é governado por um modelo multi-superfície que consegue reproduzir fratura por tração, esmagamento por compressão e deslizamento com atrito. É possível, assim, a previsão de modos de colapso de alvenaria designados por *stepped*, *toothed* ou *de-bonding*.

À macroescala (nível da estrutura), a informação proveniente da caracterização mecânica da alvenaria à escala anterior é inserida num modelo discreto de EFs. EFs quadriláteros rígidos encontram-se ligados por interfaces, que representam a informação do material fictício homogeneizado através de um modelo de plasticidade com dano. Uma representação desacoplada entre os modos de deformação no plano e para fora-do-plano é assumida. As referidas interfaces reproduzem os regimes de pré- e pós-pico do material, a sua ortotropia, o efeito da velocidade de deformação e, dependendo do modelo usado à mesoescala, os efeitos tridimensionais de corte. A estratégia é implementada num software avançado de análise estrutural e, portanto, ferramentas numéricas poderosas estão disponíveis; como o a*rc-length*, *line–search* e métodos implícitos e explícitos para resolução do sistema de equações.

A estratégia numérica é aplicada num conjunto representativo de casos de estudo. Os resultados demonstram que esta é: fiável na previsão do comportamento estático e dinâmico para fora-do-plano de estruturas de alvenaria; numericamente robusta; atrativa do ponto de vista do tempo de processamento, quando comparada às estratégias tradicionais de EFs; e apropriada para o estudo da fragilidade sísmica de estruturas de alvenaria simples.

Palavras-chave: Alvenaria, fora-do-plano, hipercubo latino, Homogeneização, multi-escala.

(vacate page)

Abstract

A two-step numerical strategy using homogenization is proposed for the nonlinear analysis of Unreinforced masonry (URM) structures for both static and dynamic regimes. It comprises two-scales of analysis, i.e. the meso and the macro. It is suitable to account with the structural system uncertainties' by making use of a Latin Hypercube Sampling method aiming the development of a seismic fragility assessment study.

At a meso-scale (level of components) two simple and reliable homogenized models are presented for the characterization of the masonry behavior via a representative volume element (RVE) defined at the structural level. A finite element (FE) meso-modelling approach within plate formulation assumptions (Kirchhoff-Love and Mindlin-Reissner theory) using Cauchy continuum hypotheses and a first-order periodic homogenization technique is adopted. Brick units are considered elastic and modelled through quadrilateral FEs with linear interpolation. Mortar joints are assumed to be inelastic and reduced to zero-thickness interface FEs. A multi-surface plasticity model governs the strength envelope of mortar joints. It can reproduce fracture, frictional slip and crushing along the interface elements, hence making possible the prediction of a stepped, toothed or de-bonding failure pattern of masonry.

At a macro-scale (structural level), the material and mechanical characterization of the masonry deduced from the mesoscopic model is employed via a discrete finite element strategy. On homogenized interfaces, between adjoining quadrilateral rigid FEs, a model governed by uncoupled in- and out-of-plane behaviors with damage and plasticity is adopted. Such homogenized interfaces can represent the material pre- and post-peak regimes, the material orthotropy, the material load rate-dependency, and depending on the resulting data from the used meso-model account by three-dimensional shear effects. It is implemented in an advanced structural analysis software and, therefore, it is possible to use powerful built-in features such as the arc-length method, line-search algorithm and implicit or explicit solver schemes within a wide range of applications.

The application of the numerical framework covers a representative repertoire of case studies. These demonstrated that the approach can reproduce with good accuracy the out-of-plane static and dynamic behavior of masonry structures. It proved to be robust, computationally attractive when compared with traditional FE strategies, and suitable to be used in seismic fragility studies of URM structures.

Keywords: Homogenization, Latin Hypercube Sampling, Masonry, multi-scale, out-of-plane.

(vacate page)

Table of Contents

(vacate page)

List of Figures

(vacate page)

List of Tables

(vacate page)

Chapter 1

1 Introduction

1.1 Unreinforced masonry (URM) structures

Masonry is an ancient but still widely used material (M. Tomaževič 1999). Its usage has been mainly fostered by the simplicity of this type of construction, where masonry units are laid together with or without the use of bonding mortar. Features such as its durability, aesthetics, low maintenance, adaptability, good sound and thermal insulation properties (Hendry 2001) are also important allowing masonry to continuously find application.

Unreinforced masonry (URM) buildings are a relevant part of the worldwide building stock. These include stone, brick, adobe or earthen masonry structures and represent in countries such as Mexico, Pakistan and Peru, more than 75% over its total buildings' inventory. In other countries as Iran, Australia, Indonesia or Italy, the relative percentage is higher than 50% (Frankie et al. 2013). A similar trend is found for the case of Portugal, with a value ranging the 50% according to the Portuguese Census of Population and housing. Note that the latter is expectable to be higher in urban historical centers (M. Tomaževič 1999), as stated by Cóias e Silva (2001) for Lisbon (the capital of Portugal). By being spread in urban historical centers, URM structures can have an important economical and societal role, being still used for commercial, services or housing purposes. Besides its functional character, these buildings tend to aggregate an intrinsic historic and cultural value (M. Tomaževič 2010) and hence symbolically be part of a societal identity.

The widespread of most of this built heritage has been achieved based on empirical knowledge passed by generation to generation and, therefore, URM structural behavior was often ill-understood. These constructions have been typically made to withstand vertical loads only being rather vulnerable to horizontal load actions. To carry out maintenance and strengthening measures over this type of buildings is of prime importance, especially evident in seismic prone areas where the need to reduce the probability of a potential collapse and associated consequences is a priority.

1.2 Seismic vulnerability of URM structures

Natural events had caused a considerable number of disasters in the last decades. The World Bank (IEG 2007) reported that the number of disasters increased, between 1975 and 2005, from an approximated number of 100 to more than 400 events.

In this scope, earthquakes are one of the most serious threats and challenges to humankind, since these represent almost 60% of all the natural disasters fatalities according with the International Disaster Database (2009). If the current trend continues it is predictable that global fatalities caused by earthquakes will augment, at the current century, to a value of 2.57±0.64 million (Holzer and Savage 2013). These inevitably leads to economic impacts (Noy 2009) but mainly to human losses. The World Bank (IEG 2007) have also identified the rise of population as a key issue. The phenomena of urbanization may endanger the situation because urban areas increase their population by a rate of 67 million people per year, being expected that 60% of the estimated global population will live in urban areas by the end of 2030 (Pickett et al. 2011); the consequence is the creation of the so-called 'megacities', which are prone to higher casualties. These issues had been addressed in the last decades by Degg (1992) and Parker and Tapsell (1995).

The report released in 2014 by the United Nations (U.N. 2014) strongly connects human development with both the populations' vulnerability and buildings' resilience to the occurrence of natural and human-induced disasters. This approach explicitly advocates the priority role of a vulnerability assessment in the risk mitigation. As stated by Calvi et al. (2006), the prediction of both the economic impact and seismic risk can be, for a given region, tackled by an earthquake loss model. Therefore, making a logical extension, a vulnerability study towards a buildings' capacity assessment is fundamental for an earthquake loss model and is, as important, as the model itself. Vulnerability studies play a key role for authorities, decision makers, stakeholders (e.g. insurance companies) and to the community itself. On one hand, these studies could minimize future economic impacts and reduce human losses; and, on the other hand, these studies could help to prevent the collapse of cultural heritage buildings.

Existing URM buildings are known to be vulnerable to collapse when subjected to a seismic action. These generally have a low strength/mass ratio which, in cases where a dynamic horizontal load is applied, makes hard to withstand the inertial forces due to the reduced strength. The poor out-of-plane capacity, which is directly associated with the low tensile strength of URM, can be a limitation of these construction type. Other reasons can explain the vulnerability as: (i) the lack of capacity to dissipate the kinetic energy transmitted by the earthquake; (ii) the lack of proper connections between structural elements which hinders the so-called box-behavior (Bruneau 1994); (iii) the flexibility of the floors; and (iv) the deterioration of materials over time (Cardoso et al. 2005). The above reasons explain why URM structures are especially prone to experience out-of-plane failure modes (Griffith and Magenes 2003) as several post-earthquakes damage surveys by Kaplan et al. (2010); D'Ayala and Paganoni (2010); Dizhur et al. (2011); Silva (2013); Sorrentino et al. (2013)

have reported. The excessive earthquake vulnerability can be controlled through strengthening actions whose viability and adequacy can be assessed, at least in theory, if a proper structural assessment is carried out beforehand.

1.3 Research scope and focus

The former section addressed the importance of carrying out urgent measures in the URM built stock. Yet, intervening in these constructions is a complex process, as stated by Lourenço (2002), due to the lack of structural information and due to their high importance. A scientifically based process is less susceptible to inadequate actions and thus, in order to avoid damaging measures, the adopted methodology should be incremental, including studies such as an historical literature review, inspections, monitoring actions, and structural analysis (Croci 1998; Binda et al. 2000). In this way, an intervention should be carried out after a careful diagnosis and evaluation of the safety of the structure in its present state, as defined by the ICOMOS recommendations (2005), where the numerical modelling is a valuable contribution.

In the scope of the structural analysis of the URM structures behavior, the prevailing design rules or the analytical approaches still are, within engineering practice, the most useful. These pose, however, several well-identified limitations that may lead to potential unrealistic or conservative results (Theodossopoulos and Sinha 2013). Other simplified procedures, as the story-mechanism (M. Tomaževič 1999) and the equivalent frame-based models (Lagomarsino et al. 2013; Quagliarini et al. 2017) can also be found in the literature but hardly consider the out-of-plane failure modes, which are disregarded in most study cases. More suitable and yet conceptually simple procedures as the rigid-body approaches (Konstantinidis and Makris 2007; D'Ayala and Shi 2011) or the well disseminated kinematic methods (Griffith and Magenes 2003; D'Ayala and Speranza 2003; Calvi et al. 2006) are useful to provide closed form solutions under dynamic excitations but are very complex for walls subjected to two-way bending.

More advanced computational strategies have been developed in the last twenty years. Conversely to concrete and steel structures, the design guidelines for masonry did not go always hand in hand with the application of innovative methods. Still, it is nowadays well accepted that sophisticated strategies, mainly based on the finite element (FE) method, constitute important tools (Lourenço 2002) and are the ones which deserve more attention from the scientific community, where three main modelling strategies can be put together, namely: (i) the direct simulation or the meso-modelling; (ii) the macro-modelling simulation; and (iii) the multi-scale computational simulation.

In the meso-modelling approach, both masonry components (units and mortar joints) are explicitly represented. These are certainly capable of well reproducing both in- and out-of-plane orthotropic nonlinear behavior of masonry but are characterized by long processing times, being only recommended for limited size structural problems (Lotfi and Shing 1994; Giambanco et al. 2001; Lemos 2007; Sejnoha et al. 2008; Adam et al. 2010; Macorini and Izzuddin 2011, 2013; Sarhosis et al. 2014). The macro-modelling strategies smear out the heterogeneous assemblage of mortar and bricks into a fictitious homogeneous anisotropic material. The use of closed-form laws to represent the complex phenomenological behavior and damage of the masonry may be cumbersome and require a calibration step (usually achieved by thorough experimental campaigns). However, this approach allows studying large-scale structures without the drawbacks exhibited by meso-modelling (Dhanasekar et al. 1985; Lourenço et al. 1997; Berto et al. 2002; Roca et al. 2013).

Multi-scale FE (or FE^2) methods are in-between the latter two FE modelling schemes. The framework is being used to investigate the response of composites with different natures, see Kouznetsova et al. (2001) and Spahn et al. (2014), but is also useful for the study of masonry structures. It typically relies on a meso and macro transition of information and is, therefore, designated as two-scale or FE^2 approaches. Full continuum based FE^2 approaches result in a good compromise between solution accuracy and computational cost. Nevertheless, these methods still constitute a challenge if one desires to account for the material non-linearity (Geers et al. 2010; Otero et al. 2015), hence are seldom used for dynamic purposes.

The last scientific community effort over the set of advanced FE numerical approaches highlights the gap which remains unsolved in multi-scale strategies. Such strategies constitute a promising alternative between the meso- and macro- FE strategies, but the classical FE^2 relies on a continuum description of the material at both scales, which can be hardly applied in the dynamic assessment study of URM structures due to the involved computational costs. A FE^2 strategy which can reproduce the orthotropy and full non-linearity of the masonry is a valuable tool, especially when facing a low computational demand. Such strategy can be used for the out-of-plane assessment of masonry walls due to horizontal actions, such as earthquake loading and, furthermore, to carry seismic vulnerability assessment by developing vulnerability or fragility functions on a URM case study (or building typology).

1.4 Objectives

This dissertation addresses the analysis of URM structures using a two-scale FE^2 strategy based on homogenization principles. The main scope is the study of the quasi-static and dynamic

mechanical behavior and failure of masonry. A focus on the out-of-plane behavior is especially stressed, since less research has been conducted when compared to the in-plane case. The methodology is developed to permit a broader application, as the use within the framework of a seismic vulnerability assessment of URM structures.

The key reason for developing such strategy originates from the computational burden of the existing continuous FE^2 methods. It is known that the use of advanced computational tools is of unequivocal importance and can be ensured, in the scope of conventional design or in large-scale structures assessment, only if time and costs are maintained as relatively low. Therefore, the objectives of this study are:

- To discuss the existing methodologies for the structural analysis of masonry structures and prove the adequacy of two-scale strategies;
- To develop a strategy at a meso-scale, within a homogenization scheme, able to account for the masonry orthotropy and softening, and to be able to reproduce the tensile, shear and compression failure modes;
- To develop a simplified discrete macro-model, based on a Rigid Body Spring Mass (RBSM) model, able to receive the homogenization material data obtained at a foregoing scale;
- To incorporate both levels within a simplified FE^2 approach and conduct its validation using experimental and numerical data available in the literature;
- To apply the simplified FE^2 approach to undertake a probabilistic-based study aiming at the derivation of seismic fragility functions, which are of prime importance in earthquake loss models.

It is noteworthy to address that the methodology is implemented within a commercial FE software. The goal is to allow the dissemination of its use by academia and professional peers. The versatility of the strategy may be also pointed out as, depending on the model used in the homogenization process (at a meso-level), allows different materials to be studied apart from masonry - following the trend of the homogenized-based methods application, i.e. oriented for composite materials in general.

1.5 Thesis outline

The thesis introduces a numerical two-scale approach for the prediction of the masonry response, its validation and application within a seismic fragility assessment of an URM structure. These tasks are presented throughout the seven chapters of the document, as represented by the flowchart of Figure 1.1. The structure of each chapter is alike, except for

the Chapters 1 and 7, and includes an introductory note preceding the body of the text and closes with a brief summary. The content of each chapter is described next:

In 'Chapter 1 - *Introduction*', the motivation, brief background and objectives of the research work are presented. The outline of the thesis is also addressed.

In 'Chapter 2 - *'Masonry modelling and vulnerability assessment'*, a literature review is conducted aiming to evaluate three topics. First, the scales of interest when analyzing the mechanical behavior of masonry structures. Second, the main current numerical strategies developed to predict the structural response of masonry, which undergoes from the analytical to the more advanced ones, with a focus on the out-of-plane behavior. Third, the existing numerical frameworks to assess the seismic fragility and vulnerability of URM structures.

In Chapter 3, *'Multi-scale analysis of masonry: meso-scale level'*, three numerical strategies based on homogenization concepts are presented to characterize, at a meso-scale, the in-plane and out-of-plane behavior of running-bond and English-bond masonries. The models differ on both complexity and computational time costs. A meso-scale validation on its accuracy is performed accounting with the masonry elastic properties, the masonry orthotropic features for one- and two-way bending, and the effect of potential pre-compression states. At last, the models are applied to study an English-bond masonry aiming to derive its homogenized out-of-plane quantities but, as well, to conclude on the differences between the proposed meso-scale approaches.

In Chapter 4, *'Multi-scale analysis of masonry: macro-scale level'*, a discrete FE-based strategy whose formulation relies on a rigid-body-spring-mass model is presented at a macro-scale. It is developed on an advanced FE software and able to read homogenized in-plane (stress-strain curves) and out-of-plane (moment-curvature curves) quantities aiming to predict the nonlinear static and dynamic behaviors of masonry structures. Its validation is conducted at both linear and nonlinear ranges and the main computational features stated.

In Chapter 5, *'Multi-scale out-of-plane static and dynamic analysis of masonry: applications'*, the proposed two-scale strategy is applied for the study of the nonlinear behavior of masonry structures. A set of case studies is selected to assess the capability of the strategy within both static and dynamic (seismic load and impact load) ranges. The obtained results are compared with existing experimental and numerical data in terms of predicted displacements and damage maps. A mesh dependency study is also conducted and the computational time costs evaluated.

In Chapter 6, *'Seismic fragility assessment of an URM structure'*, the proposed deterministic two-scale strategy is extended to account with the probabilistic (viz. uncertainty) nature of

masonry. A full parametrization of the material, mechanical and geometrical variables is ensured and the resulting stochastic model integrated within a performance-based methodology. The presented framework is applied to assess the seismic fragility of a masonry structure through fragility functions for different performance limit states.

In Chapter 7, *'General summary and conclusions'*, the general summary, main conclusions and recommendations of the research study are referred together with the presentation of further developments and works.

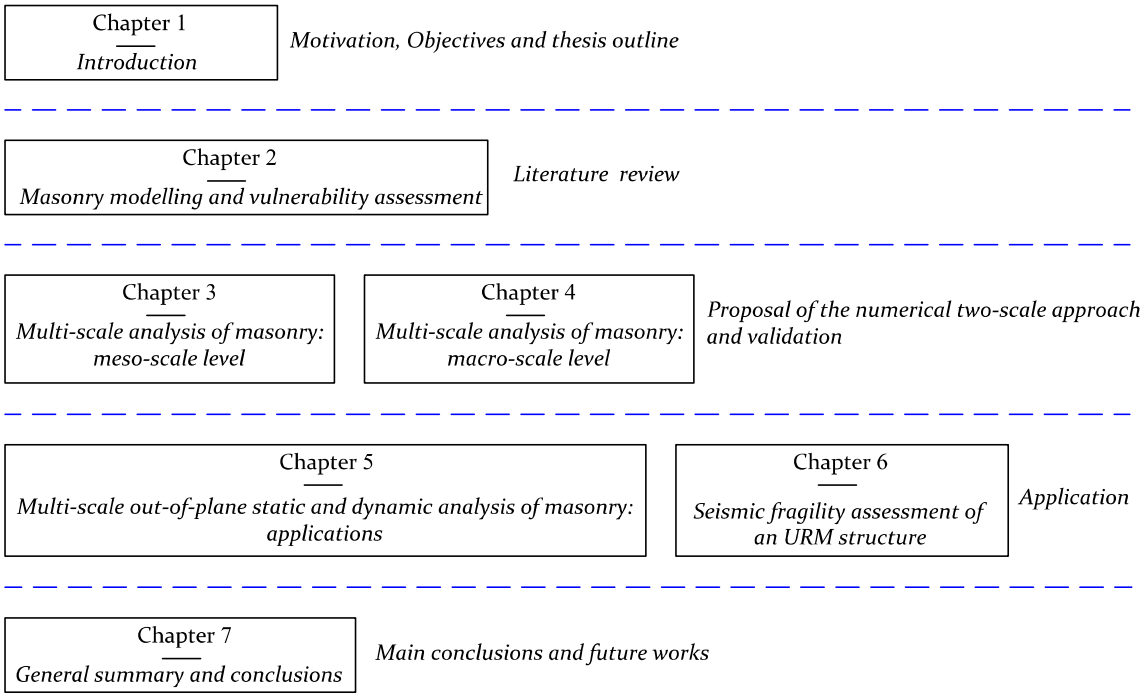

Figure 1.1 – Flowchart of the thesis outline.

(vacate page)

Chapter 2

2 Masonry modelling and vulnerability assessment

2.1 Scales of interest for masonry structures

Natural or manufactured heterogeneous materials with a random or periodic arrangement, such as composites made of material matrices with embedded inclusions (e.g. metal alloys, polymeric, ceramic or porous composites) or granular materials (e.g. masonry or concrete) may have several analysis' scales of interest (Mosby and Matouš 2015). The physical behavior of these materials is hard to predict, since it is highly dependent on the volume, shape and spatial distribution of the heterogeneities. In fact, since the pioneer investigation by Griffith (1921) where the molecular role on the material failure and the importance of the surface energy on the material strength have been addressed, topics such as material fracture and strength still constitute standing research issues due to the inherent complexity. Nowadays, the breakage of the intermolecular links (van-der-Waals forces) is widely accepted to explain the occurrence of the material failure and the following formation of a representative damage zone, see Berry (1961), DelRio et al. (2005) and Novoselov et al. (2016), generally defined through a crack-band or crack-characteristic length, hereafter referred as l_{crack}.

On one hand, the knowledge of the l_{crack} localization is, for a given material and for a given problem, important because it defines the required scale-level of analysis to properly understand the phenomenon. Experimentally measuring such l_{crack} is hard as it demands sophisticated equipment and, therefore, theoretical approaches are gaining an increasing relevance. The theoretical study by Volokh is a good case, where by relating the volumetric and surface fracture energies, the characteristic failure crack length has been obtained, e.g. $l_{crack} \sim 10$ μm for steel (Volokh 2012), $l_{crack} \sim 10^2$ μm for natural rubber (Volokh 2011) and $l_{crack} \sim 10^4$ μm for concrete (Volokh 2013). On the other hand, the material modelling at these scales is a thorough process and may be unfeasible from a structural engineering standpoint. In this scope and particularly for the masonry field, it is recognizable that two scale levels are of interest when analyzing its structural behavior (Lourenço 2009; Roca et al. 2010): the macro- and the meso-scale (see Figure 2.1). Micro-scale modelling, with an order of millimeter, is generally accounted only for non-structural problems (Geers et al. 2010), such as transport mechanism (thermal or moisture) or chemical action cases (Wu et al. 2016).

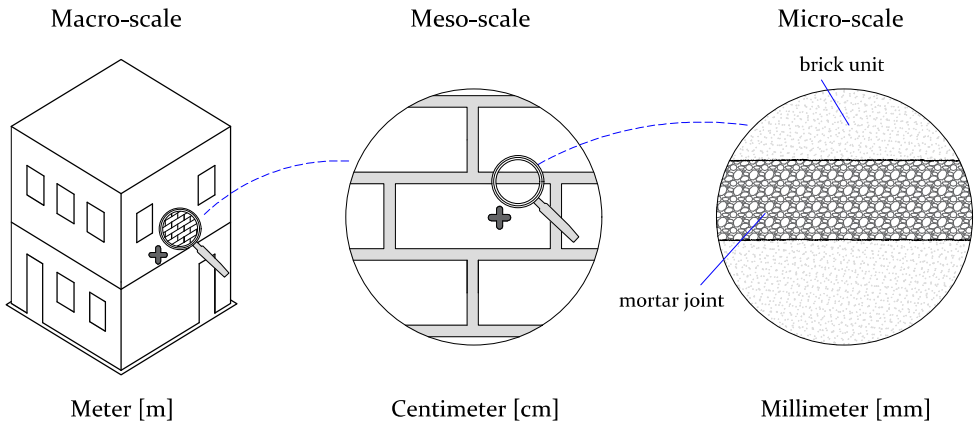

Figure 2.1 – Representation of the three scales considered for the study of the masonry: macro-scale, meso-scale and micro-scale.

The finer scale adopted in the literature for the structural analysis of masonry is designated hereafter as meso-scale. Mesoscopic[1] models discretize the media at a components level, in the order of centimeters, and seem to offer an accurate prediction of the masonry behavior (Lourenço 2002). Brick units and mortar joints are explicitly modelled being the stress and strain quantities representative of the analysis scale. This allows to easily embody masonry heterogeneity (anisotropy feature) and better track both the damage evolution and the damaged-induced anisotropy effect. As stated before, mesoscopic models demand a larger set of material parameters and are suitable only for small structures.

The coarser scale used for the study of the masonry behavior is designated as macro-level (order of meters), where the geometrical features of the structure are accounted. The study of structures with larger dimensions may allow the representation of the material using a broader domain that, in some cases, can be enough to catch the phenomenological features of interest. The underlying assumption is that the interaction between brick units and mortar joints can be neglected for the global structural behavior, and hence are valid if the difference between the macro- and meso-scales is sufficiently large; it is usually referred that a ratio smaller than 10 to 100 is questionable for periodic masonry (Mistler et al. 2007). The heterogenous masonry media is then replaced by an equivalent homogeneous material where stress and strain variables are taken as average quantities. This requires complex phenomenological formulations to reproduce material orthotropy and follow the damage onset and propagation. In this endeavor, the FE-based macroscopic strategies are the most spread in the literature where two frameworks

[1] From a structural standpoint, only two-scales are of interest in the study of the masonry behavior. Thus, some authors (see Lourenço (2002)) may use the designation of macroscopic and microscopic models. To avoid the readers' confusion, it is herein stressed that microscopic and mesoscopic models are, in the field of masonry structural analysis, equivalent.

have arisen to catch failure, i.e. using a discontinuity where cracks are explicitly modelled using the so-called cohesive zones (Barenblatt 1959; Xu and Needleman 1994; Belytschko et al. 2001) or in a continuous way using smeared-cracking models (De Borst 1987; Lourenço et al. 1997; de Borst 2002). The damage representation may lack detail at the crack level, but it is known that these numerical models are still adequate for the study of concrete, concrete-like and masonry materials at a structural level. The riddle is thus the definition of the most suitable modelling approach, according to the dimension and purpose of the study, bearing in mind that a trade-off between accuracy and practicability (also in terms of computational time) is present.

2.2 Modelling strategies: out-of-plane analysis of masonry

Several modelling strategies exist and are eligible to be used in the analysis of URM structures. A critical review, with a closer look on the out-of-plane (OOP) behavior, is presented next. Given the different theoretical backgrounds and varying complexity levels, the modelling approaches are grouped in two sections, namely analytical and advanced methods. The main advantages and drawbacks of each approach are addressed to sustain its capabilities and enforce the potential scope of application. Acknowledging the advantages and disadvantages of the modelling techniques available in the literature is of utmost importance. If the sentence by Box and Norman (1987) is extended for the problem of URM structures analysis, i.e. *'essentially all models are wrong, but some are useful'*, the latter is easily postulated. This highlights potential existing gaps aiming to develop innovative research, but it also raises awareness of practitioners over the most adequate strategy for the problem at hand.

2.2.1 Analytical methods

Analytical models are divided according to its underlying formulation, i.e. force-based approach (FBA) or displacement-based approach (DBA), as in Ferreira et al. (2014) and Sorrentino et al. (2017). Throughout this section, a general overview on the analytical models, recalled as graphical, limit analysis-based (static and kinematic theorems), flexural or rigid body methods, is addressed.

Force-Based Approach (FBA)

The first studies on the equilibrium concept by Stevin (1586) in the 16th century, where the parallelogram rule has been described graphically through force vectors (see Figure 2.2), fostered the start of equilibrium analysis and the advent of rational force-based approaches (FBA). Robert Hooke published in 1675 the principle of the inverted catenary, followed by the

development of the graphical catenary-based methods by Rankine in the 18th century and Moseley in 1833 (see Benvenuto (1991)).

Graphical approaches have been largely applied for the stability verification of vaults, arches and buttresses. Software based on such formulation has been developed, e.g. by Greenwold et al. (2003) and later enhanced by Block et al. (2006). Yet, by disregarding the possibility of local failures to occur, as local crushing, cracking and sliding effects, these tend to overestimate the structural capacity and may lead to non-conservative results. Graphical methods appear to have become outdated, since more accurate strategies are being developed – intrinsic consequence of the progressive improvement and capacity of computer technology (Lourenço 2002). Also, the OOP behavior of URM structures has been somehow disregarded (Lourenço 2008), even if its importance was firstly documented two centuries ago by Rondelet (1802). This author recalled the interest of studying the behavior of masonry walls when subjected to horizontal loads, underlying the importance of the stability role rather than strength. FBA have thus been developed through the introduction of the limit analysis theory, viz. static methods and kinematic methods. Limit analysis based on a rigid-body behavior allows the determination of the collapse load factor which activates a given failure mechanism. An FBA is within this theoretical frame of reference of application, meaning that the latter load factor can be achieved using the virtual work principle.

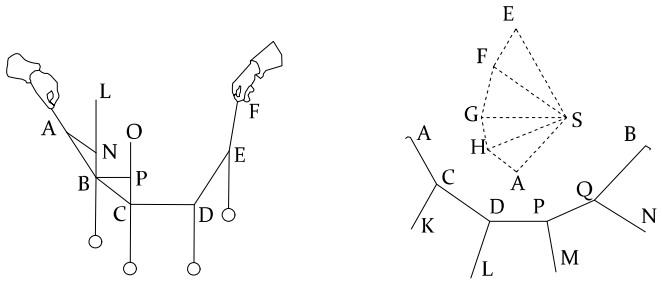

(a) (b)

Figure 2.2 – Drawings by: (a) Stevin (1586) concerning the force equilibrium of hanging weights on a string in 1586; (b) Varignon (1725) concerning the analysis of a funicular shape in 1725.

Drucker et al. (1952) were among the first authors proposing and developing the limit analysis theory in the 1950's for standard elastic-perfectly plastic three-dimensional continua. Afterwards, the relation between limit analysis and thrust lines has been introduced by Kooharian (1952). The latter led to the field of static approaches based on thrust lines and to limit state theories for masonry structures analysis (Heyman 1966). Yet, the use of thrust-line methods for the analysis of historical construction is difficult to apply; in opposition, the works of Heyman (1966) on kinematic limit analysis have been largely applied. This author accounted

for some simplifications, such as: the non-tensile masonry strength, infinite compressive strength and non-occurrence of sliding between elements.

After Heyman, other authors presented FBAs for the analysis of failure mechanisms. Giuffrè (1990) introduced the concept of analyzing each possible failure mechanism for historic masonry structures according with the mechanism features, i.e. geometry and boundary conditions. The lack of proper connections between the different structural parts of an existing URM building promote the use of such assumptions. The related drawback is its individual character, which means that an analytical formulation must be derived for each possible failure mechanism and for the associated loading and geometric conditions. Still, a limit analysis based formulation, where sub-structures are defined as macro-elements, has been extended by Giuffrè and Carocci (1993) for the seismic vulnerability study of masonry buildings. Inspired by such contribution, several authors have extended its application and developed ad-hoc expressions for other different OOP failure cases. For instance, Hobbs et al. (1994) analyzed the OOP failure of masonry walls subjected to a point load (case of an impact); and Felice and Giannini (2001) accounted for the existence of transversal walls' connections to study the OOP seismic vulnerability of URM walls.

A well-known and detailed work has been presented by D'Ayala and Speranza (2003). A set of twelve typical collapse-failure mechanisms for existing or vernacular URM buildings, see Figure 2.3, have been presented.

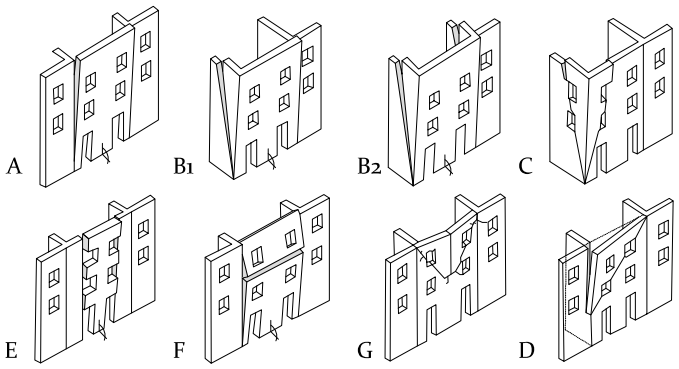

Figure 2.3 – Kinematic out-of-plane failure mechanisms collected for URM buildings (adapted from by D'Ayala and Speranza (2002)).

For each failure, a simple algebraic formula is given to obtain the limit horizontal load factor, i.e. the horizontal force that corresponds to the equilibrium limit of the geometric configuration. The analytical model accounts for connections, loading and restraint effect of horizontal structures (as the existence of ties or ring beams). It is also relevant to note the works by Casapulla (2008) and Casapulla et al. (2014), in which the work of

D'Ayala and Speranza (2003) has been considered but accounting with the friction effect (Coulomb friction).

Likewise, Restrepo-Vélez (2004) presented an analytical mechanics-based procedure for the seismic risk assessment of URM structures at a territorial scale following the works from D'Ayala and Speranza (2003). New analytical equations have been derived, through experimental data of dry-stone specimens, to calculate the collapse load multiplier of OOP mechanisms. The considered mechanisms are more complex than the preceding study and, at least for this case, the authors concluded that friction has a negligible role. A relatively recent and promising work has been presented by Milani and Tralli (2011) within an upper-bound theory. Under homogenization concepts, considering full nonlinearity on mortar joints and an associated flow rule, the behavior of two-way bending masonry walls has been studied. The authors were able to target with a good approximation both the experimental structural capacity and softening behavior.

The OOP study of URM structures through a set of homogeneous macro-elements is, from a computational point of view, very attractive. This strategy is very simple and can replace more complex numerical analysis. Several computational tools are being developed for this purpose. For instance, the software Block by Orduña (2004) (see Figure 2.4) where bi- and tri-dimensional limit analysis can be performed in a CAD-oriented environment. Its reliability is, however, only assured in the range of small displacements and rotations. In general, kinematic approaches are very practical and effective requiring the information of very few material parameters, which is important in the case of historical masonry structures due to the difficulty of their determination (Orduña 2003).

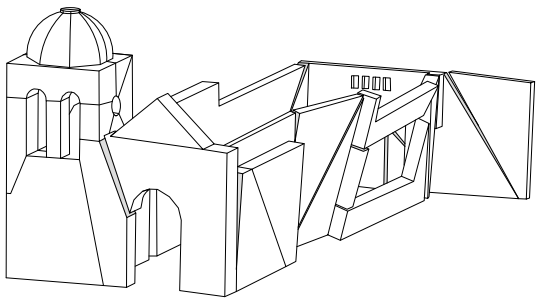

Figure 2.4 – Block software applied for the analysis of the transversal failure mechanisms of an URM Chapel (adapted from Orduña and Preciado (2008)).

Models based on the rocking of monolithic walls, i.e. macro-block approaches, can allow good estimations of the collapse load factor, as seen in Orduña and Lourenço (2005), Gilbert et al. (2006), and de Felice (2011). Still, the main drawbacks of these strategies are

threefold: (i) need to know the possible collapse mechanisms beforehand, because failure interfaces have to be defined; (ii) an expert-based decision is required to place numerical interfaces, since these may be properly aligned to represent potential and representative failure mechanisms; and (iii) a non-conservative solution may be found once the failures modes are incorrectly defined.

Displacement-based Approach (DBA)

Although force-based approaches (FBA) are often used for the analysis of URM structures, as these are naturally associated to have a low ductility degree, a displacement-based approach (DBA) may be a better choice in a seismic study context. On one hand, a DBA is more representative in the OOP study of traditional masonry elements, because such behavior is more related to velocity (energy-based) or displacement demand, rather than acceleration (i.e. force-based). It is also known that the maximum obtained displacements are a key feature in the overall structural stability (Abrams et al. 1996), so a DBA is also more suitable for ultimate limit cases. On the other hand, DBA approaches are generally associated with a flexural or rigid-body motion, easily handled by a single- and multi-degree-of-freedom (hereafter SDOF and MDOF, respectively) system. The extension to the dynamic field is paramount, since static approaches preclude important response phenomena. URM structures can usually resist forces higher than their quasi-static capacity, i.e. the concept of dynamic stability applies (Bruneau 1994; Doherty et al. 2002).

Doherty et al. (2002) presented a simplified linearized DBA, where a tri-linear force-displacement relationship to characterize the OOP behavior of masonry walls has been defined, see Figure 2.5a. The authors used the so-called '*substitute structure'* methodology introduced by Shibata and Sozen (1976), which allows to simplify the problem of representing nonlinear systems in a DBA framework. The effective secant stiffness for the URM system is obtained as illustrated in Figure 2.5b, through the defined limit displacements relationship. The displacement parameters values' Δ_1, Δ_2, Δ_3 (see Figure 2.5) are associated with the material properties and mortar joints degradation (Doherty et al. 2002). These were obtained after an experimental campaign of fourteen simply supported walls, relating each limit displacement Δ_1, Δ_2, Δ_3 as 'new', 'moderate' or 'severely' degraded state, respectively (Doherty et al. 2002).

Griffith and Magenes (2003) performed several analyses using the same trilinear force-displacement relationship approach and made important remarks. The lateral static strength and ultimate displacement of an URM wall out-of-plane loaded could be idealized as a SDOF system and are mainly dependent on its geometry, boundary conditions and pre-compression

state. Conversely, the initial stiffness and compressive strength of masonry have a lower relative importance. More recently, Derakhshan et al. (2011) performed a sensitivity study upon the procedure from Doherty et al. (2002). The results showed that the latter model overestimates both the wall instability displacement and lateral capacity. This approach is still a good alternative to the quasi-static force-based procedures, since it is a straightforward method able to predict the dynamic behavior of URM walls. However, as referred by Doherty et al. (2002), the determination of the limit states displacement is highly subjective and should rely on an extensive experimental campaign which can be a major drawback.

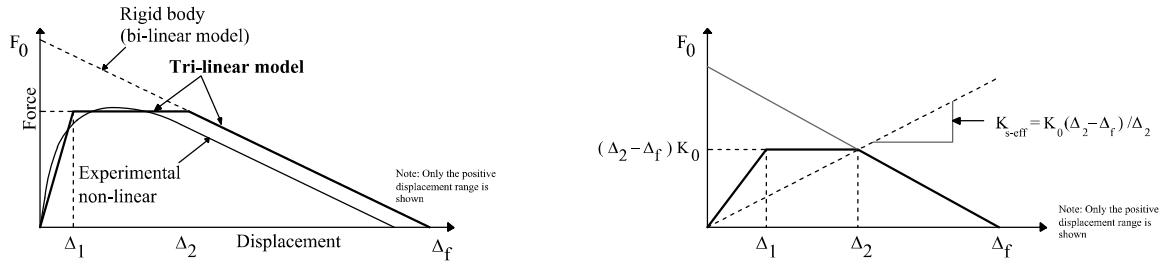

Figure 2.5 – Description defined by Doherty et al. (2002) of: (a) Simplified tri-linear force vs. displacement curve; (b) Effective secant stiffness $K_{s\text{-}eff}$ definition for semi-rigid walls.

Lagomarsino (2014) proposed a new procedure concerning the seismic rocking of masonry structures. The results from rigorous and approximate procedures have been compared. The former models account with the nonlinear dynamic response of rigid blocks and the latter models may be adopted in more complex study cases. Hence, an extensive range of masonry structures was covered, between rocky structures (archaeological remains, obelisks, columns, trilithons), arch-piers systems (e.g. triumphal arches, belfries), out-of-plane mechanisms of walls (standing out walls, façades in buildings or churches etc.) or artistic assets prone to overturn (pinnacles, statues etc.). The performance assessment by Lagomarsino (2014) upon this set of masonry structures was accomplish through a DBA following an incremental limit analysis. The incremental limit analysis allowed to obtain the capacity curve for several configurations of the model, allowing to consider the effect of geometric nonlinearity. Also, four levels of damage have been defined.

A common approach to study the masonry OOP behavior of walls is through a DBA using rigid body motion models, since masonry structures tend to behave as rigid parts subject to rocking. Based on such experimental evidence, SDOF models dealing with the free rocking motion of monolithic walls have been proposed in the recent past, following the pioneering idea by Housner (1963), see Figure 2.6a. Housner (1963) presented the behavior of a rigid block

under a constant horizontal acceleration, under a single sine pulse and under an earthquake type excitation. Several conclusions were put forth, as the existence of a *scale effect* and *loading type influence*. The former explains why geometrically larger blocks are more stable than smaller ones with the same geometrical ratio, due to the higher proportion of energy that is dissipated on impact. The author addressed, through observation, that a slender block is more stable under a random earthquake excitation than under a constant acceleration excitation; and that successive smaller pulses cause more damage than a larger one. These conclusions are somehow related with the concept of dynamic stability.

An important precursor study was Yim et al. (1980). The authors developed a computer program to describe the nonlinear motion of a rigid block on a base under both horizontal and vertical ground motions. Yim et al. (1980) stressed that the rocking response is quite sensitive to the rigid body size, slenderness ratio and to the ground motion features. Also, the block probability of exceeding a response level increases with its slenderness ratio or ground motion intensity and when its size decreases. A computer program with the same purpose was also developed by Ishiyama (1982), which noted that the rigid block motion is greatly influenced by the normal and tangent restitution coefficients. Makris and Konstantinidis (2003) compared the response of a SDOF oscillator (regular pendulum) and the rocking motion of a slender rigid body (inverted pendulum), see Figure 2.6b.

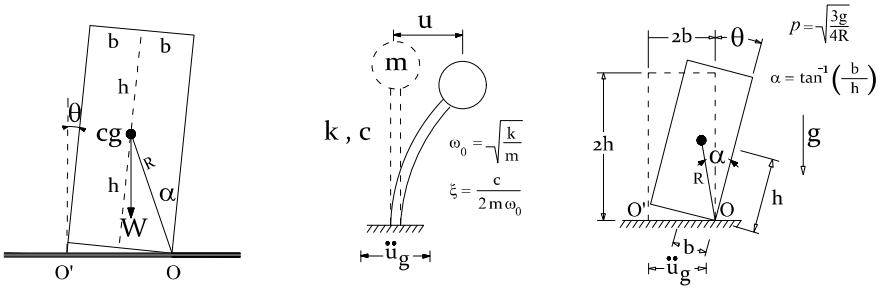

(a) (b)

Figure 2.6 – Description of: (a) Rigid block by Housner (1963); (b) Comparison between an oscillatory system and a slender rigid block response by Makris and Konstantinidis (2003).

The authors stated that the above systems are independent and different; highlighting that one should not be used to study the other. Additionally, the authors proposed a rocking spectrum to be used along with the response spectrum to be able to draw conclusions about the kinematic features of the ground motion and their effect on the response of the slender rigid block. Other important studies regarding the SDOF motion of rigid blocks in a two-dimensional Cartesian system can be named, for instance Hogan (1989), Makris and Konstantinidis (2003),

Costa et al. (2013), and Konstantinidis and Makris (2007) or Di Egidio et al. (2014) that tried to extend the concepts to a three-dimensional system. The studies from Sorrentino et al. (2008) and Shawa et al. (2012) are also noteworthy. These address the problem of real URM façades as one-sided rocking motion systems. The dynamic rocking model of the former is noteworthy, given the influence of transversal walls for geometrical imperfections, i.e. the potential out-of-plumb of the wall allows modelling the system in an asymmetric manner. In both studies, restitution coefficients have been experimentally obtained.

A deep investigation of the OOP behavior of URM structures by means of rigid-body based strategies within a multi-degree of freedom (MDOF) system is still lacking. The pioneer work by Psycharis (1990) analyzed the dynamic response of two stacked rigid blocks, in which both the blocks sliding and the uplift (rigid floor) are neglected. Psycharis (1990) outlined four possible patterns of response and impact to characterize the rocking motion of the system under vertical and horizontal ground motion, assuming a conservation of the angular momentum. Nonetheless, the approach demonstrated high complexity when assessing the rocking response, requiring the definition of equations of motions and energy dissipation for every possible mode. Based on this work, Spanos et al. (2001) extended the formulation to a more generic problem. Following the non-sliding and rigid foundation assumptions, the authors derived the nonlinear equations for each response pattern configuration. A computation tool has been developed to define the system behavior under an arbitrary base excitation.

D'Ayala and Shi (2011) developed an analytical approach to represent the OOP behavior of masonry walls through a multiple rigid body system. Three different failure patterns, based on different relative rotations between two stacked rigid blocks, have been analyzed whose nonlinear equations of motion have been programmed and solved using two commercial software's. An extensive experimental campaign data ensures the validation of the model, in terms of peak displacements, frequency and energy. Gabellieri et al. (2013) explored the effect of flexible diaphragm in the dynamic behavior of the external walls of URM historic buildings subjected to one-way bending. The walls were modelled as two rigid blocks within a 2DOF system. The main conclusion found was that the diaphragm stiffness has a strong effect on the displacement demand of the walls. It is however stated that defining a general analytical formula to predict such demand is not possible without performing dynamic analyses. Recently, Landi et al. (2015) proposed a model for the OOP simulation of slender external URM walls with flexible floors. The flexible floors are simulated through a spring element and the damping modelled by a restitution coefficient. Likewise, two degrees-of-freedom have been considered and the numerical OOP behavior validated by experimental data. The authors showed the

importance of considering the flexibility of diaphragms being the results, as expected, highly dependent on the stiffness of the spring.

The dynamic motion of SDOF rigid blocks has been widely studied. Limited research is, however, available on the response of multi-block structures, i.e. MDOF approaches. The main cause is related to the high complexity of the problem, which explains in part why most of these studies relies upon the behavior of systems with two rigid blocks only. While such studies may be useful to provide closed-form solutions under complex dynamic excitations and may fit well, in selected cases, experimental evidence, its utilization is very complex for walls subjected to two-way bending and for unknown collapse mechanisms. Furthermore, by assuming the system to move as a rigid body system, the mechanism is governed by velocity fields rather than stress fields. Accordingly, these strategies typically lead to an upper-bound or unsafe solution which can be a contentious issue.

2.2.2 Advanced numerical methods

Prevailing design rules or analytical approaches are, within engineering practice, still most useful. These pose, however, several well-identified limitations that may lead to potential unrealistic or conservative results (Theodossopoulos and Sinha 2013). A plethora of other simplified procedures, conceptually more complex, can be found in the literature. The development of these practical analysis tools has been motivated by the need of performing a nonlinear seismic structural assessment and/or proper repair interventions on URM buildings. The *story-mechanism approach* by Tomaževič (1978) is one of the first studies on the matter. It has been continuously improved and follows a 'story-mechanism' approach, i.e. each story is represented by different non-linear inter-story shear displacements (M. Tomaževič 1999). The method can simulate the shear-diagonal in-plane failure mechanisms of URM structures being governed by the masonry piers, which are idealized as elastic-plastic shear elements with limited ductility. Its conceptual simplicity and practical nature are strong points for the dissemination among practitioners, but the inability of reproducing the OOP behavior hinders its application in most of the cases.

The equivalent-frame based methods have been further developed where masonry walls are described as the assemblage of piers, spandrels and rigid nodes. Noteworthy examples are the works on the SAM (Simplified Analysis of Masonry) method by Magenes and Calvi (1997), Magenes and Della Fontana (1998), and Magenes et al. (2000), where the frame-type structure is modelled through rigid and deformable elements. Piers and spandrels are assumed to rule the structure's deformation through an elastic-plastic behavior with limited deformation. A larger

set of failures modes is accounted by the introduction of flexural or rocking failure and the possibility, even in a simplified manner, of forces redistribution after reaching the element failure threshold.

The application of the equivalent-frame method is well ensured through the development of software's, such as TREMURI (Lagomarsino et al. 2013). This software can perform nonlinear pushover and dynamic analysis of whole URM buildings when only the in-plane response is considered. Other works on the enrichment of the macro-elements, which constitute the geometric features of URM structures (such as walls, piers and spandrels), are being gradually developed. Brencich and Lagomarsino (1998) developed a three-layer macro-element that accounts for the in-plane bending and shear deformation. Employing such element within a frame-based approach can be conducted using rigid or deformable elements in-between. Furthermore, a nonlinear macro-element model has been introduced by Penna et al. (2014) to characterize, on the basis of mechanical assumptions, the bending-rocking and shear-sliding (with friction) mechanisms (and their interaction) of a whole masonry wall. In another study, Addessi et al. (2015) presented a frame model based on an enriched 2D macro-elements formulation (beam description), able to account for both stiffness and strength degradation, for the pushover study of regular masonry buildings.

The inherent simplicity of the equivalent-frame based methods make them suitable for the study of large-scale structures, due to the reduced number of degree-of-freedom involved. The material non-linearity effect of the masonry can be accounted, but these approaches suffer from a macro-element discretization-bias, demand proper strength criteria for different structural macro-elements and, more importantly, hardly consider the OOP failure modes. Besides, since they are based on the assemblage of macro-elements, the methods are particularly oriented for some classes of URM structures, i.e. with a regular openings' arrangement. For a detailed review on such methods, the reader is referred to (Quagliarini et al. 2017). In this context, the need of more general methods encouraged the development of advanced numerical methods. A brief overview on the *FE-based models* and on the *discrete element model (DEM)* is addressed next.

Finite-Element models (FEM)

Sophisticated strategies, mainly based on the finite element (FE) method, are the ones which deserve more attention from the scientific community (Lourenço 2002). FE-based methods have a broad range of application because they can be employed in complex geometric structural configurations and within static and dynamic ranges. Furthermore, the method allows to easily combine different modelling strategies and considering non-linear material constitutive models.

These are usually classified according to the followed modelling strategy, namely: (i) the direct simulation or the meso-modelling approach; (ii) the macro-modelling approach; and (iii) the multi-scale computational approach. The latter groups are described next in which both continuous and discrete FE-based models are presented.

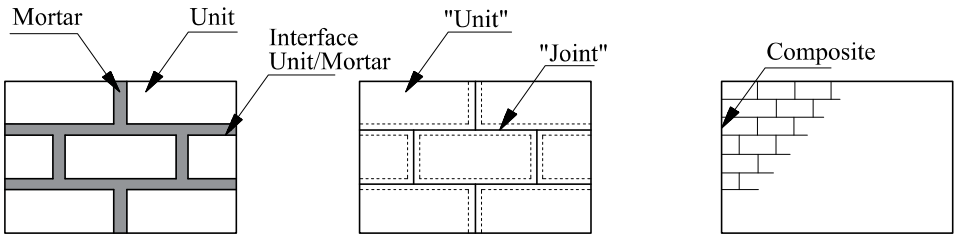

Figure 2.7 – Modelling strategies to represent the behavior of masonry: (a) detailed meso-modelling; (b) simplified meso-modelling; (c) macro-modelling (Lourenço 2008).

Meso-modelling strategy

Meso-modelling considers masonry as a two-phase material in which the masonry components, brick and mortar joints. are explicitly and individually discretized. Two strategies can be pursued, i.e. a detailed and a simplified modelling. In the former, brick units and mortar joints are modelled as continuum FE's being the mortar-brick interface modelled through discontinuous elements (interface FE's). In the latter, brick units are modelled as continuous FE's but, as simplification, mortar joints are replaced by discrete interface FE's, which try to represent the behavior of both mortar joints and brick-mortar interaction.

From the current set of eligible advanced FE-based strategies to study URM masonry behavior, the detailed meso-modelling is probably the most accurate tool. Yet, it demands more input data to characterize the behavior of the masonry components and lead to more degrees of freedom (Tzamtzis and Asteris 2003). An intensive computational effort is expected which can be, in part, lessened if a simplified meso-modelling is adopted (Roca et al. 2010). Taking into account that joints are the major contributors for the nonlinear response of masonry structures (Lourenço 1996), research tends to focus on the unit-joint interface elements characterization. Defining the brick-mortar interaction law is usually quite complex and only possible for calibration studies restricted to very small scale numerical analysis, as the study from Shieh-Beygi and Pietruszczak (2008) and Andreotti et al. (2018). Bearing in mind that failure tends to occur in the planes of weakness defined by the mortar joints (for weak joints

masonry), most of the research in the meso-modelling field tries to simulate masonry using the latter simplified approach. One of the pioneer studies has been introduced by Page (1978) in which a simplified mesoscopic model has been proposed for the in-plane analysis of clay masonry walls, with brick units assumed as elastic continuum elements and mortar joints as linkage elements. The latter work has been afterwards extended by Ali and Page (1988) for local high stress and strain gradients problems, i.e. able to account for concentrated loads. Developments have been implemented by the formulation of interface elements (with zero thickness) associated with plasticity concepts (Lourenço et al. 1997; Giambanco et al. 2001). In the work of Lourenço and Rots (1997) the interface elements are able to represent cracking, slip and crushing of the material in presence of the dilatancy effect, since non-associated flow rules are combined with Coulomb friction laws. An important achievement is the adoption of a compressive cap on the yield surface aiming to represent the crushing failure mode. The simplified mesoscopic model has been validated through comparison with experimental data from in-plane URM tests and latter extended to the three-dimensional case by Zijl (2000) being, therefore, suitable for the OOP analysis of URM structures.

Other important works have been presented on the application of such modelling strategy (Gambarotta and Lagomarsino 1997; Senthivel and Lourenço 2009; Vandoren et al. 2013). The research from Macorini and Izzuddin (2011) may be also highlighted, where a three-dimensional model including both the in- and out-of-plane behavior is developed; and then further extended to blast loading field, see Macorini and Izzuddin (2014). In this matter, one should address the research by Rafsanjani et al. (2015) where a strain-rate dependency formulation has been implemented within the multi-surface plasticity model by Lourenço and Rots (1997) and from Zijl (2000) aiming to study the behavior of URM parapets subjected to a blast load. For further works on simplified meso-modelling the reader is referred to Tzamtzis and Asteris (2003) and Theodossopoulos and Sinha (2013). In general, FE-based meso-models allow accurate results being reliable for the seismic study of URM structures. Lumping the material non-linearity on the interface elements allow to achieve a well-posed numerical problem upon the onset of cracking. A three-dimensional model is certainly capable of well reproducing both the in- and the out-of-plane orthotropic nonlinear behavior of masonry and capturing well the nonlinear deformation and cracking. However, the demand of long processing times makes the approach recommendable only in limited size structural problems and, consequently, its use in the dynamic range is hardly feasible.

Macro-modelling strategy

Macro-modelling strategies consider masonry as a one-phase material, meaning that the heterogeneous assemblage of mortar and bricks is smeared out into a continuous and fictitious homogeneous anisotropic material. Representing the phenomenological behavior of the equivalent material is a complex task but brings the advantage of reaching a quite straightforward procedure. The thorough modelling stage required by a meso-approach is avoided, since the FE mesh can be defined by a mesh generator algorithm disregarding the need of an explicit discretization of both joints and units.

A pioneer macroscopic model has been presented by Saw (1974), where the masonry is idealized as an equivalent isotropic elastic material. This strategy might be useful for the analysis of deformations at low stresses, but such formulation leads to conservative solutions by not accounting for nonlinearities. Other studies as Ganju (1977) or Samarasinghe (1982) also defined the homogeneous material based on average properties but considering the possibility of tracing local failures. Dhanasekar et al. (1985) presented a nonlinear macroscopic model for in-plane analysis, whose material average properties have been defined through bi-axial tests on masonry panels. The model is unsuitable for high stress-strain gradient problems (Tzamtzis and Asteris 2003). Lourenço (1996) and Lourenço et al. (1998) introduced a macroscopic approach with a nonlinear constitutive material model for the in-plane analysis of masonry walls, with the possibility of assuming different hardening and softening responses according to the material axis direction (masonry orthotropy). The model is based on the plasticity theory with a Hill-type yield criterion for compression and a Rankine-type yield criterion for tension. Concerning the importance of the OOP behavior of masonry, Lourenço (2000) extended the formulation to represent masonry as an anisotropic continuum model accounting for softening behavior and suitable for the study of plates, shells and 3D elements. A comparison between the numerical results and the experimental data available from Gazzola and Drysdale (1986) and Guggisberg and Thürlimann (1990) has been performed and good results achieved. Berto et al. (2002) also developed an orthotropic damage model for the analysis of quasi-brittle materials; for the masonry analysis, the angles between bed and head joints are defined to be able to reproduce the elastic and inelastic properties along each orientation.

The advantages of macroscopic models are well noticed in the literature. Its mesh discretization independency, with respect to the masonry texture, makes the strategy to be practical-oriented and suitable for the seismic analysis of both small and large URM structures, see Martínez et al. (2006), Lourenço et al. (2011, 2012), Betti and Vignoli (2011), Araujo (2012),

Pelà et al. (2013a), Roca et al. (2013) and Silva et al. (2018). The approach is, amid the advanced FE strategies and within continuous FE assumptions, the one which allows to achieve a better trade-off between the results accuracy and time to perform the analysis.

Nonetheless, the way that damage is represented still constitutes a drawback of classical FE macro-modelling strategies. It is known that in URM damage should be concentrated or locally distributed following typical failure patterns (Griffith and Magenes 2003; Roca et al. 2010). Smeared-crack models tend, however, to smear out the displacement (strain) jump over a mesh region, the so-called localization band. Several works have been developed aiming to, in the macroscopic model context, localize such damage within a narrow band and improve the directional mesh-bias issue independence through the implementation of tracking algorithms. In order to further localize the damage to a single row of finite elements and increase its real representation, Clemente et al. (2006) presented a macroscopic damage model with a novel crack-tracking algorithm. It has been modified Pelà et al. (2013b) to account for the masonry orthotropy. The reader is referred to Saloustros et al. (2018) for an extensive review on such approaches

It is important to stress, however, that there are still some important concerns pending. For instance, the adopted geometrical modelling simplifications, the type of FE used and the mesh refinement level chosen may play an important role in the required time to perform the analysis (Lourenço 2002). The use of closed-form laws to represent the complex phenomenological behavior and damage of the masonry is cumbersome and may require a calibration step. Such consideration calls for the use of constitutive models able to predict the behavior of masonry and account for failure of the homogeneous material, in which input data can be obtained by conducting thorough experimental campaigns. This may be prohibitive in most study cases due to the involved costs and time being an alternative to conduct the experimental tests on the masonry individual components and employ the derived data in a multi-scale strategy through the homogenization technique (Benedetti et al. 2008).

Multi-scale strategy

Homogenization methods, within a multi-scale framework, are in-between the latter two FE modelling schemes and constitute a promising alternative. The framework is being used to investigate the response of composites with different natures, see Feyel and Chaboche (2000), Kouznetsova et al. (2001), Miehe and Koch (2002), Mercatoris and Massart (2011), Spahn et al. (2014), Yamanaka et al. (2015), van den Eijnden et al. (2016), but is also useful

for the study of masonry structures. It typically relies on a meso and macro transition of information and is thus designated as a two-scale (FE^2) approach.

The first strategies regarding masonry homogenization tried to substitute the complex geometry into a simplified one aiming to achieve a closed-form solution in the elastic range. Studies by Pande et al. (1989), Maier et al. (1991), and Pietruszczak and Niu (1992) are, within the so-called 'two-step homogenization', important to recall. It refers to the process of geometry simplification that is performed in two steps: firstly, the homogenization is performed considering the vertical joints and leading to a horizontal layered material; secondly, the final equivalent material is obtained through the horizontal layered material by taking out the horizontal joints. The accuracy of the derived properties is dependent on the order that the homogenization steps are performed. Significant errors are expected to occur in the non-linear range, since the regular geometrical offsets of the vertical mortar joints are not accounted (Lourenço et al. 2007). Other strategies, based on the unit-cell theory, have been firstly proposed in the elastic range by Hashin and Rosen (1964) and in the nonlinear range by Dvorak and Teply (1985), through the use of the so-called hexagonal array model. Closed-form expressions are derived at a meso-scale from both equilibrium and compatibility conditions at the Representative Volume Element (RVE). After being solved or formulated these can provide the homogenized quantities or describe phenomenologically the constitutive equations at a macro-scale, see Zucchini and Lourenço (2002), Taliercio (2014), and Drougkas et al. (2015). The use of closed-formed solutions is, however, less feasible in the non-linear range, in complex loading cases or in cases where geometrical and physical changes can occur.

A more rigorous strategy in obtaining the homogenized elastic parameters of masonry is through an asymptotic model. For instance de Felice (1995) and Cecchi and Sab (2002a) formulated a meso-model considering cohesive zero thickness interface elements to solve the asymptotic problem, meaning that mortar is infinitely deformable in respect to the brick unit. An OOP extension of such asymptotic model has been presented in (Cecchi and Sab 2002b). These works are oriented to find the in- or the out-of-plane elastic stiffness values and, therefore, its application in the non-linear range may be careful analyzed. Furthermore, Cecchi and Sab (2002a) have assumed units as deformable elements in which a solution of the analytical problem fails to be formulated being, instead, derived from a FE model. To circumvent such limitation, units were considered by de Felice (1995) to be rigid blocks with the pitfall of a loss in the output accuracy, accentuated in the case of smaller stiffness ratios between the unit and mortar elastic stiffnesses.

The individual character and accuracy issues of closed-form homogenized-based techniques can be overcome using the FE method. Anthoine (1995) proposed a novel framework in which

the in-plane characteristics of masonry are obtained in just one step. The pioneer work used the FE-method to solve the homogenization Boundary Value Problem (BVP) for both stacked and running-bond masonry, but it is only set to obtain the elastic material homogenized properties. Pegon and Anthoine (1997) and Massart et al. (2004) introduced material constitutive laws of the masonry components to conduct analysis with a non-linear associated to the problem. Other approaches may be mentioned, as the meso-mechanical homogenization approach by Zucchini and Lourenço (2002) and Luciano and Sacco (1997) whereas, again, a running-bond texture is presumed. Nevertheless, the accuracy of these methods could be lessened if unexpected damaged states occur (Lourenço et al. 2007). Although general FE unit-cell models may lead to reasonably accurate and effective solutions, its integration within full continuum based FE^2 approaches is still a challenge, especially if material non-linearity is accounted as demonstrated in (Geers et al. 2010; Otero et al. 2015). In fact, the constant need of data between the macro- and meso- scales constitute a contentious issue, because a new BVP must be solved numerically for each load step and in each Gauss integration point. This compromises the utility of the approach, due to the involved computational time and thus full continuum based FE^2 approaches are seldom used for dynamic purposes and for complex structural analysis (Lourenço et al. 2007).

Bearing in mind the unequivocal importance of using advanced computational tools, several authors tried to address simplifications on two-scale frameworks to keep the time-costs as relatively small. For instance, the polynomial stress field expansion by Milani et al. (2006d), as discussed by Lourenço et al. (2007b) on the recent advances concerning homogenization tools. An adequate possibility is the use of a kinematic theorem of limit analysis at a macro-level to obtain the homogenized failure surfaces with a very limited computational effort (de Buhan and de Felice 1997; Milani et al. 2006b; Cecchi and Milani 2008). Such methods give a lower or upper bound estimate on the failure collapse load which, in some cases, can be scarce. The use of discrete FE-based methods at a macro-level is a promising alternative. Casolo (1999) defined a flexural-torsional kinematics-based model that uses quadrilateral Kirchhoff-Love plates with springs in its interfaces to study the OOP behavior of masonry façades. Milani and Tralli (2011) adopted a macro-model based on a FE-mixed formulation, where rigid triangular constant stress finite elements (from the works of Herrmann (1967)) with bending behavior lumped on its interface is used to carry the homogenized information. Discrete FE-based macro-models are very practical due to the decrease of the number of degrees-of-freedom (comparing to a continuous approach) and are especially useful to perform dynamic analysis. Several studies have shown the clear advantages of this process, since it allows a good trade-off between consumed time and results' accuracy, and enables the study of real scale buildings. The latter

is even more clear if simplifications are further assumed at both macro- or meso-scales, as observed in Milani et al. 2006b (2007), Milani and Venturini (2011), Akhaveissy and Milani (2013) and Casolo and Milani (2013).

Discrete Element Models (DEM)

Continuum finite element-based methods are nowadays very powerful. However, FE methods may not be so efficient for problems in which several discontinuous exists in the media. Specifically, when several distinct bodies exhibit large relative movements and, consequently, contact conditions vary during the analysis. Some attempts to combine FE methods in a discrete-element approach can be found in the literature, as the study by Mamaghani et al. (1999) where a discrete-fashion model has been developed, in which masonry units are idealized as rigid elements and joint interfaces as discontinuities modelled through contact elements. Such discontinuities can sustain small deformations and thus represent the split and separation between units. However, the approach was used only for simple 2D problems and, according to the author, its extension to more complex studies requires more experimental data to face the problem of the constitutive characterization of the contact elements.

The Discrete (or Distinct) Element Method (DEM) presents several advantages in comparison to the traditional FE methodologies and, therefore, a brief recall should be addressed. On one hand, bearing that masonry is the assemblage of units separated by mortared or dry joints, the method allows to represent masonry as a discontinuous media, whereas masonry units are considered as the ensemble of distinct bodies connected by contact surfaces that represent joints. On the other hand, DEM still unfolds, in such context, several modelling and analysis possibilities, as: (i) masonry units can be modelled as rigid or deformable blocks; (ii) the method is suitable to account for the nonlinear behavior of its components; (iii) the method is suitable for large displacement problems, and for static or dynamic analyses.

Since the first DEM model proposed by Cundall and Hart (1971) and the discontinuous deformation analysis (DDA) introduced by Shi and Goodman (1988), both investigations oriented for rock engineering field, several studies have been introduced and developed to contemplate other engineering fields (Lemos 2007). Focusing on masonry structures, the DDA model was applied by Ma et al. (1996), wherein masonry units are considered as deformable blocks and joints as rigid contact elements. DEM is widely applied to simple blocky structures (Roca et al. 2010), for instance in the analysis of arches to assess the collapse load (Gilbert and Melbourne 1994); static and dynamic analysis of masonry walls (Baggio and Trovalusci 1995;

Schlegel and Rautenstrauch 2004; Lemos et al. 2011; Giamundo et al. 2014; Sarhosis et al. 2016) and rocking motion of stone blocks (Peña et al. 2007).

At last, it is important to refer studies performed on classical temples, whereas the masonry units are very large and thus its idealization through rigid blocks seems to be adequate. For instance, the seismic assessment of a column-architrave of the Parthenon (Psycharis et al. 2003) and the Roman Temple of Évora (Nayeri 2012). More recently, Tran et al. (2014) used the DEM to model the behavior of a stone bridge during the phase of formwork removal. The conducted analysis allowed to obtain the displacement pattern that was validated in-situ. Software based on the formulation is being continuously presented, see Itasca (2004) and Cascini et al. (2018).

Although the inherent advantages of DEM, the modelling of 3D complex or large structures, where a high number of block elements is expected, can turn the computational time of the analysis unacceptable. Besides, simplifications concerning the mesh discretization may compromise the accuracy and thus may be taken with care. As stated by Lemos (2007), the accuracy for the OOP study of masonry is quite dependent on the number of contact points in the thickness direction. Regardless of the latter, DEM is still barely applied for 3D structures within dynamic analysis.

2.3 Seismic vulnerability assessment of masonry structures

Earthquakes are, among the set of natural events, one of the most serious threats and challenges to humankind. Seismic events represent almost 60% of all the fatalities caused by natural disasters (International Disaster Database (2009)) being predictable that the death toll will augment, at the current century, to a value of 2.57±0.64 million (Holzer and Savage 2013).

The seismic vulnerability can be defined as the susceptibility that a community faces to suffer damage or any type of loss (e.g. economic or human loss) if an earthquake occurs. If vulnerability is accounted together with the seismic hazard and exposition for a given territory, one may refer to the associated seismic risk. Since the seismic hazard is, in principle, immutable, vulnerability and exposure are of prime importance if one aims to control the associated risk. Different consequences can arise depending on the vulnerability of the community, meaning that physical, political and social conditions are variables affecting such predisposition to damage or loss (Barbat et al. 2010). This reveals the importance and the multidisciplinary character of a seismic risk mitigation process which henceforth brings the need of developing urban emergency management plans; of conducting seismic vulnerability assessment studies

over the existing building stock; and of raising the populations awareness over hazards and over the proper emergency response measures (UNDRO 1979).

A seismic vulnerability assessment is part of a loss model upon the built environment. A consistent evaluation of the seismic risk of a building structure or typology may undertake vulnerability analyses, loss assessment estimations and an evaluation of potential repair costs, since these support a well-established decision. Steps as the definition of hazard, definition of limit states, characterization of the structural state and the construction of fragility or vulnerability curves are fundamental to accomplish it.

Two main methodologies can be pursued, i.e. an empirical or analytical one; with a third option possible, designated as hybrid methods, when simultaneously considered (Calvi et al. 2006). Empirical and analytical strategies exist in the literature and aim at the prediction of the expected level of damage in a structure subjected to a given intensity measure (IM), according to pre-defined limit states. The former methods generally collect the structural damage data from conducting in-situ surveys, through statistical information or empirical knowledge; whilst, in the latter methods, a structural analysis, using simplified or more complex advanced numerical models, is performed. In this context, the way that damage is predicted constitutes the most relevant difference between the approaches.

Empirical Methods

Empirical methods are practical and widely used in the assessment of buildings at a territorial scale. Such practicability is retrieved with the cost of introducing subjectivity in the process. The works by Whitman et al. (1973) served as basis to the development of such methods, in which the authors proposed damage probability matrices (DPM) to allow the damage prediction for a building through observation. Both structural and non-structural damage are acknowledged and extrapolated for buildings with similar features (i.e. same typology) having into consideration a macro-seismic intensity scale (MSK)(Medvedev 1977) to describe the earthquake loading. Later, Braga et al. (1982) proposed a binomial distribution to define the damage pattern of a building considering, again, the MSK scale. More recently, Giovinazzi and Lagomarsino (2004) presented a macro-seismic method based on the EMS-98 scale (Grünthal 1998). The method considers six vulnerability classes of buildings, with seismic intensity levels ranging from V to XII and five damage levels. Likewise, other studies such as from Rota et al. (2008) have followed the same methodology yet assuming the peak ground acceleration (PGA) as the seismic IM. Empirical approaches based in the attribution of a vulnerability index has been also proposed, for instance by Benedetti and Petrini (1984). In

this study, the vulnerability index is calculated for each building through a survey form where eleven pre-defined building parameters need to be collected. The final index is obtained considering the relative weight of each parameter which, after normalization, is calibrated to relate the vulnerability index with a damage global factor defined for the same building typology and macro-seismic intensity or *PGA*.

Both *DPM* and *'Vulnerability Index'* empirical approaches have been largely applied in the risk assessment of urban areas, see Vicente et al. (2011). The former approach is useful to derive vulnerability curves for well-defined typologies of buildings, especially when empirical damage information is available (Rota et al. 2008). The latter approach has a broader target, since its application does not limit the building to be part of a given typology (Calvi et al. 2006), but the definition of the proper grades and weights upon the survey parameters may be questionable. Moreover, both input parameters (i.e. macro-seismic scale and vulnerability index level) are gathered through observation thus presenting some level of subjectivity. Although these steps can be processed through different manners, this still constitutes a clear drawback, because the results accuracy is highly dependent on the expert's team judgement.

Analytical Methods

In the context just defined, analytical methods are being developed in the last decades to give a more rational sense to probabilistic earthquake assessment of buildings. The introduction of spectral ordinates (displacements and accelerations) instead of macro-seismic intensities scales widens the analysis possibilities and permits to reduce the intrinsic subjectivity associated with empirical methods. Spectral ordinates allow researchers to explore new procedures in the derivation of ground-motions equations and, so, reach fragility or vulnerability curves in which the building's capacity is studied through spectral response (Calvi et al. 2006).

Few studies exist in the literature on analytical procedures for the assessment of URM buildings. Some can be still recalled as the work by Park et al. (2009), where an analytical method is adopted to generate fragility curves for a typical two-story URM building located at the central and southern regions of United States of America. To account with the high nonlinear behavior of URM structures when subjected to dynamic loads, a simple structural spring-based model has been idealized aiming, essentially, to reach low computational times. The occurrence of OOP failures is included, as well as uncertainty in both seismic excitation and material properties. The main conclusion is that the analyzed URM building type presents high seismic vulnerability and that the OOP stiffness contribution should not be disregard in the risk assessment.

Rota et al. (2010) proposed a new analytical framework to obtain fragility curves for masonry buildings prototypes using a simplified equivalent-frame model (TREMURI software by Lagomarsino et al. (2013)). The major improvement is the adoption of a detailed 3D structural modelling, whereas all the mechanical properties have been considered as random variables with a normal probability density function distribution. A total of one thousand Monte-Carlo simulations allowed to achieve multiple sets of input variables. The damage states threshold (viz. limit states) have been achieved through nonlinear static analysis thus transferring more objectivity in its definition. The authors performed dynamic analyses, for several levels of ground motion, to determine the probability density function of the displacements demand. Lognormal fragility curves have been derived by convolution of the complementary cumulative distribution of displacements demand and the probability density function of each damage state (Rota et al. 2010). The procedure follows the traces of recent proposed methodologies, as the PEER framework (Günay and Mosalam 2013), but it does not take in consideration the OOP behavior of masonry walls. It restricts the application of the method to a building typology whose connections between orthogonal walls and floors are good and in the presence of a rigid diaphragm; this means URM buildings with a box behavior. Other studies can be addressed within the same line of investigation, i.e. by using simplified analytical or numerical models, as Erberik (2007), Pasticier et al. (2007), and Kappos and Papanikolaou (2016). In fact, the seismic analytical assessment has, obviously, an enormous dependency on the approach used in the analysis. The use of equivalent frame-based methods allows to study URM buildings but precludes the consideration of OOP mechanisms rather essential in the seismic behavior. Other analytical methodologies allow a better insight of such behavior, as the collapse mechanism-based methods, capacity spectrum-based methods and fully displacement-based methods.

Regarding the collapse mechanism-based methods it is possible to state the VULNUS and the *FaMIVE* (Failure mechanism identification and vulnerability evaluation method) procedures. These try to conduct the vulnerability assessment by using collapse load multipliers according to mechanical assumptions. *VULNUS* has been developed by Bernardini et al. (1990) to study an individual or group of URM buildings and uses the fuzzy-set theory and the calculation of two collapse multipliers and a third index. The in-plane (IP) behavior parameters are computed as the ratio of shear strength of the system (two directions) and the total weight and represent the strength parameters for both directions at mid-story height of the ground floor. The OOP collapse multiplier is calculated by the ratio of the OOP strength and the total weight. This index must be calculated for each single wall and failure mode, as overturning, flexural tension and arch crushing (Bernardini et al. 1990; Restrepo-Vélez 2004). A third index

is required beforehand being obtained through the evaluation of seven vulnerability factors and respective weights. A qualitative judgement approach is followed to retrieve these parameters and, so, *VULNUS* has a hybrid character. The three indexes allow to follow the fuzzy set theory in order to compute the vulnerability value of the study case and allow, as well, the comparison with a safety criterion (see Bernardini et al. (1990) for more detail).

The *FaMIVE* is an analytical procedure based on the collapse-mechanics approach by D'Ayala and Speranza (2003) and has been extensively used, see for instance Sepe et al. (2008), and Basset-Salom and Guardiola-Víllora (2014). The method relies on limit analysis to obtain the collapse load factors of expectable IP and OOP collapse modes. The collapse multiplier is thus obtained through an equivalent static approach and hence converted in a vulnerability value. The advantages and disadvantages of the methodology are implicitly related with the analytical approach, i.e. static methods may not be sufficiently representative of a building behavior subjected to a dynamic excitation.

Aiming at the development of a national-scale methodology for loss earthquake estimation, the Federal Emergency Management Agency proposed a seismic loss estimation framework, namely HAZUS (Hazard U.S.) (Whitman et al. 1973; HAZUS 1999). HAZUS is frequently referred as a capacity-spectrum based method, since it defines the design or performance point of the building. The latter is obtained by the intersection of two curves: the first bears the ground motion information of a given scenario registered as a spectral response curve, that is scaled to account the effects of damping and duration effects; the second corresponds to the capacity curve of the building under study, typically obtained through nonlinear static analysis. Then, the building fragility curves are generated considering a lognormal distribution; whereas the distribution parameters adopted are the median capacity and damage variability (Calvi et al. 2006). HAZUS defined four limit states in a qualitative way according to the maximum drift ratio. The last could be a drawback, because even if the decision upon the damage limit states tries to cover prior experimental knowledge, it is still based on expert judgement.

Fully Displacement-Based Methods

Furthermore, strategies based on a DBA have been also investigated. Calvi (1999) firstly presented a DBA for the seismic vulnerability assessment for in-plane failure mechanisms. Three damage levels have been considered, using as limit state thresholds the inter-story drifts suggested by Magenes and Calvi (1997). These are presented as uniform probabilistic variables to introduce the associated uncertainty. The displacement demand may be obtained by an elastic response spectrum which could represent a nonlinear response simply by scaling the

spectral ordinate by a reduction factor, to account for energy dissipation of the structure. The probability of displacement exceedance is simply computed by integrating the Joint Probability Density Function for the given period and with the demand response spectrum. However, both the displacement and period of the structure are assumed as independent variables.

Bearing with the limitations of the study from Calvi (1999), Restrepo-Vélez (2004) proposed a mechanics-based approach to overcome the non-consideration of the OOP behavior and the non-independence relation between displacement (Δ) and period (T). For the OOP behavior, the capacity is obtained for a given building by applying lateral forces proportional to the stories mass. Instead, the required demand is obtained through a displacement response spectrum, which could be selected using the current seismic design codes. Analytical methods based on a displacement formulation (generally based on SDOF or MDOF systems) have an inherent simplicity which brings the advantage of being computationally effective.

Hybrid Methods

The disadvantages of analytical vulnerability curves are mainly twofold, namely: (i) the computational time cost associated with the structural analysis which leads to disregard its use in studies at an urban-scale, and (ii) the absence of a proper calibration, in most of the studies, on the analytical damage levels. To overcome these limitations, analytical and empirical methods have been combined resulting in the so-called hybrid methods.

Even if oriented to reinforced concrete structures, a pioneer study has been presented by Singhal and Kiremidjian (1996), in which the probability of each damage state has been defined through empirical knowledge and so overcoming the lack of calibration pointed out for rational methods. For masonry, the investigation conducted by Kappos et al. (1998) followed a *vulnerability index procedure* where data from past earthquakes has been used and complemented with the results of nonlinear dynamic analysis to construct DPMs. The approach has been applied in the analysis of Greek buildings with loss estimations in terms of repair cost. Likewise, Barbat et al. (1996) applied a vulnerability index procedure within a hybrid method to study the vulnerability of urban areas in Spain. Kappos et al. (2006) derived vulnerability curves considering the PGA and the spectral displacement. The authors combined available statistical data with processed results from nonlinear dynamic or static analyses aiming to extrapolate the data to PGA and spectral displacement levels where information is lacking. The vulnerability curves have been derived for several damage states and applied to buildings types located in southern Europe. Other noteworthy contribution was made by

Lagomarsino and Giovinazzi (2006) and the reader is referred to Calvi et al. (2006) and Kappos and Papanikolaou (2016) for an extensive overview of the hybrid methods application.

Herein, it is of utmost importance to stress the key advantage of the method. In fact, the method makes possible to use analytical models calibrated through past-earthquakes information that, eventually, are useful to process information for intensity seismic levels in which there is still a lack of damage data. In short, the method allows to achieve a calibrated analytical model and to reduce the required time needed to complete a set of analytical vulnerability curves of DPMs. Yet, the calibration process can be hard to carry out due to the multiple sources of uncertainty in the input of the models and, therefore, the assumptions adopted throughout the framework may be arguable, as discussed by Bommer and Crowley (2006a).

2.4 Summary

Some of the most important investigations carried out in two different masonry research fields have been briefly addressed: (i) strategies to study the structural behavior of URM structures; and (ii) methods to assess the seismic vulnerability of URM structures.

The behavior of masonry structures is difficult to predict due the inherent phenomenological complexity of the material. The overview demonstrated that the selection of the more adequate tool can be debatable. Simplified procedures are frequently designated as force- or displacement-based approaches. The former aggregates strategies as the graphical and the limit analysis methods whilst the latter aggregates strategies based on the flexural or rigid body motion (SDOF or MDOF systems) of blocky elements. It is noticeable that simplified methods are useful as they allow reaching solutions within reduced times, but the accuracy levels may be compromised and thus are conceived for ad-hoc structural problems.

In this scope, researchers are focusing in the advance of more sophisticated strategies, typically based on the FE-method and designated according to the followed modelling strategy, as: (i) direct numerical simulation or meso-modelling approach; (ii) macro-modelling approach; and (iii) multi-scale approach. The possibility of adopting different constitutive material laws, failure criterions and modelling assumptions make such methods quite interesting. Despite this, it has been seen that a direct numerical simulation may demand prohibitive computational costs for professional applications in both the pre- and processing stages (Lourenço 2002). Macro-modelling approaches are nowadays adopted for the study of large-scale structures, but the damage representation is still an open issue. They tend to smear out the damage over a mesh region (the so-called localization band) which goes against how this is generally found in

URM structures, i.e. concentrated or locally distributed following typical failure patterns (Griffith and Magenes 2003; Roca et al. 2010). In this regard, multi-scale approaches (usually two-scales or FE^2) are in-between the latter FE-modelling strategies. These rely on the homogenization principle, in which the behavior of the masonry material is characterized at a meso-scale and transferred to the macro-scale. Although seemingly very promising, the use of full-continuum FE strategies at both scales is still computationally prohibitive when material nonlinearity is accounted. This comes from the fact that a new BVP must be solved numerically for each load step, in each Gauss integration point. The adoption of simplifications at a meso- or a macro-scale can be a good way to overcome the latter problem.

Furthermore, a brief review over works in the field of the vulnerability assessment of masonry structures has been presented. The ideal methodology appears to be a combination between an empirical and an analytical approach, i.e. the so-called hybrid approach. Still, few analytical methods able to accurately predict the structural behavior of URM structures exist in the literature and, when it is the case, tend to focus on the application of structures with box behavior. Such structures possess a rigid diaphragm and a proper connection between transversal walls which allows to preclude the occurrence of OOP failures and the adoption of nonlinear static analysis to perform the seismic assessment of the structure which is, in fact, very convenient. Nonetheless, the preceding features tend to be lacking in the case of existing URM structures.

Selecting a proper computational model of the structure is essential to derive reliable fragility (or vulnerability) analytical curves (Dumova-Jovanoska 2000). So, the development of an advanced FE-approach able to be inserted within an analytical methodology for the seismic fragility (or vulnerability) assessment of URM structures is a significant achievement. This is especially prescribed if the procedure is suitable to: (i) study the OOP behavior of URM structures; (ii) account for the system and seismic load uncertainties; (iii) render a low computational effort when dynamic analyses are performed; (iv) allow a proper calibration between numerical and real damage levels; and (v) guarantee that the results have good accuracy. Therefore, the development of a simplified two-scale FE-approach to cope with these issues is an interesting and innovative stream of research. On this behalf, a novel FE^2 strategy is presented in this work where, aiming to effectively achieve improved running-times (in respect to the existing advanced FE modelling approaches), a Rigid Body Spring Mass (RBSM) model is developed at a macro-scale and implemented in the commercial software ABAQUS (2013) which has powerful built-in procedures. At a meso-scale, the data derived from different presented and validated unit-cell homogenized models is to be used.

(vacate page)

Chapter 3

3 Multi-scale analysis of masonry: meso-scale level

3.1 Introduction

The analysis of the masonry behavior in terms of strength and deformation is still a challenge. Such complexity arises from: (i) the material heterogeneity, because of the staggering between units and mortar joints; (ii) the non-linearity of the material components; and (iii) the existence of planes of weakness which tend to govern the behavior and damage, because mortar joints are typically less stiff and resistant than masonry units (Lourenço 2009).

The approach proposed in this thesis belongs to the so-called multi-scale methods based on the homogenization theory. Homogenization is an averaging procedure performed at a meso-scale upon a Representative Volume Element (RVE). On the RVE, a Boundary Value Problem (BVP) is formulated allowing an estimation of the expected average response to be used as constitutive relations at macro-level. This framework has been used to investigate the behavior of composites with different natures (Feyel and Chaboche 2000; Kouznetsova et al. 2001; Miehe and Koch 2002; Mercatoris and Massart 2011; Spahn et al. 2014; Yamanaka et al. 2015; van den Eijnden et al. 2016) but is also useful for the study of masonry structures (Pande et al. 1989; Anthoine 1995; Papa 1996; Luciano and Sacco 1997; Zucchini and Lourenço 2002; Mistler et al. 2007; Milani et al. 2007). The macro-behavior of masonry is derived by smear out the meso-scale features via a homogenization step, and thus considering its texture, components properties and expected meso-failure modes. In this way, the computational burden (in terms of CPU) is significantly reduced if compared with a fully meso-mechanical description of the material, as demonstrated in Otero et al. (2015).

The multi-scale finite element computational homogenization methods typically rely on a meso and macro transition of information and are thus designated as two-scale or FE^2 approaches, see Ghosh et al. (1995); Smit et al. (1998); Feyel and Chaboche (2000); Kouznetsova et al. (2001); Valenta et al. (2010); Mercatoris and Massart (2011); Sýkora et al. (2013). The classical models are based on a first-order homogenization scheme and, as its formulation relies on the first gradient of the kinematics field, two main limitations arise. The first limitation is related to the principle of separation of scales, which enforces the assumption of uniformity upon the macroscopic fields attributed to each RVE. It is known that in macro-regions where high deformation gradients are present, the latter assumption is not totally effective. The second limitation is related to the fact that the lengths of the two scales are not intrinsically considered in this classical formulation and, therefore, mesh-sensitivity

issues and loss of ellipticity of the equilibrium (Bažant and Oh 1983) tend to appear when softening behavior of the material is present (Geers et al. 2010). The latter demands a regularization process, for instance, based on the fracture energy (Petracca et al. 2016), to guarantee the problem objectivity. In this scope, several extensions of the homogenization process were developed trying to overcome these issues. Some authors extended the classical method to a second-order homogenization (Kouznetsova et al. 2004; Bacigalupo and Gambarotta 2012), in which the constitutive behavior is derived from the classic part and a higher gradient part, thus, linking the length scales. Other researchers developed techniques that permit the enrichment of the kinematical constraints but still allowing for the use of classical constitutive forms. This is achieved preferably through the use of Cosserat continuum models (Forest et al. 2001; Casolo 2006; Addessi et al. 2010). The well-posedness of the macroscale solution is thus achieved independently of the used mesh, even if the assumption of the separation of scales is lost.

The main advantages of the classical FE^2 approaches are twofold: (i) flexibility to be used at a meso-scale, which can be based on the FE-method (Mercatoris and Massart 2011), Fourier series (Moulinec and Suquet 1998; Vondřejc et al. 2014) or on the Voronoi method (Ghosh et al. 1995), among others; (ii) it does not require any macro-constitutive relation, because the macro-behavior is totally dependent on the homogenized response derived on the foregoing scale. Nevertheless, the classical FE^2 approaches (in particular the full continuum-FE methods) are still a challenge in the non-linear range (Geers et al. 2010; Otero et al. 2015). The advantages are especially obvious when linear elastic behavior is assumed, but obtaining a meso-scale solution at each load step of a non-linear process for each Gauss point may turn the problem prohibitive from a computational point of view. These strategies still have a higher computational cost if compared with a macro-modeling one. It is the author's belief that if one intends to use homogenization strategies for the study of large or more complex structures, the development of techniques to speed up the processing running times is critical.

Some assumptions may be undertaken which can significantly reduce the computational cost of an FE^2 approach. The use of homogenization methods based on the unit-cell theory, first proposed in the elastic range by Hashin and Rosen (1964) and in the nonlinear range by Dvorak and Teply (1985) through the use of the so-called hexagonal array model, is a possibility. In these methods (see Aboudi (1991)), closed-form expressions are derived at a meso-scale from both equilibrium and compatibility conditions at the RVE. After being solved or formulated, these can provide the homogenized quantities or describe phenomenologically the constitutive equations at a macro-scale, see Zucchini and Lourenço (2002), Taliercio (2014) and Drougkas et al. (2015). The use of closed-formed solutions is, however, not so feasible in

the non-linear range, in complex loading cases or in cases where geometrical and physical changes can occur. Another strategy is the use of the so-called adaptive multi-scale methods (Ghosh et al. 2001; Lloberas-Valls et al. 2012; Greco et al. 2016), which take advantage of the best of the first-order theory and meso-modeling approach. A first-order homogenized model represents initially the masonry behavior until a threshold criterion is reached. Such a criterion may be able to account for the onset of damage propagation or another high-gradient source. After reaching the threshold, the area of interest is replaced and kept by an explicit meso-structural description able to represent the high localized deformation without the ill-posedness of the first-order theory, see Greco et al. (2016) for the masonry field application. These numerical models could be a valuable tool due to their computational attractiveness. Many current studies on unreinforced masonry focus on in-plane cases and for quasi-static loading of running-bond masonry and, therefore, more research is required on structural models with other masonry textures and loading conditions, as out-of-plane loads or seismic excitations.

From the above considerations, the general aim of the present chapter is to formulate two unit-cell homogenized models oriented for both in- and out-of-plane analysis of unreinforced periodic masonry structures which may be linked with a proper macro-scale model. For the sake of avoiding a full three-dimensional discretization of the masonry, both homogenized strategies follow plate (but different) element formulations. Its validation is conducted considering experimental and numerical data available in the literature.

The majority of the existing research on masonry deals with running-bond texture within a single-wythe walls case (Pande et al. 1989; Lee et al. 1996; Zucchini and Lourenço 2002; Milani et al. 2007; Ghiassi et al. 2012a,b; Taliercio 2014), being the study of English-bond textures somehow under-investigated (Cecchi and Milani 2008; Casolo and Milani 2013). The novelty of this work is to present two homogenized-based models oriented for both in- and out-of-plane analysis of English-bond masonry structures. Conclusions on the influence of three-dimensional shear stresses and the effect of discontinuities/transversal joints along the masonry thickness are given. In the analysis, both linear and non-linear ranges are accounted for, in which masonry orthotropy and full softening behavior are reproduced (material nonlinearity lumped on mortar joints).

At last, the procedures are fully integrated within the commercial software DIANA (2019) by exploiting its programming features. These are ready to be combined with a FE^2 approach but, noticing the raised issues of full FE-continuum homogenized strategies, especially suitable to be linked with a discrete-FE macro model aiming to obtain reliable results with an attractive computational cost.

3.2 Outline of the approach proposed

Retrieving models at a meso-scale which are both accurate and implementable on simplified two-step procedures is of utmost importance. Here, two meso-scale homogenized models based on the theory of plates are presented aiming at the characterization of the behavior of masonry at a cell level. The accuracy of the results is evaluated through the out-of-plane (OOP) quantities only. To avoid redundancy the in-plane behavior of the elementary cell is not detailed since it is intrinsically considered to derive the OOP quantities.

Three main steps compose the classical procedure of a first-order homogenization scheme (Suquet 1987; Mistler et al. 2007): (i) the definition and solution of the meso-scale problem; (ii) the meso-to-macro transition; and (iii) the macro-scale problem solution. The present chapter focuses on the meso-level, being the formulation and solution of the mesoscopic problem herein presented. Thus, the macro-quantities which serve as input to solve the mesoscopic problem are considered as known in the theoretical formulation, as depicted in Figure 3.1. The general homogenization principles followed are exposed next.

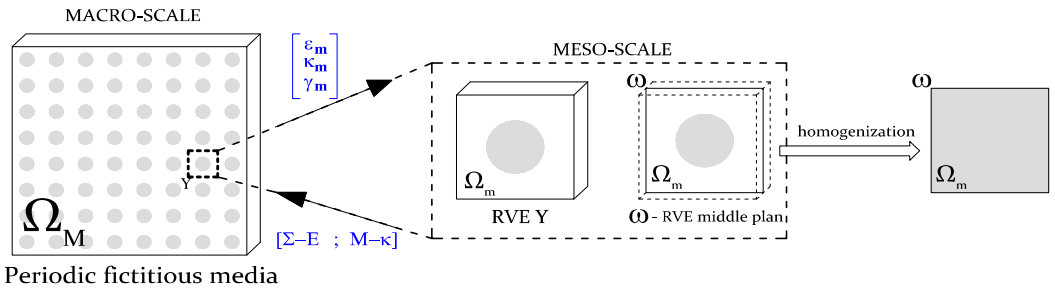

Figure 3.1 – Work-flow of the proposed unit-cell homogenized models.

3.3 Mesoscopic boundary value problem

The theoretical background for the development of the homogenized models is presented in what follows and directly applicable. The numerical models rely on a direct homogenization approach, which involves solving a meso-mechanical problem and deriving average field variables. The information is then carried out to the macro-scale so that it constitutively describes the behavior of the structure.

The definition of a proper RVE is essential, as it may be statistically representative of the body under study. It may accurately embody the heterogeneities of the material and be with a scale length sufficiently small to guarantee the validity of a first-order multi-step procedure. In the case of regular masonry, like running or English bond textures, periodicity is observed at both scales. When masonry components do not follow a random distribution but instead a periodic one, it is possible to define only one RVE. The RVE will be discussed next for each

considered texture and is herein denoted as Ω_m. The kinematical description of the homogenized based-models for the in-plane case relies on the assumption that the macroscopic strain tensor $\mathbf{E}$ is obtained as the volume average of the mesoscopic strain field $\varepsilon_m = \varepsilon_m(y)$ at each point over the associated RVE:

$$E = \frac{1}{V_m} \int_{\Omega_m} \boldsymbol{\varepsilon_m}\, dV \tag{3.1}$$

where V_m is the volume of the RVE. The mesoscopic strain field can be decomposed into a macro-scale and meso-scale contribution. The latter is referred as an additive decomposition of the mesoscopic strain tensor $\delta\boldsymbol{\varepsilon_m} = \delta\boldsymbol{\varepsilon_m}(y)$, given as:

$$\delta\boldsymbol{\varepsilon_m} = \delta\boldsymbol{E} + \nabla^{s} u_m \tag{3.2}$$

where $\delta\mathbf{E}$ is the applied constant strain tensor over the RVE and $\nabla^{s}\mathrm{u_m}$ is the gradient of the fluctuation displacement field. Taking into account that $\boldsymbol{\sigma_m}$ is the mesoscopic stress field, upon RVE equilibrium, the homogenized generalized stress can be derived. The Hill-Mandell principle is based on an energetic equivalence between the macroscopic and mesoscopic work, as follows:

$$\boldsymbol{\Sigma}\colon \delta\boldsymbol{E} = \frac{1}{V_m} \int_{\Omega_m} \boldsymbol{\sigma_m}\colon \delta\boldsymbol{\varepsilon_m}\, d\Omega \tag{3.3}$$

in which $\boldsymbol{\Sigma}$ is the macroscopic stress tensor. According to the assumed additive decomposition of the mesoscopic strain tensor of Eq. (3.2), it allows obtaining the macro-homogeneity principle as:

$$\boldsymbol{\Sigma}\colon \delta\boldsymbol{E} = \frac{1}{V_m} \int_{\Omega_m} \boldsymbol{\sigma_m}\colon \delta\boldsymbol{E}\, d\Omega + \frac{1}{V_m} \int_{\Omega_m} \boldsymbol{\sigma_m}\colon \nabla^{s} \delta u_m\, d\Omega \tag{3.4}$$

for any kinematical admissible δu_m. Periodic boundary conditions are assumed to solve the BVP. Such consideration is extensively found in homogenization procedures (Blanco et al. 2016) also for the particular case of masonry structures (Cecchi and Sab 2002b; Milani et al. 2006a; Otero et al. 2015). The periodic boundary conditions lead to a kinematical field that enforces anti-periodicity of the tractions to occur. The latter is depicted in Figure 3.2a,b for the mode-I and horizontal bending mode, which can be mathematically described for any pair of boundaries $\{\partial {Y_x}^{-}, \partial {Y_x}^{+}\} \in d\Omega_m$ as:

$$\begin{gathered}
\tilde{u}_{0,m}(\partial {Y_x}^{+}, t) = \tilde{u}_{0,m}(\partial {Y_x}^{-}, t) \text{ , for the in-plane mode-I/IV} \\
\widetilde{\mathrm{w}}_{0,\mathrm{m}}(\partial \mathrm{Y_x}^{+},\mathrm{t}) = \widetilde{\mathrm{w}}_{0,\mathrm{m}}(\partial \mathrm{Y_x}^{-},\mathrm{t}) \text{ , for the horizontal bending of a Kirchhoff-plate theory} \\
\tilde{\theta}_m(\partial {Y_x}^{+}, t) = \tilde{\theta}_m(\partial {Y_x}^{-}, t) \text{ , for the horizontal bending of a Mindlin-plate theory}
\end{gathered} \tag{3.5}$$

in which w is a transversal displacement and θ a rotation term, as depicted in Figure 3.2. Due to the periodicity of the displacement fluctuations on the boundaries, the minimal kinematic constraint required to obtain an admissible mesoscopic generalized displacement fluctuation is given by Eq. (3.6):

$$\int_{\Omega_m} \nabla^s \delta u_m \, d\Omega = 0 \tag{3.6}$$

In this way, Eq. (3.4) can be simplified and expressed as:

$$\boldsymbol{\Sigma} : \delta\mathbf{E} = \frac{1}{V_m} \int_{\Omega_m} \boldsymbol{\sigma}_m : \delta\mathbf{E} \, d\Omega, \quad \forall \delta\varepsilon \tag{3.7}$$

Thus, the corollary of the Hill-Mandell principle is that the homogeneous macroscopic stress tensor $\boldsymbol{\Sigma}$ can be written as the volume average of the mesoscopic stress field $\boldsymbol{\sigma_m} = \boldsymbol{\sigma_m}(y)$ over the RVE:

$$\boldsymbol{\Sigma} = \frac{1}{V_m} \int_{\Omega_m} \boldsymbol{\sigma}_m \, d\Omega \tag{3.8}$$

The variational principle and the use of periodic boundary conditions allow concluding that the external surface traction and body force field in the RVE are reactive terms over the imposed kinematical conditions. These kinematical boundary conditions are dependent on the deformation modes considered at the meso-mechanical level. Thus, the in-plane static equilibrium of the RVE is reached, for each kinematic constraint considered, without any external surface traction and body force terms, see Figure 3.2c.

The variational principle holds when accounting for the out-of-plane quantities to assure the energy consistency between scales. The difference lies in the replacement of generalized stresses through moment and force terms, as seen in Eq. (3.9):

$$\boldsymbol{N} : \delta\boldsymbol{E} + \boldsymbol{M} : \delta\boldsymbol{\chi} = \frac{1}{V_m} \int_{V_m} \boldsymbol{\sigma}_m \delta\boldsymbol{\varepsilon_m} \, dV_m \tag{3.9}$$

Where $\mathbf{N}$, $\mathbf{M}$, and $\boldsymbol{\chi}$ are the macroscopic membrane force, bending moment and curvature tensors, respectively and $\boldsymbol{\chi}$ is given by Eq. (3.10):

$$\boldsymbol{\chi} = -\frac{1}{V_m} \int_{\Omega_m} u_z \, dV \tag{3.10}$$

Note that u_z is the projection of the out-of-plane displacement vector defined by the periodic constraints applied to the RVE. Likewise, to consider the out-of-plane shear contribution, the term $\mathbf{T}\delta\boldsymbol{\gamma}$ may be added to the left-hand side of the variational principle of Eq. (3.9), where $\mathbf{T}$ is the macroscopic transverse shear force tensor and $\boldsymbol{\gamma}$ is the transverse shear strain vector.

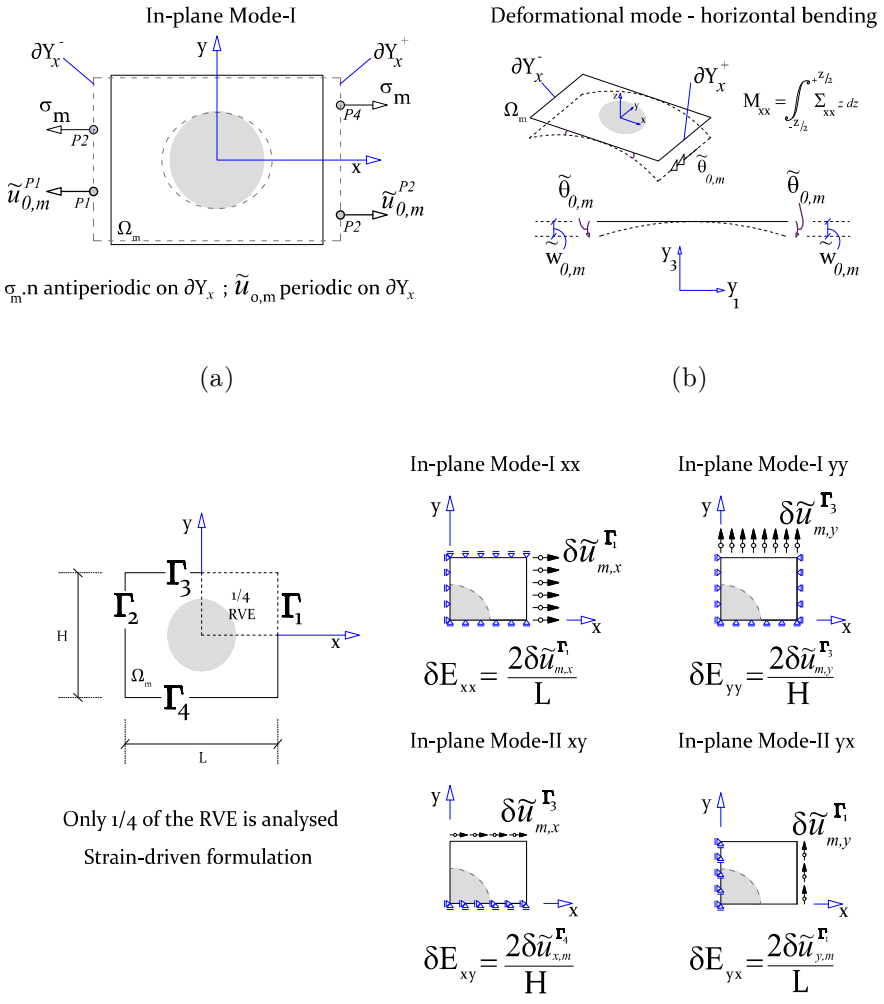

Figure 3.2 – Notation adopted at a meso-scale for a fictitious honeycombed RVE with double-symmetry: (a) for the in-plane mode-I, (b) for the horizontal bending deformation mode, and (c) representation of the boundary conditions and homogenized strain tensor components E_{ii} for the in-plane deformation modes.

3.4 Nonlinear unit-cell homogenized models

The classical first-order homogenization theory is extended to develop two meso-mechanical models within a strain-driven formulation. Both models have been developed in DIANA (2019) by exploiting the software programming capabilities and making use of the available FE library and constitutive material models. A python script has been developed to provide a fully automatic procedure between the modeling, processing and post-processing stages. The proposed homogenized procedures try to cover three features: (i) be capable of studying a RVE of a given periodic masonry texture; (ii) be accurate on estimating its mesoscopic linear and

nonlinear behavior, in terms of deformation, stresses and damage propagation; (iii) be adaptable to a FE^2 approach with the aim of estimating the macro-behavior of a given structure.

The numerical strategies that adopt FE-homogenization schemes typically consider the use of a direct numerical simulation. Plate models based on a plane-stress theory for membrane loading and within a Kirchhoff-Love or Mindlin-Reissner plate theory for out-of-plane load cases are very attractive (Cecchi et al. 2007; Milani et al. 2007; Cecchi and Milani 2008; Otero et al. 2015; Petracca et al. 2016). These strategies allow reducing the RVE three-dimensional problem to a two-dimensional one, in which the middle plane of the plate ω is considered, hence obtaining solutions with low computational processing times. Nonetheless, assuming the media as an infinitely thin membrane may not be the best procedure for problems where three-dimensional shear effects play an important role. Likewise, if discontinuities are present along the thickness direction (as it is the case of an English masonry bond), considering the material to be homogeneous over the thickness is not representative. In this context, this chapter tries to also give a contribution about the range of validity of the latter framework and if these can replace a full component description of the material.

To accomplish the purpose just stated, two homogenized–based approaches are presented in what follows for the in- and out-of-plane behavior characterization. One derives from the Kirchhoff-Love and the other from the Mindlin-Reissner plate theory, see Figure 3.3b. For the sake of conciseness, these models will be designated hereafter as KP and MP model, respectively, and an exposition of the key features will be briefly presented. For extended details on the theoretical background regarding the plates kinematics and constitutive response, the reader is referred to E. Reissner (1975); Hughes and Tezduyar (1981); and Zienkiewicz and Taylor (2000). Both KP and MP models are geometrical linear, meaning that the reference plane remains with the initial relative configuration. Instead, material nonlinearity (including cracking) is considered.

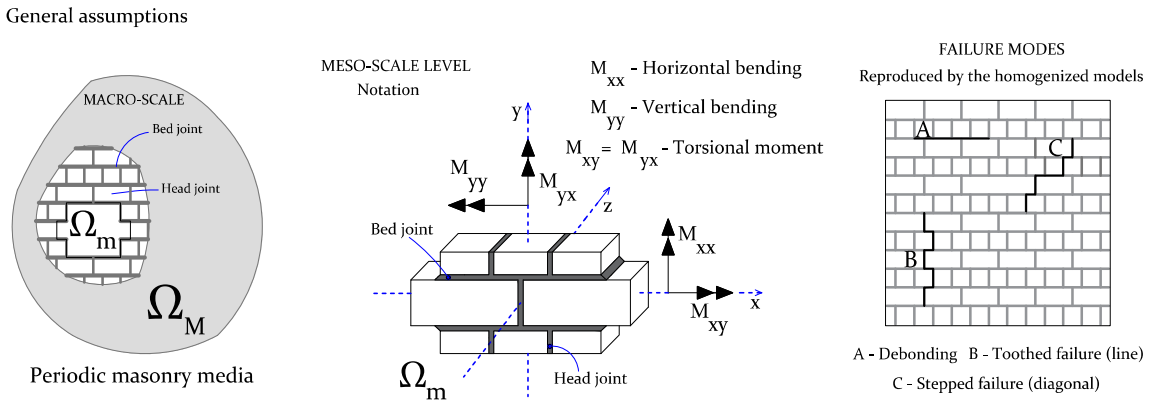

(a)

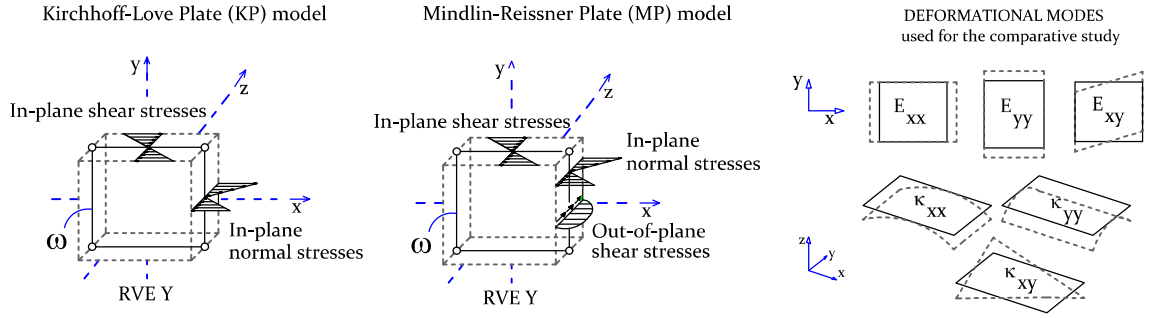

(b)

Figure 3.3 – (a) General assumptions and failure modes considered for the comparative study between the unit cell homogenization procedures. (b) A brief description of the Kirchhoff-Love and Mindlin-Reissner plate elements and the deformation modes assumed.

3.4.1 The Kirchhoff-Love plate KP homogenized model

The KP model assumes that, at the meso-scale level, masonry behaves as a planar 2D continuum according to a Kirchhoff-Love plate. This is driven by the assumption that the plane section remains normal and straight in relation to the deformed reference plane. The out-of-plane displacement does not vary in the thickness direction and it is assumed that the out-of-plane direct stress component σ_{zz} is negligible. Such hypothesis follows the plane-stress condition. The KP model is thus based on a decoupled characterization between the membrane and bending behavior, achieved respectively through a plane-stress coupled with a Kirchhoff plate bending model. The generalized displacement vector for a point of the plate is given as $u = [u_x \quad u_y \quad u_z]^T$ where u_x, u_y are the in-plane and u_z the out-of-plane displacement quantity. The normal strains ε_{zz} are negligible and disregarded. The terms θ_x and θ_y are rotations about the global coordinate system. Basically, according to the elasticity theory, the vector with the unknown quantities of the associated strains is given by $\varepsilon = [\varepsilon_{xx} \quad \varepsilon_{yy} \quad \gamma_{xy} \quad \kappa_{xx} \quad \kappa_{yy} \quad \kappa_{xy}]^T$.

Here, the in-plane strains are defined as $\varepsilon_{xx} = \frac{\partial u_x}{\partial x}, \varepsilon_{yy} = \frac{\partial u_y}{\partial y}, \gamma_{xy} = \frac{\partial u_x}{\partial y} + \frac{\partial u_y}{\partial x}$ and the curvature terms of the deflected reference mid-plane as $\kappa_{xx} = \frac{\partial \theta_y}{\partial x}, \kappa_{yy} = \frac{\partial \theta_x}{\partial y}, \kappa_{xy} = \frac{\partial \theta_y}{\partial y} - \frac{\partial \theta_x}{\partial x}$, see Figure 3.2a.

The transverse shear strains are neglected, being $\gamma_{xz}, \gamma_{yz} = 0$. The constitutive relation of the homogeneous equivalent material of the RVE is obtained for each in-plane deformation mode considered (Figure 3.3b), i.e. for the tension (mode-I), in-plane shear (mode-II) and compression (mode IV). The condition of null out-of-plane shear strains γ_{xz} and γ_{yz} imposed by the Kirchhoff plate theory leads to disregarding their effect on the resultant moments. However, the out-of-plane shear forces Q_x and Q_y are not totally omitted once their contribution is implicitly necessary to fulfil the equilibrium equation of the plate. This highlights why the comparison described next in section §3.6 is performed in terms of coupled stresses-curvature relations.

3.4.2 The Mindlin-Reissner plate MP homogenized model

It is well known that in cases where the structure follows a planar behavior or when the thickness is not relevant (usually referred as 1/10 of the structural dimension), analyzing the problem within a two-dimensional approach as the thin plate theory is appropriate. Nevertheless, for out-of-plane loading and in presence of a thick or moderately thick structural element, an enrichment of the latter theory is necessary (E. Reissner 1975; Hughes and Tezduyar 1981; Zienkiewicz and Taylor 2000; Arnold et al. 2002). Such observations are drawn upon a macro-scale level, as for instance Arnold et al. (2002) and Cecchi and Milani (2008) for the behavior of masonry structures. Nevertheless, the investigation over the difference between a three-dimensional model and two-dimensional one (as are the KP and MP models) is still lacking at a meso-scale. Even if the analyses are performed at different scales, the physical behavior is the same and thus identical conclusions are expected. Still, it is intended to carry such study to investigate the difference between strategies due to the presence of three-dimensional effects.

In this scope, a strategy based on the first-order shear deformation theory is presented (MP model) which allows including three-dimensional effects, even if in a simplified manner through the out-of-plane shear components and, consequently, increasing the results accuracy for thick and moderately thick plates. Similarly, the membrane behavior follows a plane-stress element formulation, yet the primary stresses are derived through moments and forces rather than Cauchy stresses. The bending behavior is decoupled from the latter and follows the Mindlin-Reissner theory. The in-plane strain quantities (ε_{xx} ,ε_{yy} , γ_{xy}) vary in a linear way

through the masonry thickness and the transverse shear strains are accounted and derived as $\gamma_{xz} = \frac{\partial u_z}{\partial x} + \theta_y$; $\gamma_{yz} = \frac{\partial u_z}{\partial y} - \theta_x$.

Such quantities vary in a parabolic way over the thickness but, for numerical convenience, are assumed to be constant within the classical adjustment approach (E. Reissner 1975). A shear correction factor equal to $S_r = 1.2$ affects these quantities, so that the equivalent constant shear stress diagrams have a shear strain energy similar to the actual parabolic behavior on the area under reference. So, the generalized strain vector is composed by eight unknown parameters in which the mesoscopic generalized displacement fluctuation field is decomposed in the membrane, bending and out-of-plane shear components.

For both KP and MP models, the homogenization technique is followed and, by solving the internal static RVE equilibrium using a classical FE-procedure, the homogenized Σ and E quantities are derived. Furthermore, the macro-stress couples are obtained by through-the-thickness integration of the homogeneous macro-stresses according to Eq. (3.11). The numerical integration is performed accounting only the mid-plane reference surface ω. The obtained homogenized moment-curvature relations are defined per unit of length.

$$\begin{aligned} M_{xx} &= \int_{-z/2}^{z/2} \boldsymbol{\sigma}_{m,xx} z \, dz \\ M_{yy} &= \int_{-z/2}^{z/2} \boldsymbol{\sigma}_{m,yy} z \, dz \\ M_{xy} &= \int_{-z/2}^{z/2} \boldsymbol{\sigma}_{m,xy} z \, dz \quad , \quad M_{xy} = M_{yx} \end{aligned} \tag{3.11}$$

3.4.3 RVE definition and FE-modelling assumptions

The definition of the RVE being analyzed at a meso-scale is required. It is generally accepted that the RVE needs to be statistically representative of the macro-scale level. It may contain a sufficient number of heterogeneities which possibly reproduces well the macro-behavior (Hill 1965) and sufficiently small to respect the principle of scales separation of a first-order homogenization theory. In the case of running- and English-bond masonry walls, the choice of a proper RVE is somehow simplified due to the regular and periodic disposal of the constituents' arrangement. Even so, there are several RVE possibilities but, for both the analyzed textures, the recommendations by Anthoine (1995) are followed and presented in Figure 3.4a.

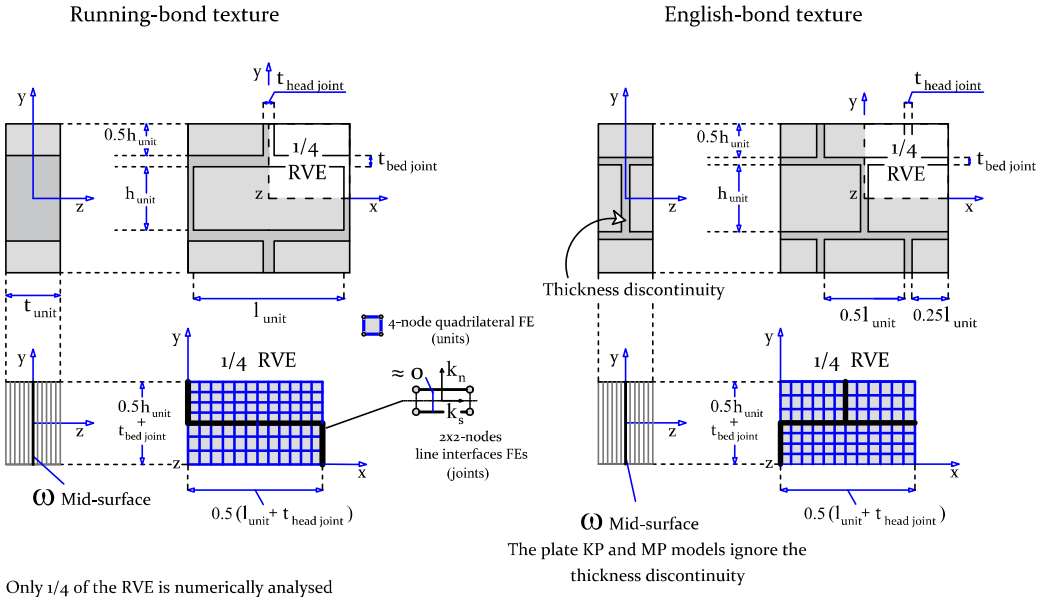

(a)

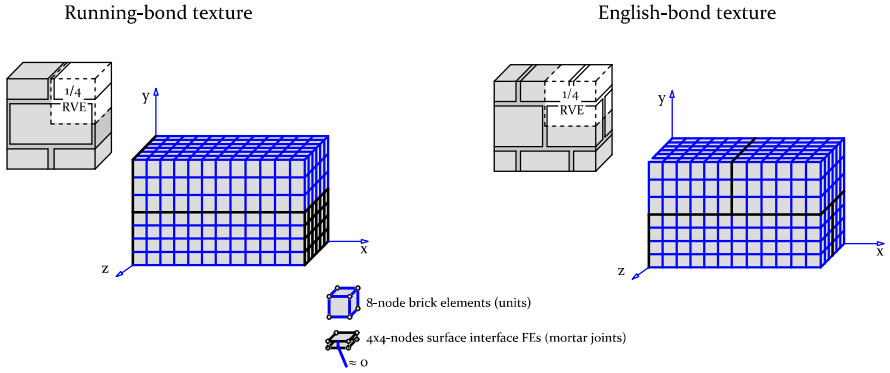

(b)

Figure 3.4 – Meso-modelling of the running- and English-bond masonry RVE considered for the: (a) KP and MP models; (b) DNS models.

In the modeling process, brick units are considered elastic and discretized as quadrilateral FE-plate elements with linear interpolation and a 2x2 Gauss-quadrature. A fine refinement has been adopted for both models, even if coarser meshes with few degrees of freedom seem adequate to assess the kinematic study of a regular and periodic RVE; as demonstrated by the simplified model of Milani et al. (2006c) and by closed-form based solutions by Taliercio (2014). Mortar joints are modeled as zero-thickness line interface elements which concentrate the material nonlinearity. Such a hypothesis seems to increase the efficiency of the framework by avoiding convergence issues related to distorted quadrilateral elements. However, the numerical consequences of using a strain-softening constitutive model may not be avoided, as stated in the application section §3.6, for the MP model in which five integration points (Simpson rule) have been defined in the thickness direction. A three-dimensional meso-model (direct numerical

simulation, DNS model) is also developed for the meso-mechanical validation described in section §3.5. In order to allow a numerical comparison and draw consistent conclusions, the DNS model follows the same modeling assumptions, i.e. in terms of material properties, plasticity model for joints and mesh-size (in the plane) with six elements in the thickness (Figure 3.4b).

To characterize the full masonry behavior, i.e. to capture the post-peak regime, nonlinear analyses need to be performed. The BVP is solved using the software DIANA (2019), where a line search algorithm has been used simultaneously with a secant BFGS method to deal with softening, see Crisfield (1981) and the DIANA (2019) documentation for more details. An arc-length procedure with a normal plane update is also at disposal, yet theoretically unnecessary within the scope of the present KP and MP homogenized schemes to find the converged solution.

3.4.4 Plasticity model for joint interfaces

Aiming at the decrease of the computational effort, the material nonlinearity is assumed to be lumped in the joints. This seems to be adequate for strong block masonry structures, since: (i) in absence or even in presence of small levels of any pre-compression state, cracking or crushing of bricks is unlikely to happen; (ii) the obtained behavior seems in agreement with experimental data, in which crack onset and propagation tend to follow a zigzag pattern along joints and between bricks (Sinha 1978; Herbert et al. 2014).

A multi-surface plasticity model from Lourenço and Rots (1997) (the so-called composite interface model) is considered for the interface elements used for the KP strategy. For the MP and DNS strategies, the model from by Zijl (2000) is adopted, which is an extension of the latter to allow its use in a three-dimensional media, see Figure 3.4b. The plasticity models can reproduce fracture, frictional slip and crushing along the interface elements.

The constitutive interface model is defined by a convex composite yield criterion with three individual functions, i.e. a tension cut-off (Eq. (3.12)), a Mohr-Coulomb criterion for shear (Eq. (3.13)) and a cap in compression (Eq. (3.14)). Softening behavior is represented in all the modes. The tensile criterion (Figure 3.5b) reads:

$$f_t(\boldsymbol{\sigma}, \kappa_t) = \boldsymbol{\sigma} - \overline{\sigma}_t(\kappa_t) \;\; and \;\; \overline{\sigma}_t = f_t \exp(-\frac{f_t}{G_f^I}\kappa_t) \tag{3.12}$$

The shear criterion (Figure 3.5c) is given as:

$$f_s(\boldsymbol{\sigma}, \kappa_s) = |\tau| + \boldsymbol{\sigma} tan\phi - \overline{\sigma}_s(\kappa_s) \;\; and \;\; \overline{\sigma}_s = c\, \exp(-\frac{c}{G_f^{II}}\kappa_s) \tag{3.13}$$

For the compressive yield function (Figure 3.5d):

$$f_c(\boldsymbol{\sigma}, \kappa_c) = {}^1\!/_2(\boldsymbol{\sigma}^T \boldsymbol{P}\boldsymbol{\sigma}) + \boldsymbol{p}^T\boldsymbol{\sigma} - \overline{\sigma}_c{}^2(\kappa_c) \tag{3.14}$$

Here, $\boldsymbol{\sigma}$ is the generalized stress, ϕ is the friction angle; $\boldsymbol{P}$ is a projection diagonal matrix and $\boldsymbol{p}$ a projection vector based on material parameters; G_f^I, G_f^{II} and G_f^{IV} are the mode-I, mode-II and the compressive fracture energy terms, respectively; $\overline{\sigma}_t$, $\overline{\sigma}_s$ and $\overline{\sigma}_c$ are the effective stresses of each the adopted yield functions, governed by the internal scalar variables κ_t, κ_s and κ_c, respectively. Note that the typical compressive hardening/softening law $\overline{\sigma}_c(\kappa_c)$ is composed by three branches as observed in Figure 3.5d. The model follows the laws $\overline{\sigma}_1(\kappa_c), \overline{\sigma}_2(\kappa_c)$ and $\overline{\sigma}_3(\kappa_c)$ defined by Lourenço and Rots (1997) and Zijl (2000).

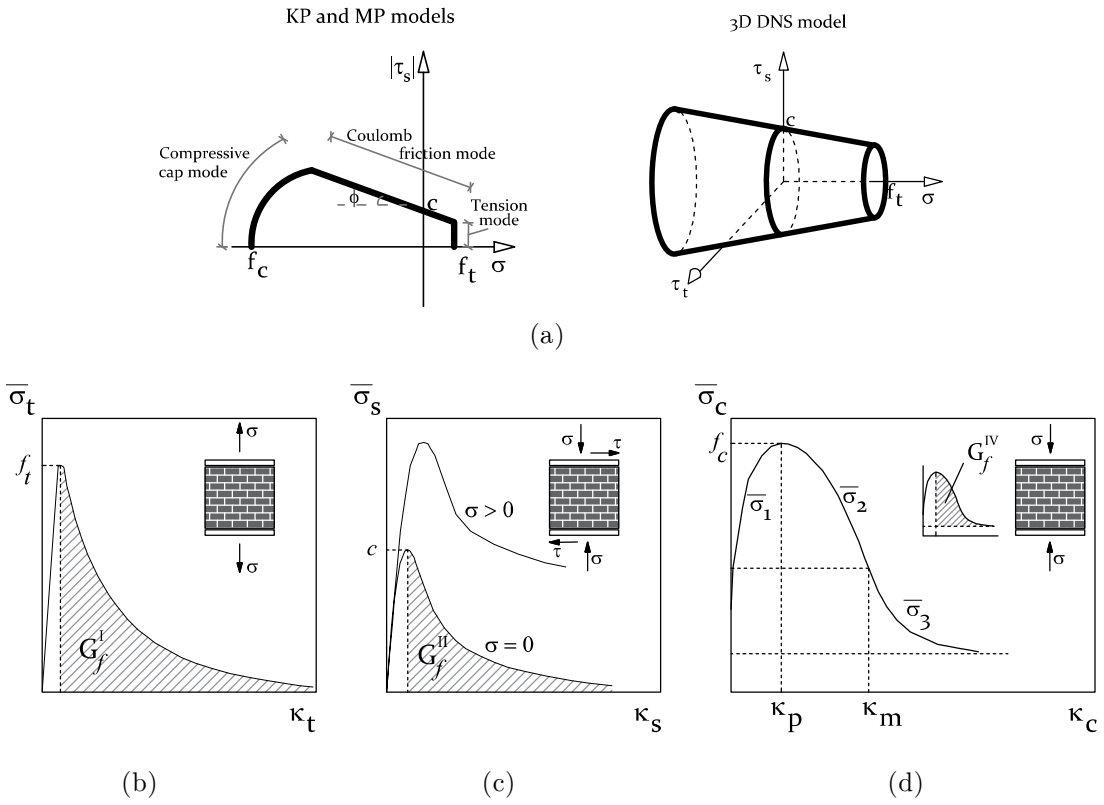

Figure 3.5 – Mortar joints: (a) adopted multi-surface plasticity model for the line (Lourenço and Rots 1997) and surface (Zijl 2000) interface FEs; Behavior of quasi-brittle materials under (b) tensile loading (mode-I, f_t is the tensile strength); (c) shear loading (mode-II, c is the cohesion) accounting with a potential pre-compression level; and (d) compressive load (f_c is the compressive strength; p and m are the peak and medium values, respectively).

It may be highlighted that a penalty approach is not followed by the adopted interface FEs to phenomenologically represent the behavior of masonry crushing. Such strategy is usually at disposal in advanced FE software's (e.g. ABAQUS (2013)), to model the physical contact

between units where impenetrability is enforced. Here, penetration and overlapping between neighboring brick units can occur which does not blur the accuracy of the in- and out-of-plane quantities derived; particularly if noted that a weak mortar masonry is being studied and so low compressive levels of stress are expected.

3.5 Meso-mechanical validation: OOP behavior of masonry

Three masonry failure modes are suitable to be represented. The first one is the debonding, toothed (line) and stepped (diagonal) failures, as denoted in Figure 3.3a. The debonding mode is dependent on the vertical bending moment faced by the masonry (one-way bending). It can occur in cases where a given wall is supported at its upper and bottom edges and laterally unrestrained. This is, for periodic bonds as the running- and English textures, the direction with lower flexural capacity since torsion plays a negligible role; hence very dependent on the level of axial compressive loading and on the boundary conditions.

The toothed and stepped type of failures are related to the horizontal bending behavior. These are typically associated with strong masonry, meaning that masonry units present much higher strength values than mortar bonds. Such assumption precludes the manifestation of units crushing. Toothed failure follows a vertical alignment defined by cracking on the head and half of the bed joints, which is generally caused by one-way bending. Torsional shear has a key role in converse to vertical flexural movements. So, the horizontal flexural strength (around head joints), torsional shear, residual friction (post-ultimate), and compressive axial loading rule the observed behavior and capacity (Lawrence 1995).

Finally, the stepped failure is associated with two-way bending leading to diagonal cracking and is thus more complex. It involves the vertical, horizontal and torsional moments actions and so both the flexure tensile and torsional capacities of the bed and head joints contribute for the ultimate strength. In this scope, the ability of the homogenization models to represent the OOP behavior of masonry is addressed next. Three main constitutive key features for numerical models aiming at the analysis of masonry are herein approached: (i) the correct representation of the elastic stiffness properties; (ii) the masonry orthotropic behavior due to the arrangement of the units and joints; and (iii) the role of the vertical membrane pre-compression states, typically due to masonry self-weight and gravity loads in general.

3.5.1 Masonry homogenized elastic stiffness

The homogenized quantities of a running-bond masonry RVE, in terms of elastic stiffness components, are derived next. The evaluation of the proposed KP and MP approaches is set through the results of a detailed FE meso-model and data from a simple closed-form solution by Zucchini and Lourenço (2002). A running bond RVE with dimensions equal to 210×100×52 mm^3 and mortar joints of 10 mm of thickness is studied. The considered material elastic properties are the following ones: $E_{brick} = 20{,}000\ MPa$; ν_{brick}=0.15; $E_{mortar} = E_{brick}/r$ and $\nu_{mortar} =$ 0.15. The elastic homogenized stiffness parameters (Young's and Shear modulus) are assessed for several ratios $r = E_{brick}/E_{mortar}$, ranging from 1 to 1000. Such broad range allows to represent the potential different stiffness ratios both in the elastic and in the inelastic range, in which the tangent and secant stiffness degradation of mortar joints occur.

Note that the linear elastic relation between the generalized stresses and strains of the interface FEs is given by the classical constitutive equation of Hooke's law, $\sigma = D\varepsilon$. Considering a line FE interface (for the adopted plate theories KP and MP models), the elastic stiffness matrix D is given as $D = diag\{k_n, k_s\}$. The values of the normal (k_n) and shear (k_s) mortar joints stiffness terms can be easily computed. One possibility is to neglect the contribution of the brick-mortar interface and to compute these parameters as $k_{n,1} = E_{mortar}/t_{joint}$ and $k_{s,1} = G_{mortar}/t_{joint}$, where $G_{mortar} = E_{mortar}/(2(1+\nu_{mortar})$ is the mortar shear modulus. Another possibility is to follow the suggestions given in CUR (1994) in which, under the assumption of a stack bond where a serial chain connection represents the masonry components (with uniform stress distributions in both unit and mortar joints), the latter stiffnesses' values read:

$$k_{n,2} = \frac{E_{brick}E_{mortar}}{t_{joint}(E_{brick} - E_{mortar})} \tag{3.15}$$

$$k_{s,2} = \frac{G_{brick}G_{mortar}}{t_{joint}(G_{brick} - G_{mortar})} \tag{3.16}$$

In this study a mean value of both approaches has been considered, meaning that k_n and k_s are given as $0.5(k_{n,1} + k_{n,2})$ and $0.5(k_{s,1} + k_{s,2})$, respectively.

An accurate detailed (interfaces explicitly modeled) FE meso-model (DNS model) is set as a reference. The use of this numerical model as a validation tool is clear since the elastic homogenized masonry stiffness calculation does not offer a complex problem nor novelty from a numerical standpoint. Such a procedure is also convenient because a numerical study encompassing a wide range of components stiffness ratios is easily carried out. Reproducing the same data experimentally would require a thorough and expensive campaign. The obtained

results are reported in Figure 3.6 and it can be observed how both the KP and MP plate models estimate well the elastic homogenized stiffness parameters. The agreement is very good according to the DNS model, being the error less than 5%. Some differences may be found with the model proposed by Zucchini and Lourenço (2002) especially for the Shear modulus (see Figure 3.6b), but still, a good agreement is achieved with a meso-mechanical procedure based on a closed-form solution.

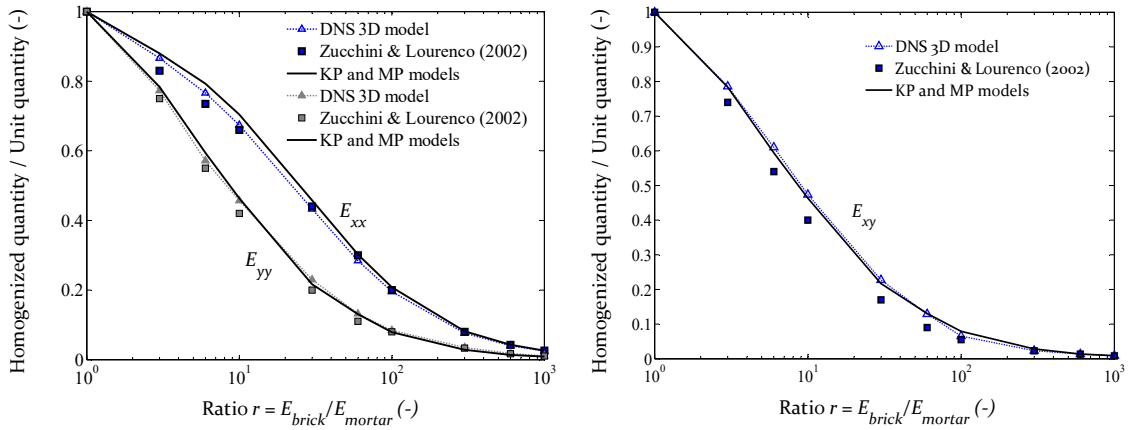

Figure 3.6 – Comparison between the homogenized in-plane elastic properties obtained with a detailed FE meso-model (DNS 3D model), the KP and MP models and from the closed-form solution by Zucchini and Lourenço (2002): (a) Young's modulus; (b) Shear Modulus.

3.5.2 Masonry orthotropic behavior: one- and two-way bending

Masonry is known to present a well-marked anisotropic behavior. The complexity increases because joints constitute planes of weakness which, depending on the stiffness ratio between mortar and brick constituents, may have a strong effect. Accounting for the non-linear behavior of masonry is of prime importance as it can have an impact on the structural overall behavior, energetic dissipation and mechanisms creation.

Two experimental campaign datasets are considered to validate the proposed homogenized models, i.e. the studies from Pluijm (1999) and Gazzola et al. (1985). The former is herein firstly addressed and focuses on the experimental test of several small panels in four-point bending, in which the bed joint angle with the normal assumes the values of 0, 30 and 90 degrees (defined as vertical, inclined and horizontal bending respectively). No pre-compression states are considered neither the post-peak information is available. Yet, both elastic limit and peak strength values are accessible within a curvature-bending moment diagram, which still constitutes a good source of information.

The panels were built with standard Dutch bricks, with dimensions 200×52×100 mm^3, and mortar joints with 10 mm of thickness. The elastic material properties assumed are the following ones: $E_{brick} = 11{,}000\ MPa$; $v_{brick} = 0.20$; $E_{mortar} = 4{,}000\ MPa$ and $v_{mortar} = 0.20$. The inelastic mechanical parameters for mortar joint interfaces are given by $f_t = 0.25\ MPa$, $G_f^I = 0.006\ N/mm$, $c = 0.60\ MPa$, $G_f^{II} = 0.035\ N/mm$, $\phi = 30$ degrees, $f_c = 20.0\ MPa$ and $G_f^{IV} = 4.0\ N/mm$. The latter values follow the average experimental values (Pluijm 1999), and include missing parameters by inverse fitting. The comparison between numerical and experimental results are summarized in Figure 3.7 in terms of bending moment vs. curvature curves. Data available from an elastic-plastic model for mortar joints by Milani and Tralli (2011) is also used for comparison purposes.

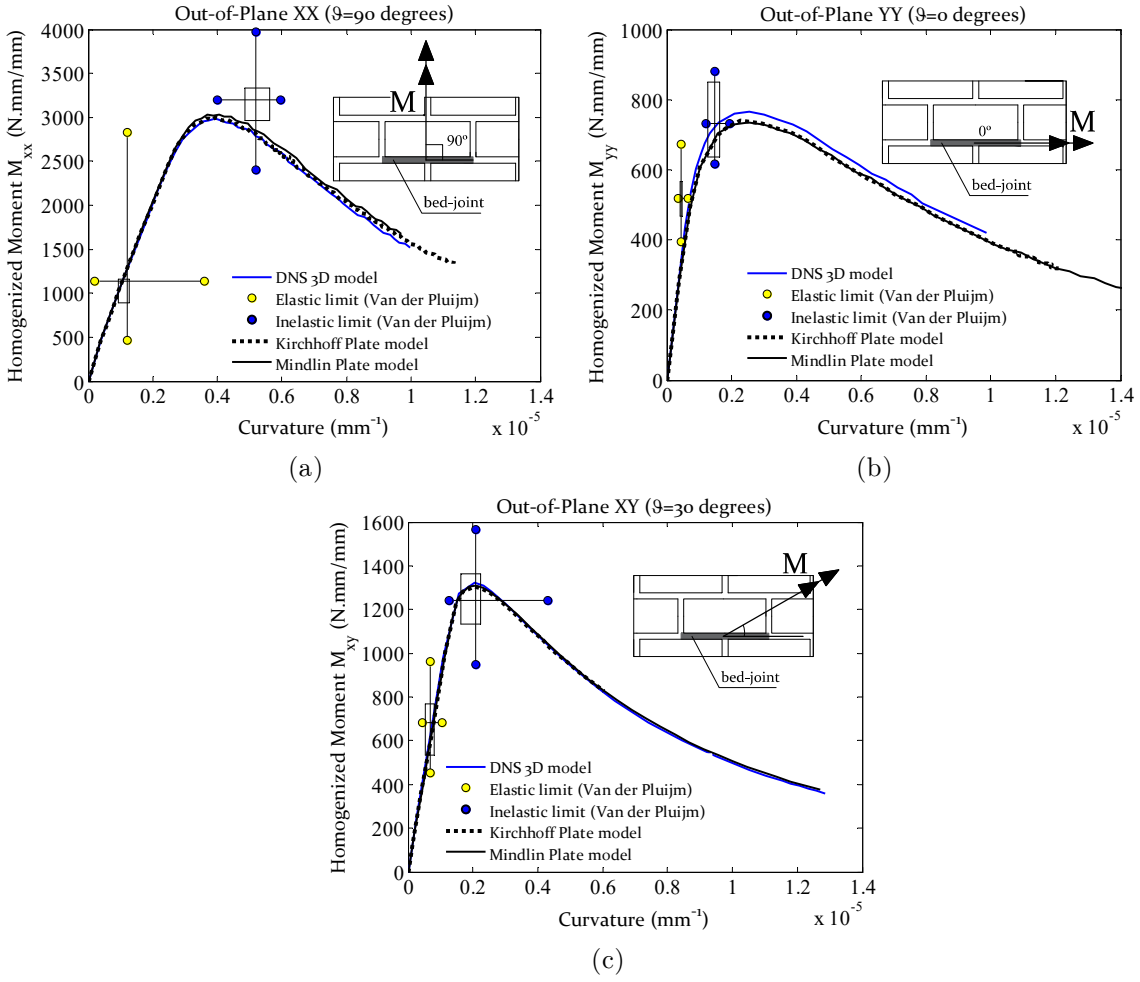

Figure 3.7 – Comparison between the experimental data (using boxplots) from Pluijm (1999) and the numerical results obtained from the homogenized procedures proposed in terms of moment vs. curvature curves: (a) moment with a ϑ=90 degrees; (b) moment with a ϑ=0 degrees; and (c) moment with a ϑ=30 degrees.

The different proposed homogenized procedures derive similar results. Thus, the three-dimensional shear effects seem to be negligible in this case, because the maximum relative

difference found is about 3% (for the vertical bending moment peaks) between the DNS model and MP or KP models. One may also conclude that, despite the existent experimental data dispersion, the models reproduce well the orthotropy of masonry and its elastic bending stiffness. The second set of experimental data used to study the material orthotropic behavior derives from the research of Gazzola et al. (1985) and Gazzola and Drysdale (1986). This will be achieved by comparing the experimental peak flexural strength values. This represents a good indicator to analyze the orthotropic behavior of masonry when subjected to OOP loading and within a de-bonding (vertical moment), stepped (inclined moment) or toothed (horizontal moment) failure pattern of masonry. The authors tested 25 wallets of hollow concrete block masonry, with different dimensions, within a running-bond texture in four-point bending. The bed joints angle with the loading direction ϑ were considered to vary between 0,15,45,75 and 90 degrees. The units' dimensions are 390×190×150 mm^3 and the mortar joints have a thickness equal to 10 mm. The elastic material properties assumed are the following: $E_{brick} = 10{,}000\ MPa$; $v_{brick} = 0.20$; $E_{mortar} = 4{,}000\ MPa$ and $v_{mortar} = 0.25$; and the inelastic mechanical parameters for mortar joint interfaces are given by: $f_t = 0.15\ MPa$, $G_f^I = 0.018\ N/mm$, $c = 0.38\ MPa$, $G_f^{II} = 0.04\ N/mm$, $\phi = 30$ degrees, $f_c = 20.0\ MPa$ and $G_f^{IV} = 4.00\ N/mm$.

Only tensile flexural strength peaks are at disposal and so the latter nonlinear material properties of mortar joints were tuned to fit the values of the horizontal ($\vartheta = 90$ degrees) and vertical ($\vartheta = 0$ degrees) flexural strengths f_{tm}, given by 0.92 MPa and 0.37 MPa respectively. The elastic material properties, even if assumed, are not relevant as these have a minor influence upon the moment capacity. The peak flexural strength is computed for each bed joint angle ϑ and the comparison between numerical and experimental data is showed in Figure 3.8.

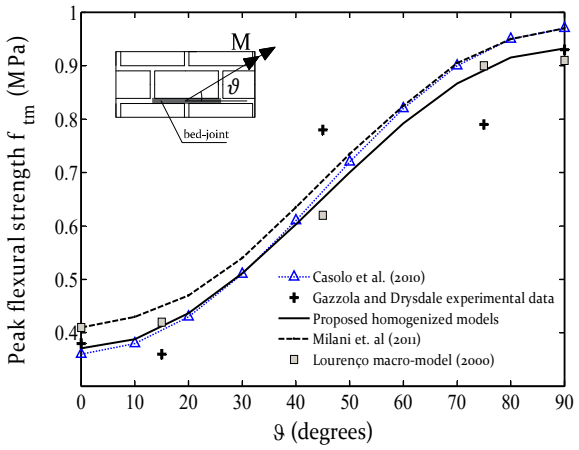

Figure 3.8 – Comparison between the experimental data from Gazzola et al. (1985) and Gazzola and Drysdale (1986) and the numerical results obtained from the proposed homogenized procedures in terms of peak flexural strengths according to the angle ϑ with the bed joint.

No significant differences can be reported among the proposed homogenization approaches and, therefore, these are merged in Figure 3.8 as one dataset and labelled as proposed homogenized models. Additionally, information regarding the anisotropic macro-model by Lourenço (2000), a simple elastic-plastic homogenized model by Milani and Tralli (2011) and a kinematic-based homogenized model by Casolo and Milani (2010) are also presented. It is possible to see that all the homogenized models seem capable to reproduce well the masonry orthotropy and provide accurate results.

3.5.3 Pre-compression state condition

The previous section demonstrated that masonry orthotropy is evident for walls exhibiting a regular texture. Masonry units staggering is responsible for a horizontal bending (i.e. with rotation along a vertical axis) stiffer and more resistant than the vertical one (i.e. with rotation along a horizontal axis), as the bed joint contributes in torque to increase stiffness and strength. This implies that tangential stresses acting on bed joints play a significant role in the horizontal bending increase, while they are not relevant in vertical bending. In this scope, the effect of pre-compression states on the ultimate torsional moment and horizontal bending capacity is assessed here.

A vertical membrane pre-compression, typically due to masonry self-weight and gravity loads in general, plays a fundamental role in the increase of the ductility and OOP strength, as shown by Milani and Tralli (2011). Two strategies can be pursued to account for this effect in the obtained homogenized curves. One is to compute the generalized pre-compression stress σ_v and invoke it within the interface Mohr-Coulomb shear criterion term $\sigma_v tan\phi$ in Eq. (3.13); the other is during the integration of the $\Sigma - \mathrm{E}$ curves by enforcing an organic force balance given by $\sum Forces = -\sigma_v t$ (t is the thickness of the wall). Both strategies are suitable, but the former is considered due to its practicability.

The experimental program performed by Willis et al. (2004) is herein used for the third and last validation key point. Firstly, the effect of pre-compression on the torsional moment capacity and residual friction are analyzed. Values of $\sigma_{\mathrm{v}} = 0.25$ MPa and $\sigma_{\mathrm{v}} = 0.50$ MPa are assumed. The test arrangement is depicted in Figure 3.9, wherein only half length of the clay brick units has been considered with the bedding mortar (only C4 batch is adopted for conciseness, see Willis et al. (2004)). The aim is to represent the overlapping between adjacent brick courses for running-bond masonry. The clay brick units have nominal dimensions of 230×65×114 mm^3 ($length \times height \times thickness$) and the mortar joints have 10 mm of thickness.

The adopted material properties have been calibrated to respect the experimental tensile flexural strengths in a uniaxial direction.

The results of this first validation are gathered in Figure 3.9. Although the experimental variability is relevant, the behavior predicted by the proposed homogenized models is in good agreement with the experimental mean one. This is especially clear for the peak moment capacity with results within 5% difference for $\sigma_v = 0.00$ MPa and $\sigma_v = 0.25$ MPa, and 10% difference for $\sigma_v = 0.50$ MPa. The experimental post-peak region has been identified by a descending branch and a horizontal plateau identifying the ultimate strength. The sharp strength deduction obtained after peak indicates a poor control of the tests and the numerical results do not have such a steep slope as the experimental mean curve. Nonetheless, the numerical curve is, for all the cases, in-between the experimental data.

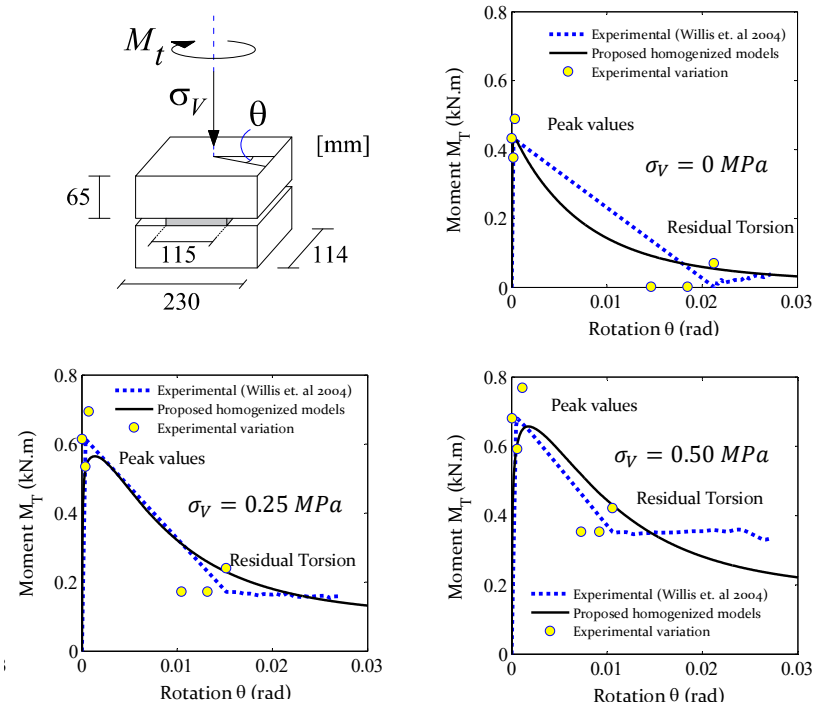

Figure 3.9 – Torsional moment capacity test: comparison between the results from the experimental torsional moment test by Willis et al. (2004) (mean curve) and the ones obtained with the proposed homogenized models.

The second experimental test used intends to study the horizontal bending moment capacity when different levels of pre-compression σ_v exist. Twenty-five brickwork panels were subjected to a two-point type of loading, and the load-deflection behavior was collected for four levels of σ_v (0.00, 0.0075, 0.15 and 0.25 MPa). The reader is referred to Willis et al. (2004) for details about the experimental setup. The experimental range of the horizontal flexural tensile strength is 0.61-0.71 N/mm^2, wherein a value of 0.66 N/mm^2 has been considered. The adopted material

properties were tuned to respect the latter value but, as well, the previous torsional capacity, especially to what concerns the shear criterion parameters (c, ϕ, G_f^{II}). The elastic properties are given as $E_{brick} = 15{,}000\ MPa$; $v_{brick} = 0.15$; $E_{mortar} = 2{,}000\ MPa$ and $v_{mortar} = 0.20$; and the inelastic mechanical parameters for mortar joint interfaces are given by: $f_t = 0.10\ MPa$, $G_f^I = 0.01\ N/mm$, $c = 0.15\ MPa$, $G_f^{II} = 0.035\ N/mm$, $\phi = 30$ degrees, $f_c = 20.0\ MPa$ and $G_f^{IV} = 4.00\ N/mm$. The results retrieved from the homogenization computations are gathered in Table 3.1. A good agreement with the experimental peak forces is found. Some deviations are noticeable for the peak displacement that may be justified by the high coefficient of variation (CoV) values found (not so successful experimental control). The case with lower experimental uncertainty concerns the test with $\sigma_v = 0.15$ MPa. In fact, from the experimental data, this was the only test where it was possible to derive the full bending moment-curvature path.

Table 3.1 – Experimental and numerical maximum load factor and deflection found for the horizontal bending test by Willis et al. (2004).

Pre-compression (MPa)	$\sigma_v = 0.00$		$\sigma_v = 0.075$		$\sigma_v = 0.15$		$\sigma_v = 0.25$	
Parameters	P_{max} (kN)	Δu_{max} (mm)	P_{max} (kN)	Δu_{max} (mm)	P_{max} (kN)	Δu_{max} (mm)	P_{max} (kN)	Δu_{max} (mm)
Experimental	12.96	0.333	15.57	0.370	14.21	0.374	15.57	0.443
(COV value)	(12%)	(22%)	(12%)	(40%)	(8%)	(14%)	(19%)	(22.5%)
Homogenized models	10.43	0.38	12.46	0.43	14.45	0.52	16.97	0.66
(difference with mean)	(24%)	(14%)	(25%)	(16%)	(2%)	(40%)	(9%)	(33%)
Casolo et. al (2010)	-	-	-	-	14.05	0.45	-	-

Figure 3.10 gathers the experimental curve which allows the comparison with the derived numerical output. The results from another numerical discrete approach from Casolo and Milani (2010) are presented. The homogenized models predict with good accuracy the elastic bending stiffness and the post-peak regime, hence indicating that the torsional calibration performed before has been well achieved. In any case, it is worth mentioning that the model is again able to reproduce well the behavior of masonry at failure in the presence of a pre-compressive state for weak mortar joints and toothed failure mechanisms.

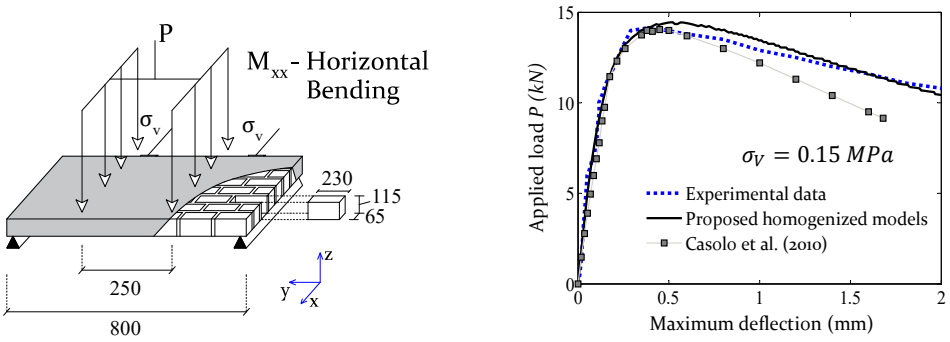

Figure 3.10 – Horizontal bending capacity test: comparison between the experimental results from Willis et al. (2004) and the numerical obtained with the proposed homogenized models and by the simplified model of Casolo and Milani (2010).

3.6 Application: English-bond pattern

After the validation tests, the proposed homogenized models are extended to characterize the OOP behavior of an English bond masonry structure. The English-bond masonry benchmark was experimentally tested by Candeias et al. (2016). Here, only the geometry and the material properties of the masonry components are required and described.

The majority of the existing research on masonry deal with running-bond texture within a single-wythe walls case (Pande et al. 1989; Lee et al. 1996; Zucchini and Lourenço 2002; Milani et al. 2007; Taliercio 2014). The analysis of the effect of potential discontinuities on the masonry thickness, when two- or three-wythes of masonry are present; the effect of three-dimensional shear stresses; and the study of other periodic textures, as the English-bond, are somehow under-investigated.

Still, some studies have been reported. In the context of simplified multi-scale methods, Casolo and Milani (2013) studied the behavior of three-leaf masonry walls and proposed, at a meso-scale, two simple unit cell homogenization models to compute the OOP homogenized quantities. One is a FE-based procedure, where bricks are assumed to be elastic and joints are reduced to interface elements, and the other is based on an analytical approach. Even if both models are accurate and relatively fast, the former does not consider the softening behavior of interfaces and the latter is an ad-hoc procedure thus demanding its extension to other components arrangements. Moreover, Cecchi and Milani (2008) characterized the meso-scale behavior of an English-bond masonry wall through a simple homogenization model. Masonry units are considered as rigid blocks and joints are modeled as 2D Reissner-Mindlin plate elements to explicitly reproduce the out-of-plane shear effects. Still, conclusions upon its influence are drawn at a structural level only through the comparison with a full FE mesoscopic model. It is also noteworthy to mention the research from Massart et al. (2005) in the field of

full-FE homogenization approaches. Even if applied to a running-bond masonry and within in-plane loading case, three-dimensional effects are reproduced through the implementation of a two-dimensional generalized plane state formulation. In this context, the experimental study upon an English-bond masonry structure benchmark constitutes an important step. The data may encourage and drive studies of different numerical strategies towards a better understanding of the latter effects. Accordingly, the current analysis tries to conclude about the effect of three-dimensional shear stresses and the role played by joints discontinuities along the thickness direction.

An English-bond masonry RVE is analyzed, see Figure 3.4a. The brick units have in-plane dimensions of 235×70×115 mm^3 ($length \times height \times thickness$) and the bed and head mortar joints have a thickness $t_{joint} = 15\ mm$. When laid and bound together in an English-bond texture the wall yields a thickness of 235 mm. The mechanical properties adopted are collected in Table 3.2 and follow the values available both from the experimental data and literature studies on the same benchmark (Mendes et al. 2014). Note that the suggestion given in CUR (1994) has been followed in this application study, and thus the computation of the normal and shear elastic stiffness terms of the interface elements are employed according to Eq. (3.15) and Eq. (3.16), respectively. The algorithm used for the application of the meso-scale strategies (KP and MP models) is briefly reported next in Figure 3.11.

Table 3.2 – Material properties adopted for the English bond masonry following literature values (Mendes et al. 2014).

Elastic Properties		Elastic and Inelastic Properties									
Brick units		Mortar joints									
E_{brick}	ν_{brick}	E_{joints}	k_n	k_s	f_t	f_c	c	G_f^I	G_f^{II}	G_f^{IV}	ϕ
11,000	0.25	2,200	183	72.6	0.105	2.84	0.20	0.012	0.05	3.97	30
N/mm²	(-)	*N/mm²*	*N/mm*	*N/mm*	*N/mm²*	*N/mm²*	*N/mm²*	*N/mm*	*N/mm*	*N/mm*	(degrees)

Four values are considered for the RVE thickness, namely $t = 470mm$, $t = 235mm$, $t = 141mm$ and $t = 70.5mm$. The results obtained with the simulations from the KP and MP models are compared with the ones derived with a three-dimensional meso-model (DNS model), as done for the previous validation steps, and depicted in Figure 3.12. Several conclusions can be put together. Firstly, and as expected, no considerable differences regarding the peak moments (M_{xx}, M_{yy}, M_{xy}) are found, between the MP and the DNS models, for all the studied thicknesses. The MP model can capture well the out-of-plane shear effects. Yet, it is important to recall that for the MP model, with the increase of the thickness value, some convergence

problems have been experienced when developing the post-peak branch due to snap-back issues. It is known that when interface elements employ a softening type of damage model, convergence problems can be experienced after the cracking onset and propagation (De Borst 1987; Hellweg et al. 1994). Thus, the issues found lead, in theory, to the requirement of improved solving techniques, see Hellwega and Crisfield (1998), or the imposition of constraints equations upon the interface nodes (De Borst 1987).

1 • Modeling stage. Input call:
2 - Selecting the masonry texture being analyzed (running or English-bond)
3 - Definition of the geometrical parameters and material data:
4 ($l_{unit}, h_{unit}, t_{unit}, t_{head\ joint}, t_{bed\ joint}$) and ($E_{brick}$, ν_{brick}, k_n, k_s, f_t, f_c, c, G_f^I, G_f^{II}, G_f^{IV}, ϕ)
5 - Define the type of analysis
6 (**If** type of analysis = nonlinear static; Activate analysis controls described in §3.4.3; **end**
7 • Processing stage:
8 IP: **for** the KP and MP models:
9 Within a strain-driven formulation, apply the periodic planar displacement increments $\tilde{u}_{0,m}$,
10 and compute:
11 **for** each in-plane deformation mode depicted in Figure 3.2:
12 **for** each applied increment:
13 Solve the BVP using the FE strategy (DIANA 2019);
14 Compute and store the average strain E and stress Σ quantities (Eq. (3.1)-(3.8));
15 **end**; **end**
16 Obtain the 5 in-plane homogenized curves: $\Sigma_{xx} - \mathrm{E}_{xx}$ (tension and compression); $\Sigma_{yy} - \mathrm{E}_{yy}$
17 (tension and compression); $\Sigma_{xy} - \mathrm{E}_{xy} = \Sigma_{yx} - \mathrm{E}_{yx}$. **end**
18 OOP: **for** the KP model:
19 Within a curvature driven formulation, apply the periodic displacement increments $\tilde{\mathrm{w}}_{0,m}$, and
20 compute:
21 **for** each out-of-plane deformation mode depicted in Figure 3.3b:
22 **for** each applied increment:
23 The integral over the thickness of the in-plane homogenized $\Sigma - \mathrm{E}$ quantities (lines 8-
24 17) and store. See Eq. 3.11.
25 **end**; **end**
26 Obtain the 3 out-of-plane homogenized curves $M_{xx} - \chi_{xx}$; $M_{yy} - \chi_{yy}$; $M_{xy} - \chi_{xy}$. **end**
27 **for** the MP model:
28 Within a curvature driven formulation, apply the periodic rotation increments $\tilde{\theta}_{0,m}$, and
29 compute:
30 **for** each out-of-plane deformation mode depicted in Figure 3.3b:
31 The solution of the BVP using the FE strategy (DIANA 2019);
32 Obtain the in-plane and transverse shear strains γ_{xz} and γ_{yz} and stresses.
33 Integrate these quantities over the thickness, holding the variational principle of Eq. (3.9),
34 and store.
35 **end**; **end**
36 Obtain the 3 out-of-plane homogenized curves $M_{xx} - \chi_{xx}$; $M_{yy} - \chi_{yy}$; $M_{xy} - \chi_{xy}$. **end**

Figure 3.11 – Algorithm adopted for the meso-scale application on an English-bond masonry wall.

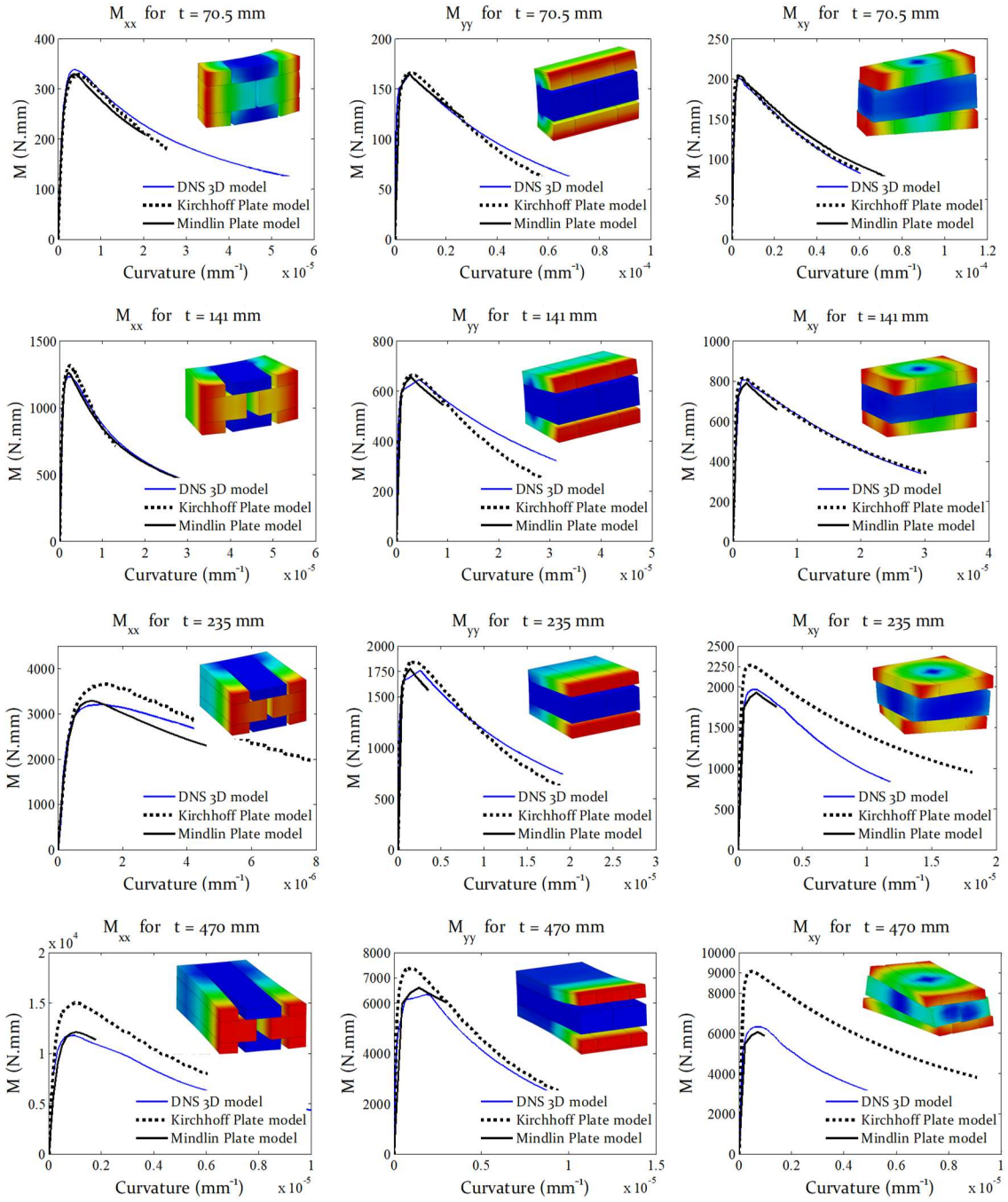

Figure 3.12 – Homogenized moment vs. curvature curves for the four RVE thickness values of the English-bond masonry texture obtained with the proposed numerical strategies: DNS 3D model, Kirchhoff plate model, and Mindlin plate model.

No convergence issues are reported for the KP model. This is based on an in-plane identification within a plane-stress formulation, from which the OOP quantities are simply obtained through the integration on wall thickness. The computational time required by the KP model to derive all the in- and out-of-plane homogenized quantities ($\Sigma_{xx}, \Sigma_{xy}, \Sigma_{yy}, \mathrm{M}_{xx}, \mathrm{M}_{xy}, \mathrm{M}_{yy}$) is around 81 seconds, which is significantly less than the MP (154 seconds) and the three-dimensional DNS (246 seconds) models. So, the KP model seems the

most suitable procedure to be integrated within a fully automatic FE^2 procedure, albeit its inability to reproduce the out-of-plane shear stresses can lead to considerable errors depending on the thickness of the RVE being analyzed. Figure 3.12 clearly shows the latter where, for a thickness of 235 mm (real dimensions) and 470 mm, an error of 14% and 23% is found, respectively. Another important feature is that the observed differences for the peak moment values are especially critical in the case of M_{xx} and M_{xy} and not relevant for the vertical bending M_{yy}. This is easily understandable from a physical standpoint. Bearing that for M_{yy} a typical de-bonding failure is achieved, see Figure 3.3a, this is mainly dependent on the tensile strength value of the horizontal joints, being the shear effect of the vertical interfaces irrelevant.

Concerning the effect of the mid-thickness vertical joint of English-bond masonry walls, two DNS models are considered. One does not take into account the discontinuity along the thickness; the other considers it, meaning that it is explicitly modeled and with a thickness of 17 mm. Figure 3.13 shows the obtained results. Again, the presence of the discontinuity has a marginal effect on the vertical bending behavior M_{yy} of the RVE. On the contrary, the model with the discontinuity manifests a lower capacity for both horizontal M_{xx} and torsional M_{xy} moments, with differences ranging 33% and 17%, respectively. Additionally, if the KP model results are considered, an error of 52% is expected for the horizontal bending moment case. Such results prove the importance of addressing the mortar discontinuities along the thickness of a masonry wall and the need to choose carefully the modeling strategy for a given case study.

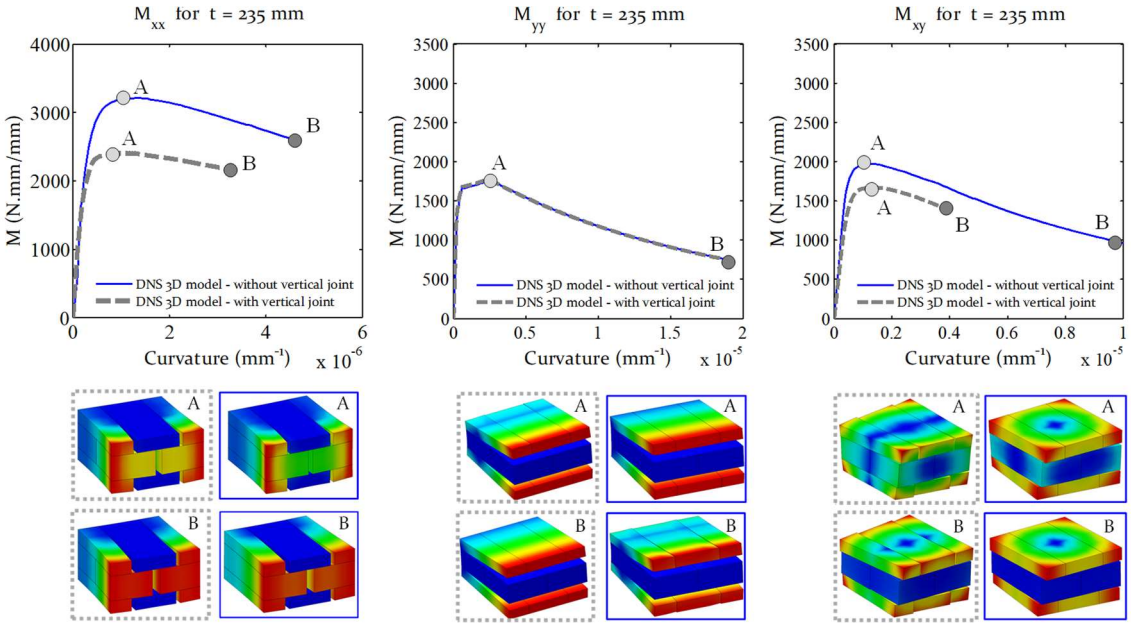

Figure 3.13 – Comparison between the homogenized moment vs. curvature curves of the English-bond masonry texture (thickness of 235mm) obtained using two DNS 3D models: one that considers and the other that excludes the existent vertical joint on the mid-thickness. Deformed configurations at the peak and ultimate post-peak point are plotted for both models.

3.7 Summary

Two mesoscopic FE-models, based on a first-order homogenization theory and within a strain driven formulation, have been formulated to characterize the behavior of masonry subjected to out-of-plane loading. A Kirchhoff-Love and Mindlin-Reissner plate theory have been adopted and designated as KP and MP models, respectively. In both strategies, a representative volume element (RVE), aimed at representing masonry by repetition, was modeled through the assemblage of quadrilateral elements with linear interpolation for bricks and line interface elements with zero-thickness for mortar joints. By solving a BVP upon the defined RVE, both the in-plane stresses and out-of-plane stress-couples were derived from the mesoscopic level. With bricks assumed to be elastic and with interface elements carrying the inelastic material information within a multi-surface plasticity model (Lourenço and Rots 1997) (an assumption plausible for strong blocks), stepped, toothed and de-bonding (straight) masonry failure patterns are suitably reproduced.

The meso-level validation of the KP and MP models has been performed. Reference available experimental data together with the results obtained via a three-dimensional meso-mechanical model (DNS model) were adopted. Three main constitutive key features have been addressed: (i) the correct representation of the elastic stiffness properties (Zucchini and Lourenço 2002); (ii) the masonry orthotropic behavior due to the arrangement of the units (Gazzola et al. 1985; Pluijm 1999); and (iii) the role of vertical membrane pre-compression states (Willis et al. 2004). The validation proved to work well, with homogenized results fitting accurately the reference data.

The application of the mesoscopic FE-homogenized based models was carried out for a real case study of an English-bond masonry mock-up tested by Candeias et al. (2016). The analyses were performed using data derived numerically, namely the homogenized out-of-plane quantities M_{xx}, M_{xy} and M_{yy}, which depend on the in-plane behavior of the masonry. Four values for the RVE thickness were adopted aiming at studying the out-of-plane shear stresses effect. The MP model follows an out-of-plane shear deformation theory and thus was able to provide similar results to the ones from the DNS model. The simplified KP model proved good accuracy for the cases where the thickness has a value which is similar or lower than the RVE dimensions (i.e. its height or length). It is worth noting that the KP strategy allows faster computations with no-convergence issues reported. Insomuch, in order to test the effect of the presence of a mortar layer on the RVE thickness (present in an English-bond texture), two mesoscopic models were further analyzed. The conclusions demonstrate that the discontinuity plays an important

role in the decrease of the horizontal bending (around 33%) and torsional moment capacities (around 17%), whereas the influence on vertical bending is minimal.

The above meso-mechanical homogenized models are characterized by several advantages, mainly related to their versatility. By exploiting the use of plate theory assumptions, the strategies allow replacing the three-dimensional mesoscopic continuum into a, mostly, two-dimensional one. Such procedures are quite convenient, due to the simplicity of application, accuracy and low computational effort required. Moreover, these are suitable to be integrated within a FE^2 approach, especially with simplified discrete methods at a macro-scale, as done in Casolo (1999) and Milani and Tralli (2011).

(vacate page)

Chapter 4

4 Multi-scale analysis of masonry: macro-scale level

4.1 Introduction

A two-step numerical framework using a novel homogenization procedure is described with an emphasis on the structural (macro) level. The main aim is its application aiming a better insight into the dynamic behavior of masonry structures. The proposed technique can determine the structural load capacity, represent the damage evolution and collect the time-history displacements. The relevance of such numerical procedure is particularly noted by current design codes, as the Eurocode 8 (2004), in which the assessment of the seismic vulnerability of masonry structures and the knowledge of the expected residual loading capacity are required after the occurrence of an earthquake.

The classical continuum FE^2 approaches still demand high computational costs (Otero et al. 2015) and, therefore, assumptions which permit the decrease of such cost without compromising the accuracy are welcomed. Besides the assumptions undertaken at a meso-scale (§Chapter 3), there is also the possibility of using simplified but still accurate methods that can be implemented at a macro-scale. This is especially convenient when the macro-model is suitable to receive the meso-scale homogenized output. Hence, the integration of these models within a meso to macro homogenized formulation, i.e. where the material constitutive information is transferred in one step from the meso- to the macro-scale, can be very promising especially for the dynamic study of masonry structures.

Some proposals can be found in the literature, as the use of limit analysis (Milani et al. 2006b) or the use of discontinuous or discrete FE-models instead of the classical macroscale continuum-FE strategies. Several works demonstrate the accuracy and computational efficiency of limit analysis when applied to in-plane (Milani et al. 2006b) and out-of-plane loaded masonry (Casolo 2006; Milani and Tralli 2011; Milani and Venturini 2011) but, as well, for masonry structures subjected to dynamic loads (Casolo and Milani 2013). The author believes that the use of advanced computational tools is of unequivocal importance and especially assured if time-costs are maintained as relatively low. Accordingly, the goal here is to prove that the proposed approach is, in the set of the more accurate advanced FE strategies, attractive from a computational burden standpoint. On this behalf, a novel FE^2 strategy is presented where, aiming to effectively achieve improved running-times (in respect to a FE macro-modeling approach), a Rigid Body Spring Mass (RBSM) model is developed at a

macro-scale and implemented in the commercial software ABAQUS (2013) which has available powerful built-in procedures.

The present chapter is organized as follows: (i) a description of the proposed approach with focus on the macro-scale level; (ii) a description of the discrete RBSM macro-model; (iii) a validation of the unit cell of the RBSM macro-model; (iv) a description of important remarks from a computational standpoint; and (v) main conclusions.

4.2 Outline of the proposed approach

A two-step numerical procedure is introduced with the aim of predicting with accuracy the dynamic behavior of masonry structures. The strategy makes use of a classical first-order homogenization scheme and is formed by three steps (Suquet 1987; Mistler et al. 2007): (i) the definition and solution of the meso-scale problem; (ii) the implementation of the meso-to-macro transition; and (iii) the solution of the macro-scale problem. The present chapter focuses on the macro-level, so that the meso-macro transition and the macro-scale problem solution steps are addressed. A discrete FE model, hereafter designated as RBSM, is applied to represent the macro-structural behavior. The methodology is briefly described in Figure 4.1.

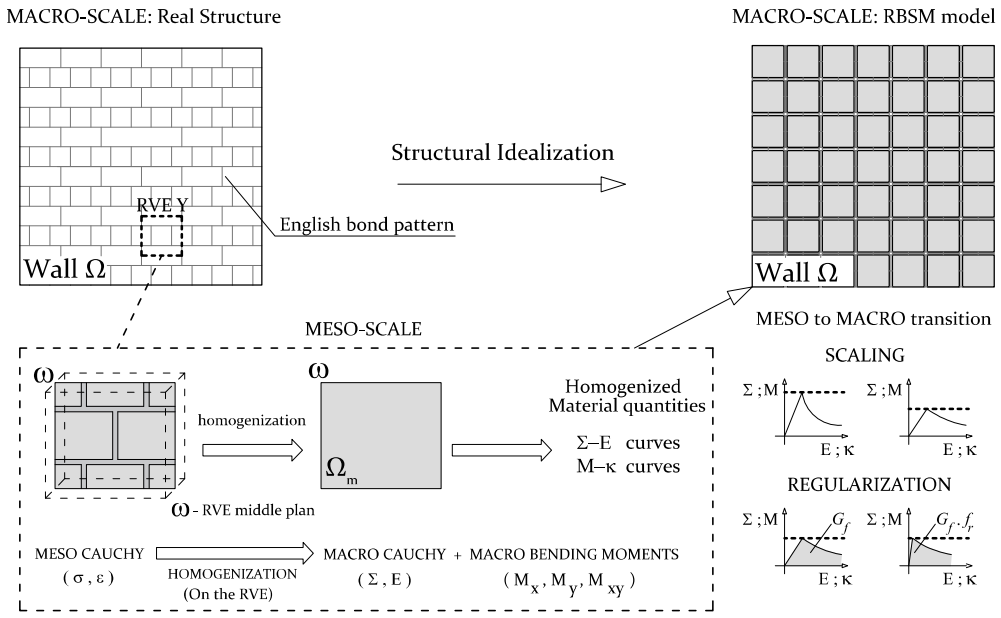

Figure 4.1 – Methodology of the proposed two-step numerical procedure.

Here, the meso-scale output is considered at disposal in terms of homogenized stress-strain ($\Sigma - \mathrm{E}$) and moments-curvature ($\mathrm{M} - \chi$) curves. This information, obtained through a unit cell homogenized procedure, is employed at a macro-level following an upward transfer of information, whereas the URM structural analysis is conducted. The application of a discrete

system may be questionable in cases where multiphase couplings can occur, as when thermal or hydro-mechanical effects exist. Still, the latter can often be disregarded in structural oriented problems and is, therefore, eligible for the present research scope.

Two steps are developed to achieve a correct upscaling, i.e. the scaling and regularization of the homogenized quantities. These appear to be critical to assure that the macro-input is independent of the macro-mesh. The governing conditions are referred to in the next section, after the introduction of the adopted macro-unit cell and the constitutive material model.

4.3 Macroscopic unit-cell

At a macro-scale level, the theoretical background of the RBSM model stems from the works of (Kawai 1977, 1978, 1991) and has been implemented in the advanced software ABAQUS (2013). The strategy is especially suited for the study of planar elements, i.e. for a three-dimensional body $\Omega_M \subseteq \Re^3$ with one dimension much smaller than the other two – typically the thickness. Such an assumption is also postulated when studying a given structure with plate or shell FE's and, therefore, the modelling using the RBSM approach tries to describe the structure using the mid-surface of the body Ω_M. Given the cartesian space and for the undeformed configuration it is assumed that the thickness t of the structure develops in the z direction ($z = [-t/2\,, +t/2]$) and that the two planar coordinates are defined through the global coordinates x and y - see Figure 4.2. Such an assumption is important to recall bearing the Cartesian system adopted at a meso-scale, because an uniformization between the allowable macro-deformation modes and the respective meso-scale ones is convenient. As depicted in Figure 4.2, the horizontal bending moment M_{xx} produces a rotation along the y-axis; the vertical bending moment M_{yy} produces a rotation along the x-axis; an horizontal in-plane force F_{xx} produces a deflection in the plane $z = 0$ following a path on the x-axis; and a vertical in-plane force F_{yy} produces a deflection in the plane $z = 0$ following a path on the y-axis.

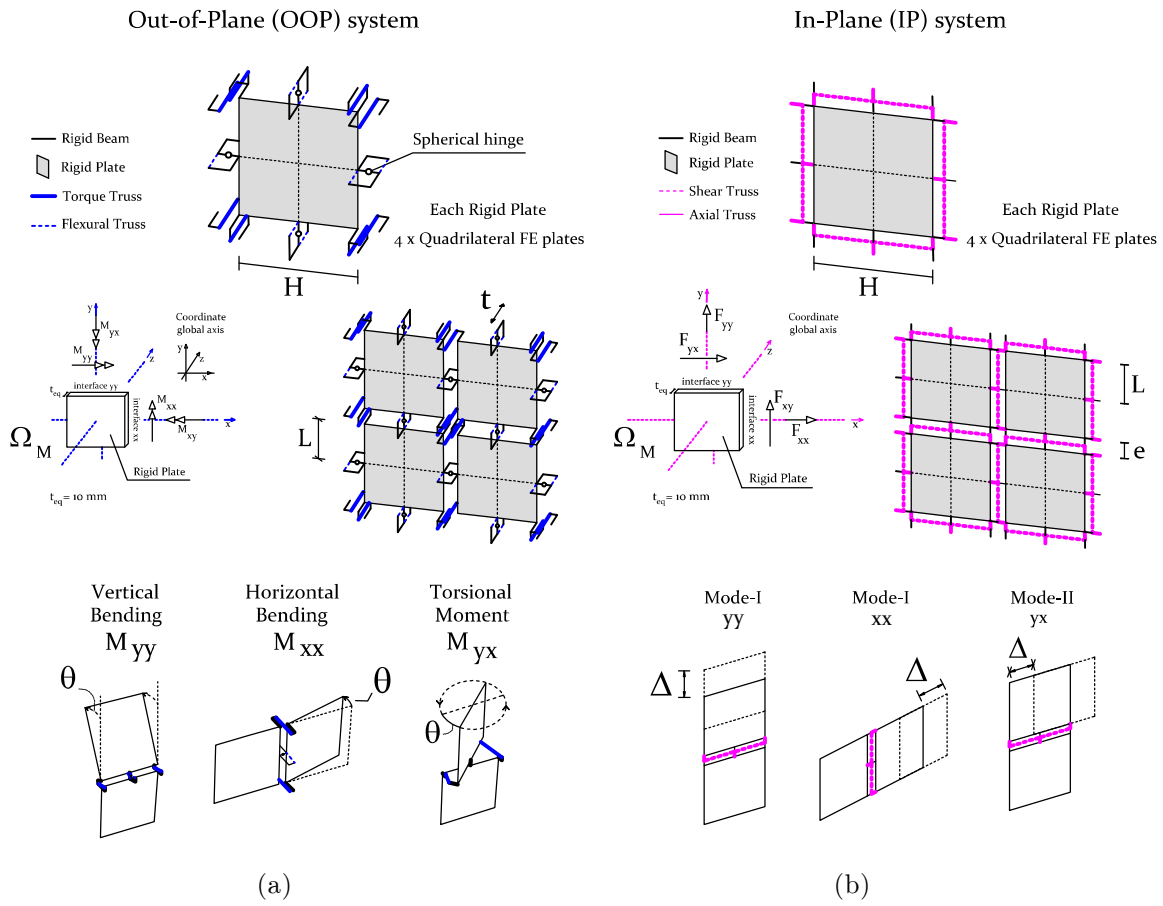

Figure 4.2 – Macro-unit cell and kinematics of the RBSM model for: (a) the out-of-plane case; and (b) the in-plane case.

The macroscopic unit-cell is composed by the assemblage of discrete quadrilateral rigid plate elements interconnected, at its interfaces, through a set of rigid and deformable FE truss-beams. The rigid plates are modeled as four linear quadrilateral elements within a finite-membrane strain formulation (designated as S4 element in ABAQUS). Full integration is adopted to preclude hourglass modes. The rigid linear elements are defined as three-dimensional Timoshenko FE beams (designated as B31 in ABAQUS). In this scope, the deformation and damage of the structure are restricted to three-dimensional two-node FE truss-beams (designated as T3D2 in ABAQUS), see Figure 4.3. These are comparable with spring elements since have just one DOF; are directly integrated; and their stiffness matrix is defined only by axial stiffness terms, given by $diag(\frac{EA}{L}, \frac{EA}{L})$, where E is the Young's modulus, A is the cross-section area of the truss element and L is its length. The macro-deformation is hence governed only by the truss-beam elements allowing to mimic the presence of the in- and out-of-plane failure modes considered in Figure 4.2, within a decoupled approach.

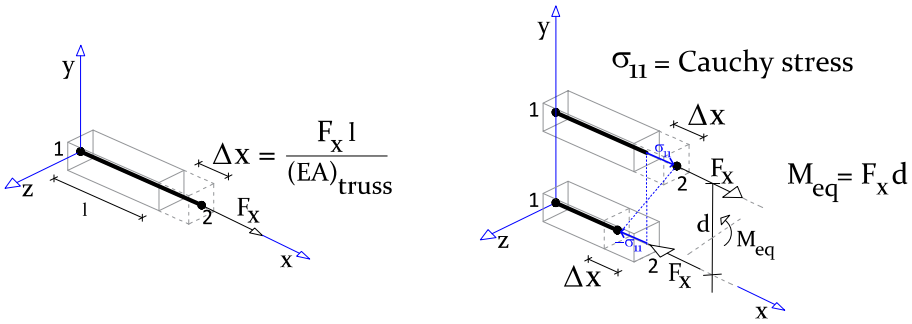

Figure 4.3 – Adopted FE truss beam with description of the in-plane (left) and out-of-plane (right) kinematic representation.

Furthermore, these elements must incorporate the material information of the meso-scale homogenized step and thus represent the masonry texture via an equivalent continuum medium. Both orthotropy and full softening behavior can be accounted by properly defining the properties of the different truss-beam for each interface side.

Regarding the OOP behavior, the macroscopic cell is composed of a set of four flexural and torsional truss-beam systems. The flexural trusses are positioned at the mid-center of each interface and the torsional trusses are positioned at each node of the squared rigid-plate. Mid-span hinges placed on interfaces allow fixing the axis of rotation for torsion movements without compromising the deformed shape. Regarding the IP behavior, truss-beams representing the axial and shear behaviors have been assumed. For the former, a total of three axial truss-beams per interface (two located in the edges and the other in the center) and a total of two shear truss-beams (defining the shear for each half length of the interface) have been assumed. The present study novelty focuses on the OOP characterization and the IP characterization is in agreement with Bertolesi et al. (2016).

Inertial forces are paramount for describing the dynamic behavior of a structure; hence the mass of the system needs to be modeled. Two approaches can be pursued, i.e. a direct lumped mass matrix or a consistent mass matrix. The former requires the computation of the representative mass for each rigid-plate and its introduction through nodal mass elements on each of the rigid plate nodes. Here, the latter has been adopted because it allows a more straightforward modeling stage and is the one typically adopted for FE-based strategies. The mass of the system is embodied by the quadrilateral rigid plates using an equivalent material density which, following a linear displacement interpolation assumption, allows to achieve a consisted mass matrix. Still, a comparison between both strategies will be assessed in the macro-validation section §4.4.1. The computation of the system density ρ_{system} is given as

$t.\rho_{masonry}/t_{eq}$, where t is the thickness of the structure, $\rho_{masonry}$ is the density of the masonry *and* t_{eq} the thickness attributed to the rigid plates (defined as 10 mm).

At last, it may be noticed that, since the RBSM model has been implemented using a Finite Element-based software, a stiffness matrix $[K] \in \mathfrak{R}^{n \times n}$ (n is the number of DOFs of the problem) has to be assembled for a given structure to compute the displacements vector $[u] \in \mathfrak{R}^n$ in respect to the action of a vector of external forces $[f] \in \mathfrak{R}^n$, through $[K][u] = [f]$. In this scope, the plates are enforced to be rigid (for both the axial and bending cases) by defining a high Young's modulus given by 10^{10} MPa (and a thickness of 10 mm). Likewise, the rigid linear elements are defined to have a high Young's modulus given by 10^{12} MPa (and a section area of 0.1 mm^2). The definition of the latter values may be questionable, as it leads that flexible elements of the system are connected with disproportionately stiffer ones. This can turn $[K]$ ill-conditioned (Kannan et al. 2014). Nonetheless, this author reports that such values have been properly defined having in mind such issue and that, for the stiffness values typically associated with concrete like materials, these can be used with no further concern.

4.3.1 Macroscopic material constitutive law

In classical continuum FE^2 homogenized approaches (see Smit et al. (1998), Feyel and Chaboche (2000), Kouznetsova et al. (2001), and Mercatoris and Massart (2011)), the macro-material information is derived from the meso-scale at each load step. The use of a simplified homogenized-based approach within an upward transfer of information between scales, processed only once, allows reducing the processing times. Therefore, a proper macro-constitutive relation must be assigned to the elements which govern both the deformation and inelastic response of the discrete model interfaces.

The constitutive model defined at the interfaces tries to mimic the material information obtained at a foregoing scale. The model should be capable to allocate the mechanical information and effectively represent the elastic and inelastic response of the defined masonry RVE. Here, an orthotropic behavior with softening is reproduced, because it derives from the presented homogenization strategies. This leads to the fundamental character that each phase has in the two-step framework. Several models can be adopted in ABAQUS (2013) as, for instance, the smeared crack concrete model, the brittle crack concrete model and the concrete damage plasticity model. These are all suitable for concrete and other quasi-brittle materials and eligible to be used to characterize the homogenized truss-beam systems. The concrete damage plasticity (hereafter, CDP) model is selected, given the better representation of the inelastic laws. The model combines a stress-based plasticity with a strain-based scalar damage.

It can reproduce several macroscopic properties for tension and compression regimes, such as: (i) different yield strengths; (ii) different stiffness degradation values; (iii) different recovery effect terms; and (iv) rate sensitivity, which can increase the peak strength value depending on the response strain rate. Moreover, it does consider the latter in the presence of interfaces dynamic and/or cyclic loading and is integrated using the backward Euler method. A general overview of the main features of CDP for the rate independent model are presented next, being the reader referred to e.g. Lubliner et al. (1989) and Lee and Fenves (1998) for further details.

Effective stresses govern the plastic part of these models (Grassl and Jirásek 2006) and the stress-strain relationship is ruled, as referred, by an isotropic damage scalar affecting the elastic stiffness of the material. According to Eq. 4.1 the nominal stress tensor $\boldsymbol{\sigma}$ reads:

$$\boldsymbol{\sigma} = (1-d)E_0^{el}(\boldsymbol{\varepsilon} - \boldsymbol{\varepsilon}^{\mathrm{pl}}) = \mathrm{E} : (\boldsymbol{\varepsilon} - \boldsymbol{\varepsilon}^{\mathrm{pl}}) \tag{4.1}$$

where E_0^{el} is the initial elastic stiffness of the material; d is the damage parameter, which defines the stiffness degradation (0 for an undamaged and 1 for a fully damaged material), and is designated as d_t and d_c for tension and compression regimes, respectively; $\boldsymbol{\varepsilon}$ is the total strain tensor; $\boldsymbol{\varepsilon}^{pl}$ is the plastic strain tensor, and E is the initial elastic stiffness of the material affected by the damage parameters (the degraded initial stiffness given by $\mathrm{E} = (1-d)\mathrm{E}_0^{el}$).
Regarding the softening variables, Eq. (4.2) describes the law $\boldsymbol{h}$ that express their evolution, in which $\dot{\varepsilon}^{\boldsymbol{pl}}$ is the plastic multiplier (assuming a non-associated potential flow), and $\tilde{\varepsilon}^{pl}$ and $\overline{\boldsymbol{\sigma}}$ the equivalent plastic strain tensor and the effective stress tensor, respectively.

$$\dot{\tilde{\varepsilon}}^{pl} = \mathrm{h}(\overline{\boldsymbol{\sigma}}, \tilde{\boldsymbol{\varepsilon}}^{pl})\dot{\varepsilon}^{\mathrm{pl}} \tag{4.2}$$

The CDP model uses a yield function based on the works of Lubliner et al. (1989) and Lee and Fenves (1998). A hardening variable K_c controls the meridians shape of the yield shape, in which a K_c=2/3 is assumed, leading to an approximation of the Mohr-Coulomb criterion. Three other dimensionless parameters need to be defined, i.e. the dilation angle Ψ, the eccentricity e, and the viscosity parameter. The dilation angle Ψ is measured in the p-q plane and gives the inclination angle of the failure surface in respect to the hydrostatic axis; from a physical standpoint, it represents the internal friction angle of the material. Here, a value of 30 degrees has been defined. The eccentricity parameter e modifies the flow potential rule, being a straight line if $e = 0$ and a hyperbola if $e = 0.1$. The default value, i.e. $\mathrm{e} = 0.1$, has been assumed. The viscosity parameter is introduced to enhance the results convergence in the presence of material and/or geometrical nonlinearities, through a viscoplastic regularization by Duvaut and Lions (1972). This parameter should be treated with care as it can misrepresent the obtained results.

For the present RBSM model, the default value of 0 (zero) has been adopted, even though it has been noticed that within a quasi-static pushover analysis a value of 1×10^{-4} can decrease the computational cost without apparently affecting the results.

Since truss beams define the material behavior of the macro-interfaces, the system will undergo only uniaxial loading conditions and, therefore, the plastic strain rates in tension, $\dot{\varepsilon}_{t}^{pl}$, and compression, $\dot{\varepsilon}_{c}^{pl}$, are a function of the uniaxial plastic strain rate $\dot{\varepsilon}_{11}^{pl}$, and read as:

$$\dot{\varepsilon}_{t}^{pl} = \dot{\varepsilon}_{11}^{pl} \quad \text{and} \quad \dot{\varepsilon}_{c}^{pl} = -\dot{\varepsilon}_{11}^{pl} \tag{4.3}$$

Likewise and, even if the CDP has been extended for the general multiaxial conditions (Lee and Fenves 1998), the uniaxial character of the system may also be adopted for the cyclic loading analysis, which simplifies to a great extent its follow-up validation. In such cases, the recovery of the elastic stiffness when the sign of the imposed load changes is an important aspect to consider. The so-called 'unilateral effect' holds both in tensile and compressive sides of the cycle, in which, for uniaxial conditions, the damage parameter variable d is given as:

$$(1-d)=(1-s_t d_c)(1-s_c d_t)\ ,\ s_t \geq 0\ ,\ s_c \leq 1 \tag{4.4}$$

Here, s_t and s_c are functions of the stress state which represents the referred stiffness recovery with the related stress reversals and are defined as:

$$\begin{cases} s_t = 1-\omega_t r^*(\overline{\sigma}_{11}) \\ s_c = 1-\omega_c\left(1-r^*(\overline{\sigma}_{11})\right) \end{cases} \tag{4.5}$$

Here, ω_t and ω_c are weight factors and assumed as input material parameters for the CDP model and limited by $0 \leq \omega_t \leq 1$ and $0 \leq \omega_c \leq 1$; and $r^*(\overline{\sigma}_{11}) = 1$ if $\overline{\sigma}_{11} > 0$ or $r^*(\overline{\sigma}_{11}) = 0$ if $\overline{\sigma}_{11} < 0$. In concrete structures, the effect is more marked when the material is in a compression regime ($\sigma_{11} < 0$), because tensile cracks tend to close (Lee and Fenves 1998). Nevertheless, the aim here is to fully reproduce the homogenized behavior in both regimes and so the *Bauschinger effect* is not reproduced. Therefore, tensile and compressive elastic stiffnesses have a full recovery effect, which is the same than defining $\omega_t = 1$ and $\omega_c = 1$.

To fulfill the input requirements of the CDP model in ABAQUS, information regarding the post-failure behavior may be introduced for each element that features material nonlinearity, i.e. the truss beams, in terms of stress and inelastic strain $\tilde{\varepsilon}^{ck}$ values. The latter must be obtained for each point of the post-peak homogenized curve by Eq. (4.6):

$$\tilde{\varepsilon}^{ck} = \varepsilon - \varepsilon_{o}^{el} \tag{4.6}$$

where ε_o^{el} is the elastic strain corresponding to the undamaged material and ε is the total axial strain of the multi-linear stress envelope. If the damage parameters d are introduced, the plasticity model is thus coupled with a damage description and is suitable for the cyclic behavior description of the material. The plastic strain values ε^{pl} are calculated, for each point of the curve, as:

$$\varepsilon^{pl} = \varepsilon^{cr} - \frac{d}{(1-d)}\frac{\sigma^P}{E_0^{el}} \tag{4.7}$$

Since the permanent plastic strain can be just positive or null, the latter can constitute a good checkpoint to foresee if the damage parameters have been properly computed. Figure 4.5 illustrates the input used for ABAQUS, where it can be seen that several steps need to be undertaken to guarantee the correct readiness of the material curves by the CDP model and, likewise, to assure the well-posedness of the macroscale solution. Note that, for simplification reasons, multi-linear curves with 5-nodes beyond the peak are introduced in ABAQUS. Also, a small plateau near the peak strength of the curve is considered, to circumvent an abrupt stiffness loss and avoid potential convergence and run time problems. The adequacy of such approximation will be discussed in section 4.4.

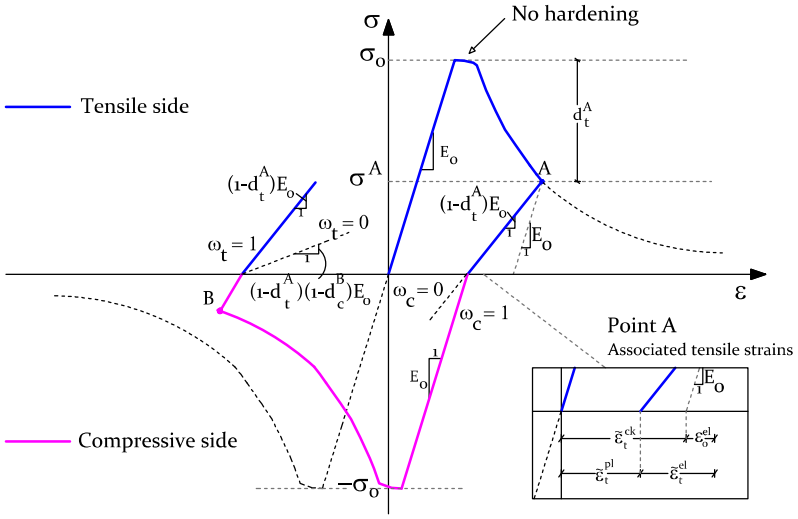

Figure 4.4 – Hysteretic curve adopted for the out-of-plane truss-beams (NOTE: for the in-plane truss beams, the tensile and compressive behaviors have different shapes which stem from the in-plane homogenized curves).

4.3.2 Meso-to-macro transition

The CDP constitutive model demands the use of stress-strain relationships as input for the elements which govern the behavior of the macro-model interfaces, i.e. the FE truss-beams.

Bearing this in mind, ad-hoc meso-to-macro transition steps are carried out with the target of correcting the material input to be used by these interfaces in ABAQUS, see Figure 4.5. Such transition is, however, only conducted after the preparation of the computational model, because it is dependent on the size of the used discrete mesh, particularly, on the values of H, e, L, t, defined below. Furthermore, squared rigid elements are assumed and so only two different angles are considered for the interfaces: *0* and *90* degrees. The material orthotropy is reproduced at a structural level because the approach offers the possibility to reproduce different input stress-strain relationships according to the trusses plane. For the in-plane behavior, the stress quantities are directly derived from the macroscopic homogenized values. For the out-of-plane system, the macroscopic homogenized moment values are adapted (so-called conversion, in Figure 4.5) to follow representative stress values for the bending and torsional truss beams through Eq. (4.8) and (4.9):

$$\sigma_{bending\ truss} = \frac{M}{(e.A_{BTruss})} \tag{4.8}$$

$$\sigma_{torque\ truss} = \frac{M}{(H.A_{TTruss})} \tag{4.9}$$

Here, M is the bending moment per unit of interface length; H is the size of each square rigid element or plate; t is the thickness of the wall, A_{BTruss} is the bending truss area; and A_{TTruss} is the torque truss area; e is the gap between the rigid plates, which ideally should be zero but in practice is assumed small enough to be able to place trusses between the elements.

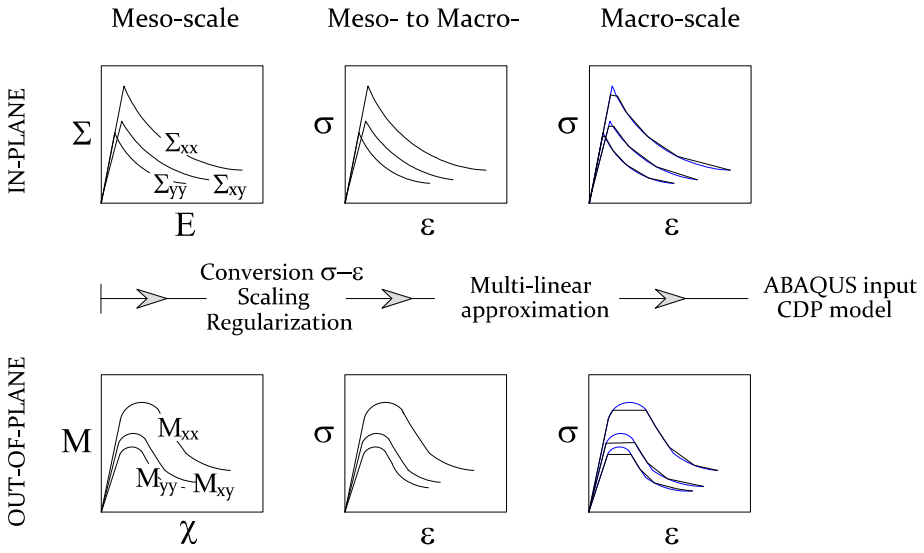

Figure 4.5 – Schematic representation of the followed methodology to convert the homogenized material curves as eligible input for the CDP model in ABAQUS.

After the previous stage, the stress-strain curves are regularized by defining the elastic stiffness and fracture energy terms. The regularization step is necessary to properly identify the elastic stiffness of each truss beam and to guarantee the input independence from the macro-mesh and thus its objectivity in the nonlinear range. This is, somehow, related with the mesh size sensitivity issue for continuous macroscopic FE models, where the fracture energy terms need to be regularized by a crack bandwidth parameter l_{crack}, as firstly documented by Bažant and Oh (1983).

Through assuring the elastic energy equivalence between the discrete model and a continuum homogeneous plate, it is possible to derive the so-called regularization factor f_r – this scaling operator affects the strain values of the curves that serve as input for the truss beams. Within a decoupled behavior, the latter is performed separately for the in-plane, axial (mode-I and mode-IV) and shear (mode-II) deformations, and out-of-plane modes, i.e. both flexural and twisting movements. In this way and, as demonstrated next in section §4.3.4, four different f_r operators can be derived, which allow holding the energy equivalence assumption.

4.3.3 Definition of the in-plane model

The definition of the discrete RBSM model has two purposes, i.e. to properly identify the elastic stiffness of the truss-beams of the system and to eliminate any trace of mesh dependency when material softening exists. As stated before, the regularization of the trusses input is accomplished though the computation of regularization factors f_r. The regularization factor is, for a specific truss set, given as the relation between the elastic stiffness of the associated homogenized meso-scale curve and the calibrated Young's modulus. This parameter affects all the strains of the homogeneous stress-strain curves of the corresponding trusses. Figure 4.6 presents the two directions of the in-plane system, i.e. the x- and y-directions; the respective tributary areas of each IP truss required to assess the aforementioned regularization factor; and the associated IP deformation modes accounted at a macro-scale.

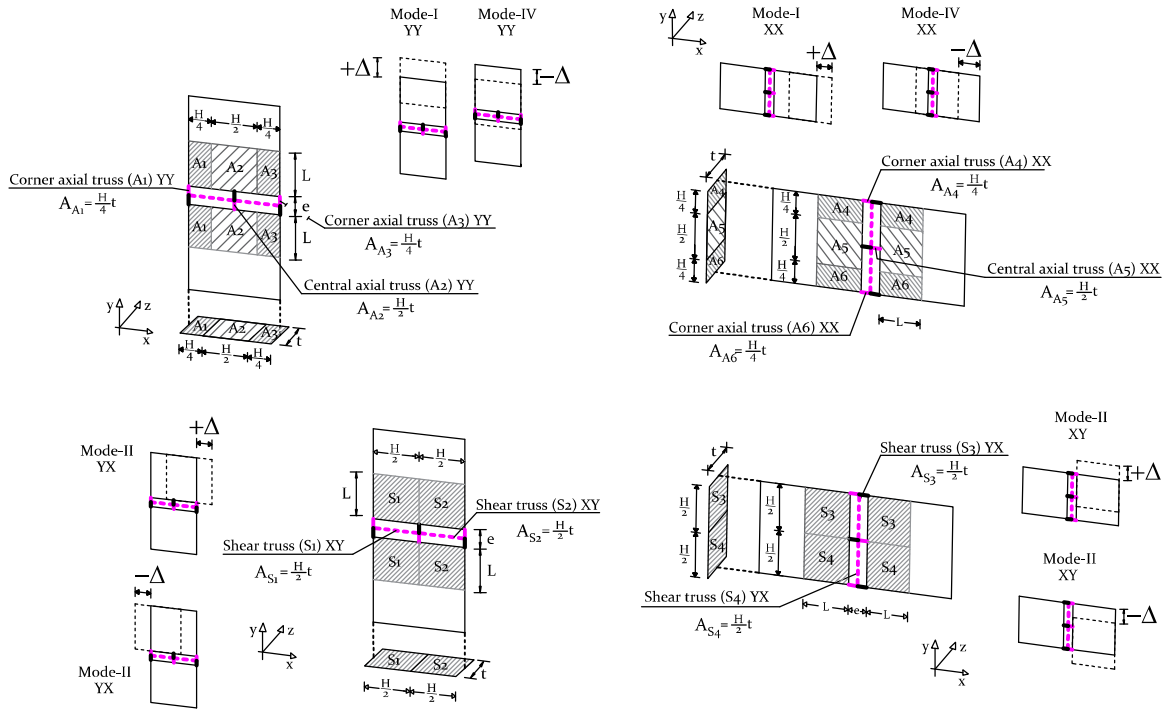

Figure 4.6 – In-plane unit cell: tributary area for each truss and kinematics of each allowable deformation mode.

Let us consider that $\bar{E}_{ii}$ is the elastic modulus of the equivalent homogeneous material ($\bar{\ }$) is the average operator and i is the corresponding axis x or y), $\bar{G}_{xy}$ the shear modulus of the equivalent homogeneous media, V the volume of the region under study and Δ a displacement increment under the studied direction. For the in-plane case, the total strain energy density is generically given by Eq. (4.10):

$$U = \frac{1}{2}\int_V \{\Sigma\}^T\{E\}\cdot d\mathrm{V} \tag{4.10}$$

Here, $\{\Sigma\}^T = \{\Sigma_{xx} \quad \Sigma_{yy} \quad \Sigma_{xy}\}$ and $\{E\} = \{E_{xx} \quad E_{yy} \quad E_{xy}\}$ are the homogenized stress and strain quantities, respectively, obtained at a meso-scale. For the mode-I, the calibrated elastic stiffness of each in-plane truss is derived through the stored strain energy in the volume V of both the discrete $\mathrm{U}^{\text{mode-I}}_{\text{discrete}}$ and the continuum homogenized media $\mathrm{U}^{\text{mode-I}}_{\text{continuum}}$.

$$U^{mode-I}_{continuum} = \frac{\sigma\varepsilon}{2}V = \frac{\bar{E}_{ii}\varepsilon^2}{2}V = \frac{H.t.\bar{E}_{ii}}{2}\frac{\Delta^2}{2L+e} \tag{4.11}$$

$$U^{mode-I}_{discrete} = V\frac{\sigma\varepsilon}{2} = \frac{H.t.E^{in-plane\ axial\ truss}_{ii}}{2}\frac{2\Delta^2}{e} \tag{4.12}$$

If both energies are equated, the Young's modulus of the in-plane axial trusses of a macro-unit cell for each plane direction (if orthotropy is considered) are derived and reads as:

$$E_{xx}^{in-plane\ axial\ truss} = \frac{\bar{E}_{xx} e}{4L + 2e} \tag{4.13}$$

$$E_{yy}^{in-plane\ axial\ truss} = \frac{\bar{E}_{yy} e}{2(H + e)} \tag{4.14}$$

The same methodology is followed for the mode-II trusses, namely the in-plane shear trusses. The stored strain energies of the continuum and discrete model are:

$$U_{continuum}^{mode-I} = \frac{H.t.\bar{G}_{xy}}{4} \frac{\Delta^2}{2L + e} \tag{4.15}$$

$$U_{discrete}^{mode-II} = \frac{e.t.E_{xy}^{in-plane\ shear\ truss} \Delta^2}{H} \tag{4.16}$$

And, consequently, the Young's modulus of the in-plane shear trusses are given by:

$$E_{xy}^{in-plane\ shear\ truss} = \frac{\bar{G}_{xy} H^2}{4e(2L + e)} \tag{4.17}$$

For more details regarding the IP formulation, the reader is referred to Bertolesi et al. (2016). Again, the main novelty of this work focuses on the OOP formulation and its proper integration with the IP case.

4.3.4 Definition of the OOP model

As for the IP model, the variational principles of energy conservation and virtual displacements were followed to derive the discrete elastic stiffnesses. The regularization factor of the OOP truss beams system is then obtained as the ratio between the strain bending energies of the discrete ($U_{discrete}^{bending}$) and continuum ($U_{continuum}^{bending}$) plate media. The $U_{continuum}^{bending}$ is derived from Eq. (4.18):

$$U = \frac{1}{2} \int_l \frac{M^2}{EI} dl \tag{4.18}$$

and given by:

$$U_{continuum}^{bending} = \frac{1}{2} (\bar{E}_{ii} I) \chi^2 (H + e) = \frac{\bar{E}_{ii} H t^3}{24(1 - \nu^2)} (H + e) \tag{4.19}$$

The stored strain bending energy of the discrete system is derived through an ad-hoc formulation. Bearing that the strain of the axial out-of-plane truss-beams is $\varepsilon = {}^{\theta e}/_{t}$ and $\theta = \chi(H + e)$, $U_{discrete}^{bending}$ is given as (see Figure 4.7):

$$U_{discrete}^{bending} = \frac{1}{2} M\theta = \frac{1}{2} \frac{E_{ii}^{bending\ truss} A_t e}{t} \theta^2 \tag{4.20}$$

By equating $U^{bending}_{continuum} = U^{bending}_{discrete}$ the correct Young's modulus of the OOP flexural trusses is calculated according to Eq. (4.21):

$$E_{ii}^{bending\ truss} = \frac{\bar{E}_{ii} t^4 H}{24e(1-\nu^2)(H+e)eA_t} \tag{4.21}$$

For the twisting movement, the same procedure is followed. Briefly, the stored strain torsional moment energies of the discrete and continuum homogeneous media are given by Eq. (4.22) and (4.23), as follows:

$$U_{continuum}^{torsional} = \frac{\bar{G} H t^3 \theta^2}{24(2L+e)} \tag{4.22}$$

$$U_{discrete}^{torsional} = \frac{E^{torsional\ truss} e H^3 \theta^2}{16t} \tag{4.23}$$

where $\bar{G}$ is the homogenized shear Modulus given directly by the slope of the shear meso-scale homogenized curve. Thus, by respecting the energy equivalence between the systems, the correct Young's modulus of the torque trusses is defined through Eq. (4.24).

$$E^{torsional\ truss} = \frac{2\bar{G} t^4}{3H^2 e(2L+e)} \tag{4.24}$$

Consider, for instance, that $\widetilde{\mathbf{E}} = [\varepsilon_1 \quad \varepsilon_2 \ \cdots \ \varepsilon_{n-1} \quad \varepsilon_n]$ and $\widetilde{\mathbf{\Sigma}} = [\sigma_1 \quad \sigma_2 \ \cdots \ \sigma_{n-1} \quad \sigma_n]$ are the n-dimensional sets which define, respectively, the stress-strain homogenized curve being regularized (n is the number of points of the curve). The correct elastic stiffness value, obtained through the energy equivalence demonstration, is computed for the point of the curve which has one third of the peak stress value, designated as point p. So, the regularization factor is generally given as $f_r = \sigma_p/(\varepsilon_p E_{corrected})$. Here, $E_{corrected}$ is the corrected Young's modulus obtained for each truss type. This procedure is followed and, consequently, four regularization factors are derived. By correcting the strain axis to calibrate the elastic stiffness value, the operator affects, as well, the post-peak curve strains and so, in an implicit way, the fracture energy itself.

Figure 4.7 represents the OOP basic cell of the macro-scale system. The geometrical parameters and the respective tributary areas for each of the flexural and torque trusses are given. Also, the kinematics of each allowable deformation mode is associated with a homogenized moment quantity.

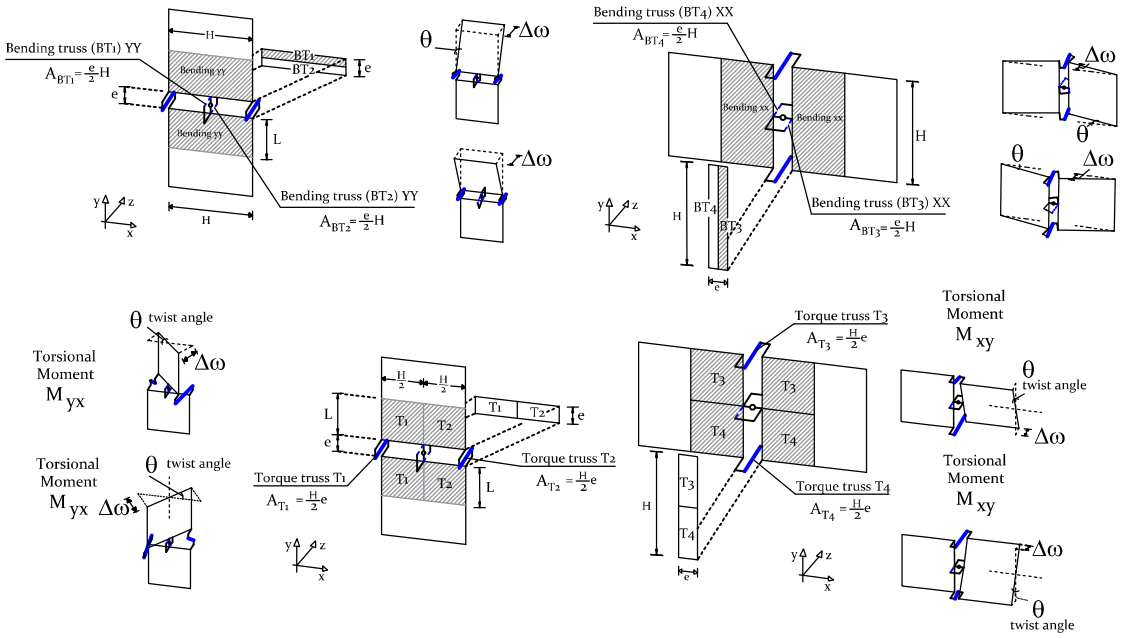

Figure 4.7 – Out-of-plane unit cell: the tributary area for each truss and kinematics of each allowable deformation mode.

4.4 Macro-mechanical validation: OOP behavior of masonry

The mechanical validation of the macro-unit cell for the study of the OOP behavior of masonry is presented next. Since the seminal works of Irons (1966), Irons and Razzaque (1972), and Irons and Loikkanen (1983), conducting patch tests become a regular step when presenting novel finite elements, see Macneal and Harder (1985), Zienkiewicz and Zhu (1992), Hughes et al. (2005), Taylor et al. (2018) and Rao and Shrinivasa (2001) for a review. Zienkiewicz and Taylor (2000) stated that, in plate problems, the 'importance of the patch test in both design and testing of the elements is paramount and this should never be omitted'.

Even if patch tests may be a trivial formality for standard finite elements, because of the shape functions continuity requirements, one may note their usefulness as a debugging step for code implementation. In this sense, some tests of comprehensiveness are employed over the novel macroscopic unit-cell discrete RBSM element aiming to assess the reliability and convergence of the solution in elastic and inelastic problems for static and dynamic ranges.

4.4.1 Linear range

Performance tests have been conducted to attest the ability of the model in (i) elasticity problems, and (ii) in vibration analysis, through the eigen-modes frequencies and deformed shapes.

Elasticity Problems

Concerning elasticity problems, the test addresses simple structural examples, namely a squared plate subjected to different loading and boundary conditions. The convergence of the discrete macro-model has been assessed by comparing the maximum elastic displacement obtained w with the exact solution w_{exact} for different mesh refinement levels N.

The squared plate benchmark with size L belongs to the set of patch test proposed by Rao and Shrinivasa (2001). Aiming to especially serve as a reference test for plate bending elements, a thickness equal to $L/100$ is assumed which approximates well thin-plate solutions. Two squared plates, one with pinned ($PPPP$) and the other with clamped supports ($CCCC$) at its edges, are subjected to a point and a pressure load. The maximum deflection obtained at the center of the plate is, for each case, normalized with the exact theoretical solution and presented in Figure 4.8. Although the discrete element apparently behaves better in the presence of simply supported edges, which is to be expected given the lower gradients of curvature, the load type seems to have a further extent on the solution accuracy. In fact, the model can better reproduce the point load behavior due to its localized effect; this goes in favor with the data from the RBSM model developed by Kawai (1977). Globally, a refinement of $N = 15$ ($H = L/15$) is a proper choice allowing estimations within 10% of maximum deflection error.

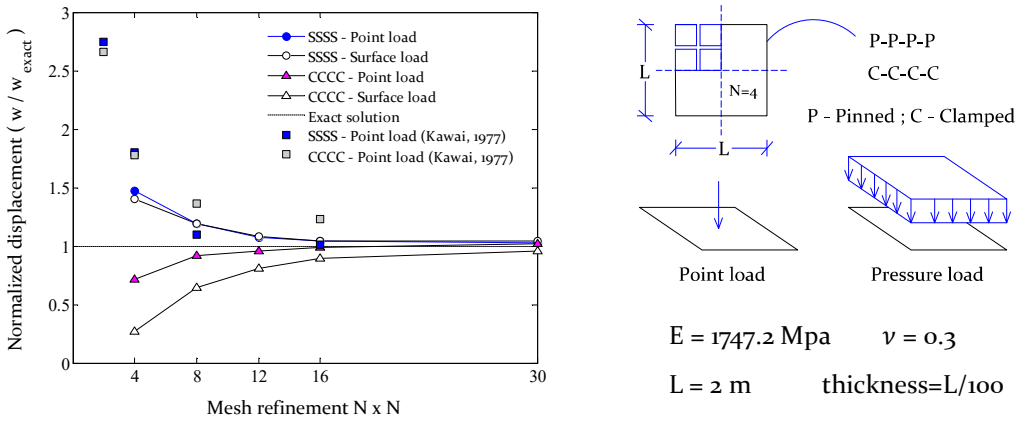

Figure 4.8 – Convergence study conducted for the squared plate test.

The plate benchmark test is inexpensive to carry out and, therefore, a time-cost analysis has been disregarded. The value of the errors found are admissible and in agreement with typical simplified mixed-FE strategies, as the RBSM by Kawai (1977) and the Hermann-Hellan constant-stress-triangular elements adopted by Turco and Caracciolo (2000). Hence, it has been considered that the discrete element passed the elastic patch tests. Besides the simplification adopted for the decoupled flexural-torsional behavior, it may be emphasized that the deviations

found, especially when clamped supported edges exist, are expected. Quadrilateral elements are adopted which restrains the model adaptability and deformability near cornered regions. A mesh-bias exist near the supports which explains why the model gives stiffer responses for the clamped edges cases; i.e. no deformation exists within a distance from the border given by the mesh size H. Moreover, the analyses can give a good indicator of the more appropriate refinement level adopted for the discrete mesh. A higher refinement is recommended for clamped edges ($N = L/16$) than simply supported edges ($N = L/12$).

Vibration Analysis

Free vibration analysis is conducted in a simply supported squared plate. The plate is isotropic and exhibits uniform thickness t and mass density values ρ. The free harmonic vibration of a thin plate is governed by the following differential equation:

$$D\nabla^4 w(x,y) - \omega^2 \rho t w(x,y) = 0 \tag{4.25}$$

Here, $w(x,y)$ is a given mode in the cartesian space, ∇^4 is the biharmonic differential operator in Cartesian coordinates, i.e. $\partial^2/\partial x^2 + \partial^2/\partial y^2$, and D is the bending stiffness given as $Et^3/12/(1-v^2)$. For the present example, a squared plate simply supported at its four edges, the solution of the vibration mode shapes has been formulated by Navier (1823):

$$w(x,y) = A_{mn} \sin\left(\frac{m\pi x}{a}\right) \sin\left(\frac{n\pi y}{a}\right) \quad , (m,n = 1,2,\dots) \tag{4.26}$$

in which, A_{mn} is the amplitude of vibration (which are the unknown coefficients), m is the number of half waves in the x-direction, n is the number of half waves in the y-direction, and a is equal to the length L of the squared plate side. By replacing the equation (4.26) in the differential equation (4.25), one obtains the exact solution for the vibration of frequencies in terms of the parameters m and n:

$$\omega = \sqrt{\frac{D}{\rho t}} \left[\left(\frac{m\pi}{L}\right)^2 + \left(\frac{n\pi}{L}\right)^2 \right] \tag{4.27}$$

By adopting different values for the integer parameters m and n, the theoretical and exact frequencies of the first 8 modes have been derived, see Table 4.1. For the discrete model, since it relies on a FE-based strategy, the natural frequencies and mode shapes have been obtained through the following matrix (weak) form equation:

$$([K] - \omega^2 [M])\{w\} = 0 \tag{4.28}$$

Here, [K] and [M] are the global stiffness and mass matrices. The mass of the discrete system is only carried by the rigid plate elements by providing a representative density value ρ_{system}. A uniform mass distribution is assumed to assemble [M], which can be achieved through a lumped or consistent strategy. The lumped strategy admits that the mass of the rigid plate is lumped in its nodes. Although only translational nodal mass elements are introduced in the system, disregarding thus the rotational inertias and mass coupling, the mass lumping allows obtaining a diagonal matrix. In the consistent strategy, mass is distributed in the rigid plates following a linear interpolation rule, as when computing the local stiffness matrix, and both translational and rotational inertias are accounted.

Towards a convergence study, four mesh refinements have been considered: $N = 4$, $N = 8$, $N = 16$ *and* $N = 30$. A thickness value of L/10 and a gap spacing between the discrete cells of $e = 20$ *mm* have been admitted. Furthermore, the analysis is complemented with the results from a standard continuum FE model (with a mapped mesh, element size of $L/30$ and with a consistent mass matrix) designated as FEA. The results have been gathered in Table 4.1 in terms of the normalized solution with the associated exact analytical angular frequency.

Table 4.1 – Convergence study: normalized natural frequencies (ω/ω_{exact}) found for the proposed macro-model and for a standard FEA.

Mode	*Proposed model (Lumped)*				*Proposed model (Consistent)*				*FEA N=30*	*Exact (rad/s)*	*m*	*n*
	N=4	*N=8*	*N=16*	*N=30*	*N=4*	*N=8*	*N=16*	*N=30*				
1	1.276	1.094	1.026	1.025	1.244	1.088	1.064	1.024	1.000	19.739	1	1
2	1.382	1.085	1.037	1.037	1.302	1.069	1.064	1.034	1.000	49.348	1	2
3	1.382	1.085	1.037	1.037	1.294	1.069	1.064	1.034	1.000	49.348	2	1
4	1.499	1.129	1.036	1.028	1.371	1.103	1.073	1.031	1.001	78.957	2	2
5	1.405	1.088	1.047	1.045	1.276	1.053	1.063	1.039	1.000	98.696	1	3
6	1.475	1.084	1.046	1.045	1.218	1.049	1.061	1.039	1.000	98.696	3	1
7	1.569	1.143	1.045	1.038	1.356	1.099	1.075	1.036	1.001	128.30	3	2
8	1.569	1.143	1.045	1.038	1.355	1.099	1.075	1.036	1.001	128.30	2	3

According to the h-refinement dependency verified in the elasticity problems considered before, higher mesh refinements inevitably lead to lower errors. Yet, a mesh size of L/16 provides solutions with an error lower than 5% (lumped approach) and, therefore, seems to constitute a sufficient refinement choice for larger case studies. A consistent mass matrix strategy yields more accurate eigen-frequency contents than the lumped one; that is especially clear for coarser meshes in which significant differences have been found (higher than 20%). On the other hand, the modal deformed shapes depicted in Figure 4.9 indicate that all the discretization fit the FEA results up to the first four modes. After that, coarser meshes are

unable to catch higher modal responses, due to the implicit mechanical arrangement of the quadrilateral rigid elements. Nonetheless, the higher refinement ($L/30$) reproduces well all the modal displacements. At last, it may be pointed out that the choice between the best approach to distribute the mass matrix is arguable, because the accuracy depends on the mesh refinement, but a consistent strategy is adopted hereafter.

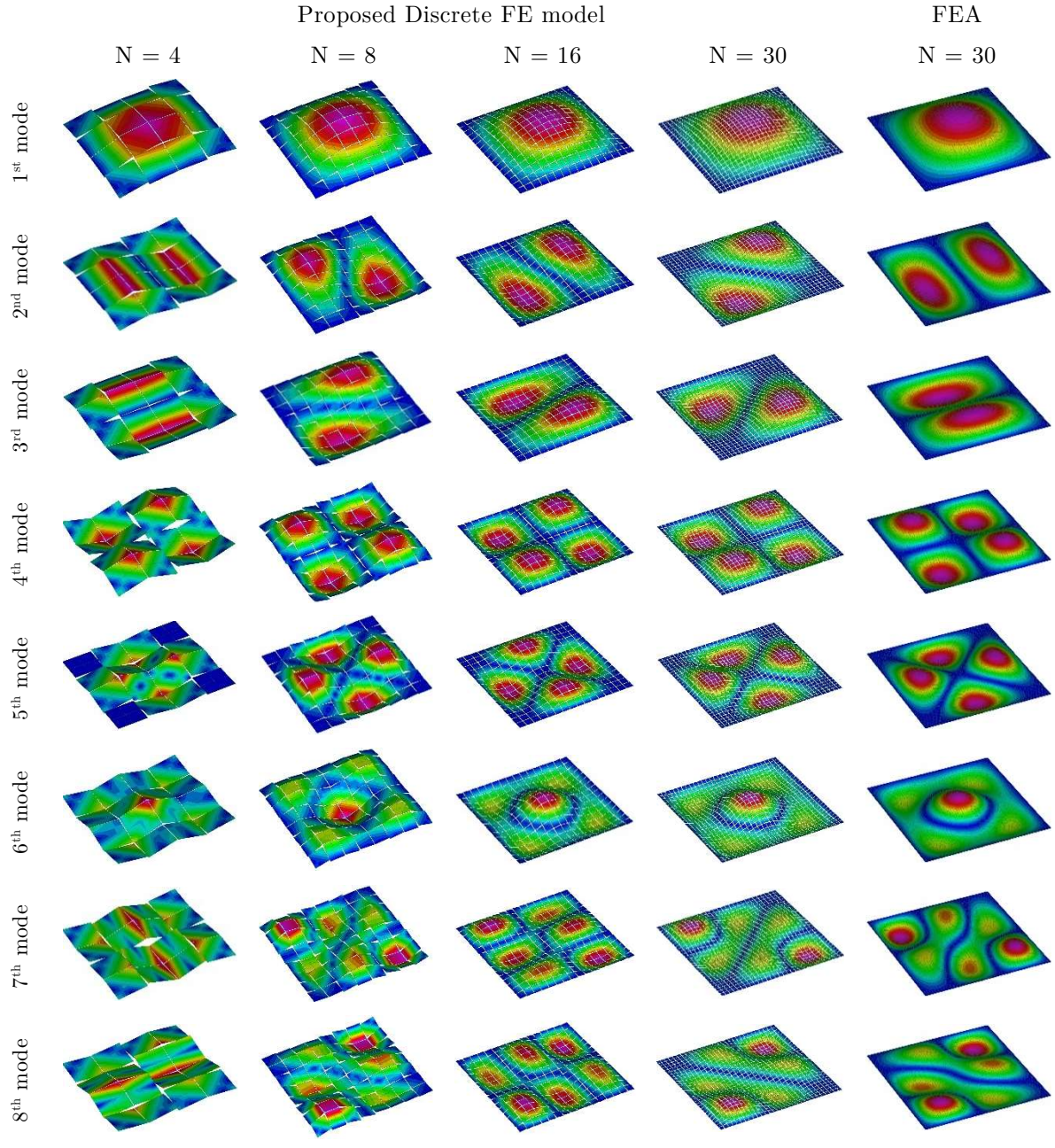

Figure 4.9 – Deformed shape of the first eight vibration modes obtained with the proposed model and in a FEA.

4.4.2 Nonlinear range

The main purpose of this section is to briefly assess if the nonlinear homogenized curve that serves as input for the Concrete Damage plasticity (CDP) model is properly attributed. This is accomplished by attesting if the CDP adopted for the macro-interfaces leads to the expected static behavior but, as well, to verify the hysteretic behavior. An ad-hoc simple case study is used for both purposes, namely a vertical masonry wall simply supported in its bottom and top edges and subjected to a centrally prescribed displacement, as depicted in Figure 4.10a.

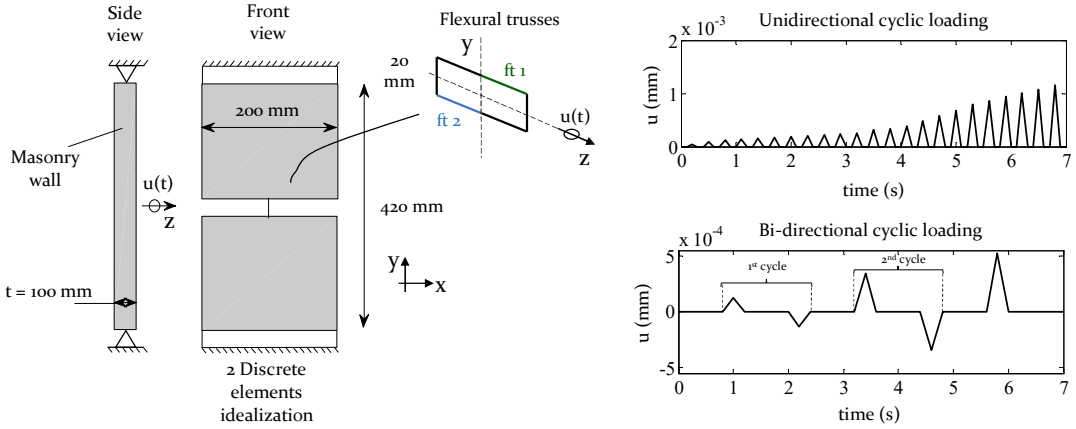

Figure 4.10 – Nonlinear validation of the macro-constitutive model with out-of-plane loaded wall: (a) discrete system representation; (b) displacement control for the uni- and bi-directional cyclic loading.

Quasi-static (monotonic) nonlinear curve

The first conceptual verification is performed through a quasi-static analysis where an OOP displacement has been applied at the center of the wall. The goal is to prove that the meso to macro transition is well performed and thus prevents mesh dependent results. The adopted homogenized in-plane curves $\Sigma_{yy} - \mathrm{E}_{yy}$ (designated as the principal quantities $\Sigma_{22} - \mathrm{E}_{22}$) are depicted in Figure 4.11 and the homogenized vertical bending moment M_{22} (designated as the principal stress couple, equivalent to M_{yy}) is obtained through-the-thickness integration of the wall using a Kirchhoff-plate theory.

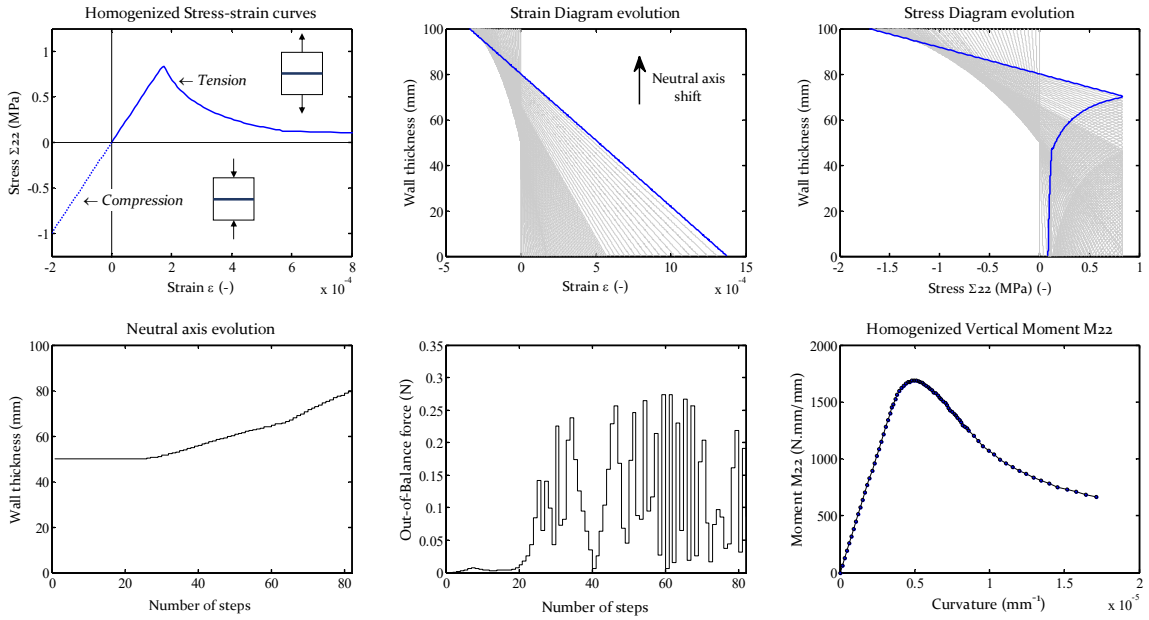

Figure 4.11 – Procedure for integrating the homogenized vertical stress-strain curves on the masonry thickness aiming to obtain the homogenized vertical bending moment curve for the benchmark test.

Following the meso-macro transitions steps addressed in section 4.3.2, the calibrated and regularized $\sigma - \varepsilon$ curves required for the vertical flexural truss beams have been identified for the present case study and gathered in Table 4.2. The quasi-static analysis allowed to reach the wall structural response whose capacity curve in terms of bending moment-curvature is represented in Figure 4.12 and compared with the expected one (M_{22} homogenized curved for an $L = 400$ mm). The results have shown that the strategy is well implemented and that adopting a simplified 6-node curve is adequate, since the stored bending energy difference is, between the obtained and the theoretical curves, less than 1%.

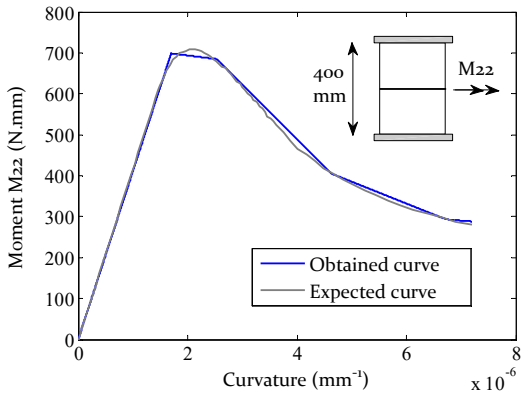

Figure 4.12 – Quasi-static test: expected vs obtained bending moment capacity curve.

Table 4.2 – Input $\sigma - \varepsilon$ curves for the CDP model.

Cracking Strain (-)	Stress (MPa)	Damage scalar d (-)
0.00E+00	9.61	0.0
5.06E-05	9.41	0.20
2.11E-04	5.57	0.42
3.49E-04	4.03	0.58
6.09E-04	3.36	0.65

Uni-directional cyclic loading

In classical plasticity theory, three main features are of utmost importance, i.e. the yield criterion, the flow rule and the hardening/softening rule (Lubliner et al. 1989). Here, a Mohr-Coulomb yield failure envelope and a non-associated flow rule have been assumed. For the hardening rule, the model depends on the definition of cracking strains associated with given effective stresses. It is the purpose of the uni-directional cyclic test to verify if the latter is well reproduced for a cyclic type of loading. Towards the latter, the same case study of Figure 4.10 has been used.

The process of strength deterioration is itself the pure representation of the softening rule evolution (Lubliner et al. 1989). Figure 4.13 shows that the obtained skeleton curve using the CDP model fits the expected quasi-static curve. The masonry strain-softening is exhibited as needed for cohesive-frictional materials.

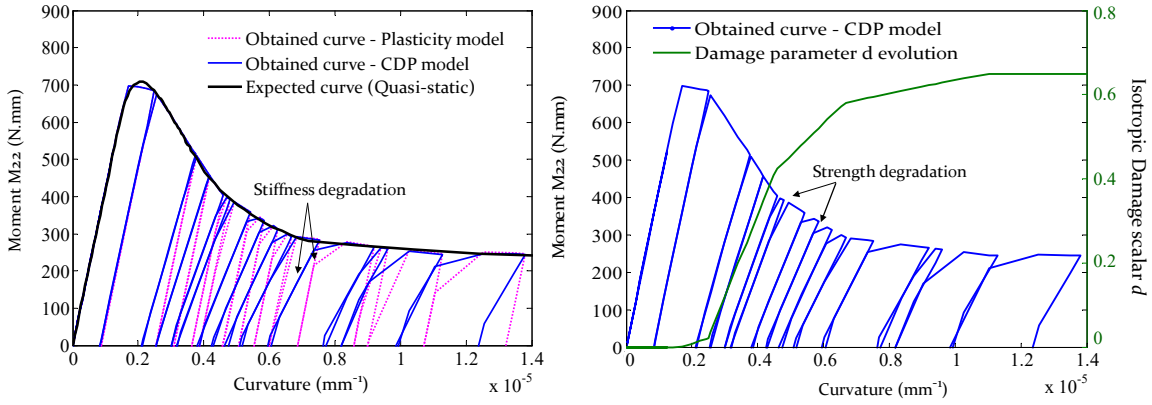

(a) (b)

Figure 4.13 – Uni-directional cyclic behavior: (a) comparison between a pure plasticity model and the damage plasticity (CDP) model; (b) damage scalar d evolution for the damage plasticity (CDP) model (NOTE: Only the positive moments are plotted, i.e. the part of the unloading branch for negative bending moments has been disregarded for the sake of readiness).

Furthermore, a damage model is coupled with the plasticity one, i.e. the softening rule is interpreted through an isotropic damage variable d which is, by itself, function of the equivalent plastic strains and thus its value never decreases. Stiffness degradation of the material after cracking should be accounted for. Figure 4.13a shows a comparison between the present CDP model and a pure plasticity model with absence of stiffness degradation. On one hand, both phenomenological representations allow to achieve permanent material plastic deformations, but these are higher if a total plasticity model with initial unloading stiffness is adopted (known to be too conservative). On the other hand, the appearance of plastic strains is a manifestation of inelastic behavior and, as Figure 4.13b proves, its evolution follows the expected path

(see Table 4.2) reaching a constant value after the ultimate strain threshold limit, correspondent to a cracking strain of 6.09E-04, in which the residual strength is defined and thus damage remains constant.

Bi-directional cyclic loading

The last test covers the bi-directional cyclic loading response of the outlined case study of Figure 4.10. The goal is to see if the expected hysteretic behavior of the flexural truss-beams is properly reproduced. Both positive and negative vertical bending capacities are similar, hence both the truss-beams ft_1 and ft_2 (see Figure 4.10) need to trace the same behavior. This is, in fact, sustained by Figure 4.14a where the Cauchy stress σ_{11} faced in both flexural trusses are similar in magnitude and, owing to the binary of the bending force, have an opposite signal.

Regarding the hysteretic behavior, after completion of the first cycle (A→F, $t = 2.25s$), as depicted in Figure 4.14c, the tensile peak is reached at A and the first tensile unloading branch initiates at B with a stiffness given by $E_B = (1 - d_t^B)E_0$ until C. The first compressive re-loading branch starts at C with a stiffness E_0, since a value of 1 has been defined for the recovery parameter ω_c and so, as predictable, the maximum compressive stress at D reaches the same magnitude than A, i.e. the maximum quasi-static envelope. In the same manner, the unloading branch (E→F) has a stiffness given by $(1 - d_c^E)E_0$, and the first re-loading tensile branch (F→G) the same stiffness than the last unloading tensile branch (B→C). This is equivalent for the first reloading compressive regime I→J, which follows the same path than the last unloading phase E→F. It is also noticeable that H and L have the same (in magnitude) axial stress σ_{11} than the last point of the quasi-static envelope. The material constitutive behavior formulation defines as minimum stress, or the designated residual strength, to be the last effective stress given as input, see Table 4.2. Thus, after reaching the point H, the damage parameter remains stationary (Figure 4.14b).

It has been demonstrated that the cyclic behavior is reproduced as it was expected and thus the proposed test has been passed. Both positive and negative vertical bending moments are represented (truss ft_1 and ft_2). It may be highlighted, again, that the latter holds true because total recovery effects have been defined for tensile and compressive regimes ($\omega_t = 1$ and $\omega_c = 1$). Furthermore, the model exhibits the capacity of allocating in memory the damage variables, for both the preceding tensile and compressive cycle of each flexural truss-beam, allowing thus the calculation of the onward un(re)-loading cycle.

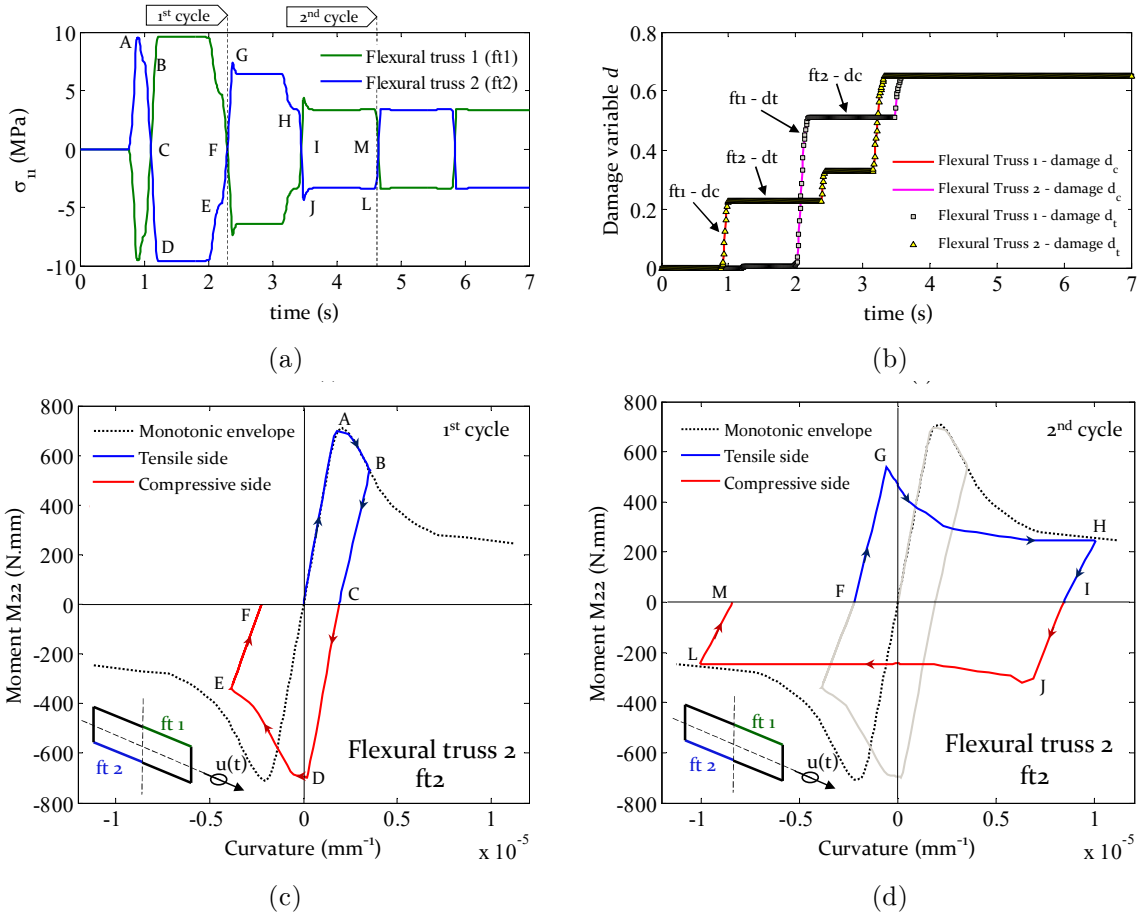

Figure 4.14 – Uniaxial cyclic loading: (a) Cauchy stress σ_{11} for the flexural truss beams; (b) Damage parameter d evolution for the flexural truss beams; (c) Vertical bending moment-curvature for the first cycle; and (d) Vertical bending moment-curvature for the second cycle.

4.5 Computational features and CPU parallelization

Selected computational features related to the RBSM model and its application on the advanced software ABAQUS are addressed next. It has been seen that the macro-scale behavior arises from the deformation of in- and out-of-plane truss beams which carry the information of the foregoing meso-scale. The advantages of restricting to linear elements the macro-response is especially related to its simplicity and one-dimensionality of the constitutive equations, cyclic behavior, strength domain, inelastic strain evolution laws, and damage evolution and tracking (closure-opening crack states).

The use of an advanced structural analysis software at a macro-scale, such as ABAQUS, brings clear benefits. In cases where a given instability renders a not purely positive definite stiffness matrix, the traditional equation solving strategies (as the Newton-Raphson, modified Newton-Raphson or secant methods) are unable to give a solution. In such situations, the software is robust because a modified Riks method (based in the works of Riks (1979, 1984)) is

at disposal. Such strategy combines a linear equation solver method as the Newton-Raphson algorithm with an arc-length algorithm (Crisfield 1981; Powell and Simons 1981) to overcome snap-back and snap-through issues; especially important for the present study when conduction quasi-static analysis in which material non-linearities are active.

A remark on the effectiveness of the FE static equation solver in terms of time costs and required RAM memory is also important to be stated. The bandwidth dimension of the global stiffness matrix [K], i.e. the number of columns from the diagonal to the last non-zero value along a row, has a high influence on the latter. Its minimization by using sparse matrixes is well-documented since the last century (Bathe and Wilson 1973; Collins 1973) with several algorithms being developed (Cuthill and McKee 1969; Bathe and Wilson 1974; Amestoy et al. 2004; Mafteiu-Scai 2014; Pop et al. 2014). A brief test consisting of a masonry wall subjected to a distributed load, and within a linear elastic analysis, has been developed. A refined mesh of 21×47 rigid quadrilateral elements represents the wall. Two algorithms for the mesh renumbering have been employed: (i) a geometric-based algorithm, whereas the mesh nodes are numbered according to a defined direction vector (length with higher dimension); and (ii) a tree-structured sparsity algorithm, in which the connectivity between adjacent elements is considered. The results are gathered in Table 4.3, whereas the differences between the models with and without a node reordering focus on the required physical memory. The computational time difference is negligible. Yet, the difference of $0.1s$ could be more relevant within a nonlinear quasi-static analysis, since several steps (and iterations) need to be solved.

Table 4.3 – Performance test on a masonry wall model (21×47 elements) for two mesh numbering algorithms.

Numbering algorithm	None	Geometric	Tree
CPU total time (s)	4.3	4.2	4.2
Optimum physical memory RAM (Mbytes)	18.4	16.2	16.1

Exploring the issue of the most efficient algorithm available in the literature is especially convenient for very large-scale structures; where powerful pre-processors software as ANSA (2017) can be used. Here, even if the performed test is simple, it aims to raise the reader awareness (or the discrete-model FE user) for the importance of using a renumbering strategy after the modeling stage. To cope with the concern of improving computational efficiency, ABAQUS offers a renumbering algorithm based on a geometrical method. This seems suitable for the dimension of the structural problems involved in the present thesis and in cases where a dominant length direction exists.

For dynamic analysis, the macro-system equilibrium can be solved using an implicit or explicit scheme, because both are eligible to be used in the software. Here, two main reasons support the selection of an implicit procedure. The first concerns the modeling of the inertial mass system which is achieved by assigning a representative density value for the rigid-plates only. In opposition to an implicit scheme, which can handle such assumption, an explicit solver demands the insertion of density values for all the elements, which would in one side turn the modelling more complex and, in the other, compromise the stability and representativeness of eigenvalues problems due to the local modal effects if truss-beam elements have an associated mass.

The second reason is linked to the intrinsic nature of each procedure. The explicit solver requires the use of considerable small time increments to avoid a system misrepresentation, i.e. suffers from a time-step solution bias. Its use is largely recommended for many problems due to its stability, as fast-dynamic problems or when interfaces contact exist (Hilber et al. 1977; Belytschko et al. 1984; Burnett et al. 2007a; Rafsanjani et al. 2015a). Bearing that the general scope of the approach is the seismic study of masonry structures, the earthquakes have a signal in the range of seconds. In case an explicit solver is used, it may lead to long and prohibitive processing times and, as well, the demand of a larger disk storage space. Conversely, an implicit procedure allows larger time increments with the setback that a converged solution must be found for each iteration.

Finally, the code is also adapted to calculate the macro-level response within parallel computing and on graphical processing units (GPU). This has a special interest to speed-up the processing times for dynamic or large-scale problems (Kruis et al. 2016; Krejčí et al. 2017) but obviously depends on the machine at disposal. Here, only the former has been explored as it will be described in the next chapter.

4.6 Summary

The present chapter focus on the macro-scale formulation of the proposed two-step strategy in the software (ABAQUS 2013). The coupling between the meso-scale models with the discrete FE-based strategy (namely, RBSM or Rigid-Body-Spring-Mass) has been also referred. The RBSM strategy is composed by quadrilateral rigid plates interconnected at its interfaces by a set of in- and out-of-plane FE truss-beam systems. More care has been given to the OOP (Out-Of-Plane) behavior since the IP (In-Plane) one derives from an already existing study. One dimensional elements only (the truss FE-beams), through a concrete damage plasticity model, can mimic the homogenized material data and govern the macro-deformation and damage of

the media. The well-posedness of the solution found is guaranteed by a regularization step which corrects the fracture energies of the stress-strain input curves according to the defined macro-mesh dimensions.

Validation and convergence tests have been performed to ascertain that the RBSM macroscopic model fulfills the requirements for: (i) elastic problems; (ii) eigenvalue problems; and (iii) nonlinear problems for monotonic and cyclic loading cases. The tests proved that the discrete model responds well to the convergence tests in both static and dynamic ranges. Likewise, it has been concluded that a refinement level given by $L/15$ (L is the length of the wall side being meshed) seems a reasonable choice for the mesh size to conduct a structural analysis if a sensitivity test is not performed. Computational recommendations have been also very briefly addressed, as the use of the arc-length method for nonlinear quasi-static tests and a renumbering algorithm to take full advantage of the computational capacity.

Lastly, it is worth noting that a decoupled characterization of flexural and torsional actions is adopted. Whilst such decoupling is certainly an approximation, it proved to be reliable, at least for levels of membrane pre-compression lower than the masonry compressive strength. In cases where pre-compression states are considerable, the results should be analyzed with more care, due to its potential non-conservative character. Furthermore, the procedure possesses a ubiquitous feature at a macro-scale, noting that the RBSM model can be implemented in any FE software, to any structural application and, more importantly, to be used by both professionals and researchers.

(vacate page)

Chapter 5

5 Multi-scale out-of-plane static and dynamic analysis of masonry: applications

5.1 Introduction

This chapter addresses the application of the two-scale numerical procedure for the analysis of Unreinforced Masonry (URM) structures. The two levels of analysis described in §Chapter 3 and §Chapter 4, i.e. the meso- and macro-scales, are herein coupled. Accordingly, the behavior characterization of the complex morphology of masonry is performed in a scaled-down model via a homogenization process. The computed data, which is able to represent the material anisotropy and full-softening regime, is used to represent the structural behavior of the masonry through a discrete Rigid Block Spring and Mass (RBSM) model.

The numerical strategy may provide an accurate prediction of the masonry behavior with a very attractive computational time cost. Since URM structures are rather vulnerable to undergo failure due to out-of-plane (OOP) mechanisms, several case studies have been carefully selected aiming to demonstrate the capability of the strategy. In this regard, the application of the two-scale numerical procedure is presented next and with the following outline: (i) static analysis of OOP loaded masonry walls in two-way bending; (ii) static and dynamic analysis of a URM structure subjected to a unidirectional seismic input; and (iii) the dynamic analysis of a URM parapet subjected to a vehicle-type impact load.

A brief overview of the problem is given for each of the selected case studies. The modelling and material assumptions considered are also detailed and the treatment of the results is carried out to allow a comparison with the experimental data at disposal. Results from other numerical frameworks are, when possible, used to complement the study.

5.2 Quasi-static analysis

5.2.1 Overview

Quasi-static analyses are performed next accounting for available experimental data of windowed and full panels in two-way bending. The panels from the studies of Gazzola and Drysdale (1986) at the University of McMaster and Chong et al. (1994) at the University of Plymouth are discussed here to show the capabilities of the procedure proposed. These traditional experimental tests for the study of the out-of-plane behavior of masonry panels use air-bags to apply the load. A constant normal pressure is thus transferred to the

masonry and, since it is gradually incremented, a quasi-static type of numerical analysis can be employed. Global pressure-displacement curves and crack patterns are available from the experimental campaigns. Numerical data from other numerical strategies is also at disposal.

5.2.2 McMaster university panels

The first masonry panels being analyzed are built with hollow concrete blocks with a running-bond texture and belong to the experimental campaign performed at the University of McMaster by Gazzola and Drysdale (1986). Although a total of five panels have been experimentally tested, only the panels designated as WF, WII and WPI are covered here, see Figure 5.1. Panel WF is simply supported in three edges and free in its top edge. Panels WII and WPI are geometrically alike, but an in-plane confining pressure of 0.2 N/mm^2 has been applied in the latter before and during the out-of-plane loading history.

The dimensions of the bricks are $390 \times 190 \times 150$ mm^3 and the thickness of the joints is 10 mm. Information concerning the assumed material and mechanical properties is reported in Table 5.1, which have been used at a meso-scale following a Kirchhoff-plate theory. The inelastic properties adopted for the masonry components have been derived from the composite material data reported by Gazzola and Drysdale (1986) (cf. section 3.5.2). The properties' identification led to a horizontal and vertical flexural strength value of $f_{tx} = 0.92$ (N/mm^2) and $f_{ty} = 0.37$ (N/mm^2), respectively. The elastic properties are unavailable and thus assumed to be equal to the ones adopted by Lourenço (2000), with an orthotropy ratio of two and a Poisson's coefficient of 0.2.

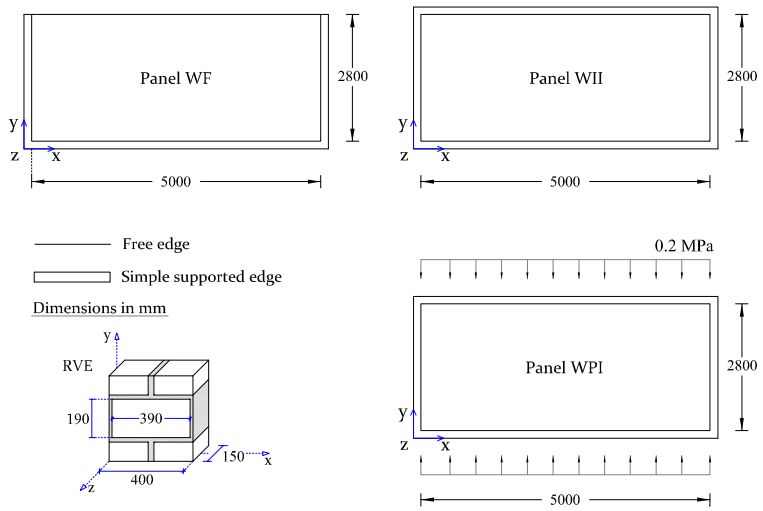

Figure 5.1 – Description of the geometry and boundary conditions of the masonry panels out-of-plane loaded at University of McMaster by Gazzola and Drysdale (1986).

Gazzola and Drysdale (1986) prepared three setups for each panel configuration, which have been out-of-plane loaded (uniform pressure p) until failure. Even though only the average collapse loads are reported in Gazzola and Drysdale (1986), the results' discussion addresses also the obtained capacity curves for the panels WI, WII and WPI. Figure 5.2 illustrates a comparison over the global force-displacement curves obtained through the present model and: (i) the average experimental collapse load (McMaster university data), (ii) an anisotropic macroscopic model by Lourenço (2000) and (iii) an upper and lower bond limit analysis by Milani et al. (2006).

Table 5.1 – Material properties adopted for the McMaster panel: elastic properties adopted for the homogeneous RVE and the inelastic properties of the mortar joints interfaces.

Elastic properties of the homogeneous RVE			
E_{xx}	E_{yy}	G_{xy}	ν_{xy}
5000 (N/mm²)	10,000 (N/mm²)	3125 (N/mm²)	0.2 (-)

Inelastic properties (mortar joints interfaces)							
f_t	f_c	c	$tan(\phi)$	Ψ	G_f^I	G_f^{II}	G_f^{IV}
0.15 (N/mm²)	20.0 (N/mm²)	0.38 (N/mm²)	0.577 (-)	45.0 (deg)	0.018 (N/mm)	0.04 (N/mm)	4.00 (N/mm)

A refined mesh size of 100 mm has been adopted, with a total of 1196 discrete elements for each panel (each discrete element has 4 quadrilateral rigid plates). Table 5.2 resumes the identification of the Young's modulus values for each macro-truss of the discrete model proposed.

Table 5.2 – Elastic identification of the discrete macro-model for the McMaster panels with a refined mesh of 100 mm size.

Elastic Parameters - Discrete macro-model (H=100 mm; e=20 mm)					
$E_{flexural\ truss}\ xx$	$E_{flexural\ truss}\ yy$	$E_{torque\ truss}\ xy$	$E_{torque\ truss}\ yx$	$A_{flexural\ truss}$	$A_{Torque\ truss}$
457,763.67 (N/mm²)	915,527.34 (N/mm²)	43,945.31 (N/mm²)	43,945.31 (N/mm²)	1000 (N/mm²)	1000 (N/mm²)

The capacity curve calculated for a point located in the center of the free edge of the panel WF is observed in Figure 5.2a. An acceptable difference of 11% is reached between the obtained peak capacity and the experimental failure load. Moreover, a good agreement is found for both the elastic response and capacity, when compared with the results from the anisotropic model of Lourenço (2000). Nonetheless, the post-peak regime is rather different, being the response of the proposed model less ductile, possibly justified by the lower tensile fracture energies adopted.

The onset of cracking is initiated near the center of the panel at its bottom half. The cracking pattern at the peak is well marked by a horizontal crack and some damage due to torsion near the two bottom corners exist, see Figure 5.3a. In the post-peak branch there is a higher redistribution of stresses, being possible to catch a well-defined yield-line type of failure for a displacement of 20 mm, see Figure 5.3a. The observation of such pattern only in the post-peak region somehow justifies the difference found with the simplified upper bound limit analysis result from Milani et al. (2006), and the apparent inability of yield-line based methods for the analysis of quasi-brittle materials.

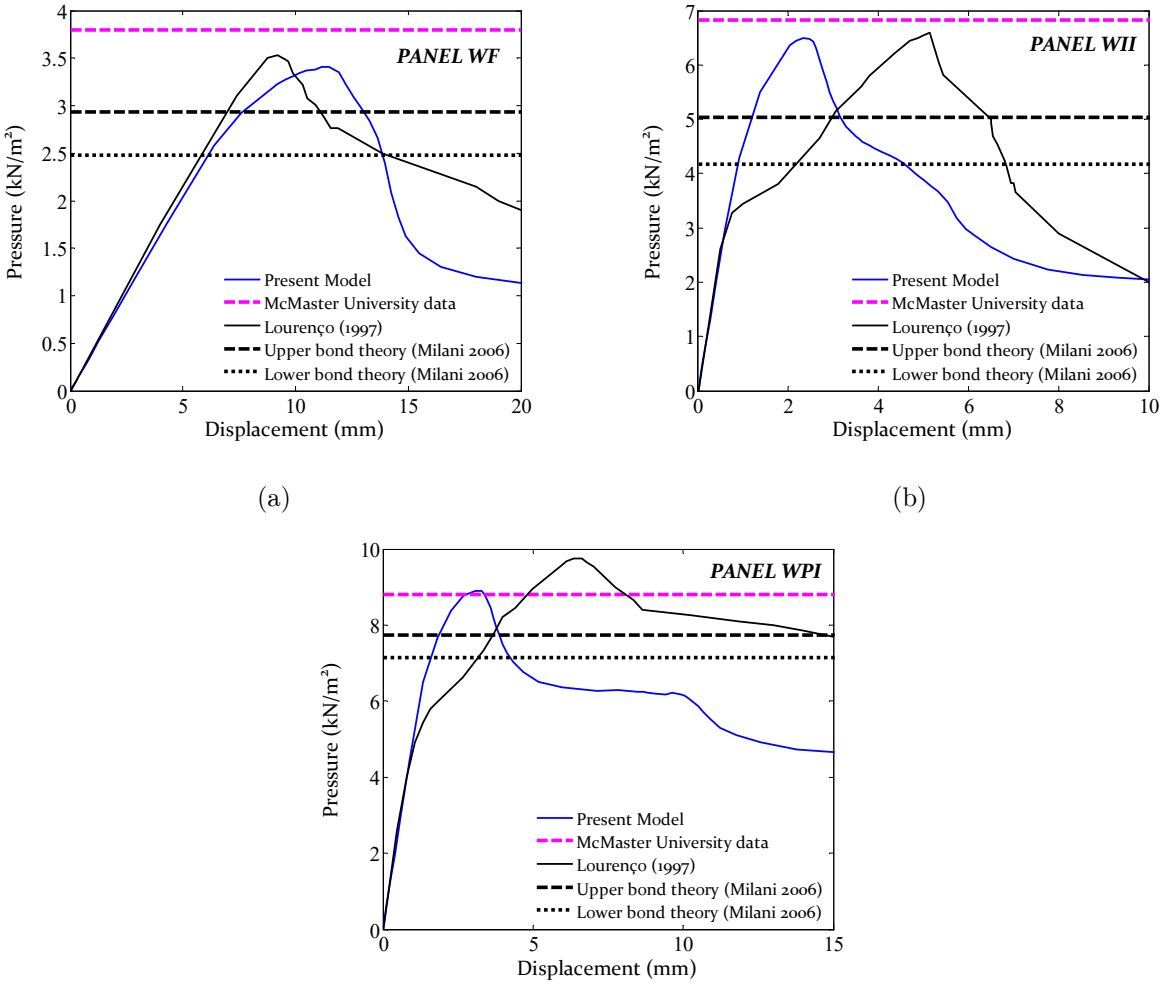

Figure 5.2 – Numerical and experimental curves of the panels tested by Gazzola and Drysdale (1986). Pressure load vs displacement for the panel: (a) WF; (b) WII; and (c) WPI.

The second panel being analyzed is referred as WII. Its response is significantly different from the previous panel (WF) due to the fact that now four supported edges exist allowing, therefore, to increase the collapse load by 40%. A difference ranging 5% is observed between the experimental data and the peak load reached with the present model. A similar result has been provided by the anisotropic model of Lourenço (2000), yet with a distinct pre-peak path. The two approaches match the initial stiffness but the latter demonstrates a considerable loss of stiffness after the onset of horizontal cracking ($p = 3.3$ kN/m^2); not observable with the present numerical approach.

Figure 5.3b shows the damage obtained at the peak, which is predominantly manifested on the mid-span area of the panel through two moderate horizontal cracks. On one hand there is low redistribution of the stresses, since residual torsional damage near the corners exist; on the other hand, the cracks orientation trails the typical response, i.e. tend to develop orthogonally to the shorter span which is also, for this case, the weaker direction (vertical bending). The so-called *X*-brace damage pattern, representing the yield-line type of failure, is only achieved for the post peak regime. The damage plot associated with a mid-span displacement of 10 mm shows two severe horizontal cracks at the center of the panel, and four cornered regions with damage concentration (mainly due to torsion movements, diagonal cracking).

The last panel, denoted as WPI, has the same geometry and boundary conditions of the panel WII. As previously mentioned, the difference is that now a vertical pre-compression state of 0.2 N/mm^2 is included. The confinement leads, theoretically, to an increase of both the capacity and ductility of the response, as seen in the section §3.5.2. Figure 5.2c corroborates the latter, as the experimental collapse load had an increase of 32%. The numerical solution matches well with the latter value (a difference below 2% of error). Considerations regarding the curve shape and its comparison with the one derived by Lourenço (2000) are alike with the ones addressed for the panel WII; likewise, subtle differences can be found concerning the damage map. Since the pre-compression state gives an extra-strength and ductility, it is observed that the damage at the peak is quantitatively less pronounced and more equally distributed. The same conclusion is drawn for the post-peak region, see Figure 5.3c, in which a yield-type of failure is now clear but still with the softening regions affected by a lower damage parameter.

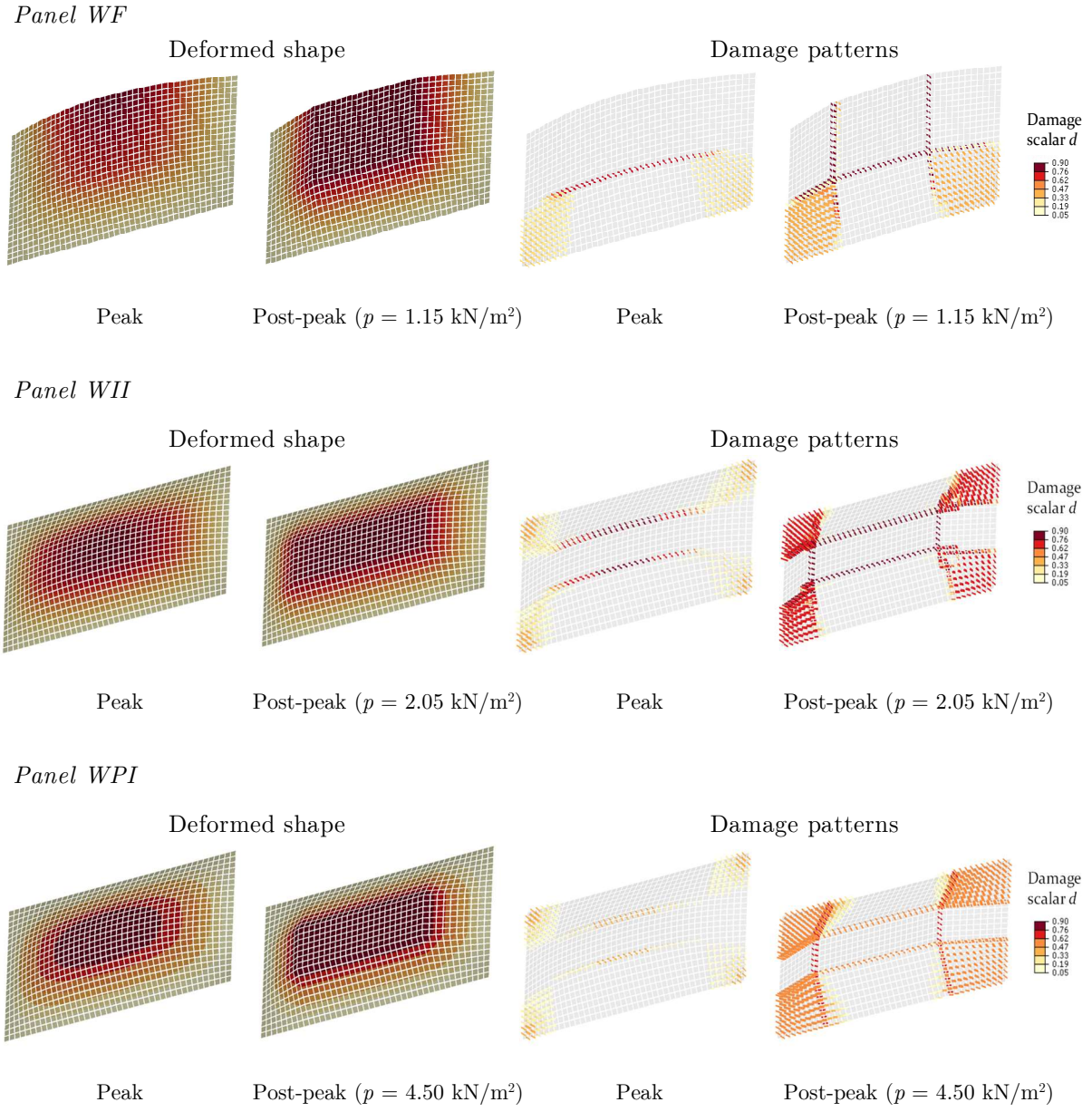

Figure 5.3 – Numerical damage patterns of the McMaster panels obtained with the proposed macro- model.

In general, a good agreement has been found between the different numerical strategies and the experimental data. The numerical model handles well the increase of both capacity and ductility in presence of an in-plane pre-compression load.

5.2.3 Plymouth university panels

The second set of out-of-plane experimental data is constituted by the panels tested at the University of Plymouth by Chong et al. (1994). Five panels in running bond masonry texture using solid clay bricks were tested and designated by SB (Chong et al. 1994; Southcombe et al.

1995). The panels SB01 and SB05 have the same geometry, hence only four panels (SB01-SB04) are considered and represented in Figure 5.4. The panels are simply supported at the lateral edges and fixed at the base. The experimental investigation aimed at a better insight on the role played by the openings size and shape. The panels have been loaded by air-bags until failure, and both the pressure and displacement at the middle span of the free edge monitored. Thus, the comparison is here done in terms of pressure load and displacement for each masonry panel.

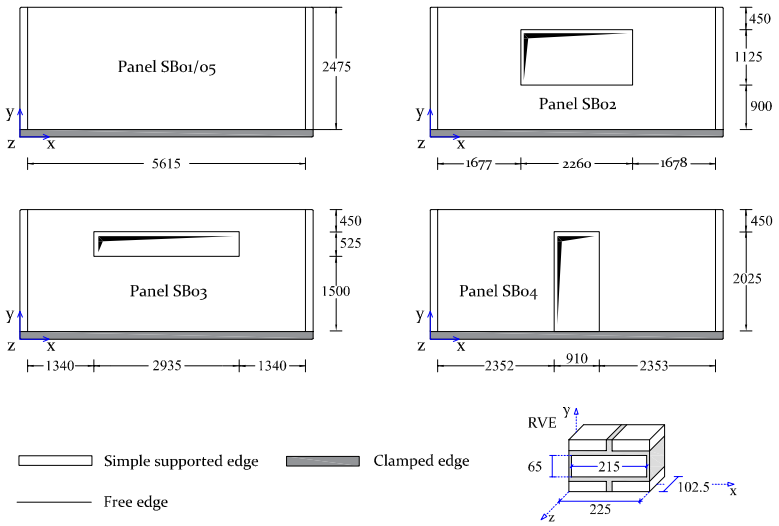

Figure 5.4 – Description of the geometry and boundary conditions for the masonry panels out-of-plane loaded at University of Plymouth by Chong et al. (1994).

The elastic and inelastic material properties adopted for the RVE characterization at a meso-scale, following a Kirchhoff-plate theory, are presented in Table 5.3. An isotropic behavior assumption is acceptable as referred by Chong et al. (1994), since the panels are built with solid brick masonry. Despite that, an orthotropic ratio of 1.2 has been derived for the composite material via homogenization process by assuming, respectively, a Young's modulus of 10,000 N/mm^2 and 3,500 N/mm^2 for brick units and mortar joints. Furthermore, the experimental data provides only the flexural tensile uniaxial strengths f_{tx} and f_{ty}, given by 2.28 and 0.97 N/mm^2, respectively. Therefore, only inelastic tensile behavior is active and the mechanical properties adopted have been tuned in order to fit the latter values. The brick units' dimensions are 215×65×102.5 mm^3 and the thickness of the joints is 10 mm.

Table 5.3 – Material properties adopted for the McMaster panel: elastic properties adopted for the homogeneous RVE and the inelastic properties of the mortar joints interfaces.

Elastic properties of the homogeneous RVE			
E_{xx}	E_{yy}	G_{xy}	ν_{xy}
9700 (N/mm²)	8000 (N/mm²)	4993 (N/mm²)	0.2 (-)

Inelastic properties (mortar joints interfaces)							
f_t	f_c	c	$tan(\phi)$	Ψ	G_f^I	G_f^{II}	G_f^{IV}
0.30 (N/mm²)	4.00 (N/mm²)	0.36 (N/mm²)	0.57 (-)	45.0 (deg)	0.015 (N/mm)	0.025 (N/mm)	1.00 (N/mm)

A refined mesh with 100 mm of size has been defined with a total of 987 discrete elements for panel SB01/05, 797 elements for panel SB02, 862 elements for panel SB03 and 834 elements for panel SB04. Table 5.4 resumes the identification of the Young's modulus values for each macro-truss of the discrete model proposed.

Table 5.4 – Elastic identification of the discrete macro-model for the Plymouth panels with a refined mesh of 100 mm size.

Elastic Parameters - Discrete macro-model (H=100 mm; e=20 mm)					
$E_{flexural\ truss}\ xx$	$E_{flexural\ truss}\ yy$	$E_{torque\ truss}\ xy$	$E_{torque\ truss}\ yx$	$A_{flexural\ truss}$	$A_{Torque\ truss}$
193630.37 (N/mm²)	159695.15 (N/mm²)	15309.27 (N/mm²)	15309.27 (N/mm²)	1000 (mm²)	1000 (mm²)

Figure 5.5 shows the comparison between the numerical and experimental results from Chong et al. (1994) taking into consideration the pressure load and displacement at the middle node of the free edge. In addition to the present model other results are gathered, namely: (i) an anisotropic macro-model (Lourenço 2000); (ii) an elastic perfectly-plastic homogenized model designated as EPP-model (Milani and Tralli 2011); (iii) a simplified deteriorating homogenized model designated as SD model (Milani and Tralli 2011), based on a limit analysis approach to define the failure mechanism; and finally (iv) a simplified quadratic programming elastic-plastic model by Milani and Tralli (2011) and designated as EPD, in which the deterioration of interfaces (ultimate bending moment) is considered.

The first panel being analyzed has no opening and is designated as SB01/05. The obtained capacity curve is plotted in Figure 5.5a. Both the elastic stiffness and the peak load are in agreement with the results found experimentally, with a difference of about 5% concerning the latter. A steep loading decrease around the 20mm of out-of-plane displacement indicates the loss of strength and consequent failure of the panel. The damage onset occurs due to vertical bending and occurs near and parallel to the fixed base of the wall, as seen by the cracking

pattern at the peak load (Figure 5.6a). After the peak, two well marked vertical cracks are formed from the center to the free edge of the panel. Extensive damage due to torsion movements occur near the lateral supports which define a diagonal failure developed from the bottom corners of the panel. The latter is in agreement with the experimental findings, in which the typical yield-line type of failure has been obtained.

For the second panel, designated as SB-02 (see Figure 5.5b), a slightly lower capacity is observed when compared with the SB01 one. This is expected since the SB-02 panel has an opening with dimensions 2260×1125 mm^2. A loss of stiffness occurs for a load given by $p =$ 2.20 kN/m^2 and the peak is reached for $p = 2.48$ kN/m^2. Although the load-displacement curve at the control node has the same shape than the experimental one, a relative difference of about 19% exists between the peak load values. Figure 5.6b shows that the damage at the peak stage surrounds the bottom corners of the opening with the formation of diagonal cracks towards the lateral supports of the panel. This is even more evident in the post-peak side ($p = 1.70$ kN/m^2), being also possible to observe a vertical crack in the top of the opening due to horizontal bending.

The third panel studied here is denoted as SB03 and has a windowed type of opening (2935×525mm^2). An alike behavior is observed with the panel SB02. A good agreement in terms of the peak load can be seen in Figure 5.5c with a deviation of 4%. The experimental curve does not possess a well develop post-peak path, still it can be noted that the shape of the numerical curve is comparable with the one from the macroscopic model by Lourenço (1997). Figure 5.6c shows that the damage at the peak is focused near the corners with slight damage at its base. Again, the post-peak behavior is characterized by the formation of diagonal cracks at the sides of the opening in the direction of the lateral supports. Likewise, the formation of the vertical crack above the opening is detected.

At last, the analysis of the panel SB04 has been carried out. A door type of opening with 910×2025 mm^2 exists. A reasonable agreement has been found between the numerical and experimental capacity curves, with a relative error of about 4% regarding the peak load. Figure 5.6d shows that the damage tends to initiate, again, near the base and parallel to the fixed support. The damage at the post-peak region for $p = 1.72$ kN/m^2 indicates that the failure occurs due to the development of a vertical crack above the opening (horizontal bending) and comprises damage due to torsional movements around the lateral supports.

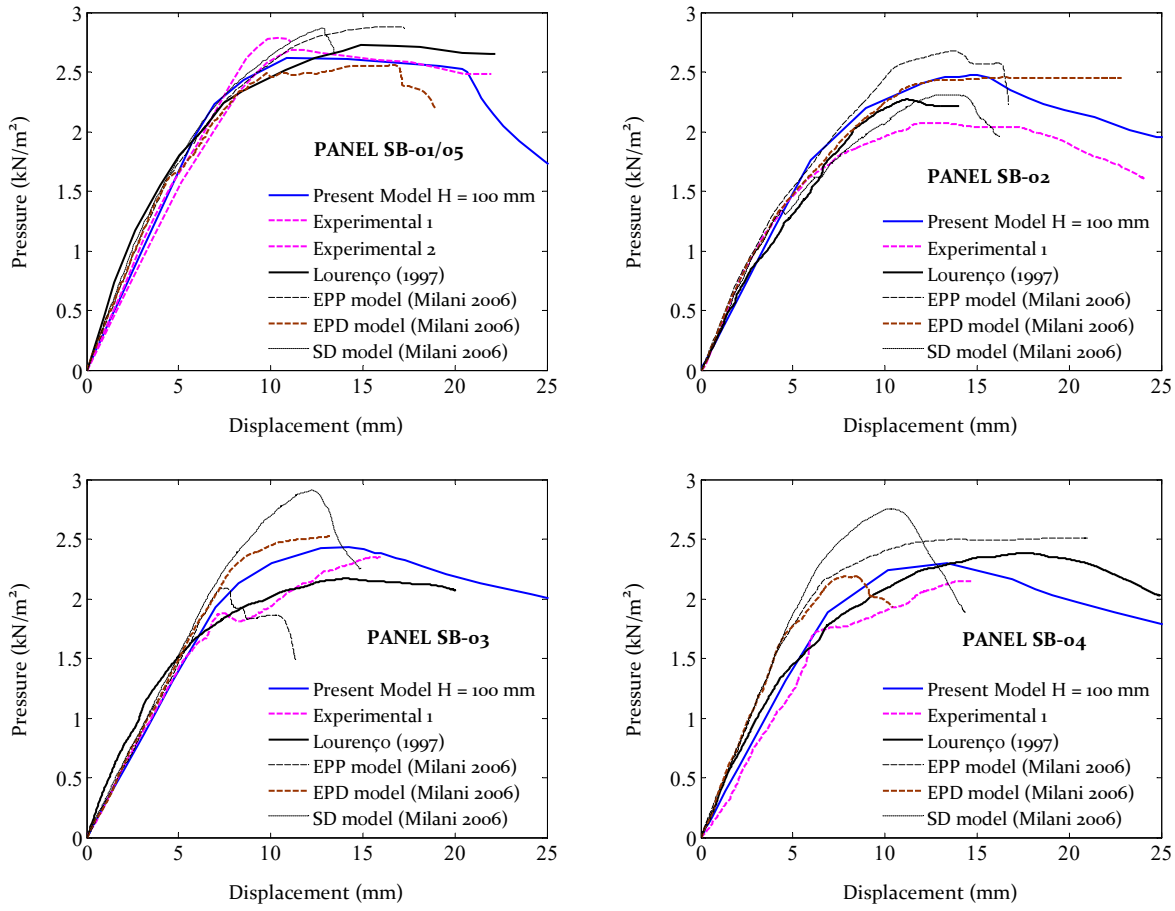

Figure 5.5 – Numerical and experimental curves for the panels experimentally tested by Chong et al. (1994): pressure load vs displacement.

In general, the comparison allows concluding that the presented numerical procedure features a good agreement for all the panels studied in the quasi-static range, both in terms of collapse load and displacements prediction. Although stemming from a simplified discrete model at a macro-scale, the proposed model can retrieve similar results to sophisticated continuum FE based strategies, such as the one presented by Lourenço (1997). Moreover, the last is especially highlighted if the results are compared with other simplified strategies that consider also a homogenization process, as the EPP, the EPD and SD models from Milani and Tralli (2011). However, in converse with these strategies that use limit analysis, the present model accounts with the full softening behavior of the material within a FE formulation without compromising the computational burden, as reported in the next section.

Panel SB01

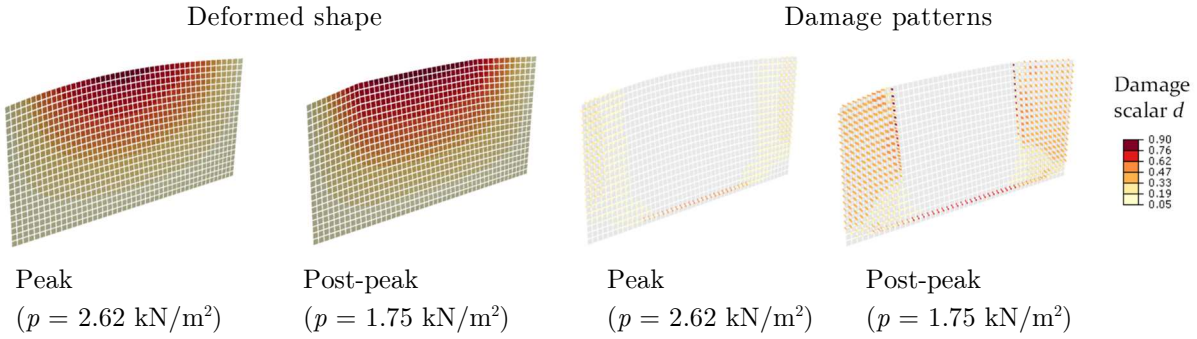

Peak ($p = 2.62$ kN/m^2) | Post-peak ($p = 1.75$ kN/m^2) | Peak ($p = 2.62$ kN/m^2) | Post-peak ($p = 1.75$ kN/m^2)

Panel SB02

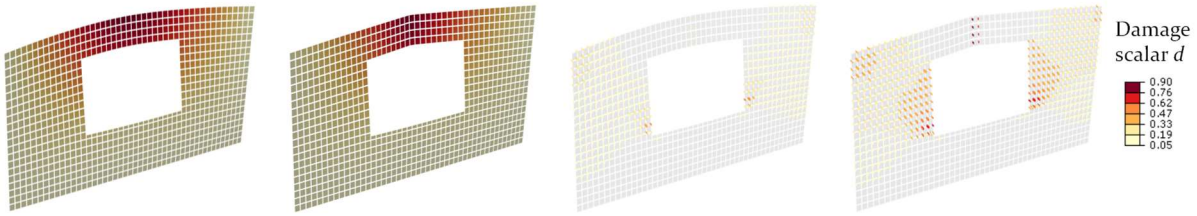

Peak ($p = 2.48$ kN/m^2) | Post-peak ($p = 1.70$ kN/m^2) | Peak ($p = 2.48$ kN/m^2) | Post-peak ($p = 1.70$ kN/m^2)

Panel SB03

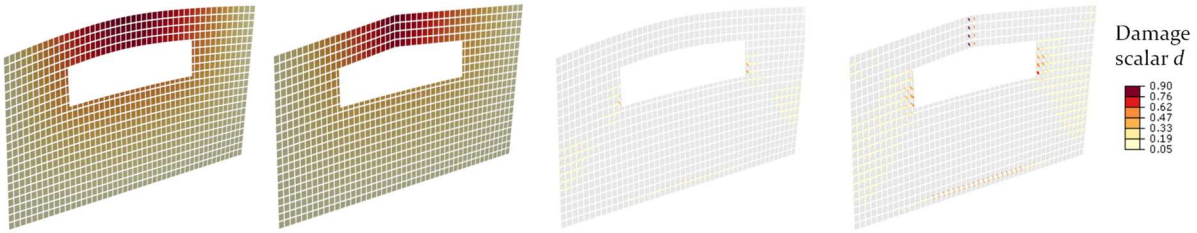

Peak ($p = 2.43$ kN/m^2) | Post-peak ($p = 1.78$ kN/m^2) | Peak ($p = 2.43$ kN/m^2) | Post-peak ($p = 1.78$ kN/m^2)

Panel SB04

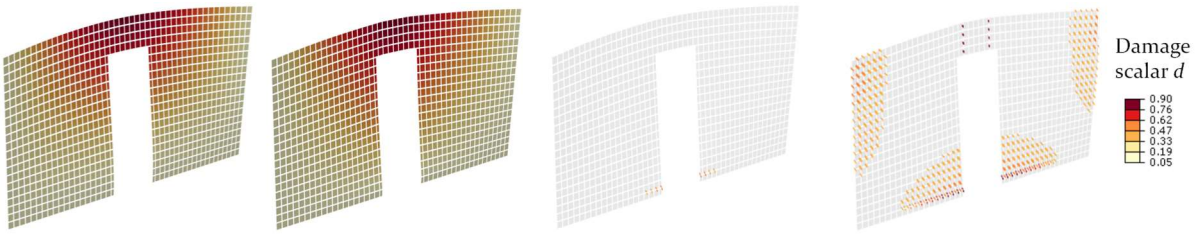

Peak ($p = 2.29$ kN/m^2) | Post-peak ($p = 1.72$ kN/m^2) | Peak ($p = 2.29$ kN/m^2) | Post-peak ($p = 1.72$ kN/m^2)

Figure 5.6 – Damage patterns obtained from the numerical analyses (mesh H=100 mm).

5.2.4 Mesh sensitivity and computation time of the solution

A mesh sensitivity study of the solution at a macro-scale is performed. This is an inevitable issue when dealing with the strain softening (and/or hardening) of materials. It has been stated, in a foregoing section (§4.3.3 and §4.3.4), that the macro-model accounts with a regularization factor aiming to remove the mesh bias of the material input given for each of the macro-trusses. Such factor is purely geometrical, meaning that is dependent only on the size of the quadrilateral squared elements and on the existing space between them; comparable with the traditional crack-band theory used for continuous FE models (Bažant and Oh 1983), in which the regularization factor is dependent on the finite element area. The study is performed on the Plymouth panels only, whereas the analyses are repeated with two less refined meshes of H=200mm and H=450mm (with respect with the brick size). The goal is to evaluate the mesh dependency in terms of results accuracy and analyze the incurring running times.

The comparison in terms of load-displacement curves is depicted in Figure 5.7. Regarding the peak loads, the differences range the 10% for the panel SB-01/05 and 5% for the panels SB02, SB03 and SB04. Some differences may be noted in the post-peak behavior and, even though are acceptable, it is well known that rigid elements, where nonlinearity is concentrated on interfaces, intrinsically suffer from limited mesh dependence on softening. In general, the results show the capacity of the model to obtain good representations of the peak and nonlinear behavior in panels with complex geometries, using several mesh refinements. Figure 5.7 demonstrates that the mesh dependency is low for the selected refinements, as the obtained difference on the pressure-displacement curve is less than 10%, which seem to be adequate within engineering applications.

In addition, it is worth noting that the required computational time is impressively reduced for the coarse mesh (only 18seconds), but still reasonable for a strong mesh refinement, see Figure 5.8 (an exponential reduction trend is observable with the increase of the mesh size). The deformed shapes of panel SB-01/05 for the three refinement levels are also presented in Figure 5.8. Note that a laptop with an i7-4710MQ CPU, 16 GB of RAM (DDR2) and with an SSD disk with a writing velocity of 512 Mbytes/s has been used.

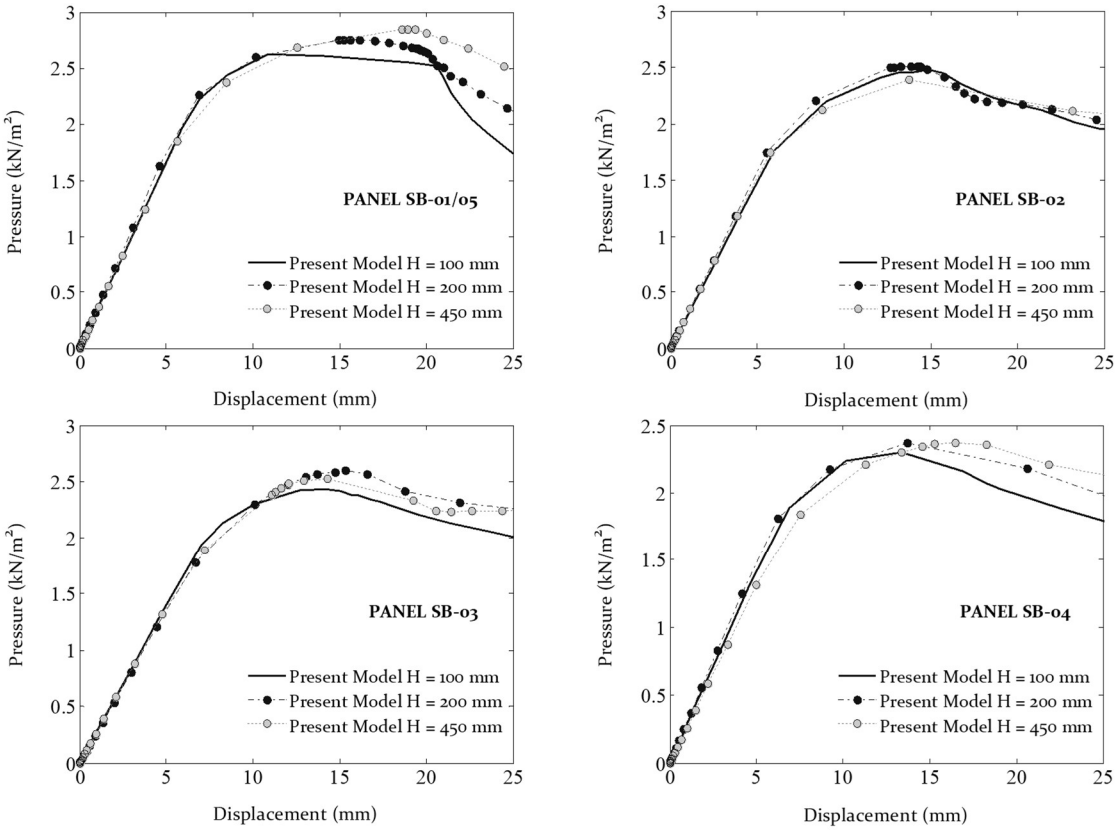

Figure 5.7 – Mesh dependency study of the solution for the Plymouth panels studied.

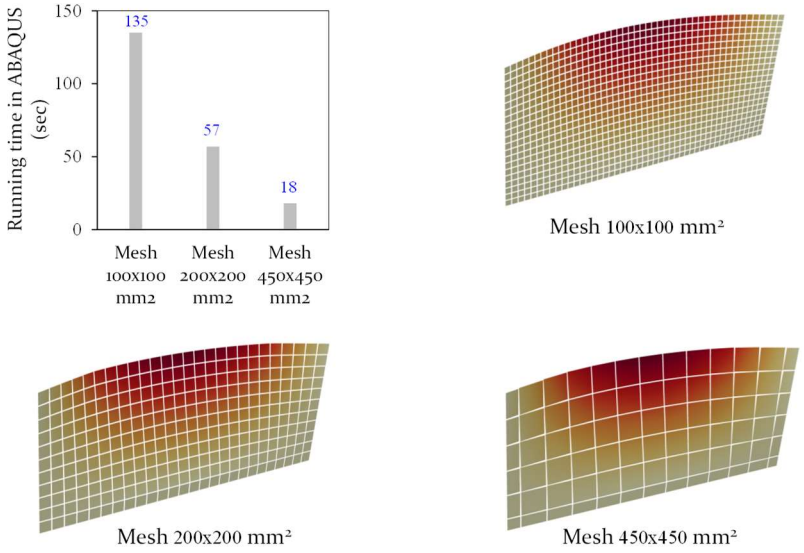

Figure 5.8 – The computation time demand to perform the quasi-static analyses for the panel SB - 01/05 using three mesh refinements. Plot of the respective deformed shapes at the peak load points of the associated curves.

5.3 Dynamic analysis: seismic loading

5.3.1 Overview

Experimental research still constitutes a crucial source of knowledge in the field of structural dynamics. The present study can contribute to enrich the available literature on the existing numerical strategies with a particular focus on the multi-scale type of analysis. The case study reports an English-bond masonry mock-up tested in the National Laboratory of Civil Engineering at Lisbon (LNEC) by Candeias et al. (2016) which, by itself, may comprise a good basis for numerical investigations since few studies still exist on such brickwork when the material nonlinearity is being assumed, for instance the works by Cecchi and Milani (2008) and Milani (2008).

This section demonstrates the ability of the procedure to reproduce the dynamic macro behavior of a complex three-dimensional masonry structure and see if similar conclusions are drawn with the previous studies on the same benchmark. The main novelties are twofold: (i) the ability of the procedure to reproduce the effect of three-dimensional effects on the macro-stress out-of-plane quantities; and (ii) the ability of the procedure to reproduce the effect of the presence of thickness discontinuities, as it is the case of the English-bond texture.

The section is organized as described next: (i) the introduction of the case study; (ii) the description of the presented numerical procedure with emphasis on the macro-level application; (iii) the application of the procedure through quasi-static and dynamic analyses, wherein the results are compared with experimental data and complemented with results from a well validated macroscopic total strain crack model in the software DIANA (2017); and, at last, (iv) the discussion of the main conclusions.

5.3.2 LNEC Brick house mock-up

The selected case study is gathered from the experimental work performed in LNEC by Candeias et al. (2016). The case study has been developed to make possible a blind test prediction by different invited authors using several advanced numerical procedures. The main results and differences between approaches, as well as open issues, are addressed in Mendes et al. (2017). The aim was to assess the collapse acceleration of the structure when subjected to a one-directional seismic input.

Two unreinforced masonry structures were tested. One mock-up is made with an English-bond brick masonry and another is made from an irregular stone masonry texture. As the principle of the scale's separation is assumed between the meso- and macro-levels, only the

study of the former benchmark is carried out. In fact, the adoption of the present strategy to the stone mock-up would be obviously possible but theoretically unfeasible, due to the large dimensions of the stone units (which define the size of the RVE) in respect to the structure ones.

The studied brick structure is composed of three walls in a U-shaped plan arrangement. The main façade (East plan) presents a gable wall and is linked with two transversal walls which act as abutments (North and South plans). These are constructed with a clay brickwork in an English-bond arrangement of 235 mm of thickness (slenderness ratio about 1:10). The clay brick units have nominal dimensions of 235x115x70 mm^3 and are laid and bound together by mortar joints with a thickness ranging from 15 to 18 mm. The geometrical features are seen in Figure 5.9a. The brick mock-up was tested up to collapse in a shaking table under a unidirectional seismic loading. The seismic input is applied in a perpendicular direction (E-W) to the main façade and derives from the N64E strong ground motion component associated with the February 21 of 2011 earthquake occurred in Christchurch, New Zealand. After the filtering and cropping of the original signal, the base input has 27 seconds of duration, 0.28g m/s^2 of PGA (Peak Ground Acceleration), 0.236 m/s PGV (Peak Ground Velocity), and 0.0258 meters of PGD (Peak Ground Displacement). The latter time signal served as a reference for the seismic input generation, whereas eight accelerograms have been derived and appended. These have been obtained from a scaling process through different increasing factors, starting from one up to three, due to the apparatus limitation. The input signal considered in the dynamic analysis is displayed in Figure 5.9b.

The structure collapsed during the last excitation (accelerogram number eight, acc08) for a PGA value of 1.27g, and the obtained failure mechanisms are depicted in Figure 5.10. The partial out-of-plane overturning of the gable wall and its tympanum has been registered, with the formation of diagonal cracks spreading from the window opening (east plan). An in-plane failure has been also obtained at the north returning wall with a well demarked horizontal cracking line defined by the bottom base of the existing opening.

For a detailed explanation regarding the assumptions that had been taken in the selection of the strong motion component, in the filtering process of the signal, the limitations of the seismic table apparatus (nominal capacity of the transverse actuator of the LNEC 3d shake table), the processing and scaling steps of the input signal, as well as information of the normalized response spectrum of the seismic action, the reader is referred to Candeias et al. (2016).

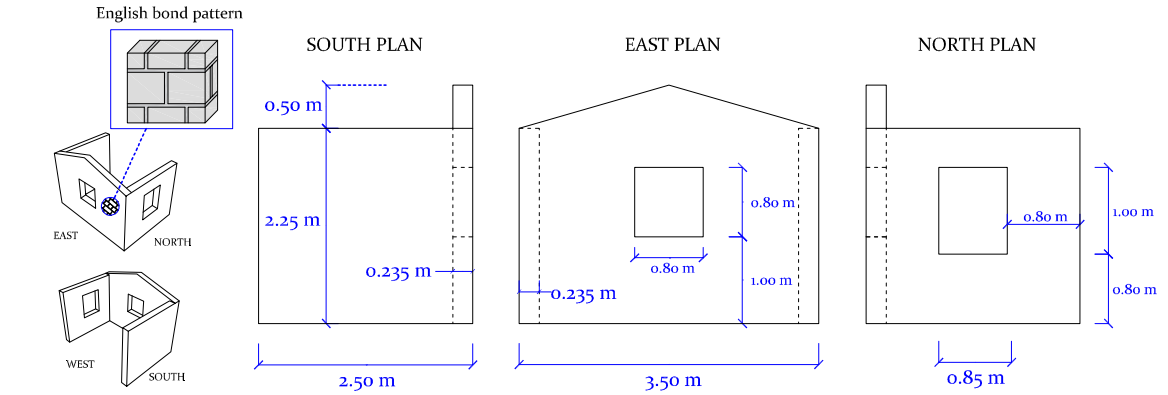

(a)

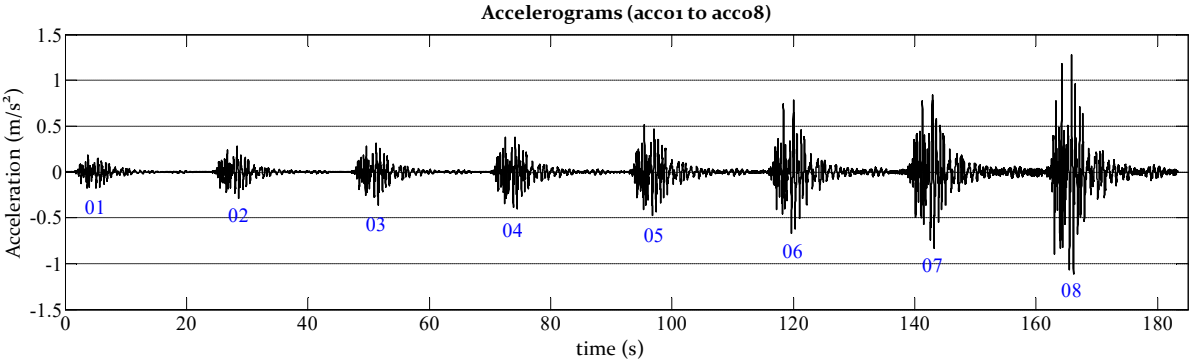

(b)

Figure 5.9 – Brick house mock-up studied: (a) geometry (dimensions in meters) (Candeias et al. 2016); (b) the experimental input seismic signal.

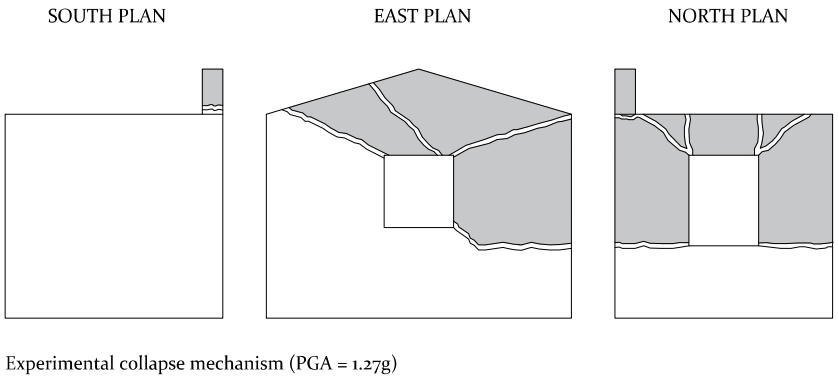

Figure 5.10 – Experimental failure mechanisms observed (adapted from Mendes et al. (2017)).

Modelling assumptions

Two macro-models are considered and designated as discrete KP and DNS models. Both have been previously described in section 3.6 (§Chapter 3). Its distinction is on the background

theory used for the homogenizing step performed at a meso-scale. The former adopts a Kirchhoff-Love plate theory and, the latter, a three-dimensional model using volume finite elements which accounts for the existent vertical discontinuity.

A refined discrete mesh with 200 mm of size has been adopted as depicted in Figure 5.11. The analyzed discrete models are designated as: (i) KP model 200, with a 200x200 mm^2 quadrilateral mesh within a Kirchhoff-plate theory at a meso-scale; and a (ii) DNS model 200, with a 200x200 mm^2 quadrilateral mesh within a three-dimensional direct numerical simulation at a meso-scale (see Figure 5.11). A DIANA macro-model, largely applied in structural problems (Lourenço 1997; Creazza et al. 2002; Araujo 2012; Silva et al. 2018), is also defined to complement the analyses. This represents masonry as an isotropic material and follows a total strain rotating crack constitutive material model, whereas an exponential and parabolic law is adopted, respectively, for the tensile and compressive behaviors. An approximated mesh size of 100 mm was defined using 3D finite elements, and such fine discretization intends to minimize numerical problems faced during the computations performed (specifically for the quasi-static analyses).

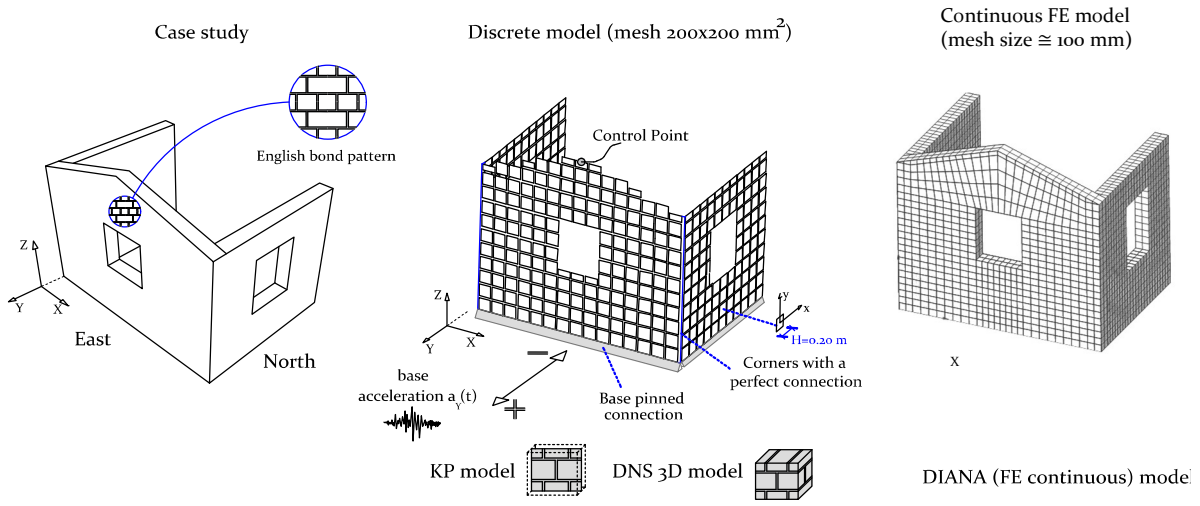

(a) (b) (c)

Figure 5.11 – (a) The geometry of case study; (b) modelling assumptions and the discrete model with H=200 mm adopted for the case study; and (c) the DIANA macroscopic model used to complement the analyses.

Along with the modelling options, two issues can be stated. Firstly, both the IP and OOP truss systems are applied to all the benchmark walls. Secondly, due to the overlapping of the brick staggering between the side walls and the main façade, the corners are expected to be stiffer. A perfect connection between walls is hence presumed being the corners modelled as

two rigid beam columns. The latter means that bending and torsional moments are fully transmitted between contiguous walls (see Figure 5.11b). At the base, the supports of the structure are considered to be pinned connections.

Material and mechanical properties

Experimental investigations on the mechanical strength characterization of the studied English-bond masonry have been carried out and reported in Candeias et al. (2016). A total of six masonry wallets were built but only three samples are defined as valid for the determination of the masonry stiffness and strength values. Briefly, it was observed that the specific mass is given by 1890 kg/m^3; the Young modulus for the masonry brickwork is equal to 5170 MPa; the compressive strength is 2.48 MPa and the tensile strength is 0.105 MPa. The latter data is summarized in Table 5.5, as well as the associated coefficients of variation. One may note the small number of representative samples, which may raise questions about the objectivity of the defined average values. Yet, this information has been given to the invited authors that conducted the blind test prediction over the benchmark (Candeias et al. 2016) and is thus, accordingly, also used here to perform the numerical analyses.

The data required to define the macro-scale constitutive CDP material model rely on the homogenized quantities resulting from the foregoing scale. Bearing the existing link between scales and its associated character, the followed experimental data and the resultant meso-scale properties are shown in Table 5.5. The homogenized elastic properties of Table 5.5 ($\bar{E}_{xx}$ and $\bar{E}_{yy}$) are used to compute the elastic stiffness of each truss-beam and determine the regularization factors for the homogenized curves obtained and depicted in Figure 5.12. These are ready to serve as macro-input after the processing of the meso-to-macro transition steps. Note that both IP and OOP homogenized quantities are displayed and interpreted by the truss beam systems (also according with the trusses plane direction). It is noticeable that the DNS model has a significantly lower capacity than the KP model for the $\Sigma_{xx}, M_{xx}, \Sigma_{xy}$ and M_{xy} curves. It is thus clear that the three-dimensional shear stresses and the vertical discontinuity in the thickness of the walls lessens the strength capacity of the masonry. Hence, it is expectable that the KP model, unable to reproduce such effects, may feature an overstrength response prediction.

Table 5.5 – Material and mechanical information obtained via experimental works (Candeias et al. 2016) given for the blind test prediction; assumed in the homogenization step at a meso-scale and assumed at the macro-scale.

Experimental data (for the blind test prediction)			
ρ = 1890 Kg/m^3 (CoV=3%)	$E_{masonry}$ = 5170 MPa (CoV = 29%)	σ_c = 2.48 MPa (CoV=14%)	σ_t = 0.105 MPa (CoV=19%)

Numerical data - Meso-Scale								
Elastic Properties (Brickwork)		Inelastic Properties (Mortar joints)						
E_{brick}	υ	f_t	f_c	c	G_f^I	G_f^{II}	G_f^{IV}	ϕ
11000 N/mm^2	0.20 (-)	0.105 N/mm^2	2.48 N/mm^2	0.20 N/mm^2	0.012 N/mm	0.05 N/mm	3.97 N/mm	30 degrees

Numerical data - Macro-scale			
Homogenized Elastic Properties			Homogenized Inelastic Properties
$\overline{E}_{xx}$	$\overline{E}_{yy}$	υ	
6400 N/mm^2	3600 N/mm^2	0.20 (-)	Homogenized curves - see Figure 5.12.

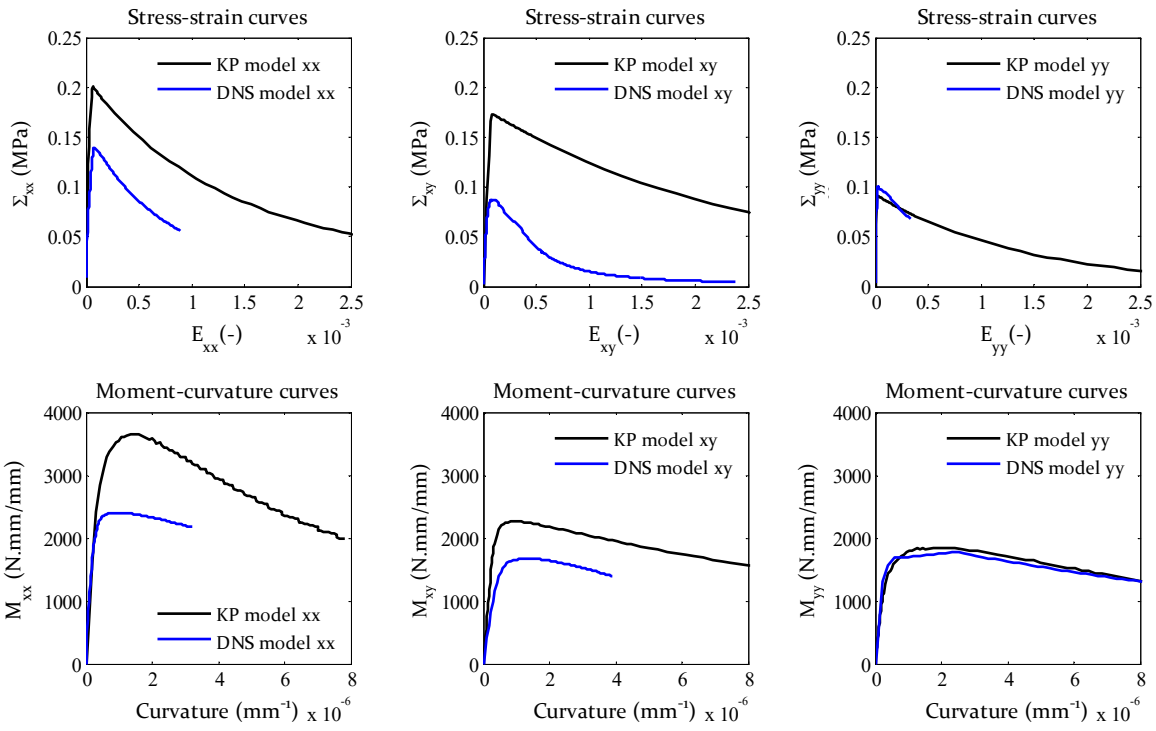

Figure 5.12 – Homogenized curves used at a macro-scale to assign the nonlinear material properties of each truss-beam system: (a) In-Plane, and (b) Out-of-Plane.

Results and discussion (blind test prediction scope)

The computations performed on the brick house mock-up are here reported. Again, the two ad-hoc models derived from the proposed framework are considered and designated as KP model 200 and DNS model 200. The selection of the KP and DNS models makes possible to draw conclusions on the effect that a Kirchhoff-Love plate theory, usually employed to simplify the analysis, brings in the macro-response of an English bond masonry structure. Despite these have been seen at a meso-scale (in section 3.6), remarks on the effect of the non-consideration of both the OOP shear stresses and the vertical discontinuity are still important to report within the macro-response. Quasi-static (pushover) and dynamic analyses have been performed. The results are compared with the available experimental information and complemented with a macroscopic model using DIANA (2017). To guarantee the comparison objectivity, the material properties used in the latter follow the data from Table 5.5, i.e. $E_{masonry} = 5170$ MPa; $\nu = 0.2$; tensile strength of 0.105 MPa; $f_c = 2.48$ MPa.

Quasi-static (*pushover*) type of analysis is usually not so representative and accurate in the evaluation of the seismic behavior of an unreinforced masonry structure, but can provide a reasonable estimate of the capacity. Even if being intrinsically incapable to reproduce dynamic effects, it may be an appropriate alternative to time costly dynamic analysis. In this case, pushover analyses are carried out to give some useful information as: (i) backtrack the origin of potential numerical problems; (ii) understand if the structural behavior and the observed failure collapse mechanisms are the expected ones; (iii) conclude on the role and the significant effect that the non-consideration of vertical discontinuities has on the English-bond masonry walls response. Analyses with a mass proportional load have been conducted for both positive (pushing) and negative (pulling) directions and their results are presented in Figure 5.13. To solve the system of nonlinear equations a Quasi-Newton technique improved with a line search algorithm and an arc-length procedure has been adopted. The experimental collapse load is also plotted, as well as the results from the DIANA macroscopic model that serves as a reference for the continuous FE-based models.

In general, a good agreement is found between all the presented numerical strategies, but some deviations are obtained in the negative direction. For each direction, all the displayed numerical approaches exhibit a similar post-peak response. The transversal walls seem to cause the differences found, which emphasizes their key role on the overall behavior. Such finding is easily corroborated by the structure deformed shape and failure patterns depicted in Figure 5.14 and Figure 5.15.

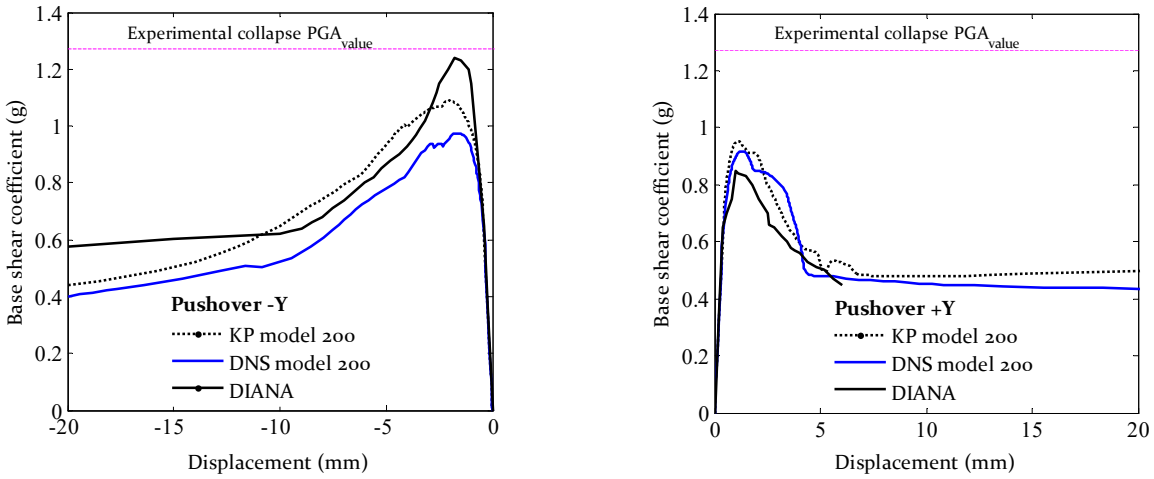

(a) (b)

Figure 5.13 – Pushover curves obtained: (a) for the negative (pulling) direction, and (b) for the positive (pushing) direction.

The negative direction has a capacity that is 6% to 14% higher than the positive one (for both the KP and DNS models). In the former direction, both transversal walls behave like abutments, in which the internal compressive and shear behavior give an extra resistance by allowing a better and effective load distribution. The OOP failure is thus postponed to a higher applied load than the one observed for the positive direction. In the latter, the response is governed by the OOP response of the East façade only, which leads to tensile stresses at the walls' connection and on the North wall piers that can be hardly withstand due to the self-nature of unreinforced masonry, see Figure 5.14d and Figure 5.15d. Such behavior can also justify the reduced dispersion observed between the numerical curves of Figure 5.13b. Hence, and with a focus on the negative direction, two findings may be addressed: (i) the KP and the DIANA macro-model lead to analogous results; (ii) conversely, owing to the lower horizontal bending capacity of the DNS model, this is the more conservative strategy.

It is important to refer that a good agreement is equally observed concerning the observed failure mechanisms for the DNS model. In fact, these resemble to be alike to the ones experimentally reported: horizontal and vertical cracking near the gable wall (Figure 5.15b,d); uplift, due to tensile stresses, of the more exterior pier in the North façade (Figure 5.15d); and shear damage in the more interior pier located in the North façade (Figure 5.15d).

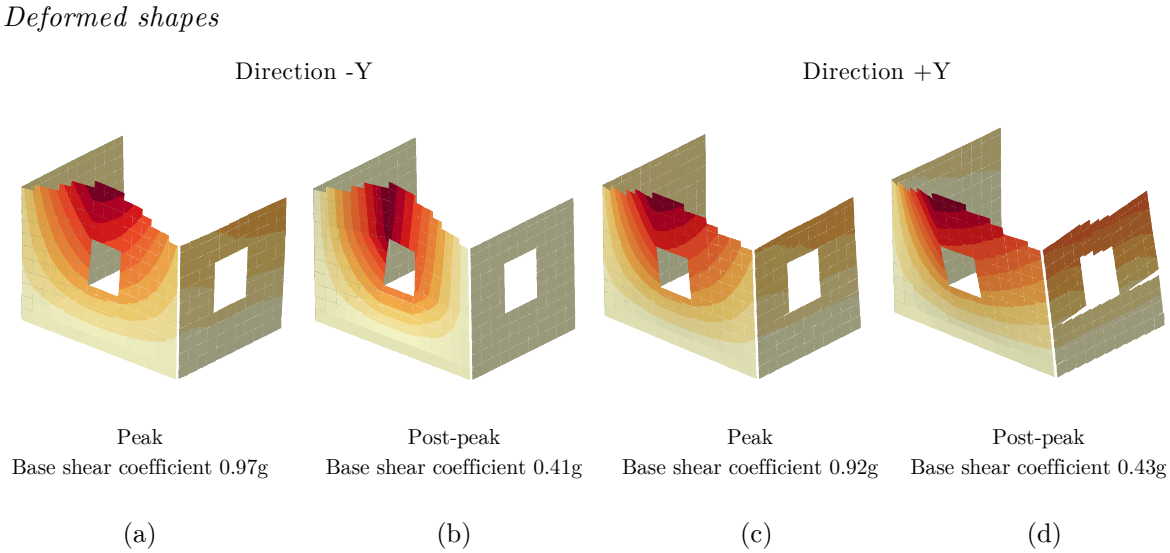

Figure 5.14 – Quasi-static (pushover) deformed shapes for the DNS model 200: (a) Direction -Y (peak); (b) Direction -Y (post-peak, displacement of -20mm); (c) Direction +Y (peak); and (d) Direction +Y (post-peak, displacement of 20 mm).

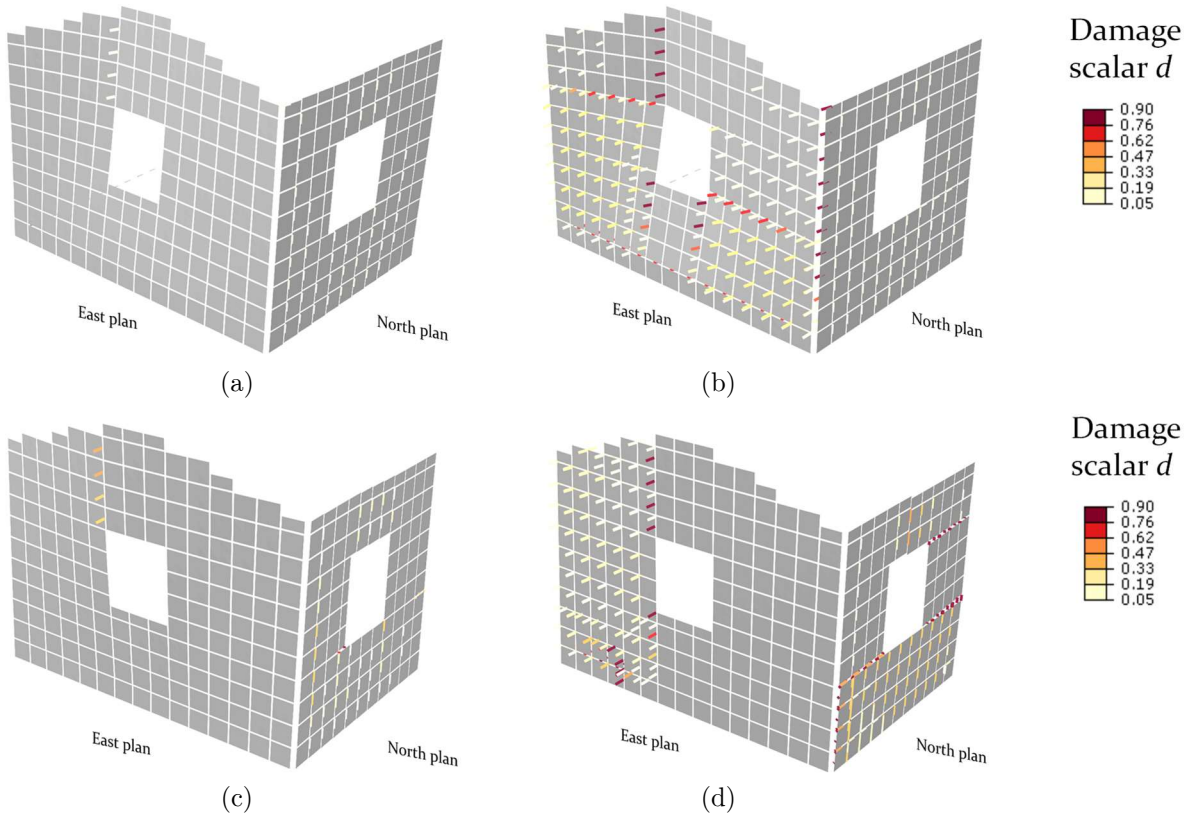

Figure 5.15 – Quasi-static (pushover) numerical damage patterns for the DNS model 200: (a) Direction -Y (peak); (b) Direction -Y (post peak, displacement of -20 mm); (c) Direction +Y (peak); and (d) Direction +Y (post-peak, displacement of 20 mm).

The seismic assessment of the brick mock-up using dynamic analysis is now reported. A set of eight seismic input signals were experimentally applied to the benchmark. Since the structure collapsed during the last accelerogram (acc08), only the results concerning the first seven accelerograms are considered here. To solve the dynamic equations of the system, an implicit procedure within a Hilber-Hughes-Taylor (HHT) time integration scheme and with a α-operator value of -0.05 (the reader is referred to Hilber et al. (1977) for further details of the method) has been assumed for this study. To avoid a needless computational effort, an available automatic time stepping algorithm is used and complemented with a maximum initial step control set to 0.005, i.e. equal to the input signal frequency. No convergence difficulty has been found to what concerns the use of the RBSM model. Such finding may stand on the fact that only one-dimensional FE rules the material non-linearity and damage. The material damping was defined via the practical approach of the equivalent Rayleigh damping (Chopra 2017). The Rayleigh parameters were computed by considering a 3% damping ratio and with a damped range of frequencies of 7-40 Hz.

The comparison between the numerical and experimental data is reached through the time history of the displacements recorded for the node located at the center of the gable wall. Figure 5.16a depicts the displacement evolution during the seven earthquakes applied. The application of the first six accelerograms led to minor damage as the response is predominantly elastic, in coherence with the experimental output. Yet, Figure 5.16b makes clear that none of the KP, DNS and DIANA numerical curves fit the experimental data for the last accelerogram (acc 7). Such evidence could, in a first glance, invoke the inability of the proposed framework to represent the dynamic behavior of masonry structures. The latter may be recognizable as a false negative type of error if one refers that, similarly to what occurred for the quasi-static analysis, the KP model derives an almost coincident output when compared with the well validated DIANA macroscopic model. In this context, several reasons can be put together to justify the results deviation.

An inaccurate modelling of the structure could be a possible source of error, but it cannot justify such larger differences. Conversely, an incorrect material damping assumption can totally lead to significant misrepresentations of the dynamic structural behavior. A value of 3% seems a rational choice and, even with a higher damping value masonry (Costa 2002; Doherty et al. 2002; Elmenshawi et al. 2010; Rabinovitch and Madah 2011; Sorrentino et al. 2011), a decrease of the peak displacements would be expectable and hence against the reported experimental values. On the other hand, defining no material damping could be a strategy but it lacks objectivity and is thus disregarded. Still, these indications are valid if the assumed average values for the material properties are correct. It is known that these derive from an

experimental campaign completed on the same brickwork but, bearing the coefficients of variation reported in Candeias et al. (2016) (see Table 5.5), the question of its representativeness can be raise.

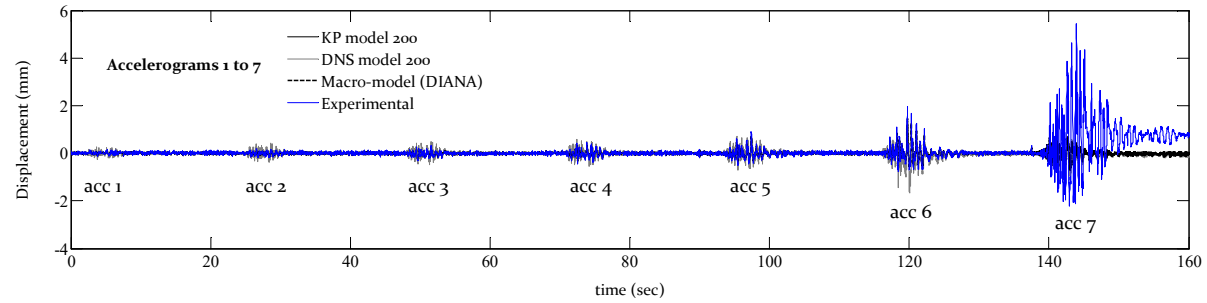

(a)

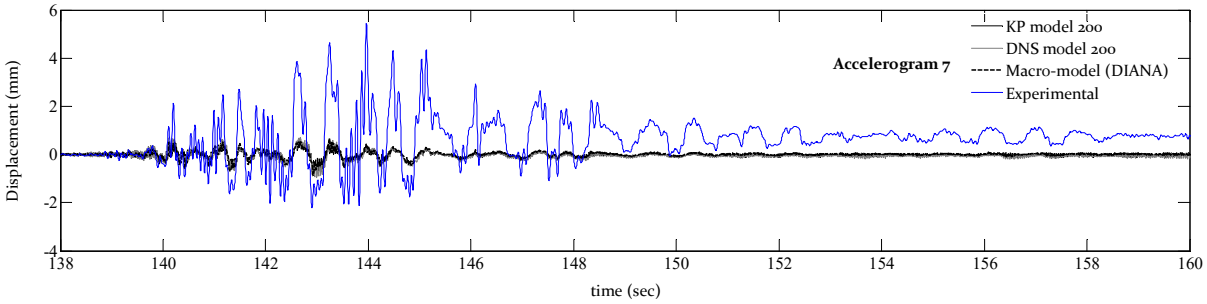

(b)

Figure 5.16 – Time-history displacements for: (a) the accelerograms 1 to 7; and (b) accelerogram 7.

In fact, a closer look to the response obtained by the numerical procedures under the acc 7 support this idea. Figure 5.17 depicts the numerical damage found by the DNS model after the occurrence of the latter accelerogram (time t=160 seconds). A dominant elastic structural behavior prevails for the transversal walls, being only noteworthy the existence of a well-marked vertical crack in the gable wall. Therefore, the current use of higher strength values for the masonry brickwork is a convincing point. This can justify why the obtained results are so different from the real response and, likewise, why analogous observations were collected by several other authors on the same brick-house mock-up. In fact, the blind test predictions performed by literature peers (using advanced methods, from the FE-based to discrete element strategies) led to an average deviation of 50%, see Mendes et al. (2017).

The difference between the KP and DNS models can be barely noted from the discrepancies obtained for the last accelerogram (Figure 5.16b). Both KP and DNS models consider the masonry orthotropy and the full non-linear softening behavior, but the latter does account it in the presence of the vertical mortar discontinuity in the English bond-masonry thickness and

taking in the effect of out-of-plane shear stresses. Thus, the DNS model seems to be the more representative one and is used next to conduct further investigations.

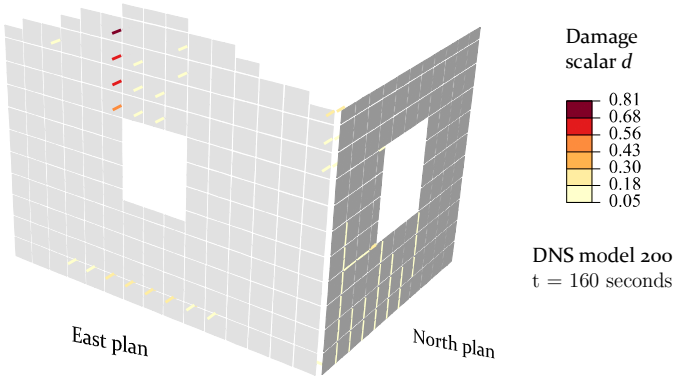

Figure 5.17 – Damage at the instant t = 160 seconds for the DNS model 200 (minor cracking).

Dynamic analysis (with post-blind prediction data)

The use of biased experimental values for the elastic stiffness and strength parameters hinders a proper fit between the numerical and the experimental response. Therefore, an inverse fitting step is conducted by exploiting the scatter of the experimental material values and the modal identification data made available after the post-blind prediction exercise (Mendes et al. 2017). The DNS model 200 and the DIANA total strain rotating crack model, using volumetric FE's, have been considered (since the KP model follows similar assumptions with the DIANA, similar results have been found and so not introduced for better readiness). The brickwork input properties have been changed towards a better numerical response by affecting: (i) its elastic Young's modulus, and (ii) its strength parameters. The value of damping was kept equal.

The calibration of the elastic brickwork stiffness has been reached by accounting with the modal identification data made available. The experimental and numerical frequencies (obtained with the RBSM model) of the first three modes are depicted in Table 5.6. All the modes are global and with well-marked flexural movements, in which the first two follow the transversal direction (N-S) and the third the longitudinal one (E-W). Such modes are the most representative ones and characterize the OOP failure of both the transversal walls and East façade as the most prone to occur. Neglecting the second mode in the fitting step, due to the lack of agreement found, it is seen that the original numerical model leads to significant differences of 22% and 17% for the first and third mode frequencies, respectively. In this context, reducing the average stiffness value by 40% enabled to fit the first mode frequency and reduce the error for the third one to 4%. The stiffness ratio between the horizontal and

vertical axis (viz. the orthotropic ratio), obtained at a meso-scale, was kept and provide the calibrated values to be $E_{xx} = 3840\ MPa$, $E_{yy} = 2160\ MPa$ and $G_{xy} = 1600\ MPa$.

Table 5.6 – Experimental and numerical frequencies for the first three vibrational modes.

	1st mode	2nd mode*	3rd mode
Experimental modal identification	10.69 Hz	15.01* Hz	21.29 Hz
Proposed model (blind test prediction – mean values)	13.71 Hz	14.43* Hz	25.67 Hz
Proposed model (calibrated)	10.63 Hz	11.03* Hz	20.45 Hz

*The second mode has been neglected due to lack of agreement.

A similar reduction strategy was followed for the strength parameters. The tensile strength and cohesion properties have been affected with a 19% reduction factor. i.e. by following the coefficient of variation reported in Table 5.5. The compressive behavior seems to have, as expected, an irrelevant role and thus the experimental average value was followed. Likewise, the parameters that control the material curves beyond the peak were kept the same, namely the fracture energies, because these refer to typical masonry literature values and no experimental reference is known. The obtained results for the accelerogram seven (acc 7) is addressed in Figure 5.18. It immediately allows concluding that the displacements are now comparable. The comparison is, for the acc 7, promising as a good agreement between the calibrated model and the experimental time-history displacements is found. Even if slight differences are visible for the peak displacements, the DNS model accurately reproduces also the residual displacement.

On the other hand, the macroscopic DIANA model seems to overestimate the structure capacity. The response is, for the acc 7 as depicted in Figure 5.18, far for being alike with the behavior reproduced by the proposed DNS procedure, despite sharing both the same material and mechanical input. The non-consideration of the masonry orthotropy and, more importantly, the disregard of the existent vertical discontinuity are key details. In fact, the latter is paramount once, when present, it decreases significantly the bending and torsional capacities. Furthermore, the DIANA (2019) macroscopic approach makes use of a hysteretic behavior with secant unloading-reloading branches, a feature that leads to the underestimation of the energy absorption and incapable to record permanent plastic deformations.

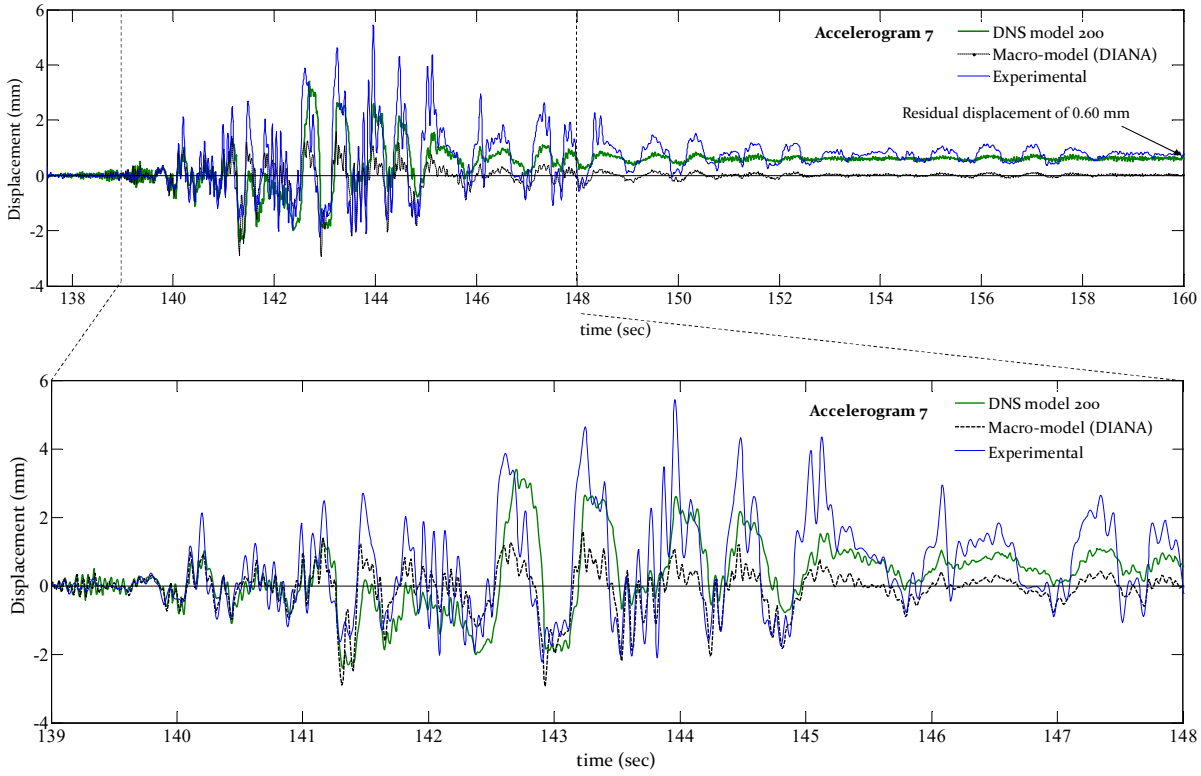

Figure 5.18 – The obtained time-history displacements after inverse fitting for the last analyzed accelerogram (acc 7).

Additionally, Figure 5.19 reports the observed experimental and numerical damage maps. From the DNS model, a vertical crack in the gable wall (due to horizontal bending) is observed, as well as the onset of cracking due to torsional movements in the east plan opening towards the corners. Moderate damage is captured in the east-north corner, even if this is not clear from the experimental observations. Some in-plane damage around the north piers is also registered. In general, a reasonable agreement has been found.

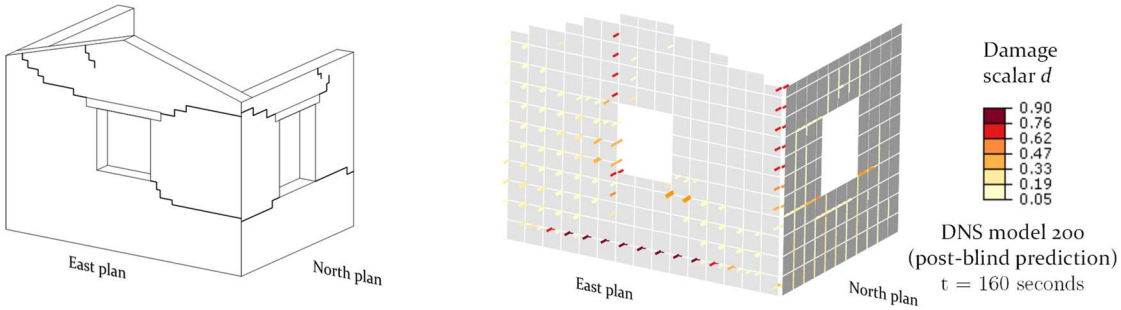

Figure 5.19 – Observed damage: (a) after the experimental series of seven accelerograms (from acc 1 to acc 7); and (b) for the calibrated DNS 200 model at the instant t = 160 seconds.

Finally, the author stresses that the KP model (or related simplified strategy) and the DIANA macroscopic approach, in which the material is modelled as homogeneous in the

thickness direction, need to be used carefully. For one-leaf walls as the running-bond case, no issues are expected yet, as concluded before, in cases where discontinuities are present, inaccurate and unconservative solutions are expected to be found due to cracks within the thickness of the wall.

5.3.3 Mesh sensitivity and computation time of the solution

An insight into the macro-mesh dependency of the results is addressed next for the dynamic range only. A coarser refinement given by H=400 mm has been defined and the dynamic analysis performed within the post-blind prediction scope repeated. Two discrete models are thus considered, the DNS model 200 with a 200x200 mm^2 mesh and the DNS model 400 with 400x400 mm^2 mesh. Figure 5.20a shows the time-history displacement for the control node. Though a more flexible response is achieved with the DNS model 400, the maximum recorded displacements are under the experimental envelope during all the intense phase of the accelerogram (acc 7).

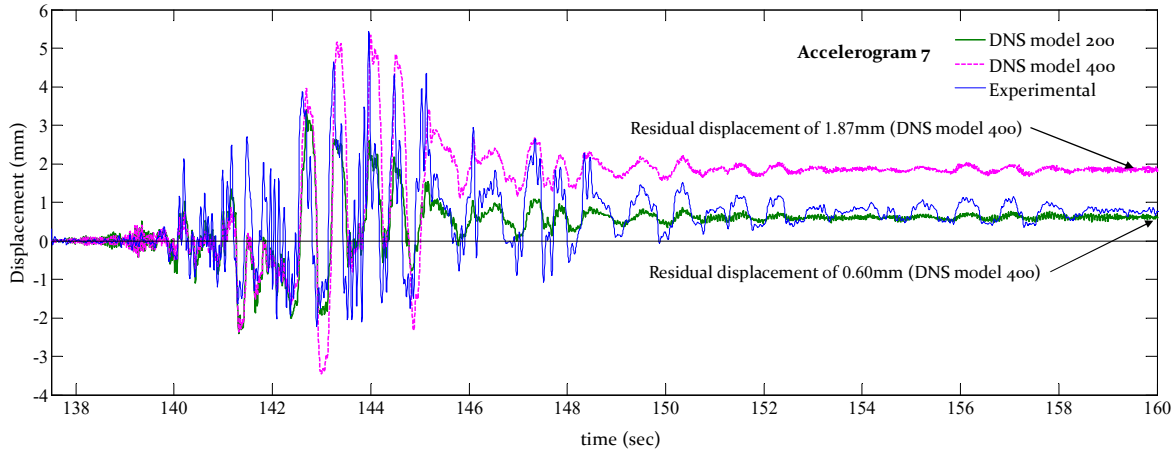

(a)

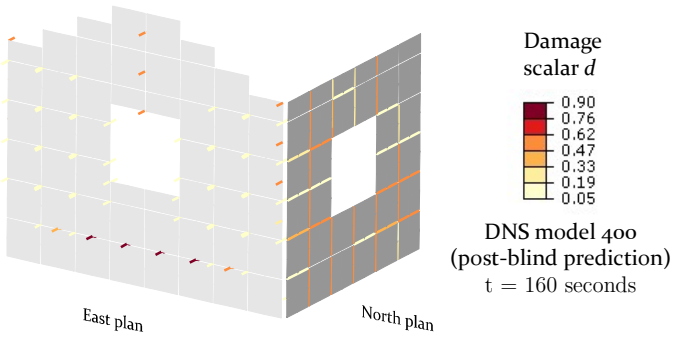

(b)

Figure 5.20 – Mesh dependency study: (a) the obtained time-history displacement for the last analyzed accelerograms (acc 7); and (b) the observed damage after the experimental series of seven accelerograms for the calibrated DNS 400 model (at the instant t = 160 seconds).

It is noticed, however, that some differences between the two refinement levels exist, as the obtained residual displacement (deviation of 67%). Such deviation is relevant, even if it is important to stress that 400 mm is a substantial large mesh for the problem at hand.

Figure 5.20b shows the damage pattern for the DNS model 400 after the series of seven accelerograms. The potential inability of coarser meshes to catch the onset of more localized cracking is visible. For instance, the vertical crack registered in the gable wall is positioned in the center of the façade, indicating that torsion has an uncertain role; clearly different than the higher refinement response addressed in Figure 5.19. The study over the mesh-bias is determinant in the results output, in respect to the accuracy of both OOP displacement and damage representation. In this regard, bypassing a coarser macro-model discretization seems to be more important within the dynamic range than within the quasi-static one. Nevertheless, the processing costs required for a finer refinement is still very promising, as seen in Figure 5.21.

Figure 5.21 graphically outlines the processing times and the disk storage usage demanded by each numerical approach. A laptop with an i7-4710MQ CPU, 16 GB of RAM (DDR2) and with an SSD disk with a writing velocity of 512 Mbytes/s has been used. The presented proposed strategies demand a significantly lower computational cost than a continuous FE macroscopic approach. In terms of the required disk space, the difference is also significant. However, one may note that the disk space refers to both displacement and damage field variable outputs (it is always dependent on the amount of output data required). In this context, it can be highlighted that the proposed goal was attained, i.e. the present approach demands significantly lower computational times than the traditional macroscopic one used for the study of large-scale structures.

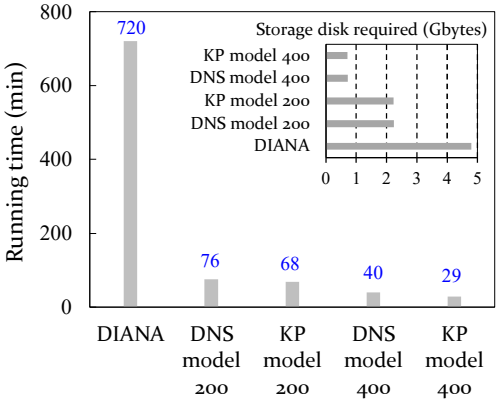

Figure 5.21 – Information of the required processing times and storage disk space for each numerical analyzed procedure.

5.4 Dynamic analysis: high strain-rate loading

5.4.1 Overview

In recent decades, a great deal of effort has been made to develop solutions to reduce destructive damage and casualties due to blast loads and impacts (also in light of a stronger protection of the built heritage against terrorist attacks). Needless to say, masonry structures are in the majority of the cases rather vulnerable to explosions and impacts. In this regard, the scientific community is eager to share advanced numerical studies conceived for a better understanding of the blast/impact structural response of masonry walls, for instance see Wang et al. (2009), Wei and Stewart (2010), Macorini and Izzuddin (2014), and Rafsanjani et al. (2015a). This is achieved in conjunction with a quantitative insight into the behavior of the masonry material at high strain rates, see Beak et al. (1994), Dennis et al. (2002), Davidson et al. (2004), Eamon et al. (2004), Wei and Stewart (2010), Pereira and Lourenço (2016a), also in regard of an optimal strengthening with innovative materials allowing for a safety increase (Pereira and Lourenço 2016b).

The city bombing event in Oklahoma (1995) addressed the importance to carry on such studies, being the target the decrease of potential casualties and buildings damage. Experimentation is still nowadays at a higher level than numerical modelling in this field. Even if more attention was devoted to concrete (Yon et al. 1992; Ross et al. 1995; Luccioni et al. 2004) and steel structures (Soroushian and Choi 1987; Balden and Nurick 2005), some different experimental campaigns are also available for masonry. For instance, some works regarding masonry panels subjected to blast loads (Varma et al. 1996; Flanagan and Bennett 1999; Eamon et al. 2004; Wesevich and Oswald 2005), and impacts (Middleton 1994; Gilbert et al. 2002a) are worth mentioning.

It is known that URM walls subjected to dynamic loads can resist accelerations higher than their static strength, the so-called dynamic stability (Bruneau 1994; Doherty et al. 2002). Additionally to the fact that the use of static or quasi-statics approaches preclude the consideration of important dynamic phenomena, see Doherty et al. (2002), existing research proved that assuming static material properties could lead to an underestimation of the bearing capacity of structures (Burnett et al. 2007a; Hao and Tarasov 2008). Therefore, material properties may exhibit a dynamic enhancement according to the applied load strain-rate, as seen in Burnett et al. (2007b) which is of utmost importance for fast dynamic loads.

Thorough experimental campaigns are difficult to carry out due to the involved costs. This brings the need of developing numerical models that may predict with accuracy the dynamic

response of structures. In this context and bearing in mind that few numerical models have the capability of accounting with such phenomenological material characteristic, the present section addresses the application of the two-step procedure for the analysis of the masonry response under high-rate loading. Firstly, a general insight describing its extension to account with the strain-rate sensitivity in the masonry response is achieved. Then, the two-step model with strain-rate dependency is used for the out-of-plane dynamic analysis of a parapet masonry wall subjected to a vehicle impact type of load.

5.4.2 Strain-rate dependence

Existing research proves that the use of static strength properties can lead to unreliable results for the masonry behavior under fast dynamic actions. Static strength material properties may exhibit an enhancement according to the strain rate level of the applied load. Research mainly focusing on concrete-like materials can be found in the literature, where assumptions intrinsically related with material effects are present to explain the phenomena, such as the lateral inertial confinement, end support friction and scale-effect (Le Nard and Bailly 2000; Hao et al. 2013; Hao and Hao 2013).

Several numerical strategies can be found in the literature to represent this phenomenological feature. The use of viscoplastic models aiming a strain-rate regularization seems adequate (Sluys and De Borst 1992; Georgin and Reynouard 2003). The plastic-damage (CDP) model adopted by the proposed framework at a macro-scale has been developed introducing the well-known Duvaut and Lions (1976) model. It embeds viscoplastic concepts into the inelastic strain and damage scalar parameter (Lee and Fenves 1998), thus linking the rate of damage with the loading strain rate. Even if numerically convenient, especially when an implicit scheme is used to solve the system of equations, the definition of the viscosity regularization parameter μ (designated as relaxation time) lacks objectivity and requires extensive sensitivity studies. Another possible strategy is the use of dynamic increase factors (*DIFs*). This is a useful and practical way to numerically represent the material properties change, since such factors directly affect the static material properties adopted. The use of *DIFs* is found suitable to study masonry structures subjected to fast loading applications (Burnett et al. 2007a; Hao and Tarasov 2008) and is herein followed.

The proposed two-step framework is eligible to receive deterministic or DIF laws (dependent on the strain rate) at a meso-scale only; therewith the homogenized-based models (cf. section 3) can compute the material input properties required to solve the unit-cell problem. The parameters that define the strength envelope of the unit cell, i.e. that directly rule the plasticity

model of the mortar interfaces, are strain-rate dependent: as the bond strength of the mortar f_t, cohesion c, compressive strength f_c and the associated G_f^I, G_f^{II} and G_f^{IV} fracture energies. In converse, the elastic properties of the masonry are considered to be rate independent. This simplification (reads limitation) is enforced by the macro-constitutive model adopted.

Briefly, the *DIFs* can be introduced in the framework via: (i) a strain-rate law, typically a logarithmic curve, for each selected parameter; or (ii) a discrete DIF value, independent from the strain rate level, which is a priori assumed and adopted as constant. The former may yield more realistic values, but the latter is straightforward, simple and more aligned with normative proposals. If these data are at disposal, homogenized in- and out-of-plane curves can be derived at a meso-scale for several a-priori established loading strain-rate values. The values of the material properties are obtained through the product between the quasi-static property values and the associated DIF, Eq. (5.1):

$$\begin{cases} f_t = DIF_{ft} \times f_t \\ c = DIF_c \times c \\ f_c = DIF_{fc} \times f_c \\ G_f^I = DIF_{GFI} \times G_f^I \\ G_f^{II} = DIF_{GfII} \times G_f^{II} \\ G_f^{IV} = DIF_{GfIV} \times G_f^{IV} \end{cases} \tag{5.1}$$

At a macro-scale, the constitutive material CDP model in ABAQUS (2013) has built-in procedures able to handle with the peak strength value rate-sensitivity. For that, it strictly requires, however, the tabulated form of the effective stress-inelastic strain relationship for, at least, two different strain rate levels. It is thus sufficient to provide a lower bond curve, given by the quasi-static data (strain rate in the range of $10^{-5}\,s^{-1}$), and an upper-bond curve, given by the maximum expectable strain rate value. The CDP model performs, for the strain rates which are in-between the defined interval, a linear interpolation to define the associated reference material constitutive behavior. A reasonable upper-bound reference value can be set, for several types of dynamic loads and for concrete-like materials, according to Bischoff and Perry (1991). For impact or blast loads, a strain-rate value over $10^{0}\,s^{-1}$ is typically found. Yet, aiming to reduce the epistemic error of a linear interpolation to a negligible margin, several input curves for several strain-rates may be processed.

5.4.3 Sheffield university parapet wall: low velocity impact test

Experimental data available from the research reported by Gilbert et al. (2002a) is used to assess the ability of the present model to represent its behavior due to a low-velocity impact load. A total of 21 full-scale unreinforced masonry parapets have been experimentally tested. These differ in both wall dimensions (length range between 5.75 and 20.0 m) and brickwork texture (running, English and English garden bonds). Here, only the running bond pattern is considered. The selected parapets are designated as C6 and C7 and are replicates. Their assemblage was executed with strong concrete blocks and weak mortar (class iii mortar according to BS-5628). The walls and brick dimensions are 9150 x 1130 x 215 mm^3 and $440 \times 215 \times 215$ mm^3, respectively. The density of the brickwork composite is 2295 kg/m^3.

At the walls' base, the surface was coated with epoxy sand to reproduce the roughness of a given street floor. For the lateral supports, two abutment blocks connected to the walls through epoxy mortar were used. Numerically, the boundary conditions are considered to be fixed for each lateral edge and simple supported at the base of the walls. For the sake of simplicity, the base-roughness was not reflected. Aiming to model a vehicle-like impact at both mid-height and length of the walls, a triangular out-of-plane load was applied through a steel plate. The load is idealized as a triangular time-history distribution, in which the peak value is equal to 110 kN. The masonry parapets representation as well as the applied force-time history for the numerical simulations are described in Figure 5.22. The deformation of the studied parapets was recorded in a node located 580 mm above the base and deviated 250 mm from the center.

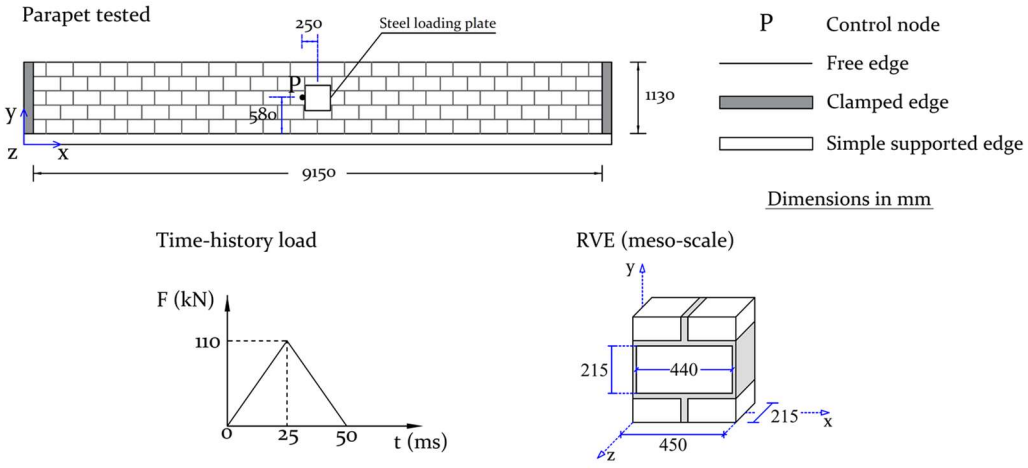

Figure 5.22 – Geometry of the running bond masonry parapets C6 and C7 tested by Gilbert et al. (2002a).

Several studies on the masonry parapets tested by Gilbert et al. (2002a) are found in the literature. For instance, the same authors proposed in Gilbert et al. (2002b) an analytical simplified approach to evaluate the response of the masonry parapets due to an impact load. This strategy allows a quick analysis, but demands the knowledge of the critical failure mechanisms beforehand. Also, the failure modes rely on a macro-block definition and may, by themselves, preclude the analysis of more general modes. Moreover, Burnett et al. (2007a) presented a simplified FE mesoscopic model that represents mortar joints with interface elements. This type of models allows a greater flexibility in the failure definition, having as limitation the increased computational time. Nevertheless, both the strategies considered by the authors are strain-rate independent, ergo their accuracy is highly dependent on the material properties adopted. The use of static strength properties instead of dynamic ones may mislead the user, i.e. an underestimation of the collapse load may occur. The study of the dynamic properties involves the definition of *DIF*s, which may turn the response highly subjective if valid experimental data is unavailable.

The numerical simulation of the parapet wall using the two-scale framework is accomplished next. Firstly, the homogenization step at a meso-scale is performed to mechanically characterize the running bond masonry behavior. The static material properties required are gathered in Table 5.7 and the rate-dependency issue is addressed. Hao and Tarasov (2008) studied the experimental dynamic behavior of a series of brick and mortar specimens under uniaxial compressive tests through a tri-axial static-dynamic apparatus. The analytical expressions required to describe the value of the *DIF*s derive from the latter research and are given by Eq. 5.2-5.4. It may be noted that the study from Rafsanjani et al. (2015b), which covers the current masonry parapets, used the same hereby presented laws to define the strain-rate dependency of masonry interfaces using a continuous mesoscopic modelling strategy. The regression equations for the ultimate compressive strength of mortar σ_{c0_mortar} used are:

$$\begin{cases} DIF = 0.0372 ln\dot{\varepsilon} + 1.4025 \ \ for \ \dot{\varepsilon} \leq 13 s^{-1} \\ DIF = 0.3447 ln\dot{\varepsilon} + 0.5987 \ \ for \ \dot{\varepsilon} > 13 s^{-1} \end{cases} \tag{5.2}$$

The regression equation for the compressive fracture energy G_f^{IV}:

$$\mathrm{DIF} = 0.15231 \ln\dot{\varepsilon} + 2.6479 \tag{5.3}$$

The regression equations for the ultimate compressive strength of the brick σ_{c0_brick}:

$$\begin{cases} DIF = 0.0268 ln\dot{\varepsilon} + 1.3504 \ for \ \dot{\varepsilon} \leq 3.2 s^{-1} \\ DIF = 0.2405 ln\dot{\varepsilon} + 1.1041 \ for \ \dot{\varepsilon} > 3.2 s^{-1} \end{cases} \tag{5.4}$$

As information regarding the strain-rate effects on tensile and shear masonry properties is lacking, the *DIF* regression equations for both tensile ultimate strength σ_{t0_mortar}, mode-I fracture energy G_f^I, cohesion c and mode-II fracture energy G_f^{II} is assigned to be equal to the compressive one. Table 5.7 shows the computed DIF values for the five strain-rate levels accounted.

Table 5.7 – Material properties and dynamic incremental factors adopted for the study of the masonry parapets subjected to an impact load.

Elastic static properties of the homogeneous RVE			
E_{xx}	E_{yy}	G_{xy}	ν_{xy}
17500 (N/mm²)	8750 (N/mm²)	6500 (N/mm²)	0.2 (-)

Inelastic static properties (mortar joints interfaces)							
f_t	f_c	c	$tan(\phi)$	Ψ	G_f^I	G_f^{II}	G_f^{IV}
0.45 (N/mm²)	30.00 (N/mm²)	0.63 (N/mm²)	0.57 (-)	45.0 (deg)	0.012 (N/mm)	0.059 (N/mm)	1.00 (N/mm)

Dynamic incremental factors (DIF's values)											
Strain rate (s^{-1})	E_{unit} (N/mm²)	E_{mortar} (N/mm²)	ν_{mortar} (-)	f_t (N/mm²)	f_c (N/mm²)	c (N/mm²)	$tan(\phi)$ (–)	Ψ (deg)	G_f^I (N/mm)	G_f^{II} (N/mm)	G_f^{IV} (N/mm)
2×10^{-5}	1	1	1	1	1	1	1	1	1	1	1
0.01	-	-	-	1.23	1.23	1.23	-	-	1.95	1.95	1.95
10	-	-	-	1.49	1.49	1.49	-	-	3.00	3.00	3.00
100	-	-	-	2.18	2.18	2.18	-	-	3.35	3.35	3.35
200	-	-	-	2.42	2.42	2.42	-	-	3.45	3.45	3.45

The implementation of such laws in the homogenized model allows deriving the stress-strain rate-dependent homogenized curves and, since the KP model is adopted here, the moment vs. curvature relationships are simply derived by the integration of the latter stress-strain curves through the thickness of the wall following a Kirchhoff-plate theory.

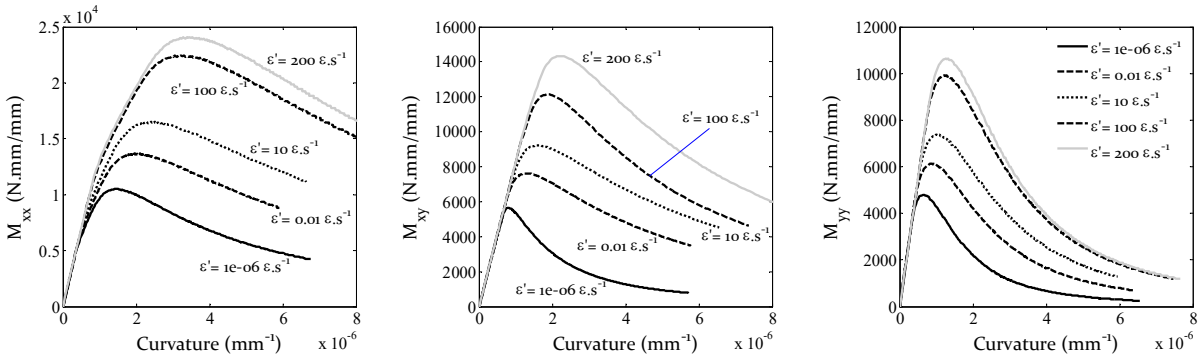

(a) (b) (c)

Figure 5.23 – Strain-rate dependent homogenized curves used for the study of masonry parapets subjected to impact load: (a) horizontal bending moment; (b) vertical bending moment; and (c) torsional moment.

Figure 5.24 reports the simulation results of the two-step framework in terms of displacement magnitude with respect to time. A numerical model with a mesh size of 100 mm has been adopted at a macro-scale (the calibrated elastic Young's modulus of the macro-trusses are given in Table 5.8). The comparison is achieved through the experimental results (Gilbert et al. 2002b) and complemented with two other numerical strategies: (i) the model by Burnett et al. (2007a), (ii) the model by Rafsanjani et al. (2015b). Figure 5.24 shows that the curve from (Burnett et al. 2007a) leads to excessive displacements (and understiff response) because it considers quasi-static values for the material parameters. Conversely, both the present and the mesoscopic model by (Rafsanjani et al. 2015b) are reasonably accurate in predicting the peak displacement, with a relative error of around 10%. Regarding the post-peak behavior, it is noticeable that the structure displacement restitution of the present numerical model is practically inexistent. Yet, similarly to the experimental results, the latter is not entirely reproduced by the other two numerical models under comparison, presenting both an out-of-plane displacement that slightly decreases in post-peak after the time instant of 180 mm. This is possibly due to the irreversible displacements computed (permanent plastic strains) within the cyclic behavior of the model, as seen in the deformed shape at t=300ms plotted in Figure 5.24. The response is still remarkable.

Table 5.8 – Elastic identification of the discrete macro-model for the parapet C6/C7 with a refined mesh of 100 mm size.

Elastic Parameters - Discrete macro-model (H=100 mm; e=20 mm)					
$E_{flexural\ truss}\ xx$	$E_{flexural\ truss}\ yy$	$E_{torque\ truss}\ xy$	$E_{torque\ truss}\ yx$	$A_{flexural\ truss}$	$A_{Torque\ truss}$
6762358.21 (N/mm²)	3381179.10 (N/mm²)	771604.39 (N/mm²)	771604.39 (N/mm²)	1000 (mm²)	1000 (mm²)

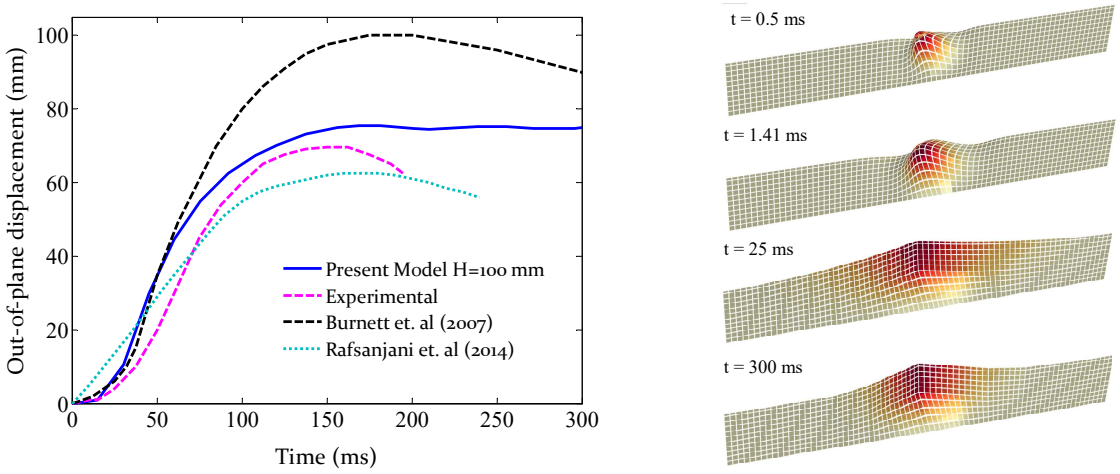

Figure 5.24 – Time history of the out-of-plane displacement obtained for the control node of the parapets C6 and C7 and deformed shapes observed with the proposed model for the time instants 0.5ms, 1.41ms, 25ms and 300 ms.

Figure 5.25 indicates the observed damage pattern. Vertical cracks are clear around both the central area and the two supported edges. Also, horizontal cracks spread from the center along the height of the masonry parapet. As expected, it is evident that damage tends to concentrate on the impact zone. This was implicitly concluded in the experiments tests by Gilbert et al. (2002a), whereas the lateral supports effect decreases with the increase of the parapet length. Thus, the central localization of the damage leads to a critical plastic deformed area that can explain the results.

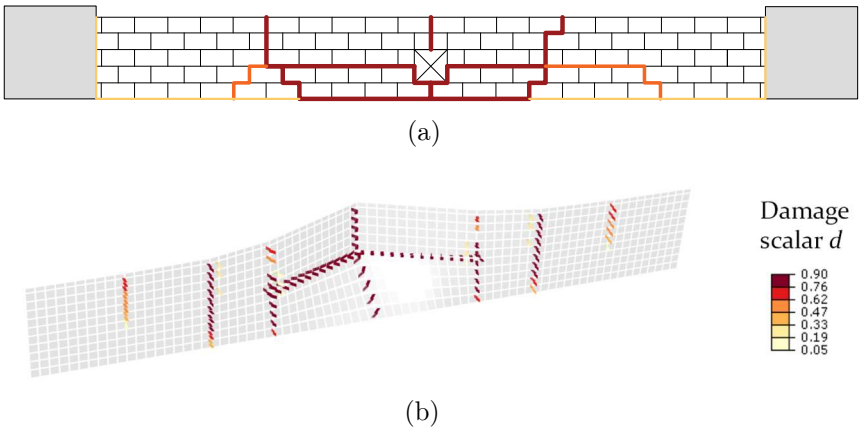

Figure 5.25 – Damage pattern for the parapet C6/C7: (a) observed after the experimental campaign (adapted from Gilbert et al. (2002a)); and (b) for the applied load wall side, horizontal cracks and vertical cracks.

5.4.4 Mesh sensitivity and computation time of the solution

A mesh sensitivity study at a macro-scale is conducted for the parapet C5/C6 subject to a low velocity load. The goal is to evaluate its dependency in terms of accuracy and computational time required. For this purpose, two less refined quadrilateral meshes were considered, i.e. 200 mm and 400 mm. Once a uniform quadrilateral mesh pattern is specified, higher mesh dimensions could lead to important geometrical misrepresentations and thus unnecessary errors. Figure 5.26 reports the results of the mesh sensitivity analysis.

Bearing as reference the curves obtained with the maximum refinement level, Figure 5.26 shows that mesh dependency is moderate from an engineering standpoint. In fact, maximum relative errors of 16% and 25% between peak curves values are found. An alike shape of the time-history displacement curves is also collected, meaning that the pre- and post-peak behavior is well captured and not perturbed with the mesh change, at least for the present control node. This is easily observed through the deformed shape presented in Figure 5.26, whereas the displacement field is smoother between adjoining discrete elements with the increase of the mesh refinement. Coarser meshes may lead to an inaccurate representation of the damage pattern due to the limited number of elements that govern it (deformable trusses).

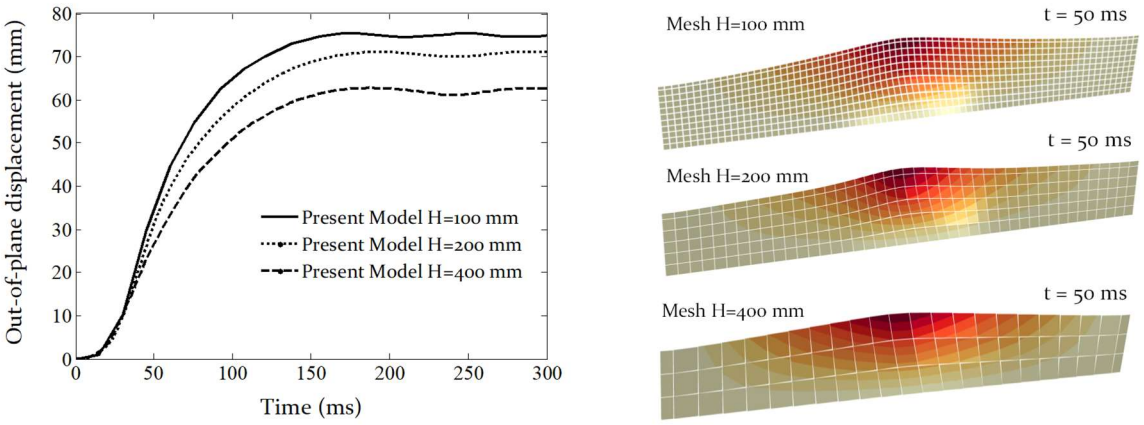

Figure 5.26 – Mesh sensitivity study in terms of time history of the out-of-plane displacement obtained for the control node of the parapets C6 and C7 with three mesh refinements, H=100, H=200 and H=400 mm. Obtained deformed shapes observed the time instant 50 ms.

On the other hand, the computational time required at a macro-scale is significantly decreased with mesh size, as seem in Figure 5.27. In this regard, the author highlights that a proper mesh size discretization is of relevance. It may minimize the errors due to possible rough geometrical modelling by the use of coarse elements, but, account also for the needed output information. For instance, if one wants to obtain a clear and accurate structural behavior in

terms of displacement and damage fields, a finer mesh is the better solution. If one is interested in obtaining a quick evaluation of the structure peak displacement or perform a thorough parametric study, a coarser mesh at a structural scale could be a possibility.

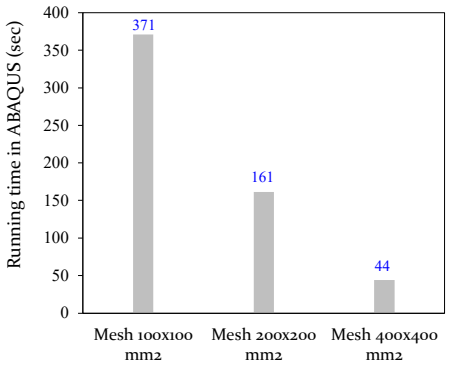

Figure 5.27 – Registered computational time for the three mesh refinements studied.

5.5 Summary

The present chapter addressed the numerical assessment of OOP loaded masonry structures using the proposed two-step procedure. A series of different experimental campaigns have been selected to ensure a study encompassing three main regimes of application: an OOP load applied in a quasi-static fashion, a seismic dynamic excitation, and an impact load (fast dynamics). The first analysis has been carried out on solid and windowed running-bond URM panels subjected to two-way bending through the application of a pressure load using airbags. Quasi-static (pushover) analyses have been performed. The comparison between the numerical and experimental data proved that the two-scale strategy represents well the structure capacity, the post-peak behavior and the observed damage patterns. Although convenient due to its practicability, a quasi-static analysis typically leads to reduced stiffness and strength values when compared to a dynamic one. This issue is especially contentious in cases where high strain–rate loads are applied, due to the enhancement effect observed on the material and mechanical properties.

In this context, a seismic dynamic analysis upon a brick URM house with an English-bond has been achieved. The referred benchmark served to foster a blind test prediction program and the obtained results showed that, in agreement with preceding observation from several research peers, the traditional methods of analysis are unable to reproduce satisfactorily the experimental observations. In converse, the proposed two-scale framework based on a direct numerical simulation (DNS) at a meso-scale allowed obtaining a good resemble in terms of experimental OOP displacements-history and damage map. The results are unequivocal and prove that reproducing the existing mortar vertical discontinuity along the English-bond

masonry thickness is of utmost importance. In fact, this configuration leads to an anisotropic behavior which cannot be well represented by the simplified Kirchhoff-based model nor by a continuous FE-based macroscopic approach. Such feature seems to have more relative importance than the OOP shear stresses effect. Even so, the latter may be re-analyzed in cases where the masonry thickness is considerable or where torsional movements are especially dominant. In this context, the author does believe that in the study of English-bond masonry structures, precluding those effects may lead to inaccurate and unconservative solutions. The third case study focused on a running-bond masonry parapet subjected to an impact load. Again, the numerical procedure exhibits a noteworthy prediction, both in terms of the OOP displacement and damage map. The ability of the proposed framework in handling the strain-rate dependency of the masonry, via a dynamic incremental factor (DIF) approach, is demonstrated and certainly a key point.

In general, although a limited (yet representative) repertoire of case studies has been considered, it has been seen that the numerical framework can reproduce with a reasonable agreement the OOP behavior of masonry structures. Insomuch, by being integrated within an advanced computer software as ABAQUS, it proved to be robust and computationally very attractive. The possibility of executing the calculations using a parallel computing system is paramount. This circumstance together with the simple numerical nature of the procedure appears to speed-up the computations and reach quite attractive running-times. As initially aimed, it can be affirmed that the presented framework demands a significantly lower computational cost than a macroscopic one, i.e. around 10 times less. Even so, despite the regularization step that corrects the fracture energies of the stress-strain input curves, it may be pointed out that: (i) the use of rigid elements, with concentrated nonlinearity on its interfaces, intrinsically suffer from limited mesh dependency on softening; (ii) discrete-based models where rigid elements are employed per se, may suffer from a perpetual geometrical limitation due to the misrepresentation that may occur when openings exist; and (iii) the discrete macro-model is not able to directly follow diagonal yield lines (zig-zag instead). Yet, the use of a refined quadrilateral mesh allows to overcome such limitation. In this context, the mesh size definition should always include the latter concerns. The mesh sensitivity studies performed seem to sustain that for practical applications the use of a coarser mesh can be appropriate. This is especially clear if one notices the improved running times achieved. Nevertheless, the results showed that bypassing a finer macro-model discretization seems to be more appropriate within the static range than within the dynamic one.

Chapter 6

6 Seismic fragility assessment of an URM structure

6.1 Introduction

Performance-based earthquake engineering (PBEE) is a methodology in which a structure is designed to reach the desired performance state given a seismic excitation level (Ghobarah 2001; Günay and Mosalam 2013). The first adoption of this philosophy dates from the Uniform Building Code (PCBO 1927) being still incorporated in current design guidelines; for instance, the FEMA 356 (2000) and ASCE/SEI 41-17 (2017), which provides the maximum probability of a structure collapse according to the level of ground motion intensity; and, at the same line, the Eurocode 8 (2004) sets the returning period of the seismic event to be considered conditioned by the type of class of the building, for both the near collapse, significant (or severe) damage, and damage limitation cases.

The 1994 M6.7 Northridge and 1995 M7.2 Hanshin-Awaji (Kobe) earthquakes showed that code-compliant design allows structures to behave well from a non-collapse requirement, but are unable to control the observed damage that led to unacceptable high downtime and repair costs. To cope with this, improvements have been introduced by PBEE frameworks whereas additional performance requirements considering direct loss and downtime costs have been presented (Welch et al. 2014). For instance, SEAOC (1995), ATC 40 (1996), FEMA 273 (1997) were developed, which aimed to be seismic provisions for building codes. Nonetheless, design codes feature a semi-probabilistic character, i.e. although the definition of the system variables is based on a simplified probabilistic estimation through safety factors, the final verification is purely deterministic because it relies on a ratio between the capacity and demand for each structural element. Such *cut and dry* approach do not guarantee the liability of engineers owing the uncertain nature of earthquakes, as seen (witnessed) in the 2011 great East Japan earthquake which caused 16,000 deaths and a total cost of $120 billion USD for building recovery activities (Norio et al. 2011).

Aiming a better control of the structural performance, reliability methods have been implemented within the PBEE frameworks; leading to the so-called second generation methods, as the PEER-PBEE developed by the Pacific Earthquake Engineering Research center, see K.A. Porter (2003). The PEER methodology introduced uncertainty in all the four stages of the seismic loss assessment: (i) hazard analysis (seismic action); (ii) structural analysis; (iii) damage analysis; and (iv) decision analysis (consequences). It is important to recall that such a framework can be applied for both new and existing structures and at a structural or at a

territorial level. In any case, this is a key tool in the decision process, as when applied to a new or existing structure, it can indicate the best design or retrofit solutions, respectively, to face a future seismic event considering both economic and downtime costs established by the owner and designer. Also, when applied at a territorial scale, the method can orient, through loss estimations in terms of economic and social impact, the most convenient solution for political and private (insurance companies) stakeholders but, as well, indicate the existence of vulnerable building stock and foster potential risk mitigation strategies.

Although the methodology is being disseminated through straightforward procedures (Günay and Mosalam 2013), its multi-disciplinarily character, complexity and computational burden still preclude its use in common engineering practice. Bearing that the structural analysis stage represents a considerable amount of time, novel probabilistic-based tools of assessment, which can be combined in such a framework have been presented in recent years. This chapter is thus intended towards the modification of the latter framework for the seismic assessment of a URM structure, yet focusing on the damage assessment and precluding, so far, the hazard and loss assessment steps. Considering the latter concerns, the proposed numerical two-step strategy is adopted for the analysis stage, because it allows fast computations even within a nonlinear dynamic analysis. The study is integrated with variables parametrization to account for the propagation of uncertainty.

6.2 Case study & outline of the stochastic framework

A methodology appropriate for the seismic vulnerability assessment of URM structures is herein described and applied next for the English-bond brick-house mock-up tested in LNEC by Candeias et al. (2016), which has been addressed in Chapter 5 (section §5.3). The probabilistic-based methodology covers two out of four PEER-PBEE approach steps, i.e. the structural and damage analyses. The final output is the computation of the probability of exceeding (POE) defined damage states, whose results may be gathered and plotted through fragility functions (viz. fragility curves). The framework aims to be general and practical, hence several assumptions are addressed to increase its computational efficiency. The main features are addressed next and presented in Figure 6.1. Each step is detailed during the application for the selected case study.

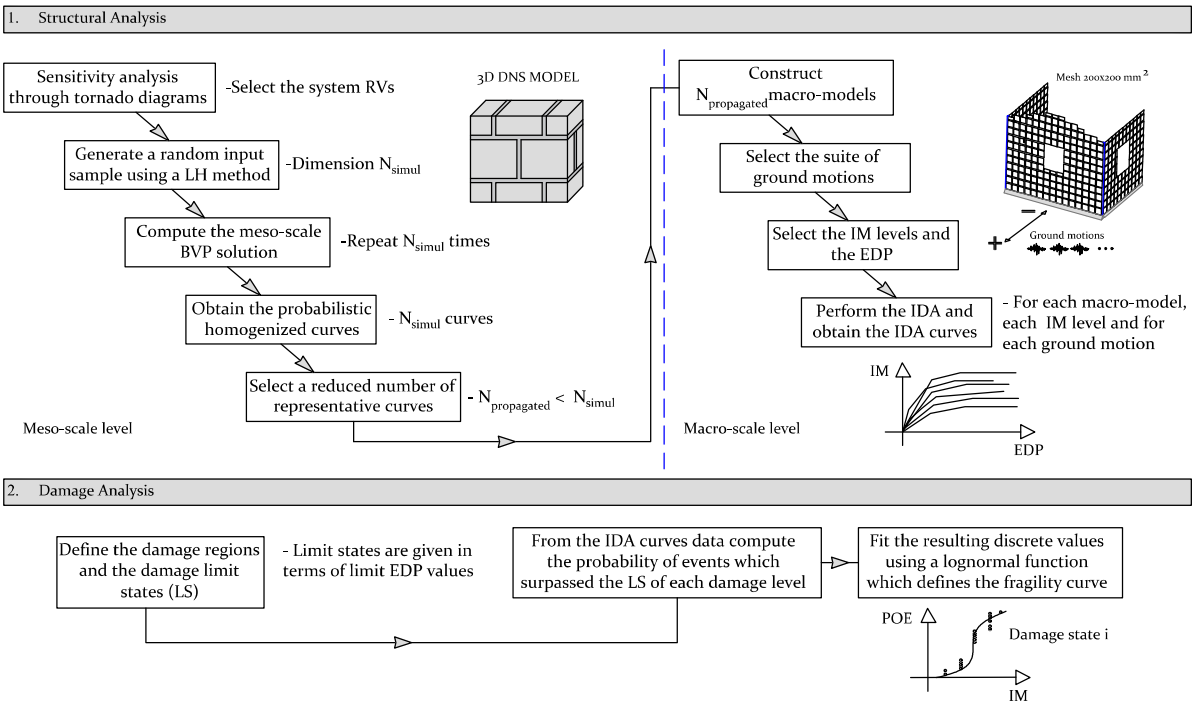

Figure 6.1 – Flow-chart of the probabilistic framework adopted for the seismic vulnerability assessment of an URM structure.

Structural analysis

Seismic fragility curves constitute a state-of-art approach when assessing the seismic risk of a structure and require the definition of both an intensity measure (IM) and an engineering demand parameter (EDP). These can be derived from the so-called capacity spectrum method (CSM) (ATC 40 1996) or through an Incremental Dynamic Analysis (IDA) (eventually seismic vulnerability curves if loss estimation was also appraised). The CSM is based on a static-type of loading and suffer, inevitably, from the perpetual limitations of static approaches, as it may mislead the energy dissipation, resulting forces and the overturning moments. The reader is referred to Krawinkler and Miranda (2004) for a further discussion concerning the CSM. In converse, the IDA brings several advantages as, besides the fact that the predicted response is the outcome from a dynamic analysis, it provides the capability of employing different Engineering Demand Parameters (namely displacement-, acceleration- or energy-based) for different earthquake Intensity Measures (such as PGA, the spectral acceleration, etc.). So, the IDA method is employed in this study.

The stochastic character of the framework is assured by incorporating uncertainty in the system variables. At a meso-scale, the material, and geometrical variables X_i are parametrized to account for probability-based concepts. Since the assessment is conditioned by the extent of system uncertainties assumed, a sensitivity study is performed to conclude on the most

important variables for the masonry response. As a result, tornado diagrams may be plotted to evaluate the less relevant system variables and, therefore, identify the ones which entail a deterministic and non-deterministic nature (read, random variables RVs) aiming to increase the computational efficiency. Afterwards, a Latin Hypercube (LH) strategy is adopted to generate the random sampling of the meso-scale input, being the BVP solved N_{simul} times using the DNS homogenized model (see section §3.6) to obtain the random homogenized quantities. The propagation of uncertainty between the meso and macro-scales is conducted by the upscaling of a set of $N_{propagated}$ stress-strain and moment-curvature quantities which represent the whole probabilistic sample. This step intends to reduce the required number of IDAs performed at a macro-scale, since $N_{propagated} \subset N_{simul}$. Note that the loading uncertainty is also acknowledged by providing different ground motions scaled for each IM analyzed.

Damage analysis

The computation of the fragility functions follows an analytical approach, meaning that the data collected from the IDA curves are used. To accomplish this goal, it is still necessary to define damage regions and the corresponding limit state (LS) levels. The structure's response represented by the IDA curves is given in terms of EDP values for each ground motion IM. Hence, it is likewise customary to describe the LS in terms of fixed EDP values (Günay and Mosalam 2013) (possibly with an associated coefficient of variation, CoV), since it allows to easily compute, through a binomial distribution approach, the number of events that surpassed or not the aforementioned limits; accordingly, it is possible to simply compute the associated POE of each LS. Finally, the construction of the fragility curves is here achieved by fitting the discrete data using a lognormal probabilistic distribution. The use of a cumulative lognormal function to express the seismic fragility curve of structures has proven to be a suitable and appropriate choice (Krawinkler and Miranda 2004).

6.3 Structural analysis (meso-scale level)

6.3.1 Sensitivity study of the input parameters

Uncertainties are commonly interpreted in engineering decision fields according to its origin and, therefore, differentiated as physical (in the sense of nature), statistical or modelling uncertainties (Nowak and Collins, R. 2012). Its representation is achieved by defining the system variables as non-deterministic or, as typically designated in the literature, as random variables (RVs) (Faber and Stewart 2003; Faber et al. 2007). Complex methods as the non–stationary stochastic processes allow to represent these RVs (Stewart and Melchers 1997;

Melchers 1999), yet the definition of simple statistical distribution functions is appropriate in the majority of the structural problems. This fact is well addressed in the probabilistic model code JCSS (2011), which puts together several valuable suggestions for a probabilistic structural design. Recommendations on the statistical distributions and the associated statistical parameters values are presented for several construction materials like concrete, timber, and masonry. Variables concerning the loading input, the material properties of the masonry and the geometry of the structure can carry the uncertainty of the system.

A proper selection of the number of RVs of the system $X = \{X_1, X_2, X_3, \dots, X_{i+1}\}$ is of utmost importance, as it has a direct effect on the required computational processing time. Table 6.1 depicts the variables that serve as meso-scale input for the homogenized 3D DNS model. The expected values and the CoV terms follow the experimental data addressed in section §5.3 and the recommendations from JCSS (2011), when applicable.

Table 6.1 – Statistical properties of the system variables to conduct the sensitivity study.

X_i	Statistical distribution	$E\left[X_i\right]$	$CoV\left[X_i\right]$
E_{brick} (N/mm^2)	LN	11000	29 % (Candeias et al. 2016)
E_{mortar} (N/mm^2)	LN	3000	25 % (JCSS 2011)
$f_{c,mortar}$ (N/mm^2)	LN	2.48	17 % (JCSS 2011)
$f_{t,mortar}$ (N/mm^2)	LN	0.105	*25 %
G_f^{IV} (N/mm)	LN	3.97	*17 %
G_f^{I} (N/mm)	LN	0.012	*25 %
G_f^{II} (N/mm)	LN	0.05	*25 %
c (N/mm^2)	LN	0.2	40 % (JCSS 2011)
Φ (degrees)	LN	30	19 % (JCSS 2011)
t (mm)	N	235	5 % (Candeias et al. 2016)
t_{joint} (mm)	N	15	20 % (Candeias et al. 2016)

* $CoV\left[X_i\right]$ value assumed by the author.

A sensitivity analysis is hereafter conducted to attest the relative significance that each one of the eleven parameters has upon the OOP homogenized quantities; specifically, on the horizontal (M_{xx}), vertical (M_{yy}) and torsional (M_{xy}) bending moment-curvature relationships. Note that, following the low experimental variability registered by Candeias et al. (2016), both the masonry density ρ and Poisson coefficient υ are given as deterministic variables. In this regard, two meso-scale homogenization problems are solved for each studied variable X_i one whereas X_i adopts a lower bound value defined to be the 5% percentile; and, the other, where X_i adopts an upper bound value defined to be the 95% percentile. The remaining random

variables are given, for both the cases, by the respective median values (50% percentile). Since this process is repeated for each of the eleven X_i, a total of 23 analyses have been developed ($X_i \times 2 + 1$); note, again, that one is provided by the reference M_{xx}, M_{yy} and M_{xy} curves retrieved when all the variables possess its median value. It is recalled that other truncation which respects the equidistance to the median is possible. This holds true because the same conclusions on the relative importance of a given variable would be found.

The latter data is assembled into tornado diagrams as seen in Figure 6.2. In this type of charts, the variables are positioned in the ordinates and the bar length represents the consequence of changing the variable to a lower and upper bound with respect to the base (median). The tornado diagrams place the most influential variables in the top of the chart, following a descending order and thus allowing to draw faster conclusions on its relative impact. Having into account that both material and geometric parameters are considered as RVs, it is expected that differences can be accountable not only on the maximum moment capacity but, as well, on the $M - \chi$ curve shape (especially in the post-peak regime). Thus, the sensitivity study has been driven for a local and global control parameter of the M_{xx}, M_{yy} and M_{xy} curves, i.e. the peak moment value and the curves stored energy, respectively.

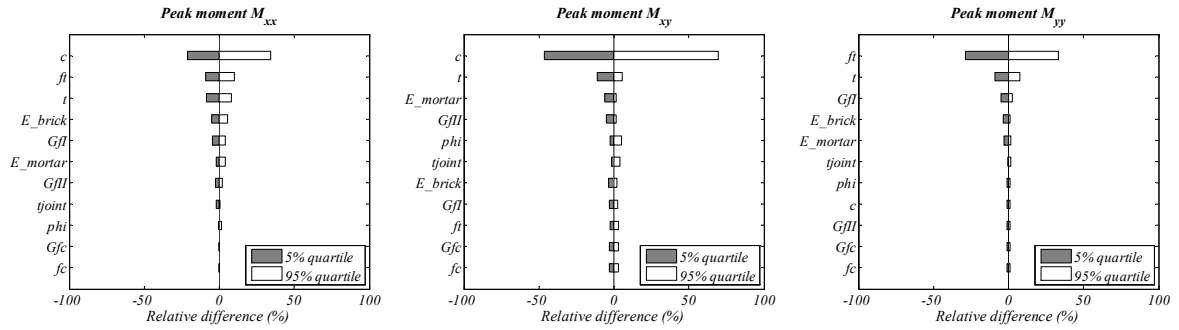

(a)

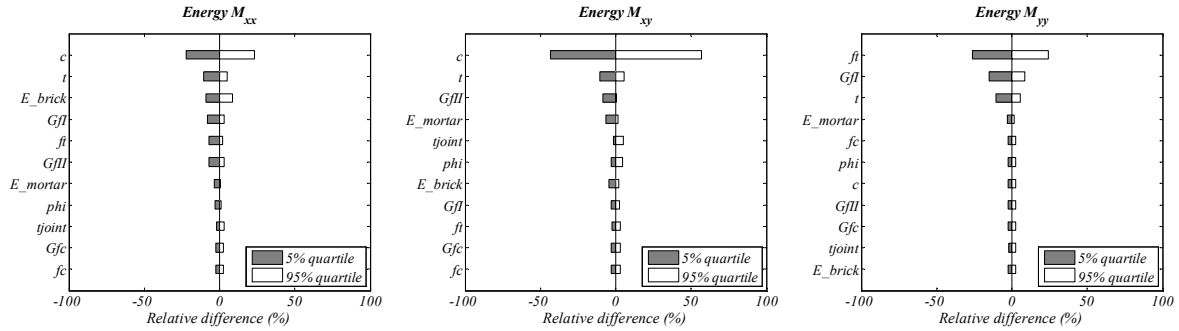

(b)

Figure 6.2 – Tornado diagrams for the eleven RVs of the system (phi = Φ): (a) local parameter given by the curves' peak; and (b) global post-peak parameter given as the stored bending energy.

The results of the tornado diagrams have shown that some parameters, as cohesion (c), tensile strength (f_t) and thickness (t) unequivocally govern both the local (peaks) and global (energy) meso-response. On the other hand, it can be also stated that the parameters concerning the compressive regime seem to have a lower effect for this case study. These findings are in agreement with the experimental evidences, i.e. in the case of weak mortar masonry, the tensile and shear regimes tend to govern the behavior of weak mortar masonry (Willis et al. 2004). Hence both the compressive strength and fracture energy terms are defined to be deterministic variables. The remaining variables seem to have a significant effect on the homogenized quantities derived and, therefore, a total of nine variables are considered to be random and carry the aleatoric uncertainty of the system:

$$X = \{E_{brick}\ , E_{mortar}\ , f_t\ , G_f^I\ , c\ , G_f^{II}, f_c\ , t_{joint}\ , t\}$$

6.3.2 Probabilistic sampling (Latin Hypercube method) of the input

In some cases, where uncertainty is considered, the failure probability can be evaluated solving the integral of the given limit state function (Faber 2009). In other cases, rather complex and within a multivariate space, the determination of the solution is necessarily achieved using an approximate strategy, as the response surface method (Bucher and Bourgund 1990) or through a *trial and error* approach using sampling methods, as the Monte Carlo (MC) or the Latin Hypercube (LH).

The MC and LH sampling techniques are widely spread in several engineering fields and follow similar methodologies, i.e. the formulation of four main steps: (i) the definition of a probability distribution function (*PDF*) and associated statistical parameters for each RV; (ii) the generation of a sample of the RVs, according to its distribution, potential correlation, and the number N_{simul} of desired simulations; (iii) finding the solution of the problems using each of the latter generated sample of variables; thus repeating the process N_{simul} times; (iv) reaching the failure probability through the ratio between the number of solutions that respect the limit function and the total of N_{simul} simulations number. The key difference between MC and LH is the way that the sampling process is performed. Both suffer from a dimensionality curse, i.e. the accuracy of the solution strongly depends on the number of simulations performed. The former approach has been developed first by Metropolis and Ulam (1949) and is conceptually more straightforward, as it uses a simple random algorithm to define the set of RVs. Still, it brings the disadvantage of demanding a high computational cost if an acceptable confidence limit is desirable. The latter technique stems from the MC method, but it adopts a rational selection of the RVs set through a stratified sampling technique which allows avoiding the

existence of overlapped simulations (McKay et al. 1979). The computational effort is thus lessened when compared to crude MC techniques (Stein 1987).

For the present application, an LHS method within an inverse transform method is chosen. The sampling process has been performed in MATLAB and intends to derive a set of $N_{simul} = 2000$ grouped values, for each RV of the array X, to allow investigate the masonry response variability. It matters recalling that some of the input variables may be dependent and, therefore, a non-identity correlation matrix has been considered. The goal is to obtain a meaningful sample of values and guarantee that only plausible physical behaviors are simulated. The built-in LHS tool of MATLAB makes use of a correlation measure based on the Person product-moment coefficient $\rho_{i,j}$ (subscripts i and j denote two given variables). Table 6.2 reports the parameters adopted (namely the covariance matrix, see McKay et al. (1979)), which are fully-based on expert judgment. Only null (independent variables) and positively correlated variables are considered. On the other hand, no spatial variability has been accounted for.

Table 6.2 – Target correlation matrix adopted between the input random variables.

	E_{brick}	E_{mortar}	f_t	G_f^I	c	G_f^{II}	Φ	t_{joint}	t
E_{brick}	1.0	0.4	0.2	0.2	0.2	0.2	0.2	0.0	0.0
E_{mortar}		1.0	0.8	0.6	0.6	0.4	0.2	0.0	0.0
f_t			1.0	0.6	0.6	0.4	0.2	0.0	0.0
G_f^I				1.0	0.6	0.4	0.2	0.0	0.0
c					1.0	0.6	0.2	0.0	0.0
G_f^{II}		sym				1.0	0.2	0.0	0.0
Φ							1.0	0.0	0.0
t_{joint}								1.0	0.2
t									1.0

The theoretical statistical distribution and the histograms obtained after the LH sampling are shown in Figure 6.3 for each RV. It is clear that a good match has been found between the generated and expected distribution curves.

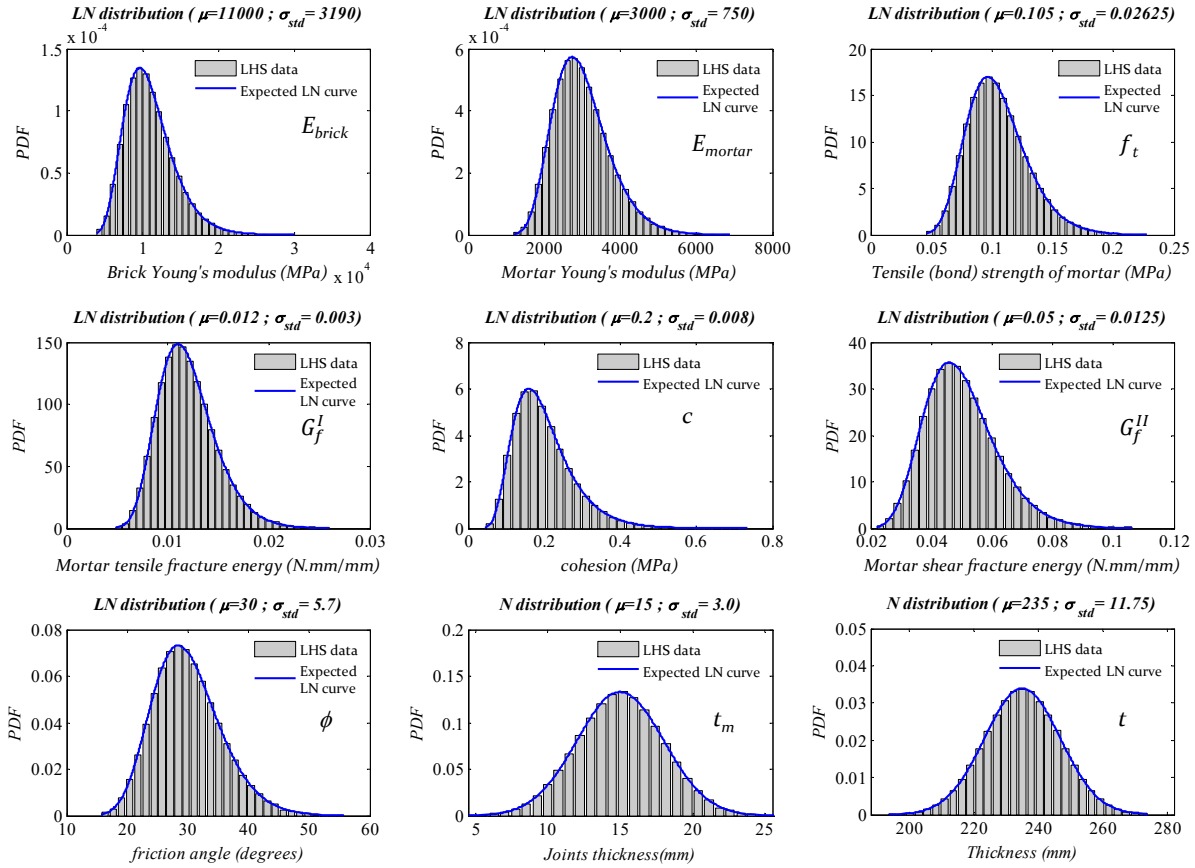

Figure 6.3 – Distribution of the generated samples of each RV after performing a LH sampling with a dimension equal to $N_{simul} = 2000$.

6.3.3 Propagation of uncertainty (meso-to-macro scale)

The process of determining the sample of values that covers the input for the 3D DNS homogenized model has been achieved through the Latin Hypercube (LH) sampling technique. A total of $N_{simul} = 2000$ simulations have been performed and the derived samples ensure the variability of the different system material, mechanical and geometrical parameters. Each generated sample serves as input for the BVP that needs to be solved at a meso-scale and, by repeating this process for every sample, a total of 2000 homogenized stress-strain and moment-curvature curves are derived, as depicted in Figure 6.4. It is clear the large variability of the meso-scale response, partly explained by the adopted high CoV values for the most critical parameters, which proves the importance of considering the material uncertainty for URM structures.

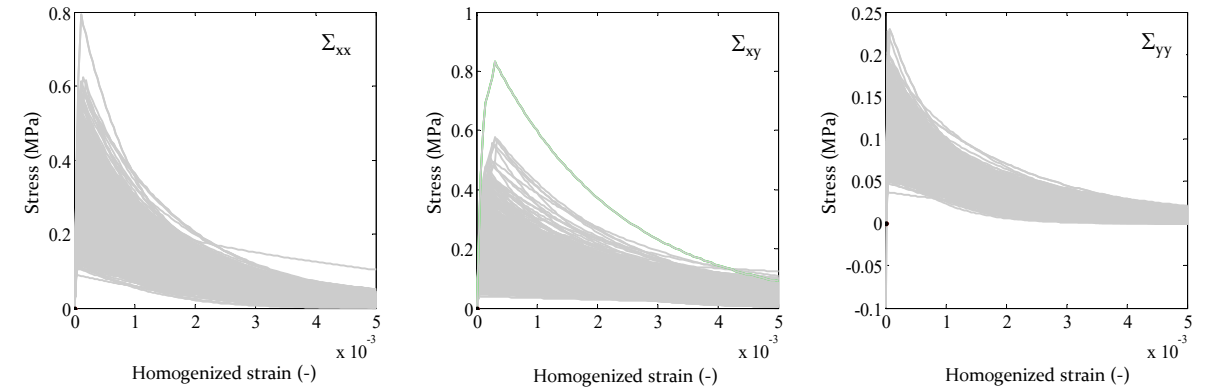

(a)

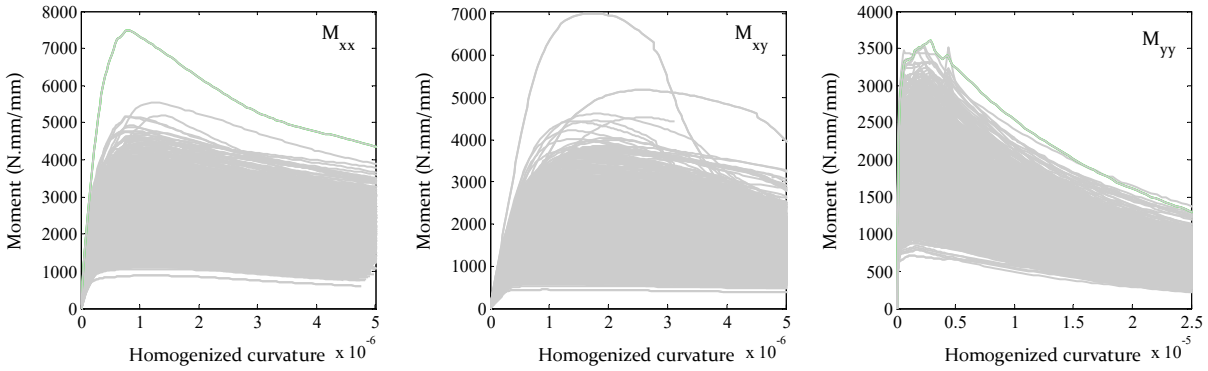

(b)

Figure 6.4 – Homogenized moment-curvature curves after the performed $N_{simul} = 2000$ simulations for the: (a) in-plane $\Sigma - E$ curves; (b) out-of-plane $M - \chi$ curves.

A convergence test has been performed to assess the adequacy of the number N_{simul}. Figure 6.5 shows that the mean peak values of the generated homogenized $M - \chi$ curves are practically stationary after a $N_{simul} = 500$ and remains below the defined tolerance of 5% (in respect to the last simulated mean value). This behavior is consistent for all the M_{xx}, M_{yy} and M_{xy} curves and, therefore, the $N_{simul} = 2000$ seems an appropriate choice (the $M - \chi$ curves are directly derived from the $\Sigma - E$ curves; hence the latter results are not plotted here).

The suite of generated stress and moment curves, developed using a LH technique and computed from the DNS homogenized model, carry the system uncertainty and make possible the probabilistic analysis of the masonry behavior at a macro-scale.

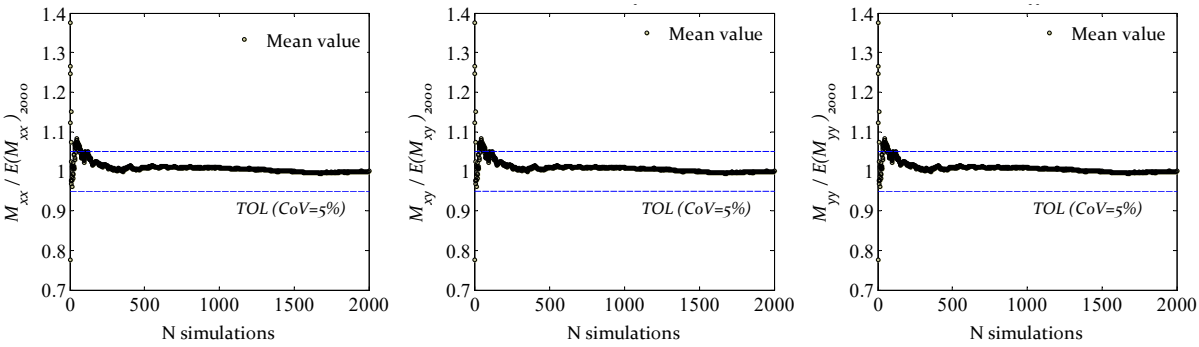

Figure 6.5 – Convergence tests performed for the obtained peak values of the M_{xx}, M_{xy} and M_{yy} quantities during the 2000 simulations performed.

The dimension of the available data is large and, in order to reduce the number of simulations performed at a macro scale, it has been decided to seek representative homogenized material curves. So, data from each quantity has been filtered to retrieve the five principal percentiles. The main purpose is the definition of five deterministic models that holistically represent N_{simul} different samples of material, mechanical and geometric parameters. However, combining the percentiles found for each of the homogenized quantities and blindly assuming that these constitute five macro models may be erroneous. In other words, the sample that originates the maximum M_{xx} peak can differ from the one which originates the maximum M_{xy} and/or M_{yy} values. This is especially critical in a multivariate system, whereas the relative importance of each variable is more diluted and thus an obvious correspondence between models is hardly found. A similar strategy has been adopted by Günay and Mosalam (2013) but focusing only on one $M-\chi$ curve input and, therefore, without the present complexity. Bearing this in mind, a correlation test between the homogenized quantities being combined is mandatory. The correlation assessment has been conducted via *q-q* plots and the results are addressed in Figure 6.6.

A local and a global parameter that characterizes the OOP homogenized quantities are accounted, namely the curve's peak value and the stored bending energy. Again, only the OOP quantities have been considered to avoid redundancy, as the $M_{xx}-\Sigma_{xx}$, $M_{xy}-\Sigma_{xy}$ and $M_{yy}-\Sigma_{yy}$ are correlated. Note that the $M-\chi$ curves are a function of the IP quantities, i.e. $M_{xx}=M_{xx}(\Sigma_{xx})$, $M_{xy}=M_{xy}(\Sigma_{xy})$ and $M_{yy}=M_{yy}(\Sigma_{yy})$. Additionally, a Kolmogorov-Smirnov (KS) test confirmed that the statistical distribution of the logarithms of both the peaks and energies for each the M_{xx}, M_{xy}, and M_{yy} curves are normally distributed within a confidence interval of 95%. This allows concluding that the latter OOP homogenized curves follow a lognormal distribution.

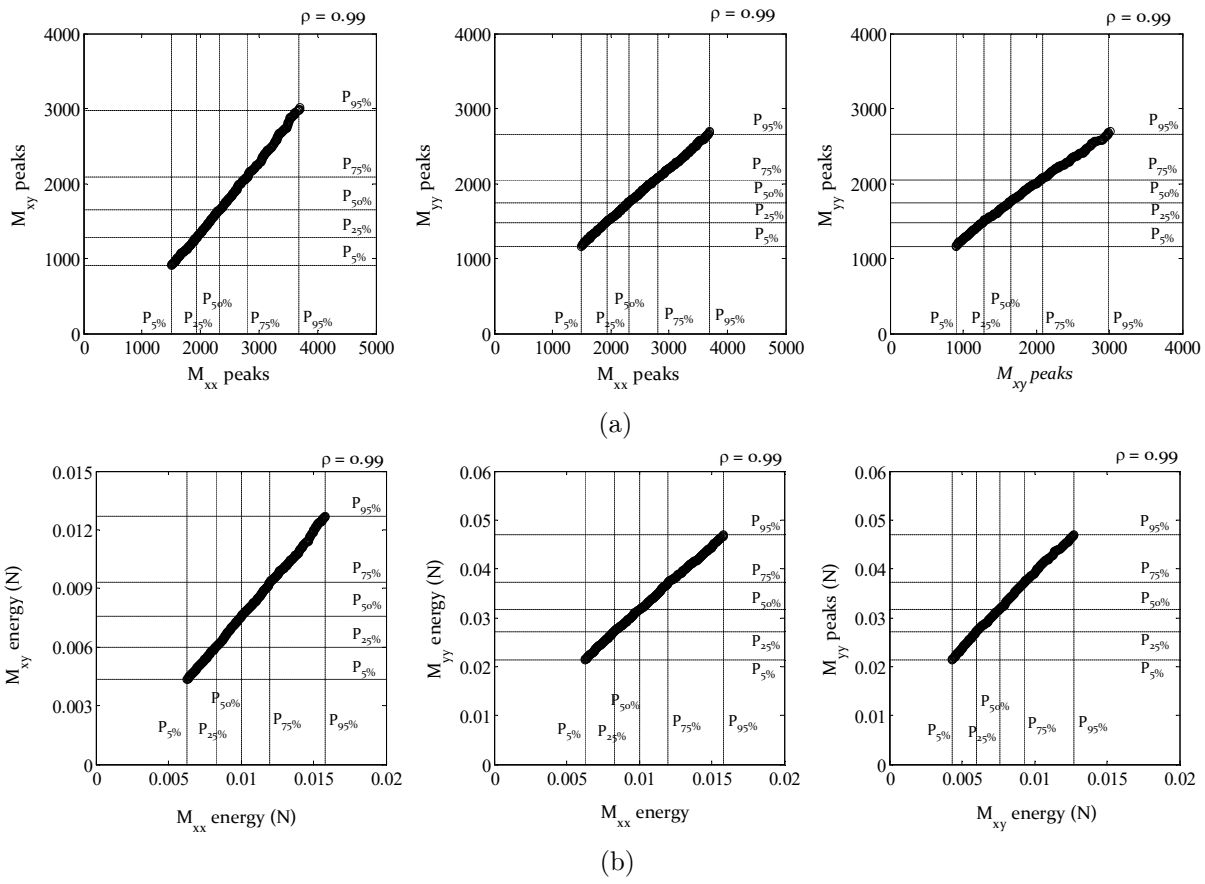

Figure 6.6 – Correlation assessment through *q-q* plots, between the obtained homogenized $M-\chi$ quantities from the 2000 simulations, in terms of (a) peak values of the curves (local parameter); (b) bending energy of the curves (global parameter). The samples have been truncated within the 95% confidence level margins.

In this regard, it is noteworthy to state that the q-q plots have confirmed that the homogenized quantities are quasi-perfect positive correlated (Pearson linear correlation coefficient of 0.99) within a confidence level of 95%. So, this supports the assumption of filtering directly five models from the sample's percentiles. The propagation of the modeling uncertainties between the meso- to the macro-scale is guaranteed by the five representative models plotted in Figure 6.7. These are designated according to the quantiles that represent, i.e. model P5%, model P25%, model P50%, model P75% and model P95%. Note that such an assumption is especially convenient as it allows reducing drastically the computational cost at a macro-scale, without losing the representativeness of the simulations performed at a meso scale.

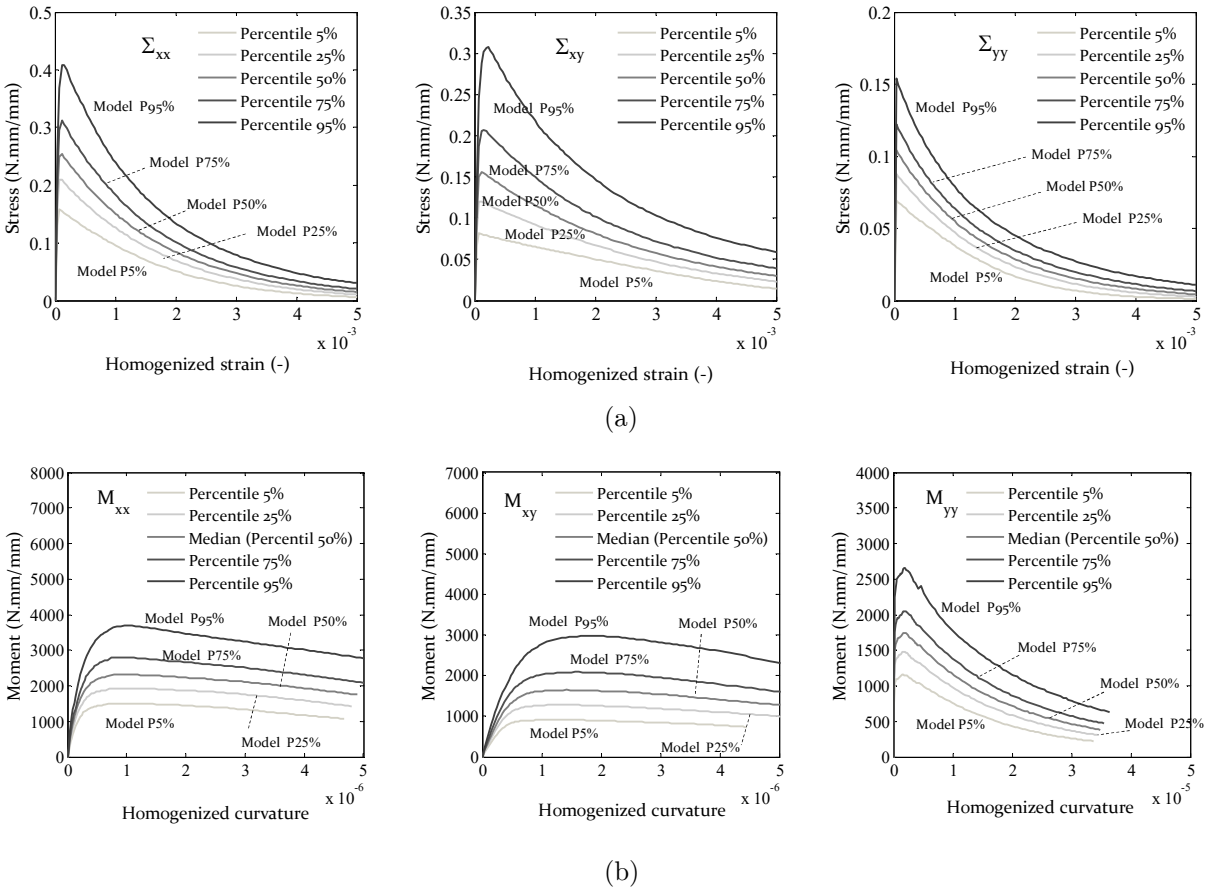

Figure 6.7 – Definition of the five models that represent the simulated sample of 2000 curves: (a) in−plane $\Sigma - \mathrm{E}$ curves; (b) out-of-plane $M - \chi$ curves.

6.4 Structural analysis (macro-scale level)

6.4.1 Load random input: artificial accelerograms

Current code guidelines, such as Eurocode 8 (2004), acknowledge the use of real and artificial accelerograms. An earthquake engineer should choose in conformity according to the nature of the application and the information at disposal. In regions where a significant set of ground motion records of damaging earthquakes is unavailable, the use of real earthquakes is difficult. Also, each record has its own features in terms of wave characteristics contents (as frequency, duration, amplitude, etc.), which makes unlikely that a similar seismic event occurs again. Bearing this in mind, artificial accelerograms compatible with the elastic response spectrum defined through design codes are used here. This is convenient once a significant number of random artificial motion records, compatible with the code design response spectrum, can be easily generated through existing tools already at disposal, as the software SIMQKE_GR (Gelfi 2006) or RASCAL (Silva and Lee 1987). For a detailed comparison between existing tools, see Iervolino et al. (2010).

A total of seven stationary signals have been generated through the software SIMQKE_GR (Gelfi 2006), which is the minimum number according to the Eurocode 8 (2004) for which a representative mean response is acceptable. The non-stationary signals (non-stationary in both amplitude and frequency content) are produced considering a trapezoidal shape for the envelope function (Gasparini and Vanmarke 1976). A total duration of 35 seconds has been defined, in which the intense phase is given to be 30seconds and the rise and decay phases are given altogether with a 5seconds duration. The signals have been high-passed in the range of frequencies of 0.2 Hz to 40 Hz and filtered using a cosine function to attenuate potential accelerations drifts. The resulting artificial accelerograms are compatible with the elastic response spectrum for an earthquake type 1 (far-fault earthquake) defined by Eurocode 8 (2004) with a returning period P_n of 475 years and for a 3% viscous damping ($\xi = 3\%$) coefficient (following the value identified in section §5.3.2), as demonstrated in Figure 6.8. The suggested parameters by the Portuguese National Annex for the region of Lisbon have been followed, i.e. an importance factor γ_I equal to 1.0 (Class B buildings); a value of $agr = 1.5$ m/s^2; and a soil type A (rock, soil factor S=1). Note that these values have been taken from the code by making some assumptions aiming to apply the framework. Therefore, these are not representative of any territory nor building.

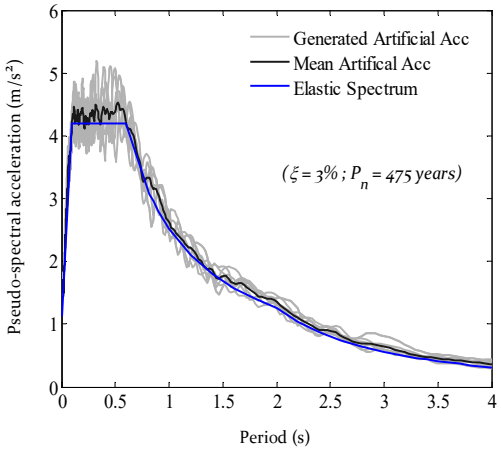

Figure 6.8 – Pseudo-acceleration response-spectrum: elastic spectrum according to Eurocode 8 (2004); response spectrum of the artificially generated earthquakes and mean spectrum of the seven artificial earthquakes.

The filtered signals compliant with the Eurocode 8 (2004) spectrum are depicted in Figure 6.9. A total of seven earthquakes, with a *PGA* tuned to 1m/s^2, serve as a reference for the scaling process. It is noteworthy to stress that the scaling of the earthquakes is performed considering an intensity measure (IM) that represents each ground motion content; this is necessary aiming to guarantee the consistency of the performed incremental dynamic analysis.

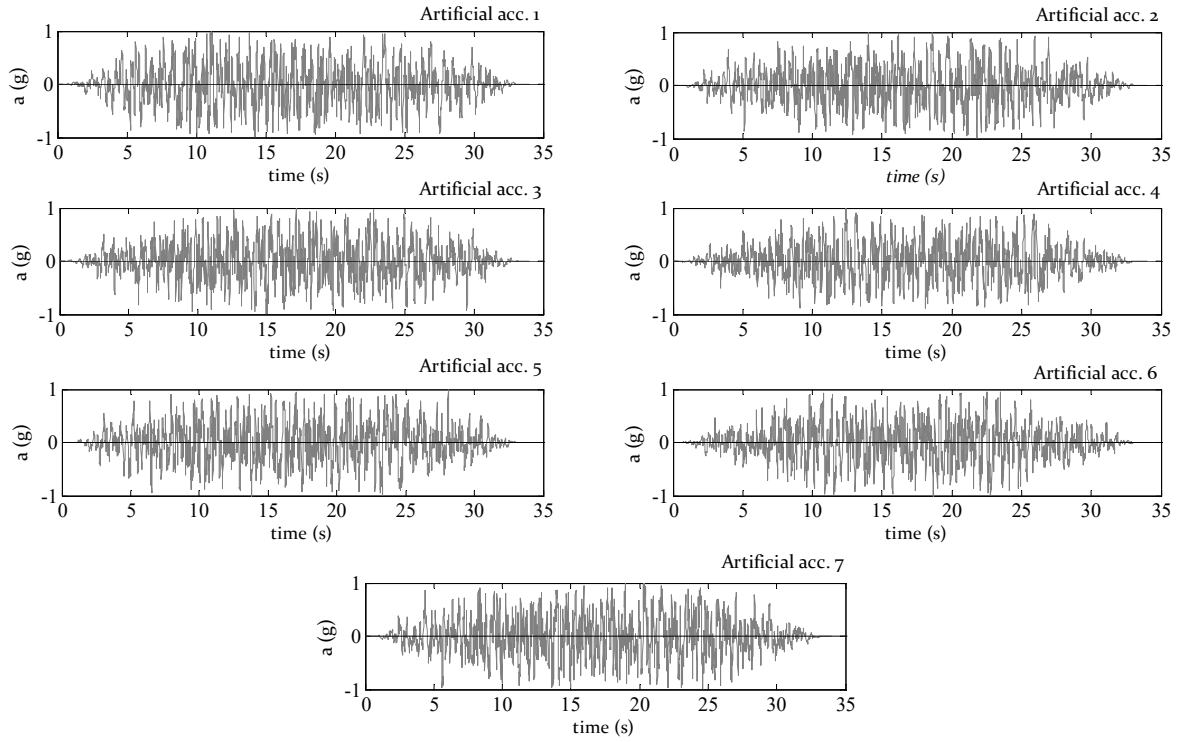

Figure 6.9 – Artificial generated accelerograms scaled to a maximum peak acceleration of 1m/s² to perform the incremental dynamic analysis (IDA).

6.4.2 Incremental dynamic analysis (IDA)

Incremental dynamic analysis (*IDA*) is an intensive method which allows obtaining a better evaluation of the seismic response of a given structure. A series of scaled accelerograms are used to perform multiple nonlinear dynamic analyses and check the response of the structure according to a defined engineering demand parameter (Vamvatsikos and Cornell 2002; Vamvatsikos and Fragiadakis 2010). Besides the selection of a proper set of ground motions, the construction of *IDA* curves demands the definition of (i) an appropriate strong motion intensity measure (*IM*); and (ii) an appropriate engineering demand parameter (*EDP*). The data gathered by the *IDA* analyses offer a comprehensive insight into the seismic response of the studied system and allow constructing important decision-tools, as seismic fragility curves or seismic vulnerability curves (if the losses are estimated). Notice that the construction of fragility curves is, in fact, the ultimate goal of the present chapter.

Intensity measure (IM)

The decision over the optimal *IM* is important for the *IDA* carried out as it may retrieve a lower dispersion on the *IDA* results. Consequently, the number of ground motions required to achieve an adequate confidence level is lower and, therefore, the computational demand

optimized. Briefly, Mackie and Stojadinoviić (2005) referred that an optimal *IM* may feature a character of: (i) practicability, in the sense that is a quantity easily understood from an engineering perspective; transversal (meaning at disposal, for instance, from hazard curves) between different seismology fields; and has a direct correlation to known engineering structural parameters; (ii) sufficiency, as it allows reducing the statistical dependence on the results concerning the ground motion characteristics, as magnitude and source distance; (iii) effectiveness, by allowing the computation of a closed-form law to derive the mean annual *POE* of an *EDP* for a given *IM* level; (iv) efficiency, as is retrieves a lower dispersion of results. An efficient *IM* requires less computational effort since a smaller number of dynamic analyses are needed to capture the predicted structural behavior; and (v) robustness, meaning that its efficiency is maintained for different structural scenarios.

The set of potential *IMs* is extensive and one can mention the *PGA*, *PDV*, *PGD*, the Arias intensity I_A, the Housner Intensity I_H, among others. The selection of the most adequate IM is still debatable. Its identification should encompass concerns related to the adopted hazard model, the system (structural or no-structural) under analysis and the data at disposal (Pitilakis 2014). Still, there are several studies, as Luco and Cornell (2007), Tothong and Luco (2007), and Mehanny (2009), which directly report different optimal IM to be used within a performance-based analysis for both new and existing structures. In this context, presumably, the most appropriate IM for the present study case is the spectral acceleration given at the first structure's period, $S_a(T_1)$ (Vamvatsikos and Cornell 2004), since the first vibration mode of the *LNEC* brick benchmark is associated with the out-of-plane translation of the west façade. This is, in fact, the dominant failure mode and wherein the control node is positioned. Such *IM* is practical, as it can be available from seismic hazard curves (as de U.S. Geological Survey) or easily derived from the response spectrum, and more efficient than the classical structure-independent PGA measure (Kazantzi and Vamvatsikos 2015; Eads et al. 2016), specifically for structures with a low fundamental period. Still, the period of a rocking structure depends on the displacement and may be unsuitable for the out-of-plane collapse of existing masonry structures.

Ground specific intensity measures as the *PGA* (or related *PGV* and *PGD* fields) are likewise practical, but may constitute an inefficient choice for long-period structures (lacks robustness). Even though, the *PGA* has been defined to be the one used as *IM*. On one hand, this is a traditional option that has been largely applied, also in agreement with the existing design codes wherein is included, for instance, in both the hazard definition and in motion attenuation relationships. On the other hand, and perhaps more importantly, such *IM* has been adopted during the input scaling of the experimental data (section §5.3). The use of the *PGA* as *IM* is

thus convenient, as prior knowledge of the structure response is somehow known beforehand. The *IDA* impose the scaling of a ground motion set in terms of *PGA* that may cover the elastic and inelastic behavior of the structure. Hence, even if this suite of earthquakes is different in terms of frequency, duration and amplitude contents, the use of *PGA* as *IM* is still helpful as it pertains a crude reference of comparison with the experimental *PGA* values of Candeias et al. (2016). Here, *IM* levels equally spaced of 0.1g have been set, starting from a PGA of 0.1g up to 0.7g. For a better comprehension on the response of the models P75% and P95%, the maximum IM has been defined to be 0.9g and the spacing equal to 0.05g.

Engineering Demand Parameter (EDP)

A series of nonlinear dynamic analyses may be carried out considering different *IM* levels aiming to plot the final *IDA* curves. This goal is only accomplishable if an adequate parameter, designated in the literature as Engineering Demand Parameter *(EDP*), is established to assess the response of the system. As referred by Krawinkler and Miranda (2004), the *EDP* selection depends on the performance target and on the type of system under investigation.

The present study focuses on the structure only, being the non-structural sub-components of the building disregarded. In such a context, the selected *EDP* may give direct information about the masonry structural behavior and, therefore, carry the uncertainty of the system: aleatory, namely the material and mechanical properties derived at a meso-scale (only from the masonry ones, since no-other material nor the soil-foundation have been considered) and epistemic, namely the modelling-related assumptions, the drawback of scaling only the amplitude (*PGA*) and not the frequency content of the ground motions, and the potential prediction inaccuracy of the two-scale numerical framework.

Possible *EDPs* include story drifts; rotation values; total or inelastic deformations; floor accelerations or velocities; internal forces of elements; strength degradation or energy dissipation values, among others. Here, the total deformation given by the maximum out-of-plane displacement component obtained at the top of the gable wall (δ_{EDP}) has been assumed. It should be mentioned that a displacement-based parameter is typically adopted within analytical frameworks to derive the seismic fragility curves of URM structures, as Calvi et al. (2006), Park et al. (2009), Rota et al. (2010), Frankie et al. (2013), and/or given in seismic URM buildings seismic provisions, as FEMA 368 (2001).

Incremental Dynamic Analysis (IDA) curves

The IDA curves are given by plotting *IM-EDP* curves after performing a series of dynamic analyses (Vamvatsikos and Cornell 2002). Here, seven artificial seismic records have been assumed and scaled to comprise seismic intensity measures ranging the 0-0.9g (PGA levels). These have been only applied in the longitudinal direction of the LNEC brick house. The propagation of the material and geometrical uncertainty traced back at the meso-scale is represented by the usage of five macro-models with corresponding $\Sigma - \mathrm{E}$ and $M - \chi$ capacities: model P5%, model P25%, model P50%, model P75% and model P95%. Accordingly, a total of 266 analyses have been performed which, in practice, cover a total of 2000 samples with different material and geometrical inputs. A confidence interval of 95% is assured by the lower (model P5%) and upper (model P95%) limits. The continuous IDA curves obtained for each macro-model are presented in Figure 6.10, whereas a linear interpolation between the discrete result pairs (IM,δ_{EDP}) from the dynamic analyses is assumed.

These allow concluding that for the models that represent the percentile 5%, percentile 25% and median of the homogenized material curves, the structure shows a steep increase of the displacements after a PGA of 0.4g, 0.5g, and 0.6g, respectively. After these PGA levels, it is clear the development of a degrading plateau. On the other hand, the two models that have higher strength values (percentile 75% and percentile 95%) do not present any significant difference in the displacements found for these PGAs. The onset of the degrading effects is only visible after an IM of 0.7g. The conditional dispersion of the results in terms of *IM* and *EDP*, i.e. $\sigma_{\mathrm{EDP|IM}}$, is higher for the model P5%. Such finding is somehow expected since the model P5% is the one associated with low strength values and hence the one which is more sensitive to the variability of the ground motion characteristics. At last, focusing on the model P50%, as it is the one comparable with the numerical model studied in section §5.3, it is noticeable that the inelastic phase is especially visible after a PGA of 0.7g. This is consistent with the results found experimentally and numerically, as no visible damage was obtained until a PGA of 0.56g (acc 6, see section §5.3).

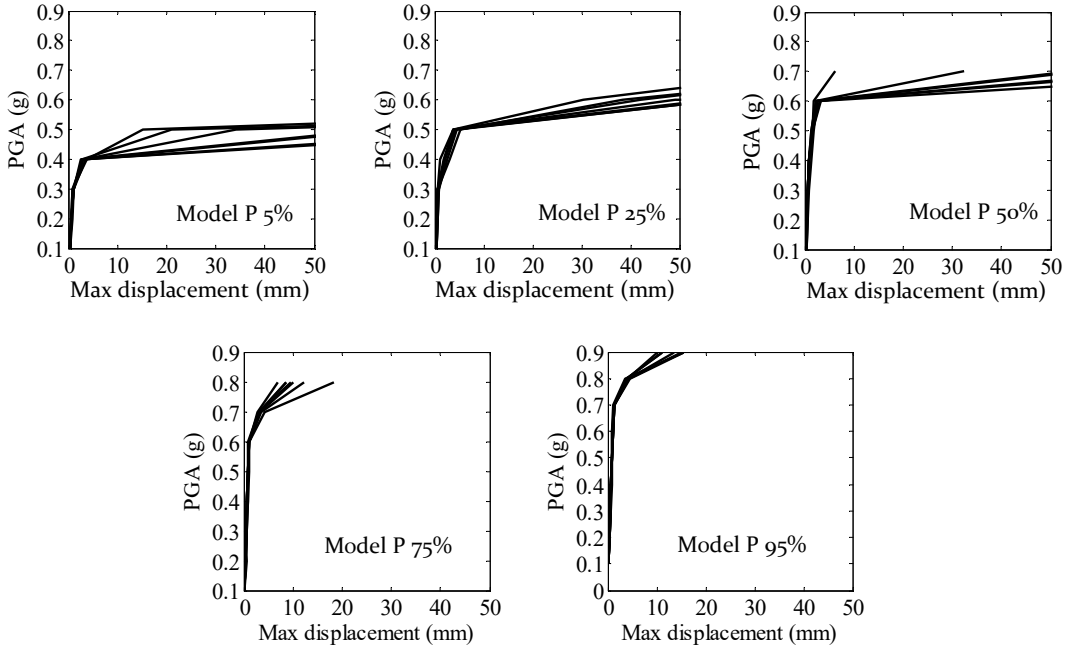

Figure 6.10 – Incremental dynamic analyses (IDA) curves obtained for each of the defined five macro−models.

6.5 Damage analysis (macro-scale level)

The damage analysis is a key step of PBEE methodologies, in which it is intended to develop seismic fragility curves (Günay and Mosalam 2013). Fragility curves give the conditional distribution of the probability of exceeding a specific performance state limit (or demand parameter) as a function of an *IM* of hazard. It constitutes a noteworthy base of information for the stakeholders involved in the decision-making process of a structural intervention and/or design.

Several frameworks exist to develop fragility curves, which goes from the expert-judgment, empirical, analytical or hybrid methods. Here, an analytical approach has been followed based on the data that results from the IDA performed. However, it is still necessary to describe the demand parameters in terms of performance levels of the structure, usually associated with the observed damage and hence designated as damage limit states (*LS*).

6.5.1 Performance levels of the structure

Performance levels can be expressed by targeting discrete thresholds for the *EDP* on the structure's response. Such levels or limit states (*LS*) separate different damage regions, which can be further on associated with different retrofitting and/or repair actions (and costs) to bring it to the original (undamaged) state. The connection between realistic damage states and quantitative *EDPs* represents the main struggle of the process and, when accomplished, fragility

curves on the probability of reaching/exceeding a damage level according to a seismic IM can be drawn.

Although the selection of the *EDP* that better correlates with the structural damage level is questionable, the adoption of a displacement-based parameter (usually drift values) tends to be generally used by guidelines (SEAOC 1995; ATC 40 1996; FEMA 273 1997; FEMA 306 1998; HAZUS 1999; FEMA 356 2000; Eurocode 8 2004; ASCE/SEI 41-17 2017; NZSEE 2017) and in literature-related works (Calvi et al. 2006; Rota et al. 2010; Kappos 2016). Again, this supports the decision over a displacement quantity to serve as *EDP*. A comprehensive overview of the seismic performance code provisions in terms of drift-ratio values is addressed by Petry and Beyer (2014). For instance, one may highlight FEMA 356 (2000), which instructs the use of maximum drift ratios of 0.3%, 0.6% and 1.0% to bound, respectively, the performance damage states in terms of Immediate Occupancy, Life Safety, and Collapse Prevention. Also, the Eurocode 8 (2004) proposes three LS, i.e. the Damage Limitation associated with the drift-ratio for the first-yielding displacement of the global capacity curve of the structure; the maximum limit for the Significant Damage region has associated a drift-ratio of 0.4% if a shear failure occurs or 0.8% H_0/L if a flexure failure occurs (H_0 is the effective height and L the length of the wall); and Near Collapse whose limit drift-ratio is computed to be 4/3 higher than the previous *LS*.

Guidelines data are especially suitable for in-plane failure modes and a better insight into the safety margin due to out-of-plane collapses is still needed. This concern has been recently addressed in the standard ASCE/SEI 41-17 (2017), in which the masonry provisions suffered some updates concerning the out-of-plane actions for URM structures. Moreover, existing URM buildings, in which a box-type of behavior is not present, are typically conditioned by the fragility of a component rather than the global system one. In this scope, such traditional URM structures feature a fragility whose associated seismic response is hardly consistent with the provisions met by standards Eurocode 8 (2004) and ASCE/SEI 41-17 (2017). For the present case study, three damage regions have been defined following the states preconized by Eurocode 8 (2004): damage limitation (DL), significant (or severe) damage (SD) and near collapse (NC). The performance limit states are attained by the results from the nonlinear static pushover analyses conducted for the DNS model 200 with the median material parameters (model P50%), as depicted in Figure 6.11 and expressed in Table 6.3. Note that:

- The DL region implies that the building is safe to be occupied after the earthquake. The limit state is described as δ_{DL} and is given by the yielding point of the capacity curve;

- The SD region implies that the building shows clear damage, but still retains a seismic safety margin. The limit state is described as δ_{SD} and it is equal to $0.75\delta_{NC}$ as denoted in Eurocode 8 (2004) (δ_{NC} is the NC limit state);
- The NC region implies that the building is severally damaged and, even though it still shows support under gravity loads, it has no seismic safety margin. The limit state is described as δ_{NC} and is given as the post-peak displacement for which the structure loses 20% of the peak strength capacity (according to Rota et al. (2010)).

So, instead of using full code-based *LS*, which are formulated to give a reasonable generic solution, the bespoke *LS* states thresholds exhibit higher representativeness. Uncertainty is, however, being introduced in the system, since the most appropriate strategy would demand the computation of nonlinear static pushover analyses for all the five macro-systems (models P5%, P25%., P50%, P75% and P95%). To cope with the lack of practicability of conducting the latter identification, a CoV value of 15% (within a normal probabilistic distribution) has been assumed for each of the *LS*s parameters. The variability of the *LS* thresholds may also dilute the epistemic uncertainties, regarding the scaling process of the ground motions and intrinsic inaccuracy of the homogenized two-scale model of reproducing the real displacements.

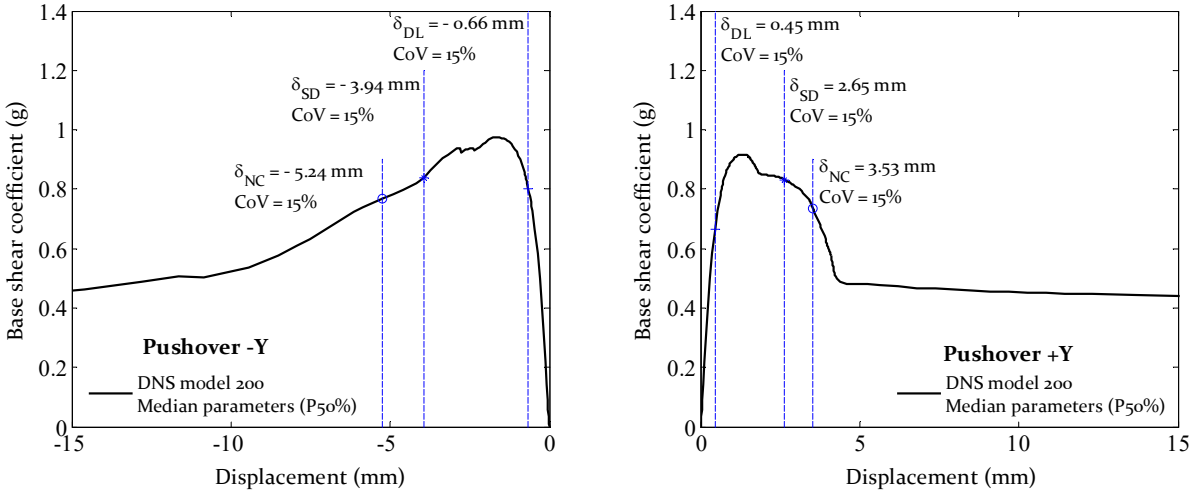

(a) (b)

Figure 6.11 – Nonlinear pushover curves and the definition of the performance limit states (LS): direction -Y; and (b) direction +Y.

Different performance limits have been accounted for each longitudinal direction of the structure as seen in Table 6.3, as its behavior differs due to the lack of symmetry. In this regard, the weakest link theory is considered, meaning that the overall damage state of the structure is given by the limit value exceeded first according to the displacement δ_{EDP} sign.

Table 6.3 – Structural performance levels adopted (longitudinal direction only).

Limit State (LS)	Negative direction (-Y)		Positive direction (+Y)	
	δ_{EDP} (mm)	CoV (%)	δ_{EDP} (mm)	CoV (%)
DL	-0.66	15%	0.45	15%
SD	-3.94	15%	2.65	15%
NC	-5.24	15%	3.53	15%

6.5.2 Displacement-based seismic fragility curves

The last step of the followed framework is the generation of seismic fragility curves which allows assessing the seismic vulnerability of the masonry structure. According to the defined performance limit states, and with the structural response information for a series of ground motions, it is possible to define fragility expressions. These relate the probability of exceeding (POE) a given damage threshold as a function of the *IM* of the strong ground motion. Mathematically, one can refer as follows:

$$Frag(IM;\delta_{EDP}) = P[EDP \geq \delta_{EDP}|IM] \tag{6.1}$$

where $Frag(IM;\delta_{EDP})$ is the fragility at a given ***IM*** and for a limit state which as an associated *EDP* limit δ_{EDP}. Several analytical functions can be used to estimate the fragility curves, being herein assumed that these follow a cumulative lognormal distribution, as commonly seen in field-related literature (Krawinkler and Miranda 2004; Porter et al. 2007; Baker 2014). A lognormal fragility curve determined for a generic *LS*, with an associated *EDP* limit given as δ_{EDP} reads as:

$$P[C|IM = x] = \Phi\left(\frac{\ln\left(x/\theta\right)}{\beta}\right) \tag{6.2}$$

where $P[C|IM = x]$ is the probability of the structure to reach or exceeds the *LS* when subjected to a given ground motion with an $IM = x$; $\Phi(.)$ is the standard normal cumulative distribution function; θ is the median and β is the standard deviation of $ln(IM)$. The estimation of the lognormal parameters of each LS curve can be achieved using different methodologies: by the method of moments; by the minimization of the weighted sum of the squared error; and by the maximum likelihood method. While the former may be disregarded for the problem at hand, since few *IMs* levels have been studied, the last two are eligible. Even though, the maximum likelihood method has been assumed, as it seems to give accurate estimations of $\hat{\theta}$ and $\hat{\beta}$ ($\hat{}$ denote an estimated parameter) (Baker 2014).

The maximum likelihood estimation method

The method computes the estimated moments $\hat{\theta}$ and $\hat{\beta}$ through a maximization problem on the likelihood of the predicted data in fitting with the expected one (numerical discrete points). Prior to the optimization step itself, the computation of the number of events n_c (out of the total N_{event}) whose *EDP* value exceeded the limit value δ_{LS} is needed, for each defined *LS* and accounting with all the *IM* levels. Hence, following a binomial distribution, the probabilities of collapse can be easily computed:

$$P(n_c \text{ out of } N_{events}|IM = x) = \binom{N_{events}}{n_c} p^{n_c}(1-p_i)^{N_{events}-n_c} \tag{6.3}$$

in which p is the probability of reaching/exceeding the LS at $IM = x$. After repeating this process for all the *IM* values, the likelihood of the entire set of analysis is given as the product of the individual likelihoods. In this regard, the optimization function is written over the total likelihood (the sum of the individual likelihoods) and, owing to a mathematical convenience, in the logarithmic form and so reads (Baker 2014):

$$\left\{\hat{\theta}, \hat{\beta}\right\} = \arg\max_{\theta,\beta} \sum_{j=1}^{m} \left[n_c \ln\left(\Phi\left(\frac{\ln\left(x/\theta\right)}{\beta}\right)\right) + (N_{events} - n_c)\ln\left(1 - \Phi\left(\frac{\ln\left(x/\theta\right)}{\beta}\right)\right)\right] \tag{6.4}$$

This process has been performed in MATLAB (through the use of function *fminsearch*) for each *LS* and the estimated lognormal distribution parameters $\hat{\theta}$ and $\hat{\beta}$ are depicted in Table 6.4. In general, one may note that the median values $\hat{\theta}$ of the fragility curves are between 0.15g-0.29g, 0.37g-0.73g and 0.44g-0.84g for the DL, SD and NC states, respectively. The relative difference between the P95% and P5% results of the median $\hat{\theta}$ is, for all the damage states, approximated and is in the range of 200%. This is a relevant value and may be explained by the considerable variability of the macro-input, which propagates from the material and mechanical uncertainties of the system. Also, in Table 6.4 it is shown that the standard deviation values are particularly high for the DL state. In fact, steeper curves are found for the SD and NC states, as seen in Figure 6.12, which is in agreement with the low energy dissipation capacity that URM structures possess when damage is active.

The analysis led concluding with a 100% probability, and within a 95% confidence level, that: (i) the yielding of the structure will occur for a PGA equal or higher than 0.4g; the structure will suffer significant damage for a PGA equal or higher than 0.8g; and that the structure will collapse for a PGA equal or higher than 0.9g. Such results are in agreement with the experimental campaign, as residual damage has been witnessed for a PGA of 0.56g (acc 5);

moderate damage has been witnessed for a PGA of 0.84g (acc 7), and the collapse of the structure has been witnessed for a PGA of 1.27g (acc 8).

Table 6.4 – Fitted Lognormal distribution parameters of the fragility curves representing the response of the five macro-models studied foe each defined limit state.

Limit States (LS)	Model P5%		Model P25%		Model P50%		Model P75%		Model P95%	
	$\hat{\theta}$	$\hat{\beta}$	$\hat{\theta}$	$\hat{\beta}$	$\hat{\theta}$	$\hat{\beta}$	$\hat{\theta}$	$\hat{\beta}$	$\hat{\theta}$	$\hat{\beta}$
DL	0.15	0.06	0.17	0.28	0.18	0.25	0.25	0.22	0.29	0.16
SD	0.37	0.13	0.43	0.06	0.59	0.06	0.63	0.04	0.73	0.04
NC	0.44	0.02	0.52	0.05	0.64	0.05	0.72	0.03	0.84	0.04

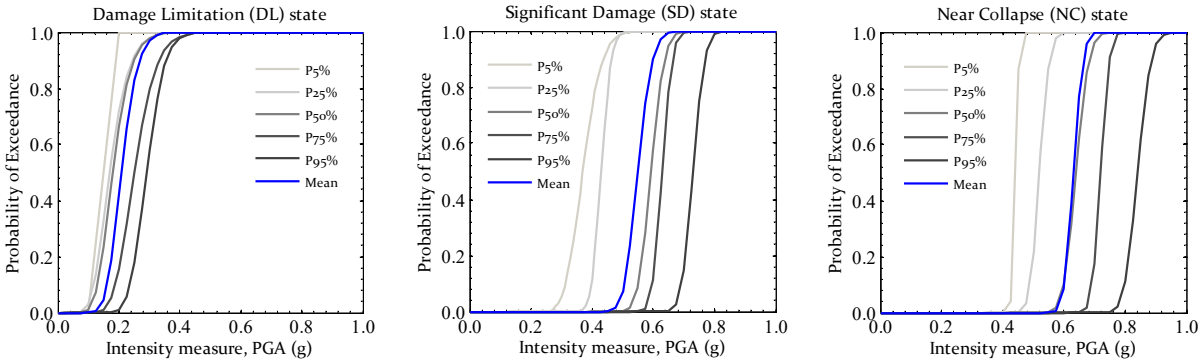

Figure 6.12 – Fragility curves obtained for each of the macro-models defined at for each damage state: (a) damage limitation (DL) state; (b) significant damage (SD) state; and (c) near collapse (NC) state.

At last, and aiming a clear comparison between the fragility curves of each damage state, the mean fitted lognormal distributions are calculated and the associated statistical parameters given in Table 6.5. The median values found for the SD and NC states are less spaced when compared with the DL case. So, one may refer that the structure has low capacity to withstand damage, as it is foreseen that the structure can go from a situation of relevant damage to collapse situation with a PGA value increase of only 0.1g. An insight over the position of the performance targets δ_{SD} and δ_{NC} (Table 6.3) leads to conclude that these are close to each other and a low ductility index exist, which allow understanding the fragile character of the masonry structure, also keeping in mind the steep shape of the fragility curves of Figure 6.13. Yet, the damage assessment results may be conservative because those LS are found through a static analysis.

In this regard and for the present study case, the contriving of a strengthening scheme which can postpone the out-of-plane failure of the tympanum wall seems fundamental to reduce the human and economic losses in the aftermath of a seismic event. Nevertheless, such a decision should be made simultaneously with information from a hazard probability curve (which will

potentially be the output of a future work), as PGA values higher than 0.6g could have associated high seismic recurrence times (for the region of Lisbon) and thus hinder any action due to its unprofitable character from the investor perspective.

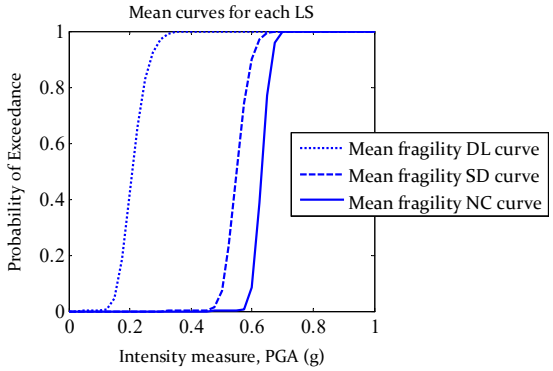

Figure 6.13 – Mean of the fitted fragility curves for the three limit states defined.

Table 6.5 – Mean fragility curves parameters for each defined limit state.

Limit states (LS)	$\hat{\theta}$	$\hat{\beta}$
DL	0.21	0.19
SD	0.55	0.07
NC	0.63	0.04

6.6 Summary

A stochastic framework aiming at the seismic performance evaluation of masonry structures has been proposed in this chapter. It has background on the existing PBEE approaches (Krawinkler and Miranda 2004) and, therefore, intends to give a broader insight into the masonry structural response. Although only the structural and damage analyses are conducted (hazard analysis and loss estimation and have been disregarded) it aims to influence the decision process over the need and/or comparison between retrofitting and/or design strategies. To attest its adequacy, the framework has been applied in the seismic performance investigation of a masonry structure. The case study is the English-bond brick house mock-up tested in *LNEC* by Candeias et al. (2016), which has been studied in §Chapter 5. The preceding observations of its dynamic response (only in the longitudinal direction) showed that the governing failure mode is given by the out-of-plane collapse of the tympanum of the gable wall. Hence, the seismic vulnerability is assessed accounting with such collapse mode.

The framework relies on the two-step numerical procedure presented in §Chapters 3 and 4 and, therefore, appends two levels of analysis: (i) at a meso-scale, in which the material, mechanical and geometrical variables are parametrized to carry the masonry uncertainty and compute the random homogenized quantities; and (ii) at a macro-scale, where the meso-scale uncertainty is propagated through the selection of representative $\Sigma - \mathrm{E}$ and $M - \chi$ curves to be used within the RBSM model. Here, the loading uncertainty is also ensured by using several ground motions compliant with the Eurocode 8 (2004) elastic spectrum. The seismic vulnerability has been evaluated through the generation of fragility curves. Three damage

regions have been set following the Eurocode 8 (2004) recommendations, i.e. damage limitation, significant damage and near collapse states; and the performance targets, namely limit states (*LS*), defined accordingly but using the information from the quasi-static pushover curves obtained with the median values of the system variables. Analytical fragility functions have been derived from an incremental dynamic analysis (*IDA*), in which a successive set of ground motions (a total of seven) scaled for different intensity measures, here defined to be Peak Ground Acceleration, were applied to the structure. The structure response has been evaluated according to an engineering demand parameter (*EDP*) given by the out-of-plane displacement component of the top gable wall node. A total of 2000 homogenized curves have been collected at a meso-scale, whose sample served to perform 266 dynamic analyses at a macro-scale. Such extensive numerical data allowed the computation of three displacement-based lognormal fragility functions for the three damage states in which a 95% confidence level was acquired. A maximum-likelihood method has been used to estimate the fitted lognormal distribution parameters.

The main remarks are: (i) the fragility curves that define the 95% confidence level envelope show, for all the damage states considered, a well distinct response. This highlights the relative effect that the system uncertainties have in the response; (ii) the observation supports the experimental campaign, as there are 100% of probability that the structure will suffer significant damage for a *PGA* higher than 0.8g; and that the structure will collapse for a *PGA* equal or higher than 0.9g; (iii) the structure shows low capacity to dissipate energy, as low standard deviation values have been identified for the significant and near collapse damage states. Lastly, it matters also addressing that even though the case study is not representative of any building typology, it has been suitable to prove that the framework is appropriate and applicable. This is especially important when connected with the level of detail and computational attractiveness that the procedure offers when compared with the existing advanced numerical strategies for the nonlinear dynamic study of masonry. Additionally, since the approach is based on an analytical methodology, there is further space for both improvement and investigation, namely: (i) the study the ideal number of simulations required at a meso-scale; (ii) the study the effect of performance limit states definition; (iii) the study on the relative effect of the loading uncertainty when compared with the material one; (iv) the adoption of other *IM* apart from the structure-independent *PGA* measure; (v) the use of a methodology within a broader application, perhaps in larger and complex structures, which is particular interesting if one notices that the results can be generalized if applied to a building typology; and (vi) the incorporation of hazard and loss analyses to the framework.

Chapter 7

7 General summary and conclusions

Experimentation is of utmost importance in all subjects of knowledge and surely necessary in the structural and dynamic analysis of masonry structures. This is fundamental to support the validation of theoretical hypotheses through observation but, additionally, to make data available that serve as ground validation for the development of computational methods. The inherent phenomenological complexity of masonry makes hard the prediction of the mechanical response of unreinforced masonry (URM) structures. The analysis of masonry using experimental campaigns only is thorough and difficult to carry out, bearing also in mind the involved costs and required time, which brings the need of developing proper numerical models to predict with accuracy the response of masonry structures.

Computational methods have become daily instruments in both structural and dynamic engineering fields for both the professional and scientific communities. This is not the end of the story since open issues need to be solved and there is always space for further improvements. By recognizing the importance of such methods in offering solutions (even if approximated ones), together with the societal importance of the masonry-built heritage and its associated seismic fragility, the present research addressed the following two key points:

(i) Proposal of a simplified two-step numerical framework, based on homogenization principles, aiming the study of the quasi-static and dynamic mechanical behavior and failure of masonry. The strategy allows obtaining adequate solutions with relatively low time-costs when compared to the existing advanced FE-based computational methods.
(ii) Application of the proposed numerical strategy for the seismic fragility assessment of a URM structure.

In such scope, the study tried to address an investigation on two different masonry research fields, one concerning the study of the structural behavior of URM structures and, the other, concerning the methods to assess the seismic performance of URM structures. A general summary is presented next following the logical order of the contents presented throughout the study. Lastly, some suggestions for future works are stated.

The scope of the proposed multi-scale approach

A set of different analytical and numerical strategies exist in the literature. The most simplified ones, typically designated as a force- and displacement-based approaches, are useful because

demand low computational effort, but its accuracy can be compromised being so especially conceived for ad-hoc structural problems.

In contrast, the so-called advanced strategies are progressively being developed following the increase of computational power and are thus suitable to accurately study the mechanical behavior of masonry. Finite element techniques grasped special attention. are designated in the literature according to the level of modeling detail as (i) direct numerical simulation or meso-modeling approach; (ii) macro-modeling approach; and (iii) multi-scale approach.

Although a direct numerical simulation (meso-modeling) provides the most accurate solutions, it lacks practicability since it demands prohibitive computational costs even when used for the study of small structures. On the other hand, macro-modeling approaches assume masonry as a fictitious homogeneous material and are more indicated for the study of large-scale structures. Yet, the damage representation is still physically poorly represented as it is based on FE smeared-crack models. Multi-scale methods based on computational homogenization schemes (usually two-scales or FE^2 are considered for masonry) are in-between the latter FE-modelling approaches. These rely on the homogenization principle, in which the behavior of the masonry material is characterized at a meso-scale and transferred to the macro-scale. Although seem to be very promising, the use of full-continuum FE strategies at both scales is still computationally prohibitive when material nonlinearity is accounted. This results from the fact that a new BVP must be solved numerically for each load step, in each Gauss integration point. To cope with this issue, the adoption of a simplified framework that makes use of a unit-cell model at a meso-scale integrated with a macro-scale model constitutes the main core of this thesis.

Meso-scale level

The accuracy of multi-scale approaches strongly depends on the mesoscopic constitutive models adopted. Two FE unit-cell mesoscopic models, based on a first-order periodic homogenization technique and within a strain-driven formulation, have been formulated to characterize the masonry behavior subjected to in-plane and out-of-plane loading. These were designated as KP and MP models following the assumed underlying plate theories, i.e. Kirchhoff-Love and Mindlin-Reissner theories, respectively. Both running-bond and English-bond are suitable to be studied and the models were fully implemented in advanced commercial software. The representative volume element (RVE) aimed at representing masonry by repetition was modeled with brick units composed by quadrilateral elements with linear interpolation and mortar joints with zero-thickness line interface elements. By solving a boundary value problem upon the

defined RVE, both the in-plane stresses and out-of-plane stress-couples are derived. Note that bricks are assumed to be elastic and the interface elements carry the inelastic material information within a multi-surface plasticity model (an assumption plausible for strong blocks). The meso-scale validation proved to work well and three main constitutive key features were addressed: (i) the correct representation of the elastic stiffness properties; (ii) the masonry orthotropic behavior due to the arrangement of the units; and (iii) the role of vertical membrane pre-compression states. A stepped, toothed and de-bonding (straight) masonry failure patterns are suitably reproduced.

The models were applied for the mechanical study of the out-of-plane homogenized quantities of an English-bond masonry. The analyses allowed concluding that the simplified KP model allows faster computations with no-convergence issues reported. Yet, due to the inability of reproducing the effect of three-dimensional shear stresses, the KP model proved good accuracy for the cases where the thickness has a value similar or lower than the RVE dimensions (i.e. its height or length); a maximum of 15% deviation was found for the homogenized horizontal and torsional moments. In contrast, the MP model follows an out-of-plane shear deformation theory and was thus able to provide similar results to the ones derived from the DNS model.

Insomuch, the investigation demonstrates that the mid-thickness mortar discontinuity of an English-bond masonry plays an important role in the decrease of the horizontal bending (around 33%) and torsional moment capacities (around 17%), whereas the influence on vertical bending is minimal. Meso-mechanical homogenized-based models as the KP and MP, which exploit the use of plate theory assumptions to replace the three-dimensional mesoscopic continuum into a, mostly, two-dimensional one, are quite convenient. These are of a simple application, accurate and demand low computational effort, however, need to be used with care in cases where a discontinuity exists in the structure's thickness.

Macro-scale level

The macro-scale formulation of the proposed two-step strategy resorts in a Rigid Body Spring Mass (RBSM) model. It is composed by quadrilateral rigid plates interconnected at its interfaces by a set of in- and out-of-plane FE truss-beam systems and was implemented in advanced commercial software. The system can mimic, in a decoupled fashion, the deformation modes established at a meso-scale.

One-dimensional elements only (the truss FE-beams), through a concrete damage plasticity model, can mimic the homogenized material data and govern the macro-deformation and damage of the media. Furthermore, material anisotropy and full softening behavior are

represented. The linking steps between the meso-macro scales involve: the conversion of the homogenized $\Sigma - \mathrm{E}$ and $M - \chi$ curves to stress-strain curves eligible to serve as input for the truss-FE beams; the identification of the Young's modulus of the truss-FE beam elements according to energy principles; and a regularization step which corrects the fracture energies of the stress-strain input curves according to the defined macro-mesh dimensions. The obtained macro-input is representative of the obtained homogenized meso-scale elastic and inelastic properties and guarantees the well-posedness of the solution found, as it is independent of the macroscopic mesh adopted.

The validation and convergence tests confirmed that the RBSM macroscopic model fulfills the requirements for (i) elastic problems; (ii) eigenvalue problems; and (iii) nonlinear problems for monotonic and cyclic loading cases. Likewise, the conducted mesh sensitivity studies allowed to conclude that a refinement level given by $L/15$ (L is the length of the wall side being meshed) seems a reasonable choice for the mesh size to conduct a structural analysis (if a sensitivity test is not performed beforehand). Computational recommendations have been also very briefly addressed, as the use of the arc-length method for nonlinear quasi-static tests and a renumbering algorithm to take full advantage of the computational capacity.

Proposed two-step approach: application

The application of the proposed two-step approach comprised three main regimes: (i) an out-of-plane load applied in a quasi-static fashion; (ii) a seismic dynamic excitation; and (iii) an impact load (fast dynamics). Firstly, the two-scale model was applied for the analyses of solid and windowed running-bond URM panels subjected to two-way bending through the application of a pressure load using airbags. Quasi-static (pushover) analyses have been performed. The comparison between the numerical and experimental data proved that the two-scale strategy represents well the structural capacity, the post-peak behavior and the observed damage patterns.

Secondly, the two-scale model was applied for the seismic dynamic analysis of a brick URM house with an English-bond. The referred benchmark served to foster a blind test prediction program and the obtained results showed that, in agreement with the preceding observations from several research peers, the traditional methods of analysis are unable to reproduce satisfactorily the experimental observations. In converse, the proposed two-scale framework based on a direct numerical simulation (DNS) at a meso-scale allowed obtaining a good resemble in terms of experimental out-of-plane displacements-history and damage map. The results are unequivocal and prove that reproducing the existing mortar vertical discontinuity along the

English-bond masonry thickness is of utmost importance. In fact, the English-bond configuration leads to an anisotropic behavior which cannot be well represented by the simplified Kirchhoff-based model nor by a continuous FE-based macroscopic approach. Such feature seems to have more relative importance than the out-of-plane shear stresses effect.

Thirdly, the two-scale model was applied for the study of a running-bond masonry parapet subjected to an impact load. The procedure exhibits a noteworthy prediction, both in terms of the out-of-plane displacement and damage map. The ability of the proposed framework in handling the strain-rate dependency of the masonry, via a dynamic incremental factor (DIF) approach, is demonstrated and certainly a key point.

Mesh sensitivity studies were performed for all the study cases. These sustain that for practical applications the use of a coarser mesh can be appropriate. This is especially clear if one notices the improved running times achieved. The study over the mesh-bias is determinant in the results output with respect to the accuracy of both out-of-plane displacement and damage representation. Nevertheless, the results showed that bypassing a finer macro-model discretization seems to be more appropriate within the static range than within the dynamic one.

Lastly, it is worth noting that a decoupled characterization between the in-plane and out-of-plane modes is adopted. Whilst such decoupling is certainly an approximation, it proved to be reliable, at least for levels of membrane pre-compression lower than the masonry compressive strength. In cases where pre-compression states are considerable, the results should be analyzed with more care, due to its potential non-conservative character (strength is overestimated). In general, although a limited repertoire of case studies has been considered, it has been seen that the numerical framework can reproduce with a reasonable agreement the out-of-plane behavior of masonry structures. Insomuch, by being integrated into advanced computer software, it proved to be robust and computationally very attractive. The possibility of executing the calculations using a parallel computing system is paramount. This circumstance together with the simple numerical nature of the procedure appears to speed-up the computations and reach quite attractive running-times. As initially aimed, it can be affirmed that the presented framework demands a significantly lower computational cost than a macroscopic one, i.e. around 10 times less.

Probabilistic seismic fragility analysis

The solution bias of computational methods stems from the inaccuracy (or inability) of the numerical description of the masonry physical behavior and ascertains, as well, on the aleatoric

randomness of the materials, geometrical, and loading parameters. To account with such variability, a stochastic framework aiming the seismic performance evaluation of masonry structures was proposed. The two-step approach was extended to include the possibility of a probabilistic description of the input variables. At a meso-scale, the material, mechanical and geometrical variables are parametrized to carry the masonry uncertainty. The computation of the random homogenized quantities is achieved using a Latin Hypercube Sampling (LHS) method to generate the input of the meso-scale problem. At a macro-scale, the uncertainty is propagated through the selection of a statistical representative $\Sigma - \mathrm{E}$ and $M - \chi$ meso-scale homogenized curves to be used within the RBSM model. The loading uncertainty can be also ensured through the use of a number of real or artificial ground motions (if compliant with the normative requirements).

The probabilistic two-step approach was applied in an English-bond brick house mock-up. Focusing on the structural and damage analyses only, the main aim was the seismic fragility assessment of the URM structure for different performance limit states; as typically preconized in Performance-Based Earthquake Engineering (PBEE) approaches. A total of 2000 homogenized curves have been collected at a meso-scale, from which five representative macro-models were selected. An incremental dynamic analysis (IDA) was performed accounting with a total of seven earthquakes (artificially generated records) that were scaled for several ground motion intensity measures (PGA) and a total of 266 IDA curves were obtained (macro-scale). Such extensive numerical data allowed the computation of three displacement-based lognormal fragility functions for three damage regions in which a 95% confidence level was acquired. The damage regions have been set following the Eurocode 8 (2004) recommendations, i.e. damage limitation, significant damage and near collapse states; and the performance targets, namely limit states (LS), defined using the information from the quasi-static pushover curves obtained with the median values of the system variables. A maximum-likelihood method has been used to estimate the fitted lognormal distribution parameters.

Four main findings are important to recall here: (i) the use of a reduced number of macro-models, which statistically represent a total of 2000 meso-scale simulations, is only possible because the homogenized quantities derived are correlated; (ii) a significant variability has been found for the fragility curves of each damage state, which highlights the relative effect that the system uncertainties have in the response; (iii) the numerical observation support the experimental data, as there is 100% of probability that the structure will suffer significant damage if subjected to an earthquake with a PGA higher than 0.8g; and that the structure collapse for a PGA equal or higher than 0.9g; (iv) the structure showed low capacity to dissipate energy, as a low standard deviation values have been identified for the significant and near

collapse damage states. This defers with the typical fragility associated with masonry structures when subjected to out-of-plane loading. Lastly, it matters also addressing that even though the case study is not representative of any building typology, it has been suitable to prove that the framework is appropriate and applicable. This is especially important when seen together with the level of detail and computational attractiveness that the procedure offers when compared with the existing advanced FE-based numerical strategies for the nonlinear dynamic study of masonry.

Suggestions for future works

The investigation attempted to provide a numerical tool to describe the nonlinear response of URM structures with a focus on the out-of-plane behavior. The seismic fragility assessment was also appraised and a stochastic framework proposed. Although the main objectives have been accomplished, there is still room for further works. Therefore, future developments are listed next:

1. The incorporation, at a meso-scale, of interface elements embedded in the brick units to account with the masonry crushing failure mode (compression) for the case of strong mortar masonries.
2. Extend the meso-scale models to automatically generate other periodic brick masonries, as stack and Flemish textures, or stone masonries, as ashlar and rubble textures. Yet, the priority should resort on the study of irregular masonry textures, as it seems an under-developed topic in the field.
3. The application of the numerical framework in the analysis of other case studies. Examples comprise the infill-walls or larger structures, for instance, a typological or historical URM structure. Perhaps the seismic assessment of a larger structure seems the most convenient one, as it can clearly take advantage of the real potentialities of the procedure. i.e. the computational attractiveness in terms of processing time.
4. The investigation on some aspects of the stochastic model proposed, namely: (i) study the ideal number of simulations required at a meso-scale; (ii) study the effect of performance limit states definition; (iii) study on the relative effect of the loading uncertainty when compared with the material one; and (iv) the adoption of other intensity measures (IM) apart from the structure-independent Peak Ground Acceleration.
5. The integration of the stochastic framework within a loss assessment methodology for URM structures. This may be an important achievement together with the practicability of such frameworks, as these may influence the decision process over the need and/or comparison

between retrofitting and/or design strategies. This is especially clear if the methodology is applied to an URM building typology, whose results can be further generalized.

6. The procedure possesses a ubiquitous feature and, therefore, it may be of interest to implement the RBSM model in another FE software or within an open source-platform, especially that handles a non-scripted language. If so, this may largely foster its use by both professionals and researchers.

References

ABAQUS (2013) Finite Element Analysis (Theory manual). RI: Dassault Systèmes Simulia Corporation, Providence

Aboudi J (1991) Mechanics of composite materials: a unified micromechanical approach

Abrams DP, Angel R, Uzarski J (1996) Out-of-Plane Strength of Unreinforced Masonry Infill Panels. Earthquake Spectra 12:825–844. doi: 10.1193/1.1585912

Adam JM, Brencich A, Hughes TG, Jefferson T (2010) Micromodelling of eccentrically loaded brickwork: Study of masonry wallettes. Engineering Structures 32:1244–1251. doi: https://doi.org/10.1016/j.engstruct.2009.12.050

Addessi D, Liberatore D, Masiani R (2015) Force-Based Beam Finite Element (FE) for the Pushover Analysis of Masonry Buildings. International Journal of Architectural Heritage 9:231–243. doi: 10.1080/15583058.2013.768309

Addessi D, Sacco E, Paolone A (2010) Cosserat model for periodic masonry deduced by nonlinear homogenization. European Journal of Mechanics - A/Solids 29:724–737. doi: 10.1016/j.euromechsol.2010.03.001

Akhaveissy AH, Milani G (2013) A numerical model for the analysis of masonry walls in-plane loaded and strengthened with steel bars. International Journal of Mechanical Sciences 72:13–27. doi: 10.1016/j.ijmecsci.2013.03.003

Ali SS, Page AW (1988) Finite Element Model for Masonry Subjected to Concentrated Loads. Journal of Structural Engineering 114:1761–1784. doi: 10.1061/(ASCE)0733-9445(1988)114:8(1761)

Amestoy PR, Davis TA, Duff IS (2004) Algorithm 837: AMD, an Approximate Minimum Degree Ordering Algorithm. ACM Trans Math Softw 30:381–388. doi: 10.1145/1024074.1024081

Andreotti G, Graziotti F, Magenes G (2018) Detailed micro-modelling of the direct shear tests of brick masonry specimens: The role of dilatancy. Engineering Structures 168:929–949. doi: https://doi.org/10.1016/j.engstruct.2018.05.019

ANSA (2017) The advanced CAE pre-processing software for complete model build up. In: OpenFOAM User Meeting Stammtisch United. Kassel, Germany

Anthoine A (1995) Derivation of the in-plane elastic characteristics of masonry through homogenization theory. International Journal of Solids and Structures 32:137–163. doi: 10.1016/0020-7683(94)00140-R

Araujo A (2012) Seismic Assessment of St James Church by Means of Pushover Analysis – Before and After the New Zealand Earthquake. TOCIEJ: The Open Civil Engineering Journal 6:. doi: http://dx.doi.org/10.2174/1874149501206010160

Arnold DN, Madureira AL, Zhang S (2002) On the Range of Applicability of the Reissner–Mindlin and Kirchhoff–Love Plate Bending Models. Journal of Elasticity 67:171–185. doi:

10.1023/A:1024986427134

ASCE/SEI 41-17 (2017) Seismic Evaluation and Retrofit of Existing Buildings, ASCE/SEI 4. American Society of Civil Engineers

ATC 40 (1996) Seismic evaluation and retrofit of concrete buildings. Redwood City (CA): Applied Technology Council

Bacigalupo A, Gambarotta L (2012) Computational two-scale homogenization of periodic masonry: Characteristic lengths and dispersive waves. Computer Methods in Applied Mechanics and Engineering 213–216:16–28. doi: 10.1016/j.cma.2011.11.020

Baggio C, Trovalusci P (1995) Stone assemblies under in-plane actions. Comparison between nonlinear discrete approaches. Comput Methods Structural Masonry 184–193

Baker JW (2014) Efficient Analytical Fragility Function Fitting Using Dynamic Structural Analysis. Earthquake Spectra 31:579–599. doi: 10.1193/021113EQS025M

Balden VH, Nurick GN (2005) Numerical simulation of the post-failure motion of steel plates subjected to blast loading. International Journal of Impact Engineering 32:14–34. doi: 10.1016/j.ijimpeng.2005.07.013

Barbat AH, Carreño ML, Pujades LG, et al (2010) Seismic vulnerability and risk evaluation methods for urban areas. A review with application to a pilot area. Structure and Infrastructure Engineering 6:17–38. doi: 10.1080/15732470802663763

Barbat AH, Moya FY, Canas J (1996) Damage Scenarios Simulation for Seismic Risk Assessment in Urban Zones. Earthquake Spectra 12:371–394. doi: 10.1193/1.1585889

Barenblatt GI (1959) The formation of equilibrium cracks during brittle fracture. General ideas and hypotheses. Axially-symmetric cracks. Journal of Applied Mathematics and Mechanics 23:622–636. doi: https://doi.org/10.1016/0021-8928(59)90157-1

Basset-Salom L, Guardiola-Víllora A (2014) Seismic performance of masonry residential buildings in Lorca's city centre, after the 11th May 2011 earthquake. Bulletin of Earthquake Engineering 12:2027–2048. doi: 10.1007/s10518-013-9559-8

Bathe K-J, Wilson EL (1973) Solution methods for eigenvalue problems in structural mechanics. International Journal for Numerical Methods in Engineering 6:213–226. doi: 10.1002/nme.1620060207

Bathe KJ, Wilson EL (1974) NONSAP — A nonlinear structural analysis program. Nuclear Engineering and Design 29:266–293. doi: https://doi.org/10.1016/0029-5493(74)90128-9

Bažant ZP, Oh BH (1983) Crack band theory for fracture of concrete. Matériaux et Constructions 16:155–177. doi: 10.1007/BF02486267

Beak M, Colwell SA, Crowhurst D, Eliis BR (1994) The behaviour of masonry and concrete panels under explosion and static loading. Institution of chemical Engineers Symposium series 134:227–247

Belytschko T, Lin JI, Chen-Shyh T (1984) Explicit algorithms for the nonlinear dynamics of shells. Computer Methods in Applied Mechanics and Engineering 42:225–251. doi: https://doi.org/10.1016/0045-7825(84)90026-4

Belytschko T, Moës N, Usui S, Parimi C (2001) Arbitrary discontinuities in finite elements. International Journal for Numerical Methods in Engineering 50:993–1013. doi: 10.1002/1097-0207(20010210)50:4<993::AID-NME164>3.0.CO;2-M

Benedetti A, Pelà L, Aprile A (2008) Masonry properties determination via splitting tests on cores with a rotated mortar layer. Instanbul Technical University

Benedetti D, Petrini V (1984) Sulla Vulnerabilità Di Edifici in Muratura: Proposta Di Un Metodo Di Valutazione. L'Industria delle Costruzioni 149:66–74

Bernardini A, Gori R, Modena C (1990) An application of coupled analytical models and experiential knowledge for seismic vulnerability analyses of masonry buildings. Engineering aspects of earthquake phenomena

Berry JP (1961) Fracture processes in polymeric materials. I. The surface energy of poly(methyl methacrylate). Journal of Polymer Science 50:107–115. doi: 10.1002/pol.1961.1205015313

Berto L, Saetta A, Scotta R, Vitaliani R (2002) An orthotropic damage model for masonry structures. International Journal for Numerical Methods in Engineering 55:127–157. doi: 10.1002/nme.495

Bertolesi E, Milani G, Lourenço PB (2016) Implementation and validation of a total displacement non-linear homogenization approach for in-plane loaded masonry. Computers & Structures 176:13–33. doi: https://doi.org/10.1016/j.compstruc.2016.08.001

Betti M, Vignoli A (2011) Numerical assessment of the static and seismic behaviour of the basilica of Santa Maria all'Impruneta (Italy). Construction and Building Materials 25:4308–4324. doi: 10.1016/j.conbuildmat.2010.12.028

Binda L, Saisi A, Tiraboschi C (2000) Investigation procedures for the diagnosis of historic masonries. Construction and Building Materials 14:199–233. doi: 10.1016/S0950-0618(00)00018-0

Bischoff PH, Perry SH (1991) Compressive behaviour of concrete at high strain rates. Materials and Structures 24:425–450. doi: 10.1007/BF02472016

Blanco PJ, Sánchez PJ, de Souza Neto EA, Feijóo RA (2016) Variational Foundations and Generalized Unified Theory of RVE-Based Multiscale Models. Archives of Computational Methods in Engineering 23:191–253. doi: 10.1007/s11831-014-9137-5

Block P, DeJong M, Ochsendorf J (2006) As Hangs the Flexible Line: Equilibrium of Masonry Arches. Nexus Network Journal 8:13–24. doi: 10.1007/s00004-006-0015-9

Bommer JJ, Crowley H (2006) The Influence of Ground-Motion Variability in Earthquake Loss Modelling. Bulletin of Earthquake Engineering 4:231–248. doi: 10.1007/s10518-006-9008-z

Box GEP, Norman RD (1987) Empirical Model-Building and Response Surfaces. Wiley

Braga F, Dolce M, Liberatore D (1982) A statistical study on damaged buildings and an ensuing review of the M.S.K.-76 scale. In: Proceedings of the 7th Earthquake Engineering. Athens

Brencich A, Lagomarsino S (1998) A macroelement dynamic model for masonry shear walls. Computer methods in structural masonry 4:67–75

Bruneau M (1994) Seismic evaluation of unreinforced masonry buildings - a state-of-the-art report. Canadian Journal of Civil Engineering 21:512–539

Bucher CG, Bourgund U (1990) A fast and efficient response surface approach for structural reliability problems. Structural Safety 7:57–66. doi: https://doi.org/10.1016/0167-4730(90)90012-E

Burnett S, Gilbert M, Molyneaux T, et al (2007a) The performance of unreinforced masonry walls subjected to low-velocity impacts: Finite element analysis. International Journal of Impact Engineering 34:1433–1450. doi: 10.1016/j.ijimpeng.2006.08.004

Burnett S, Gilbert M, Molyneaux T, et al (2007b) The response of masonry joints to dynamic tensile loading. Materials and Structures 40:517–527. doi: 10.1617/s11527-006-9160-6

Calvi GM (1999) A displacement-based approach for vulnerability evaluation of classes of buildings. Journal of Earthquake Engineering 3:411–438. doi: 10.1080/13632469909350353

Calvi GM, Pinho R, Magenes G, et al (2006) Development of seismic vulnerability assessment methodologies over the past 30 years. ISET Journal of Eathquake Technology 43:75–104

Candeias PX, Costa AC, Mendes N, et al (2016) Experimental Assessment of the Out-of-Plane Performance of Masonry Buildings Through Shaking Table Tests. International Journal of Architectural Heritage 1–28. doi: 10.1080/15583058.2016.1238975

Cardoso R, Lopes M, Bento R (2005) Seismic evaluation of old masonry buildings. Part I: Method description and application to a case-study. Engineering Structures 27:2024–2035. doi: 10.1016/j.engstruct.2005.06.012

Casapulla C (2008) Lower and upper bounds in closed form for out-of-plane strength of masonry structures with frictional resistances. In: Proceedings of 6th International Conference SAHC08. Bathe (UK), pp 1191–1198

Casapulla C, Cascini L, Portioli F, Landolfo R (2014) 3D macro and micro-block models for limit analysis of out-of-plane loaded masonry walls with non-associative Coulomb friction. Meccanica 49:1653–1678. doi: 10.1007/s11012-014-9943-8

Cascini L, Gagliardo R, Portioli F (2018) LiABlock_3D: A Software Tool for Collapse Mechanism Analysis of Historic Masonry Structures. International Journal of Architectural Heritage 1–20. doi: 10.1080/15583058.2018.1509155

Casolo S (1999) Rigid element model for non-linear analysis of masonry façades subjected to out-of-plane loading. Communications in Numerical Methods in Engineering 15:457–468

Casolo S (2006) Macroscopic modelling of structured materials: Relationship between orthotropic Cosserat continuum and rigid elements. International Journal of Solids and Structures 43:475–

496. doi: 10.1016/j.ijsolstr.2005.03.037

Casolo S, Milani G (2013) Simplified out-of-plane modelling of three-leaf masonry walls accounting for the material texture. Construction and Building Materials 40:330–351. doi: 10.1016/j.conbuildmat.2012.09.090

Casolo S, Milani G (2010) A simplified homogenization-discrete element model for the non-linear static analysis of masonry walls out-of-plane loaded. Engineering Structures 32:2352–2366. doi: 10.1016/j.engstruct.2010.04.010

Cecchi A, Milani G (2008) A kinematic FE limit analysis model for thick English bond masonry walls. International Journal of Solids and Structures 45:1302–1331. doi: 10.1016/j.ijsolstr.2007.09.019

Cecchi A, Milani G, Tralli A (2007) A Reissner–Mindlin limit analysis model for out-of-plane loaded running bond masonry walls. International Journal of Solids and Structures 44:1438–1460. doi: 10.1016/j.ijsolstr.2006.06.033

Cecchi A, Sab K (2002a) A multi-parameter homogenization study for modeling elastic masonry. European Journal of Mechanics - A/Solids 21:249–268. doi: https://doi.org/10.1016/S0997-7538(01)01195-0

Cecchi A, Sab K (2002b) Out of plane model for heterogeneous periodic materials: the case of masonry. European Journal of Mechanics - A/Solids 21:715–746. doi: 10.1016/S0997-7538(02)01243-3

Chong V, Southcombe C, May I (1994) The behavior of laterally loaded masonry panels with openings. In: Proceedings of 3rd international masonry conference. London, UK: Proceedings of the British Masonry Society. pp 178–82

Chopra AK (2017) Dynamics of structures: theory and applications to earthquake engineering. Pearson Prentice Hall

Clemente R, Roca P, Cervera M (2006) Damage model with crack localization–application to historical buildings. Structural Analysis of Historical Constructions, New …

Cóias e Silva V (2001) Viabilidade técnica de execução do “Programa de Redução da Vulnerabilidade Sísmica do Edificado". In: In SPES & GECoRPA. Redução da Vulnerabilidade Sísmica do Edificado

Collins RJ (1973) Bandwidth reduction by automatic renumbering. International Journal for Numerical Methods in Engineering 6:345–356. doi: 10.1002/nme.1620060306

Costa A (2002) Determination of mechanical properties of traditional masonry walls in dwellings of Faial Island, Azores. Earthquake Engineering & Structural Dynamics 31:1361–1382. doi: 10.1002/eqe.167

Costa AA, Arêde A, Penna A, Costa A (2013) Free rocking response of a regular stone masonry wall with equivalent block approach: experimental and analytical evaluation. Earthquake Engineering & Structural Dynamics 42:2297–2319. doi: 10.1002/eqe.2327

Creazza G, Matteazzi R, Saetta A, Vitaliani R (2002) Analyses of Masonry Vaults: A Macro Approach based on Three-Dimensional Damage Model. Journal of Structural Engineering 128:646–654. doi: 10.1061/(ASCE)0733-9445(2002)128:5(646)

Crisfield MA (1981) A fast incremental/iterative solution procedure that handles "snap-through." Computers & Structures 13:55–62. doi: https://doi.org/10.1016/0045-7949(81)90108-5

Croci G (1998) The conservation and structural restoration of architectural heritage. Computational Mechanics Publications, Southampton

Cundall P, Hart P (1971) A computer model for simulating progressive large scale movements in blocky rock systems. In: Proc. Symp. Rock Fracture (ISRM). Nancy, France, p II-8

CUR (1994) Structural masonry: a experimental/numerical basis for practical design rules (in Dutch). Report 171:

Cuthill E, McKee J (1969) Reducing the Bandwidth of Sparse Symmetric Matrices. In: Proceedings of the 1969 24th National Conference. ACM, New York, NY, USA, pp 157–172

D'Ayala D, Shi Y (2011) Modeling Masonry Historic Buildings by Multi-Body Dynamics. International Journal of Architectural Heritage 5:483–512. doi: 10.1080/15583058.2011.557138

D'Ayala D, Speranza E (2003) Definition of Collapse Mechanisms and Seismic Vulnerability of Historic Masonry Buildings. Earthquake Spectra 19:479–509. doi: 10.1193/1.1599896

D'Ayala D, Speranza E (2002) An integrated procedure for the assessment of seismic vulnerability of historic buildings. 12th European Conference on Earthquake Engineering

D'Ayala DF, Paganoni S (2010) Assessment and analysis of damage in L'Aquila historic city centre after 6th April 2009. Bulletin of Earthquake Engineering 9:81–104. doi: 10.1007/s10518-010-9224-4

Davidson JS, Porter JR, Dinan RJ, et al (2004) Explosive Testing of Polymer Retrofit Masonry Walls. Journal of Performance of Constructed Facilities 18:100–106. doi: 10.1061/(ASCE)0887-3828(2004)18:2(100)

de Borst R (2002) Fracture in quasi-brittle materials: a review of continuum damage-based approaches. Engineering Fracture Mechanics 69:95–112. doi: 10.1016/S0013-7944(01)00082-0

De Borst R (1987) Computation of post-bifurcation and post-failure behavior of strain-softening solids. Computers & Structures 25:211–224. doi: 10.1016/0045-7949(87)90144-1

de Buhan P, de Felice G (1997) A homogenisation approach to the ultimate strength of brick masonry. Journal of the Mechanics and Physics of Solids 45:1085–1104. doi: 10.1016/S0022-5096(97)00002-1

de Felice G (1995) Metodi di omogeneizzazione per sistemi regolari di corpi rigidi. In: Proceedings of the XII AIMETA Congress. Naples, Italy. Naples, Italy, pp 453–479

de Felice G (2011) Out-of-Plane Seismic Capacity of Masonry Depending on Wall Section Morphology. International Journal of Architectural Heritage 5:466–482. doi:

10.1080/15583058.2010.530339

Degg M (1992) Natural Disasters: Recent Trends and Future Prospects. Geography 77:198–209

DelRio FW, de Boer MP, Knapp JA, et al (2005) The role of van der Waals forces in adhesion of micromachined surfaces. Nature Materials 4:629

Dennis ST, Baylot JT, Woodson SC (2002) Response of 1/4-Scale Concrete Masonry Unit (CMU) Walls to Blast. Journal of Engineering Mechanics 128:134–142. doi: 10.1061/(ASCE)0733-9399(2002)128:2(134)

Derakhshan H, Griffith MC, Ingham JM (2011) Out-of-Plane Behavior of One-Way Spanning Unreinforced Masonry Walls. Journal of Engineering Mechanics

Dhanasekar M, Kleeman P, Page A (1985) The failure of brick masonry under biaxial stresses. Proceedings of the Institution of Civil Engineers 79:295–313. doi: 10.1680/iicep.1985.992

Di Egidio A, Zulli D, Contento A (2014) Comparison between the seismic response of 2D and 3D models of rigid blocks. Earthquake Engineering and Engineering Vibration 13:151–162. doi: 10.1007/s11803-014-0219-z

DIANA (2019) User's manual

Dizhur D, Ingham J, Moon L, et al (2011) Performance of Masonry Buildings and Churches in the 22 February 2011 Christchurch Earthquake. Bulletin of the New Zealand Society for Earthquake Engineering 44:

Doherty K, Griffith MC, Lam N, Wilson J (2002) Displacement-based seismic analysis for out-of-plane bending of unreinforced masonry walls. Earthquake Engineering & Structural Dynamics 31:833–850. doi: 10.1002/eqe.126

Drougkas A, Roca P, Molins C (2015) Analytical micro-modeling of masonry periodic unit cells – Elastic properties. International Journal of Solids and Structures 69:169–188. doi: 10.1016/j.ijsolstr.2015.04.039

Drucker D, Prager W, Greenberg H (1952) Extended limit design theorems for continuous media

Dumova-Jovanoska E (2000) Fragility curves for reinforced concrete structures in Skopje (Macedonia) region. Soil Dynamics and Earthquake Engineering 19:455–466. doi: https://doi.org/10.1016/S0267-7261(00)00017-8

Duvaut G, Lions JL (1972) Les inéquations en mécanique et en physique. New York

Dvorak GJ, Teply JL (1985) Periodic Hexagonal Array Models for Plasticity of Composite Materials. In: Plasticity Today: Modeling, Methods and Applications. Elsevier Science Publishers B. V., pp 623–642

E. Reissner (1975) On transverse bending of plates, including the effect of transverse shear deformation. International Journal of Solids and Structures 11:569–573. doi: 10.1016/0020-7683(75)90030-X

Eads L, Miranda E, Lignos D (2016) Spectral shape metrics and structural collapse potential. Earthquake Engineering & Structural Dynamics 45:1643–1659. doi: 10.1002/eqe.2739

Eamon CD, Baylot JT, O'Daniel JL (2004) Modeling Concrete Masonry Walls Subjected to Explosive Loads. Journal of Engineering Mechanics 130:1098–1106. doi: 10.1061/(ASCE)0733-9399(2004)130:9(1098)

Elmenshawi A, Sorour M, Mufti A, et al (2010) Damping mechanisms and damping ratios in vibrating unreinforced stone masonry. Engineering Structures 32:3269–3278. doi: https://doi.org/10.1016/j.engstruct.2010.06.016

Erberik MA (2007) Generation of fragility curves for Turkish masonry buildings considering in-plane failure modes. Earthquake Engineering & Structural Dynamics 37:387–405. doi: 10.1002/eqe.760

Eurocode 8 (2004) Eurocode 8. Design provisions for earthquake resistance of structures. Part 1-1: General rules – seismic actions and general requirements for structures. Brussels, Belgium: European Commitee for Standardization

Faber MH, Maes MA, Baker JW, et al (2007) Principles of risk assessment of engineered systems. In: Kanda, Takada, Furuta (eds) 10th International Conference on Applications of Statistics and Probability in Civil Engineering. Taylor & Francis Group, London, ISBN 978-0-415-45211-3, The University of Tokyo, Kashiwa Campus, Japan

Faber MH, Stewart MG (2003) Risk assessment for civil engineering facilities: critical overview and discussion. Reliability Engineering & System Safety 80:173–184. doi: 10.1016/S0951-8320(03)00027-9

Faber PDMH (2009) Risk and Safety in Engineering. Swiss Federal Institute of Technology, Zurich

Felice G de, Giannini R (2001) Out-of-plane seismic resistance of masonry walls. Journal of Earthquake Engineering 5:253–271. doi: 10.1080/13632460109350394

FEMA 273 (1997) NEHRP Guidelines for the Seismic Rehabilitation of Buildings. Washington, DC, USA

FEMA 306 (1998) Evaluation of earthquake damaged concrete and masonry wall buildings. Basic Procedures Manual. Washington, DC, USA

FEMA 356 (2000) Prestandard and Commentary for the Seismic Rehabilitation of Buildings. Washington, DC, USA

FEMA 368 (2001) NEHRP recommended provisions for seismic regulations for new buildings and other structures

Ferreira TM, Costa AA, Costa A (2014) Analysis of the Out-Of-Plane Seismic Behavior of Unreinforced Masonry: A Literature Review. International Journal of Architectural Heritage 9:949–972. doi: 10.1080/15583058.2014.885996

Feyel F, Chaboche J-L (2000) FE2 multiscale approach for modelling the elastoviscoplastic behaviour of long fibre SiC/Ti composite materials. Computer Methods in Applied Mechanics

and Engineering 183:309–330. doi: 10.1016/S0045-7825(99)00224-8

Flanagan RD, Bennett RM (1999) Bidirectional Behavior of Structural Clay Tile Infilled Frames. http://dx.doi.org/101061/(ASCE)0733-9445(1999)125:3(236). doi: 10.1061/(ASCE)0733-9445(1999)125:3(236)

Forest S, Pradel F, Sab K (2001) Asymptotic analysis of heterogeneous Cosserat media. International Journal of Solids and Structures 38:4585–4608. doi: 10.1016/S0020-7683(00)00295-X

Frankie TM, Gencturk B, Elnashai AS (2013) Simulation-Based Fragility Relationships for Unreinforced Masonry Buildings. Journal of Structural Engineering 139:400–410. doi: 10.1061/(ASCE)ST.1943-541X.0000648

Gabellieri R, Landi L, Diotallevi PP (2013) 2-DOF model for the dynamic analysis of unreinforced masonry walls in out-of-plane bending. In: COMPDYN 2013 - 4th ECCOMAS Thematic Conference on Computational Methods in Structural Dynamics and Earthquake Engineering. Kos Island (Greece), pp 3510–3522

Gambarotta L, Lagomarsino S (1997) Damage models for the seismic response of brick masonry shear walls. Part II: the continuum model and its applications. Earthquake engineering & …

Ganju T (1977) Non-linear finite element analysis of clay brick masonry. Proc 6th Australasian Conf on Mech of Structures and Materials 59–65

Gasparini DA, Vanmarke EH (1976) Simulated earthquake motions compatible with prescribed response spectra. Evaluation of Seismic Safety of Buildings

Gazzola EA, Drysdale RG (1986) A Component Failure Criterion for Blockwork in Flexure. In: Advances in Analysis of Structural Masonry. ASCE, pp 134–154

Gazzola EA, Drysdale RG, Essawy AS (1985) Bending of concrete masonry walls at different angles to the bed joints. In: Proc. of the 3rd North Am. Masonry Conference

Geers MGD, Kouznetsova VG, Brekelmans WAM (2010) Multi-scale computational homogenization: Trends and challenges. Journal of Computational and Applied Mathematics 234:2175–2182. doi: 10.1016/j.cam.2009.08.077

Gelfi P (2006) SIMQKE-GR - Software for generating artificial accelerograms compatible with the response spectrum

Georgin JF, Reynouard JM (2003) Modeling of structures subjected to impact: concrete behaviour under high strain rate. Cement and Concrete Composites 25:131–143. doi: 10.1016/S0958-9465(01)00060-9

Ghiassi B, Soltani M, Tasnimi AA (2012a) A simplified model for analysis of unreinforced masonry shear walls under combined axial, shear and flexural loading. Engineering Structures 42:396–409. doi: https://doi.org/10.1016/j.engstruct.2012.05.002

Ghiassi B, Soltani M, Tasnimi AA (2012b) Seismic Evaluation of Masonry Structures Strengthened with Reinforced Concrete Layers. Journal of Structural Engineering 138:729–743. doi:

10.1061/(ASCE)ST.1943-541X.0000513

Ghobarah A (2001) Performance-based design in earthquake engineering: state of development. Engineering Structures 23:878–884. doi: https://doi.org/10.1016/S0141-0296(01)00036-0

Ghosh S, Lee K, Moorthy S (1995) Multiple scale analysis of heterogeneous elastic structures using homogenization theory and voronoi cell finite element method. International Journal of Solids and Structures 32:27–62. doi: 10.1016/0020-7683(94)00097-G

Ghosh S, Lee K, Raghavan P (2001) A multi-level computational model for multi-scale damage analysis in composite and porous materials. International Journal of Solids and Structures 38:2335–2385. doi: 10.1016/S0020-7683(00)00167-0

Giambanco G, Rizzo S, Spallino R (2001) Numerical analysis of masonry structures via interface models. Computer Methods in Applied Mechanics and Engineering 190:6493–6511. doi: 10.1016/S0045-7825(01)00225-0

Giamundo V, Sarhosis V, Lignola GP, et al (2014) Evaluation of different computational modelling strategies for the analysis of low strength masonry structures. Engineering Structures 73:160–169. doi: 10.1016/j.engstruct.2014.05.007

Gilbert M, Casapulla C, Ahmed HM (2006) Limit analysis of masonry block structures with non-associative frictional joints using linear programming. Computers & Structures 84:873–887. doi: 10.1016/j.compstruc.2006.02.005

Gilbert M, Hobbs B, Molyneaux TC. (2002a) The performance of unreinforced masonry walls subjected to low-velocity impacts: mechanism analysis. International Journal of Impact Engineering 27:253–275. doi: 10.1016/S0734-743X(01)00050-1

Gilbert M, Hobbs B, Molyneaux TC. (2002b) The performance of unreinforced masonry walls subjected to low-velocity impacts: experiments. International Journal of Impact Engineering 27:231–251. doi: 10.1016/S0734-743X(01)00049-5

Gilbert M, Melbourne C (1994) Rigid-block analysis of masonry structures. Structural Engineer 72:

Giovinazzi S, Lagomarsino S (2004) A macroseismic method for the vulnerability assessment of buildings. In: 13th world conference on Earthquake Engineering. Vancouver, Canada

Giuffrè A (1990) Letture sulla meccanica delle murature storiche. Rome, Itally: Kappa

Giuffrè A, Carocci C (1993) Statica e dinamica delle costruzioni murarie storiche. In: Editore MA (ed) Atti del Convegno internazionale CNR “Le pietre da costruzione: il tufo calcareo e la pietra leccese.” Bari, pp 539–598

Grassl P, Jirásek M (2006) Damage-plastic model for concrete failure. International Journal of Solids and Structures 43:7166–7196. doi: 10.1016/j.ijsolstr.2006.06.032

Greco F, Leonetti L, Luciano R, Nevone Blasi P (2016) An adaptive multiscale strategy for the damage analysis of masonry modeled as a composite material. Composite Structures 153:972–988. doi: 10.1016/j.compstruct.2016.06.066

Greenwold S, Allen E, Zalewski W (2003) Active statics. Cambridge, MA: MIT

Griffith AA (1921) VI. The phenomena of rupture and flow in solids. Philosophical Transactions of the Royal Society of London Series A, Containing Papers of a Mathematical or Physical Character 221:163 LP-198

Griffith M, Magenes G (2003) Evaluation of out-of-plane stability of unreinforced masonry walls subjected to seismic excitation. Journal of Earthquake Engineering 7:141–169

Grünthal G (1998) Cahiers du Centre Européen de Géodynamique et de Séismologie: Volume 15– European Macroseismic Scale 1998. In: European Center for Geodynamics and Seismology. Luxembourg

Guggisberg R, Thürlimann B (1990) Failure criterion for laterally loaded masonry walls. In: Proc., 5th North Am. Masonry Conf. pp 949–958

Günay S, Mosalam KM (2013) PEER Performance-Based Earthquake Engineering Methodology, Revisited. Journal of Earthquake Engineering 17:829–858. doi: 10.1080/13632469.2013.787377

Hao H, Tarasov B (2008) Experimental Study of Dynamic Material Properties of Clay Brick and Mortar at Different Strain Rates. Australian Journal of Structural Engineering 8:117

Hao Y, Hao H (2013) Numerical Investigation of the Dynamic Compressive Behaviour of Rock Materials at High Strain Rate. Rock Mechanics and Rock Engineering 46:373–388. doi: 10.1007/s00603-012-0268-4

Hao Y, Hao H, Li ZX (2013) Influence of end friction confinement on impact tests of concrete material at high strain rate. International Journal of Impact Engineering 60:82–106. doi: 10.1016/j.ijimpeng.2013.04.008

Hashin Z, Rosen BW (1964) The Elastic Moduli of Fiber-Reinforced Materials. Journal of Applied Mechanics 31:223–232

HAZUS (1999) NIBS - National Institute of Building Science. HAZUS 99 earthquake loss estimation methodology: technical manual. Federal Emergency Management Agency, Washington D.C.

Hellweg H-B, Crisfield MA, Davies GAO (1994) Failure analysis of composite structures using interface elements. In: Eggington RE (ed) NAFEMS Conf. Application of Finite Elements to Composite Materials. pp 6–9

Hellwega H-B, Crisfield MA (1998) A new arc-length method for handling sharp snap-backs. Computers & Structures 66:704–709. doi: 10.1016/S0045-7949(97)00077-1

Hendry EAW (2001) Masonry walls: materials and construction. Construction and Building Materials 15:323–330. doi: https://doi.org/10.1016/S0950-0618(01)00019-8

Herbert DM, Gardner DR, Harbottle M, Hughes TG (2014) Uniform lateral load capacity of small-scale masonry wall panels. Materials and Structures 47:805–818. doi: 10.1617/s11527-013-0092-7

Herrmann LR (1967) Finite element bending analysis for plates. Journal of Engineering Mechanics

Division 93:13–26

Heyman J (1966) The stone skeleton. International Journal of Solids and Structures 2:249–279. doi: 10.1016/0020-7683(66)90018-7

Hilber HM, Hughes TJR, Taylor RL (1977) Improved numerical dissipation for time integration algorithms in structural dynamics. Earthquake Engineering & Structural Dynamics 5:283–292. doi: 10.1002/eqe.4290050306

Hill R (1965) A self-consistent mechanics of composite materials. Journal of the Mechanics and Physics of Solids 13:213–222. doi: 10.1016/0022-5096(65)90010-4

Hobbs H, Ting M, Gilbert M (1994) An analytical approach for walls subjected to static and dynamic out-of-plane point loads. In: 0th International Brick and Block Masonary Conference. Alberta, Canada

Hogan SJ (1989) On the Dynamics of Rigid-Block Motion Under harmonic Forcing. Proceedings of the Royal Society A: Mathematical, Physical and Engineering Sciences 425:441–476. doi: 10.1098/rspa.1989.0114

Holzer TL, Savage JC (2013) Global Earthquake Fatalities and Population. Earthquake Spectra 29:155–175. doi: 10.1193/1.4000106

Housner GW (1963) The behavior of inverted pendulum structures during earthquakes. Bulletin of the Seismological Society of America 53:403–417

Hughes TJR, Cottrell JA, Bazilevs Y (2005) Isogeometric analysis: CAD, finite elements, NURBS, exact geometry and mesh refinement. Computer Methods in Applied Mechanics and Engineering 194:4135–4195. doi: https://doi.org/10.1016/j.cma.2004.10.008

Hughes TJR, Tezduyar TE (1981) Finite Elements Based Upon Mindlin Plate Theory With Particular Reference to the Four-Node Bilinear Isoparametric Element. Journal of Applied Mechanics 48:587. doi: 10.1115/1.3157679

ICOMOS Recommendations (2005) International Council on Monument and sites, Recommendation for the analysis, conservation and Structural restoration of Architectural Heritage

IEG (2007) Development Actions and the Rising Incidence of Disasters. Washington, D.C.

Iervolino I, De Luca F, Cosenza E, Manfredi G (2010) Real, Scaled, Adjusted and Artificial Records: A Displacement and Cyclic Response Assessment BT - Advances in Performance-Based Earthquake Engineering. In: Fardis MN (ed). Springer Netherlands, Dordrecht, pp 39–47

Irons B, Loikkanen M (1983) An engineers' defence of the patch test. International Journal for Numerical Methods in Engineering 19:1391–1401. doi: 10.1002/nme.1620190908

Irons BM (1966) Numerical integration applied to finite element methods. In: Conference on Use of Digital Computers in Structural Engineering. University of Newcastle

Irons BM, Razzaque A (1972) Experience with the patch test for convergence of finite elements. In: Aziz AKBT-TMF of the FEM with A to PDE (ed) The Mathematical Foundations of the

Finite Element Method with Applications to Partial Differential Equations. Academic Press, pp 557–587

Ishiyama Y (1982) Motions of rigid bodies and criteria for overturning by earthquake excitations. Earthquake Engineering and Structural Dynamics 10:635–650

Itasca (2004) UDEC - Universal Distinct Element Code. Itasca Consulting Group Inc.

JCSS (2011) Joint Committee on Structural Safety - Probabilistic Model Code PART 3: Resistance Models

K.A. Porter (2003) An overview of PEER's performance-based earthquake engineering methodology. In: Ninth International Conference on Applications of Statistics and Probability in Engineering. San Francisco, California

Kannan R, Hendry S, Higham NJ, Tisseur F (2014) Detecting the causes of ill-conditioning in structural finite element models. Computers & Structures 133:79–89. doi: https://doi.org/10.1016/j.compstruc.2013.11.014

Kaplan H, Bilgin H, Yilmaz S, et al (2010) Structural damages of L'Aquila (Italy) earthquake. Natural Hazards and Earth System Sciences 10:499–507

Kappos A, Panagopoulos G, Panagiotopoulos C, Penelis G (2006) A hybrid method for the vulnerability assessment of R/C and URM buildings. Bulletin of Earthquake Engineering 4:391–413. doi: 10.1007/s10518-006-9023-0

Kappos AJ (2016) An overview of the development of the hybrid method for seismic vulnerability assessment of buildings. Structure and Infrastructure Engineering 12:1573–1584. doi: 10.1080/15732479.2016.1151448

Kappos AJ, Papanikolaou VK (2016) Nonlinear dynamic analysis of masonry buildings and definition of seismic damage states. The Open Construction and Building Technology Journal 10:192–209

Kappos AJ, Stylianidis KC, Pitilakis K (1998) Development of Seismic Risk Scenarios Based on a Hybrid Method of Vulnerability Assessment. Natural Hazards 17:177–192. doi: 10.1023/A:1008083021022

Kawai T (1977) New Discrete Structural Models and Generalization of the Method of Limit Analysis. In: Finite Elements in Nonlinear Mechanics, P.G. Bergan et al. eds. Tapir Publishers, pp 885–906

Kawai T (1991) Discrete Limit Analysis of Reinforced Concrete Structures Using Rigid Bodies-Spring Models. In: The finite element method in the 1990's. Springer Berlin Heidelberg, Berlin, Heidelberg, pp 182–191

Kawai T (1978) New discrete models and their application to seismic response analysis of structures. Nuclear Engineering and Design 48:207–229. doi: 10.1016/0029-5493(78)90217-0

Kazantzi AK, Vamvatsikos D (2015) Intensity measure selection for vulnerability studies of building classes. Earthquake Engineering & Structural Dynamics 44:2677–2694. doi: 10.1002/eqe.2603

Konstantinidis D, Makris N (2007) The dynamics of a rocking block in three dimensions. Proceedings of the 8th HSTAM International Congress on Mechanics 12–14

Kooharian A (1952) Limit Analysis of Voussoir (Segmental) and Concrete Archs. Journal Proceedings 49:317–328

Kouznetsova V, Brekelmans WAM, Baaijens FPT (2001) An approach to micro-macro modeling of heterogeneous materials. Computational Mechanics 27:37–48. doi: 10.1007/s004660000212

Kouznetsova VG, Geers MGD, Brekelmans WAM (2004) Multi-scale second-order computational homogenization of multi-phase materials: a nested finite element solution strategy. Computer Methods in Applied Mechanics and Engineering 193:5525–5550. doi: 10.1016/j.cma.2003.12.073

Krawinkler H, Miranda E (2004) Performance-Based Earthquake Engineering. In: Bozorgnia Y, Bertero V V. (eds) Earthquake Engineering: From Engineering Seismology to Performance-Based Engineering. CRC Press: Boca Raton, Florida, pp 560–636

Krejčí T, Kruis J, Šejnoha M, Koudelka T (2017) Hybrid parallel approach to homogenization of transport processes in masonry. Advances in Engineering Software 113:25–33. doi: https://doi.org/10.1016/j.advengsoft.2016.08.009

Kruis J, Krejčí T, Šejnoha M (2016) Parallel Computing in Multi-scale Analysis of Coupled Heat and Moisture Transport in Masonry Structures. In: Kozubek T, Blaheta R, Šístek J, et al. (eds) High Performance Computing in Science and Engineering. Springer International Publishing, Cham, pp 50–59

Lagomarsino S (2014) Seismic assessment of rocking masonry structures. Bulletin of Earthquake Engineering 13:97–128. doi: 10.1007/s10518-014-9609-x

Lagomarsino S, Giovinazzi S (2006) Macroseismic and mechanical models for the vulnerability and damage assessment of current buildings. Bulletin of Earthquake Engineering 4:415–443. doi: 10.1007/s10518-006-9024-z

Lagomarsino S, Penna A, Galasco A, Cattari S (2013) TREMURI program: An equivalent frame model for the nonlinear seismic analysis of masonry buildings. Engineering Structures 56:1787–1799. doi: 10.1016/j.engstruct.2013.08.002

Landi L, Gabellieri R, Diotallevi PP (2015) A model for the out-of-plane dynamic analysis of unreinforced masonry walls in buildings with flexible diaphragms. Soil Dynamics and Earthquake Engineering 79:211–222. doi: 10.1016/j.soildyn.2015.09.013

Lawrence SJ (1995) The Behaviour of masonry in Horizontal Flexure. In: Proceedings of the 7th Canadian Masonry Symposium. Canada, pp 525–536

Le Nard H, Bailly P (2000) Dynamic behaviour of concrete: the structural effects on compressive strength increase. Mechanics of Cohesive-frictional Materials 5:491–510. doi: 10.1002/1099-1484(200008)5:6<491::AID-CFM106>3.0.CO;2-R

Lee J, Fenves GL (1998) Plastic-Damage Model for Cyclic Loading of Concrete Structures. Journal of Engineering Mechanics 124:892–900. doi: 10.1061/(ASCE)0733-9399(1998)124:8(892)

Lee JS, Pande GN, Middleton J, Kralj B (1996) Numerical modelling of brick masonry panels subject to lateral loadings. Computers & Structures 61:735–745. doi: 10.1016/0045-7949(95)00361-4

Lemos J, Costa A, Bretas E (2011) Assessment of the Seismic Capacity of Stone Masonry Walls with Block Models. Computational Methods in Earthquake Engineering 221–235

Lemos J V. (2007) Discrete Element Modeling of Masonry Structures. International Journal of Architectural Heritage 1:190–213. doi: 10.1080/15583050601176868

Lloberas-Valls O, Rixen DJ, Simone A, Sluys LJ (2012) On micro-to-macro connections in domain decomposition multiscale methods. Computer Methods in Applied Mechanics and Engineering 225–228:177–196. doi: 10.1016/j.cma.2012.03.022

Lotfi HR, Shing PB (1994) Interface Model Applied to Fracture of Masonry Structures. Journal of Structural Engineering 120:63–80. doi: 10.1061/(ASCE)0733-9445(1994)120:1(63)

Lourenço PB (1996) Computational strategies for masonry structures. PhD Thesis. Delft University of Technology, Delft, The Netherlands

Lourenço PB (2000) Anisotropic Softening Model for Masonry Plates and Shells. Journal of Structural Engineering 126:1008–1016. doi: 10.1061/(ASCE)0733-9445(2000)126:9(1008)

Lourenço PB (1997) An anisotropic macro-model for masonry plates and shells: implementation and validation. TNO Building and Construction Research - Computational Mechanics 34–91

Lourenço PB (2002) Computations on historic masonry structures. Progress in Structural Engineering and Materials 4:301–319. doi: 10.1002/pse.120

Lourenço PB (2009) Recent advances in masonry structures: Micromodelling and homogenisation. In: Galvanetto U, Aliabadi MHF (eds) Multiscale Modeling in Solid Mechanics. Imperial College Press, pp 251–294

Lourenço PB (2008) Structural masonry analysis : recent developments and prospects. In: Proceedings of the 14th International brick and block masonry conference. University of Newcastle, Australia, Sydney

Lourenço PB, De Borst R, Rots JG (1997) A plane stress softening plasticity model for orthotropic materials. International Journal for Numerical Methods in Engineering 40:4033–4057. doi: 10.1002/(SICI)1097-0207(19971115)40:21<4033::AID-NME248>3.0.CO;2-0

Lourenço PB, Mendes N, Ramos LF, Oliveira D V. (2011) Analysis of Masonry Structures Without Box Behavior. International Journal of Architectural Heritage 5:369–382. doi: 10.1080/15583058.2010.528824

Lourenço PB, Milani G, Tralli A, Zucchini A (2007) Analysis of masonry structures: review of and recent trends in homogenization techniques. Canadian Journal of Civil Engineering 34:1443–1457. doi: 10.1139/L07-097

Lourenço PB, Rots JG (1997) Multisurface Interface Model for Analysis of Masonry Structures. Journal of Engineering Mechanics 123:660–668. doi: 10.1061/(ASCE)0733-9399(1997)123:7(660)

Lourenço PB, Rots JG, Blaauwendraad J (1998) Continuum Model for Masonry: Parameter Estimation and Validation. Journal of Structural Engineering 124:642–652. doi: 10.1061/(ASCE)0733-9445(1998)124:6(642)

Lourenço PB, Trujillo A, Mendes N, Ramos LF (2012) Seismic performance of the St. George of the Latins church: Lessons learned from studying masonry ruins. Engineering Structures 40:501–518. doi: 10.1016/j.engstruct.2012.03.003

Lubliner J, Oliver J, Oller S, Oñate E (1989) A plastic-damage model for concrete. International Journal of Solids and Structures 25:299–326. doi: 10.1016/0020-7683(89)90050-4

Luccioni B., Ambrosini R., Danesi R. (2004) Analysis of building collapse under blast loads. Engineering Structures 26:63–71. doi: 10.1016/j.engstruct.2003.08.011

Luciano R, Sacco E (1997) Homogenization technique and damage model for old masonry material. International Journal of Solids and Structures 34:3191–3208. doi: 10.1016/S0020-7683(96)00167-9

Luco N, Cornell CA (2007) Structure-Specific Scalar Intensity Measures for Near-Source and Ordinary Earthquake Ground Motions. Earthquake Spectra 23:357–392. doi: 10.1193/1.2723158

M. Tomaževič (1999) Earthquake-resistant design of masonry buildings, Vol. 1. World Scientific

Ma M, Pan A, Luan M, Gebara J (1996) Seismic analysis of stone arch bridges using discontinuous deformation analysis. In: Proceedings of the 11th world conference on earthquake engineering. Elsevier, Amsterdam, p paper nº 1551

Mackie K, Stojadinoviić B (2005) Fragility basis for California highway overpass bridge seismic decision making. PEER report 2005/02

Macneal RH, Harder RL (1985) A proposed standard set of problems to test finite element accuracy. Finite Elements in Analysis and Design 1:3–20. doi: https://doi.org/10.1016/0168-874X(85)90003-4

Macorini L, Izzuddin BA (2011) A non-linear interface element for 3D mesoscale analysis of brick-masonry structures. International Journal for Numerical Methods in Engineering 85:1584–1608. doi: 10.1002/nme.3046

Macorini L, Izzuddin BA (2014) Nonlinear Analysis of Unreinforced Masonry Walls under Blast Loading Using Mesoscale Partitioned Modeling. Journal of Structural Engineering 140:A4014002. doi: 10.1061/(ASCE)ST.1943-541X.0000931

Macorini L, Izzuddin BA (2013) Nonlinear analysis of masonry structures using mesoscale partitioned modelling. Advances in Engineering Software 60–61:58–69. doi: 10.1016/j.advengsoft.2012.11.008

Mafteiu-Scai LO (2014) The Bandwidths of a Matrix. A Survey of Algorithms. Annals of West University of Timisoara - Mathematics and Computer Science 52:183–223. doi: https://doi.org/10.2478/awutm-2014-0019

Magenes G, Bolognini D, Braggio C (2000) Metodi semplificati per l'analisi sismica non lineare di edifici in muratura. CNR-Gruppo Nazionale per la Difesa dai …

Magenes G, Calvi GM (1997) In-plane seismic response of brick masonry walls. Earthquake Engineering & Structural Dynamics 26:1091–1112. doi: 10.1002/(SICI)1096-9845(199711)26:11<1091::AID-EQE693>3.0.CO;2-6

Magenes G, Della Fontana A (1998) Simplified non-linear seismic analysis of masonry buildings. Proc of the British Masonry Society 8:190–195

Maier G, Papa E, Nappi A (1991) On damage and failure of brick masonry. In: Experimental and numerical methods in earthquake engineering. Balkema: Brussels and Luxembourg, pp 223–245

Makris N, Konstantinidis D (2003) The rocking spectrum and the limitations of practical design methodologies. Earthquake Engineering & Structural Dynamics 32:265–289. doi: 10.1002/eqe.223

Mamaghani I, Aydan O, Y K (1999) Analysis of masonry structures under static and dynamic loading by discrete finite element method. Structural Eng/Earthq Eng JSCE 16:75–86

Martínez G, Roca P, Caselles O, Clapés J (2006) Characterization of the dynamic response for the structure of Mallorca Cathedral. In: Structural analysis of historical Constructions. New Delhi, India

Massart TJ, Peerlings RHJ, Geers MGD (2004) Mesoscopic modeling of failure and damage-induced anisotropy in brick masonry. European Journal of Mechanics - A/Solids 23:719–735. doi: 10.1016/j.euromechsol.2004.05.003

Massart TJ, Peerlings RHJ, Geers MGD, Gottcheiner S (2005) Mesoscopic modeling of failure in brick masonry accounting for three-dimensional effects. Engineering Fracture Mechanics 72:1238–1253. doi: 10.1016/j.engfracmech.2004.09.007

MATLAB 2015a, The MathWorks, Inc., Natick, Massachusetts, United States.

McKay MD, Beckman RJ, Conover WJ (1979) Comparison of Three Methods for Selecting Values of Input Variables in the Analysis of Output from a Computer Code. Technometrics 21:239–245. doi: 10.1080/00401706.1979.10489755

Medvedev S (1977) Seismic intensity scale MSK-76. Publ Inst Geophys Pol Acad Sc 117:95–102

Mehanny SSF (2009) A broad-range power-law form scalar-based seismic intensity measure. Engineering Structures 31:1354–1368. doi: https://doi.org/10.1016/j.engstruct.2009.02.003

Melchers RE (1999) Structural Reliability Analysis and Prediction, 2nd editio. Wiley

Mendes N, Costa AA, Lourenço PB, et al (2017) Methods and Approaches for Blind Test Predictions of Out-of-Plane Behavior of Masonry Walls: A Numerical Comparative Study. International Journal of Architectural Heritage 11:59–71. doi: 10.1080/15583058.2016.1238974

Mendes N, Lourenço PB, Campos-Costa A (2014) Shaking table testing of an existing masonry

building: assessment and improvement of the seismic performance. Earthquake Engineering & Structural Dynamics 43:247–266. doi: 10.1002/eqe.2342

Mercatoris BCN, Massart TJ (2011) A coupled two-scale computational scheme for the failure of periodic quasi-brittle thin planar shells and its application to masonry. International Journal for Numerical Methods in Engineering 85:1177–1206. doi: 10.1002/nme.3018

Metropolis N, Ulam S (1949) The Monte Carlo Method. Journal of the American Statistical Association 44:335–341. doi: 10.1080/01621459.1949.10483310

Middleton WG (1994) Research projects into the upgrading of unreinforced masonry parapets. In: Barr B, Evans HR, Haring JE (eds) Bridge assessment management and design: Proceedings of the Centenary Year Bridge Conference. Elsevier, Cardiff, U.K., pp 229–234

Miehe C, Koch A (2002) Computational micro-to-macro transitions of discretized microstructures undergoing small strains. Archive of Applied Mechanics (Ingenieur Archiv) 72:300–317. doi: 10.1007/s00419-002-0212-2

Milani G (2008) 3D upper bound limit analysis of multi-leaf masonry walls. International Journal of Mechanical Sciences 50:817–836. doi: 10.1016/j.ijmecsci.2007.11.003

Milani G, Lourenço P, Tralli A (2007) 3D homogenized limit analysis of masonry buildings under horizontal loads. Engineering Structures 29:3134–3148. doi: 10.1016/j.engstruct.2007.03.003

Milani G, Lourenço P, Tralli A (2006a) Homogenization Approach for the Limit Analysis of Out-of-Plane Loaded Masonry Walls. Journal of Structural Engineering 132:1650–1663. doi: 10.1061/(ASCE)0733-9445(2006)132:10(1650)

Milani G, Lourenço PB, Tralli A (2006b) Homogenised limit analysis of masonry walls, Part II: Structural examples. Computers & Structures 84:181–195. doi: 10.1016/j.compstruc.2005.09.004

Milani G, Lourenço PB, Tralli A (2006c) Homogenised limit analysis of masonry walls, Part I: Failure surfaces. Computers & Structures 84:166–180. doi: https://doi.org/10.1016/j.compstruc.2005.09.005

Milani G, Tralli A (2011) Simple SQP approach for out-of-plane loaded homogenized brickwork panels, accounting for softening. Computers & Structures 89:201–215. doi: 10.1016/j.compstruc.2010.09.005

Milani G, Venturini G (2011) Automatic fragility curve evaluation of masonry churches accounting for partial collapses by means of 3D FE homogenized limit analysis. Computers & Structures 89:1628–1648. doi: 10.1016/j.compstruc.2011.04.014

Mistler M, Anthoine A, Butenweg C (2007) In-plane and out-of-plane homogenisation of masonry. Computers & Structures 85:1321–1330. doi: 10.1016/j.compstruc.2006.08.087

Mosby M, Matouš K (2015) On mechanics and material length scales of failure in heterogeneous interfaces using a finite strain high performance solver. Modelling and Simulation in Materials Science and Engineering 23:85014

Moulinec H, Suquet P (1998) A numerical method for computing the overall response of nonlinear composites with complex microstructure. Computer Methods in Applied Mechanics and Engineering 157:69–94. doi: 10.1016/S0045-7825(97)00218-1

Navier CLMH (1823) Extrait des recherches sur la flexion des plans elastiques. Bull Sci Soc Philomarhique de Paris 5:95–102

Nayeri SA (2012) Seismic Asessment of the Roman Temple in Évora, Portugal. University of Minho

Norio O, Ye T, Kajitani Y, et al (2011) The 2011 eastern Japan great earthquake disaster: Overview and comments. International Journal of Disaster Risk Science 2:34–42. doi: 10.1007/s13753-011-0004-9

Novoselov KS, Mishchenko A, Carvalho A, Castro Neto AH (2016) 2D materials and van der Waals heterostructures. Science 353:. doi: 10.1126/science.aac9439

Nowak AS, Collins, R. K (2012) Reliability of Structures, Second. CRC Press, Taylor & Francis Group

Noy I (2009) The macroeconomic consequences of disasters. Journal of Development Economics 88:221–231. doi: 10.1016/j.jdeveco.2008.02.005

NZSEE (2017) The Seismic Assessment of Existing Buildings - Technical Guidelines for Engineering Assessments. Part A: Assessment Objectives and Principles. New Zealand

Orduña A (2004) Block user's manual. Guimarães: University of Minho Also available at http://www civil uminho pt/masonry

Orduña A (2003) Seismic assessment of ancient masonry structures by rigid blocks limit analysis. University of Minho

Orduña A, Lourenço PB (2005) Three-dimensional limit analysis of rigid blocks assemblages. Part I: Torsion failure on frictional interfaces and limit analysis formulation. International Journal of Solids and Structures 42:5140–5160. doi: 10.1016/j.ijsolstr.2005.02.010

Orduña A, Preciado A (2008) Vulnerability assessment of churches at Colima by 3D limit analysis models. In: Proceedings of the 6th international conference on structural analysis of historical constructions (SAHC)

Otero F, Oller S, Martinez X, Salomón O (2015) Numerical homogenization for composite materials analysis. Comparison with other micro mechanical formulations. Composite Structures 122:405–416. doi: 10.1016/j.compstruct.2014.11.041

Pacific Coast Building Officials (PCBO) (1927) Uniform Building Code. Whittier, California

Page AW (1978) Finite Element Model for Masonry. Journal of the Structural Division 104:1267–1285

Pande GN, Liang JX, Middleton J (1989) Equivalent elastic moduli for brick masonry. Computers and Geotechnics 8:243–265. doi: 10.1016/0266-352X(89)90045-1

Papa E (1996) A unilateral damage model for masonry based on a homogenisation procedure. Mechanics of Cohesive-frictional Materials 1:349–366. doi: 10.1002/(SICI)1099-1484(199610)1:4<349::AID-CFM18>3.0.CO;2-M

Park J, Towashiraporn P, Craig JI, Goodno BJ (2009) Seismic fragility analysis of low-rise unreinforced masonry structures. Engineering Structures 31:125–137. doi: 10.1016/j.engstruct.2008.07.021

Parker D, Tapsell S (1995) Hazard transformation and hazard management issues in the London megacity. GeoJournal 37:313–328. doi: 10.1007/BF00814011

Pasticier L, Amadio C, Fragiacomo M (2007) Non-linear seismic analysis and vulnerability evaluation of a masonry building by means of the SAP2000 V.10 code. Earthquake Engineering & Structural Dynamics 37:467–485. doi: 10.1002/eqe.770

Pegon P, Anthoine A (1997) Numerical strategies for solving continuum damage problems with softening: Application to the homogenization of Masonry. Computers & Structures 64:623–642. doi: 10.1016/S0045-7949(96)00153-8

Pelà L, Aprile A, Benedetti A (2013a) Comparison of seismic assessment procedures for masonry arch bridges. Construction and Building Materials 38:381–394. doi: 10.1016/j.conbuildmat.2012.08.046

Pelà L, Cervera M, Roca P (2013b) An orthotropic damage model for the analysis of masonry structures. Construction and Building Materials 41:957–967. doi: 10.1016/j.conbuildmat.2012.07.014

Peña F, Prieto F, Lourenço PB, et al (2007) On the dynamics of rocking motion of single rigid–block structures

Penna A, Lagomarsino S, Galasco A (2014) A nonlinear macroelement model for the seismic analysis of masonry buildings. Earthquake Engineering & Structural Dynamics 43:159–179. doi: 10.1002/eqe.2335

Pereira JM, Lourenço PB (2016a) Experimental Characterization of Masonry and Masonry Components at High Strain Rates. Journal of Materials in Civil Engineering 04016223. doi: 10.1061/(ASCE)MT.1943-5533.0001755

Pereira JM, Lourenço PB (2016b) Experimental bond behaviour of GFRP and masonry bricks under impulsive loading. Materials and Structures 49:4799–4811. doi: 10.1617/s11527-016-0826-4

Petracca M, Pelà L, Rossi R, et al (2016) Regularization of first order computational homogenization for multiscale analysis of masonry structures. Computational Mechanics 57:257–276. doi: 10.1007/s00466-015-1230-6

Petry S, Beyer K (2014) Influence of boundary conditions and size effect on the drift capacity of URM walls. Engineering Structures 65:76–88. doi: https://doi.org/10.1016/j.engstruct.2014.01.048

Pickett STA, Cadenasso ML, Grove JM, et al (2011) Urban ecological systems: scientific foundations and a decade of progress. Journal of environmental management 92:331–62. doi:

10.1016/j.jenvman.2010.08.022

Pietruszczak S, Niu X (1992) A mathematical description of macroscopic behaviour of brick masonry. International Journal of Solids and Structures 29:531–546. doi: 10.1016/0020-7683(92)90052-U

Pitilakis K (2014) Earthquake Risk Assessment: Certitudes,Fallacies,Uncertainties and the Quest for Soundness. In: Pitilakis K, Crowley H, Kaynia AM (eds) SYNER-G: Typology Definition and Fragility Functions for Physical Elements at Seismic Risk: Buildings, Lifelines, Transportation Networks and Critical Facilities. Springer Netherlands, Dordrecht, pp 59–95

Pluijm van der RR (1999) Out-of-plane bending of masonry: behaviour and strength. Doctoral dissertation, Technische Universiteit Eindhoven

Pop P, Matei O, Comes C-A (2014) Reducing the bandwidth of a sparse matrix with a genetic algorithm. Optimization 63:1851–1876. doi: 10.1080/02331934.2013.830120

Porter K, Kennedy R, Bachman R (2007) Creating Fragility Functions for Performance-Based Earthquake Engineering. Earthquake Spectra 23:471–489. doi: 10.1193/1.2720892

Powell G, Simons J (1981) Improved iteration strategy for nonlinear structures. International Journal for Numerical Methods in Engineering 17:1455–1467. doi: 10.1002/nme.1620171003

Psycharis IN (1990) Dynamic behaviour of rocking two-block assemblies. Earthquake Engineering & Structural Dynamics 19:555–575. doi: 10.1002/eqe.4290190407

Psycharis IN, Lemos J V., Papastamatiou DY, et al (2003) Numerical study of the seismic behaviour of a part of the Parthenon Pronaos. Earthquake Engineering & Structural Dynamics 32:2063–2084. doi: 10.1002/eqe.315

Quagliarini E, Maracchini G, Clementi F (2017) Uses and limits of the Equivalent Frame Model on existing unreinforced masonry buildings for assessing their seismic risk: A review. Journal of Building Engineering 10:166–182. doi: 10.1016/j.jobe.2017.03.004

Rabinovitch O, Madah H (2011) Finite element modeling and shake-table testing of unidirectional infill masonry walls under out-of-plane dynamic loads. Engineering Structures 33:2683–2696. doi: 10.1016/j.engstruct.2011.05.019

Rafsanjani SH, Lourenço PB, Peixinho N (2015a) Implementation and validation of a strain rate dependent anisotropic continuum model for masonry. International Journal of Mechanical Sciences 104:24–43. doi: 10.1016/j.ijmecsci.2015.10.001

Rafsanjani SH, Lourenço PB, Peixinho N (2015b) Dynamic interface model for masonry walls subjected to high strain rate out-of-plane loads. International Journal of Impact Engineering 76:28–37. doi: 10.1016/j.ijimpeng.2014.09.002

Rao KM, Shrinivasa U (2001) A set of pathological tests to validate new finite elements. Sadhana 26:549–590. doi: 10.1007/BF02703459

Restrepo-Vélez LF (2004) Seismic risk of unreinforced masonry buildings. Individual Study. Pavia, Italy: Rose School. University of Pavia.

Riks E (1979) An incremental approach to the solution of snapping and buckling problems. International Journal of Solids and Structures 15:529–551. doi: 10.1016/0020-7683(79)90081-7

Riks E (1984) Some computational aspects of the stability analysis of nonlinear structures. Computer Methods in Applied Mechanics and Engineering 47:219–259. doi: 10.1016/0045-7825(84)90078-1

Roca P, Cervera M, Gariup G, Pela' L (2010) Structural Analysis of Masonry Historical Constructions. Classical and Advanced Approaches. Archives of Computational Methods in Engineering 17:299–325. doi: 10.1007/s11831-010-9046-1

Roca P, Cervera M, Pelà L, et al (2013) Continuum FE models for the analysis of Mallorca Cathedral. Engineering Structures 46:653–670. doi: 10.1016/j.engstruct.2012.08.005

Rondelet J (1802) Traité théorique et pratique de l'art du batir

Ross CA, Tedesco JW, Kuennmen ST (1995) Effects of Strain Rate on Concrete Strength. ACI Materials Journal 92:37–47. doi: 10.14359/1175

Rota M, Penna A, Magenes G (2010) A methodology for deriving analytical fragility curves for masonry buildings based on stochastic nonlinear analyses. Engineering Structures 32:1312–1323. doi: 10.1016/j.engstruct.2010.01.009

Rota M, Penna A, Strobbia CL (2008) Processing Italian damage data to derive typological fragility curves. Soil Dynamics and Earthquake Engineering 28:933–947. doi: 10.1016/j.soildyn.2007.10.010

Saloustros S, Cervera M, Pelà L (2018) Challenges, Tools and Applications of Tracking Algorithms in the Numerical Modelling of Cracks in Concrete and Masonry Structures. Archives of Computational Methods in Engineering. doi: 10.1007/s11831-018-9274-3

Samarasinghe W (1982) A Finite-Element model for the inplane behaviour of brickwork. In: Proceedings of the Institution of Civil Engineers, Part 2 - Reseach and Theory. pp 171–178

Sarhosis V, Bagi K, Lemos J V., Milani G (eds) (2016) Computational Modeling of Masonry Structures Using the Discrete Element Method. IGI Global

Sarhosis V, Tsavdaridis K, Giannopoulos I (2014) Discrete Element Modelling (DEM) for Masonry Infilled Steel Frames with Multiple Window Openings Subjected to Lateral Load Variations. The Open Construction and Building Technology Journal 8:93–103. doi: 10.2174/1874836801408010093

Saw CB (1974) Linear elastic finite element analysis of masonry walls on beams. Building Science 9:299–307. doi: 10.1016/0007-3628(74)90029-2

Schlegel R, Rautenstrauch K (2004) Failure analysis of masonry shear walls. Numerical Model Discrete Mater 15–18

SEAOC (1995) Vision 2000, Performance based seismic engineering of buildings - vol I and II: Conceptual framework. Sacramento (CA), USA

Sejnoha J, Sejnoha M, Zeman J, et al (2008) A mesoscopic study on historic masonry. Structural Engineering & Mechanics 30:99–117. doi: 10.12989/sem.2008.30.1.099

Senthivel R, Lourenço PB (2009) Finite element modelling of deformation characteristics of historical stone masonry shear walls. Engineering Structures 31:1930–1943. doi: https://doi.org/10.1016/j.engstruct.2009.02.046

Sepe V, Speranza E, Viskovic A (2008) A method for large-scale vulnerability assessment of historic towers. Structural Control and Health Monitoring 15:389–415. doi: 10.1002/stc.243

Shawa O Al, Felice G, Mauro A, Sorrentino L (2012) Out-of-plane seismic behaviour of rocking masonry walls. Earthquake Engineering & Structural Dynamics 41:949–968. doi: 10.1002/eqe.1168

Shi G hua, Goodman RE (1988) Discontinuous Deformation Analysis - A New Method Forcomputing Stress, Strain And Sliding Of Block Systems. The 29th U.S. Symposium on Rock Mechanics (USRMS)

Shibata A, Sozen MA (1976) Substitute-Structure Method for Seismic Design in R/C. Journal of the Structural Division 102:1–18

Shieh-Beygi B, Pietruszczak S (2008) Numerical analysis of structural masonry: mesoscale approach. Computers & Structures 86:1958–1973. doi: 10.1016/j.compstruc.2008.05.007

Silva LC (2013) Analysis of Christchurch Catholic Basilica, New Zealand. University of Minho. Integrated Master Thesis

Silva LC, Mendes N, Lourenço PB, Ingham J (2018) Seismic Structural Assessment of the Christchurch Catholic Basilica, New Zealand. Structures 15:115–130. doi: https://doi.org/10.1016/j.istruc.2018.06.004

Silva W-, Lee K (1987) WES RASCAL code for synthesizing earthquake ground motions.

Singhal A, Kiremidjian AS (1996) Method for Probabilistic Evaluation of Seismic Structural Damage. Journal of Structural Engineering 122:1459–1467. doi: 10.1061/(ASCE)0733-9445(1996)122:12(1459)

Sinha BP (1978) A Simplified ultimate load analysis of laterally-loaded model orthotropic brickwork panels of low tensile strength. Structural Engineering ASCE 56B:81–84

Sluys LJ, De Borst R (1992) Computational modeling of impact tests on steel fibre reinforced concrete beams. Heron 37:3–15

Smit RJM, Brekelmans WAM, Meijer HEH (1998) Prediction of the mechanical behavior of nonlinear heterogeneous systems by multi-level finite element modeling. Computer Methods in Applied Mechanics and Engineering 155:181–192. doi: 10.1016/S0045-7825(97)00139-4

Soroushian P, Choi K (1987) Steel Mechanical Properties at Different Strain Rates. Journal of Structural Engineering 113:663–672. doi: 10.1061/(ASCE)0733-9445(1987)113:4(663)

Sorrentino L, AlShawa O, Decanini LD (2011) The relevance of energy damping in unreinforced

masonry rocking mechanisms. Experimental and analytic investigations. Bulletin of Earthquake Engineering 9:1617–1642. doi: 10.1007/s10518-011-9291-1

Sorrentino L, D'Ayala D, de Felice G, et al (2017) Review of Out-of-Plane Seismic Assessment Techniques Applied To Existing Masonry Buildings. International Journal of Architectural Heritage 11:2–21. doi: 10.1080/15583058.2016.1237586

Sorrentino L, Kunnath S, Monti G, Scalora G (2008) Seismically induced one-sided rocking response of unreinforced masonry façades. Engineering Structures 30:2140–2153. doi: 10.1016/j.engstruct.2007.02.021

Sorrentino L, Liberatore L, Decanini LD, Liberatore D (2013) The performance of churches in the 2012 Emilia earthquakes. Bulletin of Earthquake Engineering 12:2299–2331. doi: 10.1007/s10518-013-9519-3

Southcombe C, May I, Ching V (1995) The behavior of brickwork panels with openings under lateral load. In: Proceedings of the 4th international masonry conference, vol. 1. British Masonry Society, London, pp 105–10

Spahn J, Andrä H, Kabel M, Müller R (2014) A multiscale approach for modeling progressive damage of composite materials using fast Fourier transforms. Computer Methods in Applied Mechanics and Engineering 268:871–883. doi: 10.1016/j.cma.2013.10.017

Spanos PD, Roussis PC, Politis NPA (2001) Dynamic analysis of stacked rigid blocks. Soil Dynamics and Earthquake Engineering 21:559–578. doi: 10.1016/S0267-7261(01)00038-0

Stein M (1987) Large Sample Properties of Simulations Using Latin Hypercube Sampling. Technometrics 29:143–151. doi: 10.1080/00401706.1987.10488205

Stevin S (1586) De beghinselen der weeghconst. Leiden 1:

Stewart MG, Melchers RE (1997) Probabilistic Risk Assessment of Engineering Systems. ITP

Suquet PM (1987) Elements of Homogenization for Inelastic Solid Mechanics. In: Homogenization techniques for composite media. Springer-Verlag, pp 193–278

Sýkora J, Šejnoha M, Šejnoha J (2013) Homogenization of coupled heat and moisture transport in masonry structures including interfaces. Applied Mathematics and Computation 219:7275–7285. doi: https://doi.org/10.1016/j.amc.2011.02.050

Taliercio A (2014) Closed-form expressions for the macroscopic in-plane elastic and creep coefficients of brick masonry. International Journal of Solids and Structures 51:2949–2963. doi: 10.1016/j.ijsolstr.2014.04.019

Taylor RL, Simo JC, Zienkiewicz OC, Chan ACH (2018) The patch test—a condition for assessing FEM convergence. International Journal for Numerical Methods in Engineering 22:39–62. doi: 10.1002/nme.1620220105

The International Disaster Database (2009) Disasters in numbers

Theodossopoulos D, Sinha B (2013) A review of analytical methods in the current design processes

and assessment of performance of masonry structures. Construction and Building Materials 41:990–1001. doi: 10.1016/j.conbuildmat.2012.07.095

Tomaževič M (2010) Heritage Masonry Buildings and Reduction of Seismic Risk: The Case of Slovenia. In: Netherlands S (ed) Materials, Technologies and Practice in Historic Heritage Structures. pp 327–350

Tomaževič M (1978) The computer program POR. Ljubljana, Hungary

Tothong P, Luco N (2007) Probabilistic seismic demand analysis using advanced ground motion intensity measures. Earthquake Engineering & Structural Dynamics 36:1837–1860. doi: 10.1002/eqe.696

Tran VH, Vincens E, Morel JC, et al (2014) 2D-DEM modelling of the formwork removal of a rubble stone masonry bridge. Engineering Structures 75:448–456. doi: 10.1016/j.engstruct.2014.05.048

Turco E, Caracciolo P (2000) Elasto-plastic analysis of Kirchhoff plates by high simplicity finite elements. Computer Methods in Applied Mechanics and Engineering 190:691–706. doi: 10.1016/S0045-7825(99)00438-7

Tzamtzis A, Asteris P (2003) Finite element analysis of masonry structures: Part I: Review of previous work. In: 9th North American masonry conference. pp 101–111

U.N. (2014) Human Development Report; Sustaining Human Progress: Reducing Vulnerabilities and Building Resilience

UNDRO (1979) Natural disasters vulnerability analysis. New York

Valenta R, Sejnoha M, Zeman J (2010) Macroscopic Constitutive Law for Mastic Asphalt Mixtures from Multiscale Modeling. International Journal for Multiscale Computational Engineering 8:131–149. doi: 10.1615/IntJMultCompEng.v8.i1.100

Vamvatsikos D, Cornell CA (2002) Incremental dynamic analysis. Earthquake Engineering & Structural Dynamics 31:491–514. doi: 10.1002/eqe.141

Vamvatsikos D, Cornell CA (2004) Applied Incremental Dynamic Analysis. Earthquake Spectra 20:523–553. doi: 10.1193/1.1737737

Vamvatsikos D, Fragiadakis M (2010) Incremental dynamic analysis for estimating seismic performance sensitivity and uncertainty. Earthquake Engineering & Structural Dynamics 39:141–163. doi: 10.1002/eqe.935

van den Eijnden AP, Bésuelle P, Chambon R, Collin F (2016) A FE2 modelling approach to hydromechanical coupling in cracking-induced localization problems. International Journal of Solids and Structures 97–98:475–488. doi: 10.1016/j.ijsolstr.2016.07.002

Vandoren B, De Proft K, Simone A, Sluys LJ (2013) Mesoscopic modelling of masonry using weak and strong discontinuities. Computer Methods in Applied Mechanics and Engineering 255:167–182. doi: 10.1016/j.cma.2012.11.005

Varignon P (1725) Nouvelle mécanique ou statique. 2 vols. Paris: C Jombert

Varma RK, Tomar CPS, Parkash S, V. S. S (1996) Damage to Brick Masonry Panel Walls Under High Explosive Detonations. Asme-Publications-Pvp 351:207–216

Vicente R, Parodi S, Lagomarsino S, et al (2011) Seismic vulnerability and risk assessment: case study of the historic city centre of Coimbra, Portugal. Bulletin of Earthquake Engineering 9:1067–1096. doi: 10.1007/s10518-010-9233-3

Volokh KY (2012) Characteristic length of damage localization in steel. Engineering Fracture Mechanics 94:85–86. doi: https://doi.org/10.1016/j.engfracmech.2012.07.010

Volokh KY (2011) Characteristic Length of Damage Localization in Rubber. International Journal of Fracture 168:113–116. doi: 10.1007/s10704-010-9563-9

Volokh KY (2013) Characteristic length of damage localization in concrete. Mechanics Research Communications 51:29–31. doi: https://doi.org/10.1016/j.mechrescom.2013.04.007

Vondřejc J, Zeman J, Marek I (2014) An FFT-based Galerkin method for homogenization of periodic media. Computers & Mathematics with Applications 68:156–173. doi: 10.1016/j.camwa.2014.05.014

Wang M, Hao H, Ding Y, Li Z-X (2009) Prediction of fragment size and ejection distance of masonry wall under blast load using homogenized masonry material properties. International Journal of Impact Engineering 36:808–820. doi: 10.1016/j.ijimpeng.2008.11.012

Wei X, Stewart MG (2010) Model validation and parametric study on the blast response of unreinforced brick masonry walls. International Journal of Impact Engineering 37:1150–1159. doi: 10.1016/j.ijimpeng.2010.04.003

Welch DP, Sullivan TJ, Calvi GM (2014) Developing Direct Displacement-Based Procedures for Simplified Loss Assessment in Performance-Based Earthquake Engineering. Journal of Earthquake Engineering 18:290–322. doi: 10.1080/13632469.2013.851046

Wesevich JW, Oswald CJ (2005) Empirical Based Concrete Masonry Pressure-Impulse Diagrams for Varying Degrees of Damage. In: Structures Congress 2005. American Society of Civil Engineers, Reston, VA, pp 1–12

Whitman R, Reed JW, Hong ST (1973) Earthquake damage probability matrices. In: Proceedings of the Fifth World Conference on Earthquake Engineering. Rome, Italy, pp 2531–2540

Willis CR, Griffith MC, Lawrence SJ (2004) Horizontal Bending of Unreinforced Clay Brick Masonry. Masonry International 17:109–121

Wu L, Lucas V, Nguyen V-D, et al (2016) A stochastic multi-scale approach for the modeling of thermo-elastic damping in micro-resonators. Computer Methods in Applied Mechanics and Engineering 310:802–839. doi: https://doi.org/10.1016/j.cma.2016.07.042

Xu X-P, Needleman A (1994) Numerical simulations of fast crack growth in brittle solids. Journal of the Mechanics and Physics of Solids 42:1397–1434. doi: https://doi.org/10.1016/0022-5096(94)90003-5

Yamanaka T, Ghiasi H, Heidari-Rarani M, et al (2015) Multiscale finite element analysis of mode I

delamination growth in a fabric composite. Composite Structures 133:157–165. doi: 10.1016/j.compstruct.2015.07.094

Yim C, Chopra A, Penzien J (1980) Rocking response of rigid blocks to earthquakes. Earthquake Engineering and Structural Dynamics 565–587

Yon J-H, Hawkins NM, Kobayashi A (1992) Strain-Rate Sensitivity of Concrete Mechanical Properties. ACI Materials Journal 89:146–153. doi: 10.14359/2223

Zienkiewicz OC, Taylor RL (2000) The Finite Element Method: Solid mechanics. (Vol. 2). Butterworth-Heinemann

Zienkiewicz OC, Zhu JZ (1992) The superconvergent patch recovery (SPR) and adaptive finite element refinement. Computer Methods in Applied Mechanics and Engineering 101:207–224. doi: https://doi.org/10.1016/0045-7825(92)90023-D

Zijl GPAG (2000) Computational Modelling of Masonry Creep and Shrinkage. Delft University of Technology

Zucchini A, Lourenço P (2002) A micro-mechanical model for the homogenisation of masonry. International Journal of Solids and Structures 39:3233–3255. doi: 10.1016/S0020-7683(02)00230-5